Journal of the

ENGINEERING MECHANICS DIVISION

Proceedings of the American Society of Civil Engineers

ENGINEERING MECHANICS DIVISION
EXECUTIVE COMMITTEE
Daniel C. Drucker, Chairman; Dan H. Pletta, Vice-Chairman;
Egor P. Popov; Bruce G. Johnston; Edward Wenk, Jr., Secretary

COMMITTEE ON PUBLICATIONS
Dan H. Pletta, Chairman; John S. Archer; W. Douglas Baines; Hans Bleich;
Albert G. H. Dietz; Robert J. Hansen; Eivind Hognestad; Ernest F. Masur

CONTENTS

October, 1959

Papers

	Page
Elastic Bending of Layered Plates by K. S. Pister and S. B. Dong	1
Flexible Surfaces on Viscoelastic Subgrades by B. C. Hoskin and E. H. Lee	11
Solutions for One-Dimensional Structural Lattices by Donald L. Dean and Selmo Tauber	31
Electrical Analog for Earthquake Yield Spectra by G. N. Bycroft, M. J. Murphy and K. J. Brown	43
The Neutral Axis in Plastic Bending of Beams by Aris Phillips	65
Laterally Loaded Thin Flat Plates by William A. Bradley	77
Behavior of Structures During Earthquakes by G. W. Housner	109

(Over)

Copyright 1959 by the American Society of Civil Engineers.

Page

Commentary on Plastic Design in Steel: Additional Design Considerations - I
Progress Report No. 3 of the Joint WRC-ASCE Committee on Plasticity Related to Design. 131

Commentary on Plastic Design in Steel: Additional Design Considerations - II
Progress Report No. 4 of the Joint WRC-ASCE Committee on Plasticity Related to Design. 157

Discussion 187

Journal of the
ENGINEERING MECHANICS DIVISION
Proceedings of the American Society of Civil Engineers

ELASTIC BENDING OF LAYERED PLATES

K. S. Pister,[1] A. M. ASCE and S. B. Dong,[2] A. M. ASCE

ABSTRACT

A system of equations governing the non-linear bending of plates consisting of two or more bonded, thin layers is presented. The effects of both transverse and in-plane loading and thermal gradients through the plate thickness as well as over the plate faces are included. Specialization of the equations for particular classes of problems is shown.

NOMENCLATURE

Conventional symbols used in plate theory are employed. (See, for example, Reference [1]. Other symbols are defined below.

T	- temperature difference with respect to an initial equilibrium state.
α	- linear coefficient of thermal expansion.
N_T, M_T	- thermal stress and moment resultants
u_o, v_o, w_o	- displacement vector components of a point on the top surface of the plate.
ϵ_{xo}, ϵ_{yo}, γ_{xyo}	- strain tensor components on the top surface of the plate.
h_k	- distance from the top of the plate to the top of the k th plate lamina.
B, C, D, K	- composite plate parameters

Note: Discussion open until March 1, 1960. To extend the closing date one month, a written request must be filed with the Executive Secretary, ASCE. Paper 2194 is part of the copyrighted Journal of the Engineering Mechanics Division, Proceedings of the American Society of Civil Engineers, Vol. 85, No. EM 4, October, 1959.

1. Associate Prof. of Civ. Eng., Univ. of California, and Engr., Univ. of California Radiation Lab., Berkeley, Calif.
2. Graduate Student in Civ. Eng., Univ. of California, Berkeley, Calif.

INTRODUCTION

This paper is concerned with formulation of a system of equations governing the elastic bending of plates consisting of two or more thin, bonded layers of isotropic materials. The equations are developed within the framework of the von Karman theory of bending, which ignores the effect of transverse shear deformation, but accounts for deflections which are of the order of the plate thickness. The effect of transverse and in-plane forces as well as thermal gradients through the plate thickness and over the plate faces is considered. Although problems of layered plates have received some attention in the past, emphasis has been placed upon symmetric, sandwich type construction. A general treatment of the linear theory of bimetallic shells and axisymmetric bending of circular plates including thermal effects has been given by Grigolyuk.(2) An independent formulation of the latter problem has also been given by Vinson,(3) who further restricted the problem to layers with the same Poisson's ratio. Numerical results for a number of circular plate problems appear in a paper by Korolev.(4) The objective of the present paper is to extend previous work to include non-linear effects and to systematize the computation of the elastic parameters entering into the formulation of the problem for multi-layer plates.

Specification of the Temperature Distribution

In many problems of interest coupling in the heat flow equations may be neglected and the temperature distribution in each layer determined from appropriate solutions of the Fourier heat conduction equation. In such cases the temperature in each layer can be expressed as

$$T(x,y,z,t) = T_k(x,y,z,t),\ h_{k-1} \leq z \leq h_k \tag{1}$$

where a plate element with the associated coordinate system is shown in Fig. 1. Assuming no contact resistance at internal interfaces, the temperature distribution will be continuous through the thickness. Proper account of contact resistance can be taken with no difficulty. For sufficiently thin layers the temperature distribution through the plate approaches piece-wise linearity. For time-dependent temperature distribution, the elastic response of the plate can be regarded as quasi-static in most cases.

Equations of the Large Deflection Theory

The von Karman displacement assumptions for plate bending referred to the coordinate system shown are:

$$\begin{aligned} u &= u_o - z\,w_{,x} \\ v &= v_o - z\,w_{,y} \\ w &= w_o \end{aligned} \tag{2}$$

where u_o, v_o, w_o, (the displacement components of a point on the top surface of the plate) are understood to be functions of x, y. The comma denotes partial differentiation. The strain-displacement equations associated with the von Karman theory are:

$$\epsilon_x = u_{o,x} + \frac{1}{2}w_{,x}^2 - z w_{,xx} = \epsilon_{xo} - z w_{,xx}$$

$$\epsilon_y = v_{o,y} + \frac{1}{2}w_{,y}^2 - z w_{,yy} = \epsilon_{yo} - z w_{,yy} \tag{3}$$

$$\gamma_{xy} = v_{o,x} + u_{o,y} + w_{,x} w_{,y} - 2 z w_{,xy} = \gamma_{xyo} - 2 z w_{,xy}$$

For plane stress* in a lamina in the i th layer, Hookes Law gives

$$\epsilon_x^{(i)} = \frac{1}{E_i}\left[\sigma_x^{(i)} - \nu_i \sigma_y^{(i)}\right] + \alpha_i T_i$$

$$\epsilon_y^{(i)} = \frac{1}{E_i}\left[\sigma_y^{(i)} - \nu_i \sigma_x^{(i)}\right] + \alpha_i T_i \tag{4}$$

$$\gamma_{xy}^{(i)} = \frac{2}{E_i}\left[1 + \nu_i\right]\tau_{xy}^{(i)}$$

Substituting (3) into (4) and inverting gives

$$\sigma_x^{(i)} = \frac{E_i}{1-\nu_i^2}\left[\epsilon_{xo} - z w_{,xx} + \nu_i(\epsilon_{yo} - z w_{,yy}) - \alpha_i(1+\nu_i)T_i\right] \tag{5a}$$

$$\sigma_y^{(i)} = \frac{E_i}{1-\nu_i^2}\left[\epsilon_{yo} - z w_{,yy} + \nu_i(\epsilon_{xo} - z w_{,xx}) - \alpha_i(1+\nu_i)T_i\right] \tag{5b}$$

$$\tau_{xy}^{(i)} = \frac{E_i}{2(1-\nu_i^2)}\left[(\gamma_{xyo} - 2 z w_{,xy})(1-\nu_i)\right] \tag{5c}$$

Stress resultants and stress couples can now be defined as for homogeneous plates by integrating Eqs. (5) over each layer and summing the resulting expressions over the n plate layers.

$$N_x, N_y, N_{xy} = \sum_{k=1}^{n} \int_{h_{k-1}}^{h_k} (\sigma_x, \sigma_y, \tau_{xy})^{(k)} \, dz \tag{6}$$

$$M_x, M_y, M_{xy} = \sum_{k=1}^{n} \int_{h_{k-1}}^{h_k} (\sigma_x, \sigma_y, \tau_{xy})^{(k)} \, z \, dz \tag{7}$$

Upon integration and collection of terms there results:

$$N_x = B\epsilon_{xo} + B_\nu \epsilon_{yo} - C w_{,xx} - C_\nu w_{,yy} - N_T \tag{8a}$$

$$N_y = B\epsilon_{yo} + B_\nu \epsilon_{xo} - C w_{,yy} - C_\nu w_{,xx} - N_T \tag{8b}$$

$$N_{xy} = \frac{1}{2}(B - B_\nu)\gamma_{xyo} - (C - C_\nu) w_{,xy} \tag{8c}$$

*Results obtained for beams indicate that this is a satisfactory approximation provided that temperature and/or surface pressure gradients in the x, y directions are not severe.(5)

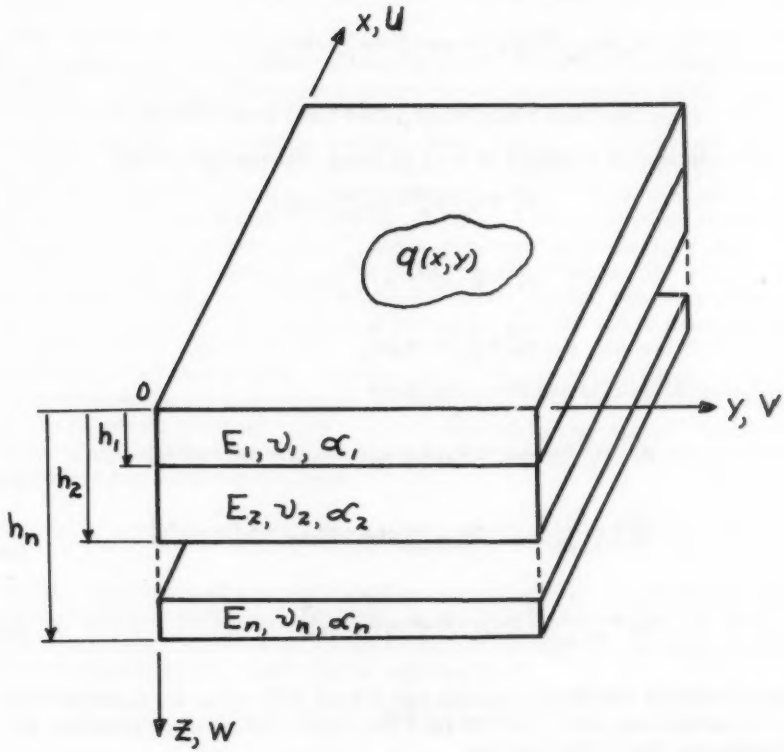

Fig. 1

$$M_x = -Dw_{,xx} - D_\nu w_{,yy} + C\epsilon_{xo} + C_\nu \epsilon_{yo} - M_T \tag{9a}$$

$$M_y = -Dw_{,yy} - D_\nu w_{,xx} + C\epsilon_{yo} + C_\nu \epsilon_{xo} - M_T \tag{9b}$$

$$M_{xy} = \frac{1}{2}(C - C_\nu)\gamma_{xyo} - (D - D_\nu)w_{,xy} \tag{9c}$$

The elastic constants appearing in the above Eqs. are identified as follows: (all sums are over the range 1, 2, . . . n)

$$B = \sum_k \frac{E_k}{1-\nu_k^2}(h_k - h_{k-1}) \qquad B_\nu = \sum_k \frac{E_k \nu_k}{1-\nu_k^2}(h_k - h_{k-1}) \tag{10a, b}$$

$$C=\sum_k \frac{E_k}{1-\nu_k^2}\frac{(h_k^2-h_{k-1}^2)}{2} \qquad C_\nu=\sum_k \frac{E_k\nu_k}{1-\nu_k^2}\frac{(h_k^2-h_{k-1}^2)}{2} \tag{11a, b}$$

$$D=\sum_k \frac{E_k}{1-\nu_k^2}\frac{(h_k^3-h_{k-1}^3)}{3} \qquad D_\nu=\sum_k \frac{E_k\nu_k}{1-\nu_k^2}\frac{(h_k^3-h_{k-1}^3)}{3} \tag{12a, b}$$

The thermal stress resultant and thermal moment associated with the temperature distribution are

$$N_T=\sum_k \frac{E_k\alpha_k}{1-\nu_k}\int_{h_{k-1}}^{h_k} T_k\,dz \tag{13}$$

$$M_T=\sum_k \frac{E_k\alpha_k}{1-\nu_k}\int_{h_{k-1}}^{h_k} T_k\,z\,dz \tag{14}$$

In the sequel the following additional constants will be useful:

$$D^*=D-CK_1-C_\nu K_2 \qquad D_\nu^*=D_\nu-C_\nu K_1-CK_2 \tag{15a, b}$$

$$K_1=\frac{BC-B_\nu C_\nu}{B^2-B_\nu^2} \qquad K_2=\frac{BC_\nu-B_\nu C}{B^2-B_\nu^2} \qquad K_3=\frac{1}{B+B_\nu} \tag{16a, b, c}$$

It is convenient to regard the transverse displacement w and the stress resultants N_x, N_y, N_{xy} as primary dependent variables. The three equations of equilibrium for the plate element supplemented by the compatibility equation for the in-plane strain components at the top surface of the plate constitute the determinative system for these variables. These equations are:

$$N_{x,x}+N_{xy,y}=0 \qquad N_{xy,x}+N_{y,y}=0 \tag{17a, b}$$

$$M_{x,xx}+2M_{xy,xy}+M_{y,yy}=-(q+N_x w_{,xx}+2N_{xy}w_{,xy}+N_y w_{,yy}) \tag{17c}$$

$$\epsilon_{xo,yy}+\epsilon_{yo,xx}-\gamma_{xyo,xy}=w_{,xy}^2-w_{,xx}w_{,yy} \tag{17d}$$

From Eq. (8) the strain components are

$$\epsilon_{xo}=\frac{B}{B^2-B_\nu^2}N_x-\frac{B_\nu}{B^2-B_\nu^2}N_y+K_1w_{,xx}+K_2w_{,yy}+K_3N_T \tag{18a}$$

$$\epsilon_{yo}=\frac{B}{B^2-B_\nu^2}N_y-\frac{B_\nu}{B^2-B_\nu^2}N_x+K_1w_{,yy}+K_2w_{,xx}+K_3N_T \tag{18b}$$

$$\gamma_{xyo}=\frac{2N_{xy}+2(C-C_\nu)w_{,xy}}{B-B_\nu} \tag{18c}$$

Substituting Eqs. (18) into (9):

$$M_x = -D^* w_{,xx} - D_\nu^* w_{,yy} + K_1 N_x + K_2 N_y + K_3(C + C_\nu) N_T - M_T \tag{19a}$$

$$M_y = -D^* w_{,yy} - D_\nu^* w_{,xx} + K_1 N_y + K_2 N_x + K_3(C + C_\nu) N_T - M_T \tag{19b}$$

$$M_{xy} = (K_1 - K_2) N_{xy} - (D^* - D_\nu^*) w_{,xy} \tag{19c}$$

Now all terms appearing in the determinative Eqs. (17) are expressed in terms of the fundamental variables.

Eqs. (17a, b) are satisfied identically by introducing the Airy Stress function F(x,y) such that

$$N_x = F_{,yy} \qquad N_y = F_{,xx} \qquad N_{xy} = -F_{,xy} \tag{20}$$

Substituting Eqs. (19) and (20) in (17c) gives

$$D^* \nabla^4 w - K_2 \nabla^4 F = \nabla^2 \left[K_3(C + C_\nu) N_T - M_T \right] + q + F_{,yy} w_{,xx} - 2F_{,xy} w_{,xy} + F_{,xx} w_{,yy} \tag{21}$$

Substituting Eqs. (18) into (17d):

$$\frac{B}{B^2 - B_\nu^2} \nabla^4 F + K_2 \nabla^4 w = -K_3 \nabla^2 N_T + w_{,xy}^2 - w_{,xx} w_{,yy} \tag{22}$$

Eqs. (21) and (22), from which w and F can be obtained, are generalizations of the von Karman equations, modified to take into account the properties of a plate made of bonded layers of different materials and to include the effect of temperature gradients.* The presence of the term $K_2 \nabla^4 F$ in Eq. (21) and $K_2 \nabla^4 w$ in Eq. (22) indicates the coupling effect introduced by the layered construction, i.e., in-plane forces affect bending equilibrium. Since the four boundary conditions associated with the system of equations do not differ from those which obtain in the theory for single-layer plates, no further mention will be made here. In view of the difficulty in obtaining solutions of Eqs. (21) and (22) even in the case of a homogeneous, single layer plate it seems desirable to investigate the form taken by the equations in particular cases.

Reduction to Single-Layer Homogeneous Plates

For a single layer plate Eqs. (21) and (22) take the form

$$D_1 \nabla^4 w = \nabla^2 \left[\frac{h N_T}{2} - M_T \right] + q + F_{,yy} w_{,xx} - 2F_{,xy} w_{,xy} + F_{,xx} w_{,yy} \tag{23}$$

$$\nabla^4 F = -(1 - \nu) \nabla^2 N_T + E h (w_{,xy}^2 - w_{,xx} w_{,yy}) \tag{24}$$

where $D_1 = \dfrac{Eh^3}{12(1 - \nu^2)}$, and N_T and M_T represent thermal stress and thermal moment resultants, respectively. These are the classical von Karman

*Similar equations were obtained for a bimetallic shell of constant curvature by Grigolyuk.(2) Unfortunately, however, the equations were not simplified to the extent shown to be possible here.

equations modified to include thermal effects.* If the non-linear terms are neglected in Eq. (24), uncoupled, small deflection equations are obtained. Eq. (24) is then the thermo-elastic compatibility equation for plane stress and Eq. (23) is the equilibrium equation for a plate subjected to in-plane and transverse loads combined with thermal gradients. If a linear temperature gradient through the plate thickness is assumed, these equations reduce to the standard form shown on pages 27 and 59 of Reference (6).

Specialization for Constant Poisson's Ratio

In many instances the value of Poisson's ratio may be very nearly constant for materials with appreciably different moduli of elasticity. Assuming this to be the case, the following simplications of the constants appearing in Eqs. (21) and (22) occur:

$$K_2 = 0 \qquad K_3(C+C_\nu) = \frac{C}{B} \qquad \frac{B}{B^2-B_\nu^2} = \frac{1}{B(1-\nu^2)}$$

Accordingly, these equations take the simpler form

$$D^* \nabla^4 w = \nabla^2\left[\frac{C}{B}N_T - M_T\right] + q + F_{,yy}w_{,xx} - 2F_{,xy}w_{,xy} + F_{,xx}w_{,yy} \qquad (21')$$

$$\nabla^4 F = -(1-\nu)\nabla^2 N_T - B(1-\nu^2)(w_{,xy}^2 - w_{,xx}w_{,yy}) \qquad (22')$$

The equations are now of the same form as for a single layer plate, permitting transposition of known solutions and use of existing methods for new problems.

Equations of the Small Deflection Theory

For deflections which are small compared to plate thickness, the quadratic terms in the strain-displacement Eqs. (3) are dropped. This results in setting equal to zero the corresponding terms in the compatibility Eq. (22); all other equations remain the same. Accordingly, it is possible to simplify the fundamental system as follows. From Eq. (22) with the above simplification,

$$\nabla^4 F = -\frac{K_3(B^2-B_\nu^2)}{B}\nabla^2 N_T - \frac{K_2(B^2-B_\nu^2)}{B}\nabla^4 w \qquad (22'')$$

Eqs. (22") and (21) may now be combined to give the single Eq. governing deflection:

$$\frac{BD-C^2}{B}\nabla^4 w = \nabla^2\left[\frac{C}{B}N_T - M_T\right] + q + N_x w_{,xx} + 2N_{xy}w_{,xy} + N_y w_{,yy} \qquad (21'')$$

Since in the small deflection theory the in-plane forces and transverse deflection are uncoupled, Eq. (21") for w can be solved in terms of prescribed in-plane forces and/or transverse loads and thermal gradients. Note again that solutions may be obtained directly from corresponding single-layer plate problems by transposition. The strain components at the top surface of the plate can be found in terms of the specified forces N_x, N_{xy}, N_y from Eqs. (18) and the deflection w obtained from the solution of Eq. (21").

*Solutions of the one-dimensional large deflection problem of a homogeneous plate strip subjected to temperature changes and transverse load have been given by Williams,[7] using displacement equations of equilibrium.

In view of the invariance of the operators occurring in Eqs. (21) and (22) transformation to polar coordinates is limited to transforming the terms on the right hand side as follows:

$$N_r = \frac{1}{r}\frac{dF}{dr} \qquad N_\theta = \frac{d^2F}{dr^2} \qquad N_{r\theta} = 0 \tag{25a}$$

$$F_{,yy}w_{,xx} - 2F_{,xy}w_{,xy} + F_{,xx}w_{,yy} = \frac{1}{r}\frac{d}{dr}\left(\frac{dF}{dr}\frac{dw}{dr}\right) \tag{25b}$$

$$w_{,xy}^2 - w_{,xx}w_{,yy} = -\frac{1}{2r}\frac{d}{dr}\left(\frac{dw}{dr}\right)^2 \tag{25c}$$

Accordingly, Eqs. (21) and (22) assume the form

$$D^*\nabla^4 w - K_2\nabla^4 F = \nabla^2\left[K_3(C+C_\nu)N_T - M_T\right] + q + \frac{1}{r}\frac{d}{dr}\left(\frac{dF}{dr}\frac{dw}{dr}\right) \tag{26}$$

$$\frac{B}{B^2 - B_\nu^2}\nabla^4 F + K_2\nabla^4 w = -K_3\nabla^2 N_T - \frac{1}{2r}\frac{d}{dr}\left(\frac{dw}{dr}\right)^2 \tag{27}$$

where

$$\nabla^2 = \frac{1}{r}\frac{d}{dr}\left(r\frac{d}{dr}\right)$$

First integrals of these equations may be obtained at once upon multiplying through by r and integrating:

$$D^*\frac{d}{dr}(\nabla^2 w) - K_2\frac{d}{dr}(\nabla^2 F) = \frac{d}{dr}\left[K_3(C+C_\nu)N_T - M_T\right] + \frac{1}{r}\int q\,r\,dr + \frac{1}{r}\frac{dF}{dr}\frac{dw}{dr} + \frac{a_1}{r} \tag{26'}$$

$$\frac{B}{B^2 - B_\nu^2}\frac{d}{dr}(\nabla^2 F) + K_2\frac{d}{dr}(\nabla^2 w) = -K_3\frac{dN_T}{dr} - \frac{1}{2r}\left(\frac{dw}{dr}\right)^2 + \frac{a_2}{r} \tag{27'}$$

where a_1, a_2 are constants.

Eqs. (8), (9) and (19) for stress resultants and stress couples may be easily transformed into appropriate expressions in polar coordinates. The elastic constants will of course remain unchanged.

Small deflection equations can be obtained from (26) and (27) by dropping non-linear terms as for rectangular plates. However, the problem is more conveniently formulated in this case by choosing u_o, the top surface radial displacement, and w, the transverse displacement, as primary variables. Substituting stress-resultant and stress-couple expressions in the two appropriate equilibrium equations in polar coordinates leads to (8):

$$\frac{d^2u_o}{dr^2} + \frac{1}{r}\frac{du_o}{dr} - \frac{u_o}{r^2} = \frac{1}{C^2 - BD}\left[-DN_T + CM_T - CQ\right] \tag{28}$$

$$\frac{d^3w}{dr^3} + \frac{1}{r}\frac{d^2w}{dr^2} - \frac{1}{r^2}\frac{dw}{dr} = \frac{1}{C^2 - BD}\left[-CN_T + BM_T - BQ\right] \tag{29}$$

where $Q = \frac{1}{r}\int q\,r\,dr$.

It will be noted that the equations are not coupled and solutions for various types of boundary conditions can be obtained without difficulty. Examples of solutions of a similar set of equations for bimetallic plates are given in (2).

Transverse Shear Resultants and Shear Stresses

Although transverse shear deformation is neglected in the theory discussed, transverse shear resultants can be determined from equilibrium considerations. The resultants are defined as

$$Q_x = \sum_k \int_{h_{k-1}}^{h_k} \tau_{xz}^{(k)}\, dz \qquad Q_y = \sum_k \int_{h_{k-1}}^{h_k} \tau_{yz}^{(k)}\, dz \tag{30a, b}$$

These stress resultants are determined from the moment equilibrium Eqs.:

$$Q_x = M_{x,x} + M_{xy,y} \qquad Q_y = M_{xy,x} + M_{y,y} \tag{31a, b}$$

Combining these Eqs. with (19) gives

$$Q_x = -D^*(\nabla^2 w)_{,x} + K_2(N_{y,x} - N_{xy,y}) + K_3(C + C_\nu)N_T - M_{T,x} \tag{32a}$$

$$Q_y = -D^*(\nabla^2 w)_{,y} + K_2(N_{x,y} - N_{xy,x}) + K_3(C + C_\nu)N_T - M_{T,y} \tag{32b}$$

The distribution of shear stresses τ_{xz}, τ_{yz} is most easily obtained by considering first the interface shear stresses denoted by $\tau_x^{(k)}$ and $\tau_y^{(k)}$ in Fig. 2. Equilibrium of the finite element in the x and y directions requires that

$$\tau_x^{(k)} = -\sum_{i=1}^{k} \left[N_{x,x}^{(i)} + N_{xy,y}^{(i)} \right] \qquad \tau_y^{(k)} = -\sum_{i=1}^{k} \left[N_{xy,x}^{(i)} + N_{y,y}^{(i)} \right] \tag{33a, b}$$

Accordingly, the shear stress in the k th layer can be written

$$\tau_{xz}^{(k)} = \tau_x^{(k-1)} - \int_{h_{k-1}}^{z} \left[\sigma_{x,x}^{(k)} + \tau_{xy,y}^{(k)} \right] dz$$

A similar expression results for $\tau_{yz}^{(k)}$. Since both σ_x and τ_{xy} are linear functions of z, the shear stresses will follow a parabolic law, as for single-layer plates.

REFERENCES

1. Timoshenko, S., "Theory of Plates and Shells", McGraw-Hill Book Company, Inc., New York, 1940.
2. Grigolyuk, E. I., "Theory of Bimetallic Plates and Shells", Akademiia Nauk, USSR, Inst. Mekhaniki, Inzhenernyi Sbornik, Vol. 17, pp. 69-120, 1953.
3. Vinson, J. R., "Thermal Stresses in Laminated Circular Plates", Presented at the 3rd U. S. National Congress of Applied Mechanics, Brown University, Providence, Rhode Island, June 1958.
4. Korolev, V. I., "Thin Double-layer Plates and Shells", Akademiia Nauk, USSR, Inst. Mekhaniki, Inzhenernyi Sbornik, Vol. 22, pp. 98-110, 1955.

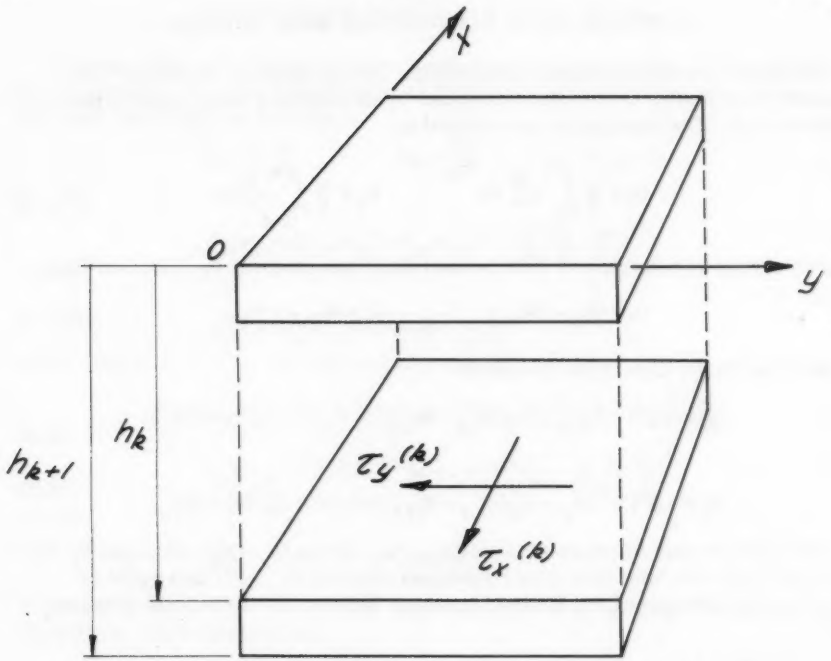

Fig. 2

5. Boley, B. A., "The Determination of Temperature, Stresses, and Deflections in Two-dimensional Thermoelastic Problems," J. Aero. Sci., Vol. 23 (1), pp. 67-75, 1956.

6. Melan, E. and Parkus, H., "Warmespannungen", Springer-Verlay, Vienna, 1953.

7. Williams, M. L., "Further Large Deflection Analysis for a Plate Strip Subjected to Normal Pressure and Heating", Journal of Applied Mechanics, Paper No. 57-A-14, June 1958.

8. Dong, S. B., "Elastic Bending of Layered Plates", M. S. Thesis in Civil Engineering, Graduate Division, University of California, Berkeley, 1958.

Journal of the
ENGINEERING MECHANICS DIVISION
Proceedings of the American Society of Civil Engineers

FLEXIBLE SURFACES ON VISCOELASTIC SUBGRADES[a]

B. C. Hoskin,[1] and E. H. Lee[2]

ABSTRACT

This report is concerned with the analysis of stress and deformation of a subgrade strengthened by a flexible surface plate subjected to a load distribution. Rate effects, creep and stress relaxation in components of such foundations are included through the application of linear viscoelastic theory. It is shown that elastic analyses for such situations which have been actively developed in recent years can be directly extended to treat the analogous problem including viscoelastic effects. Particular examples are presented for constant loads suddenly applied and maintained. In contrast to elastic solutions, the rate influence causes variation of deflection, subgrade pressure and plate bending moments as the constant loads are maintained for extended periods. The significance of the problem and the discussion of particular solutions are given in Sections 1 and 4 of the report. Sections 2 and 3 deal with the general development of the theory.

1. INTRODUCTION

A problem of considerable interest in several fields of civil engineering is that of determining the efficiency of a plate as a means of transferring a relatively localised applied load to a flexible foundation (Fig. 1). This situation arises, for instance, in the design of footings for columns and also in the

Note: Discussion open until March 1, 1960. To extend the closing date one month, a written request must be filed with the Executive Secretary, ASCE. Paper 2195 is part of the copyrighted Journal of the Engineering Mechanics Division, Proceedings of the American Society of Civil Engineers, Vol. 85, No. EM 4, October, 1959.

a. The results presented in this paper were obtained in the course of research sponsored by the Office of Ordnance Research, Dept. of the Army, under Contract No. DA-19-020-3648

1. Scientific Officer, Aeronautical Research Labs., Melbourne, Australia, formerly Brown Univ.
2. Prof. of Applied Math., Div. of Applied Math., Brown Univ., Providence, R. I.

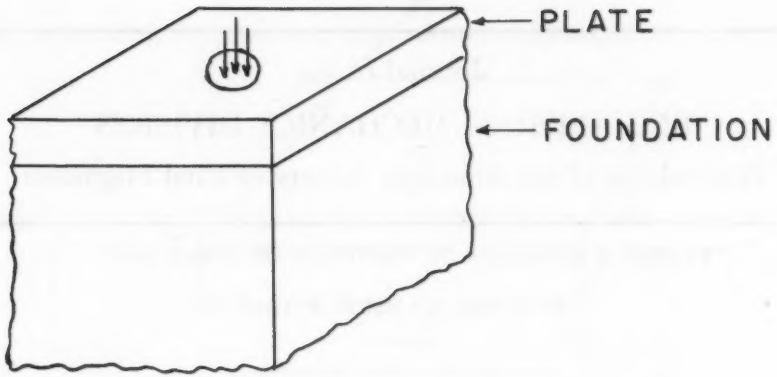

FIG. 1

design of airport pavements. Most of the theoretical work aimed at obtaining rational design formulae for the above problem has dealt with elastic plates on elastic foundations and results of proven practical value have been obtained on this basis.[1,2,3] Nevertheless, it often happens that real foundations are not truly elastic; in particular they may be subject to time effects as is generally the case for a soil foundation. In this paper elastic plates supported by visco-elastic foundations are considered in order that analytical formulae, suitable for application to situations wherein time effects in a foundation are of importance, can be obtained. Some preliminary work on this problem has already been reported[4] and recently the related problem of beams on visco-elastic foundations has been treated by Freudenthal and Lorsch.[5]

In recent years it has been shown that in certain circumstances the stress and deflection analysis of a system including linear visco-elastic components can be treated in terms of the analogous elastic problem having the same geometry and boundary conditions. In the case of a system, the geometry of which does not change during the loading program, and for which boundary conditions remain of the same type at each boundary point, for example prescribed load or prescribed deflection, application of the Laplace transform removes the time dependence and transforms the problem into an associated elastic problem[6] to which standard methods of elastic analysis can be applied. Loaded flexible surfaces over subgrades with prescribed surface loading fall into this category. The present report shows how general problems of this type can be treated by this method, and illustrates the procedure through specific examples.

Linear viscoelastic materials comprise those for which the relationship between stress and strain is a linear differential or integral operator with respect to time. In addition to instantaneous elastic response to stress, such materials exhibit delayed elasticity and viscous flow, and for example respond to a pulse of constant stress as indicated in Fig. 2. Such laws are commonly written:

(1.1)

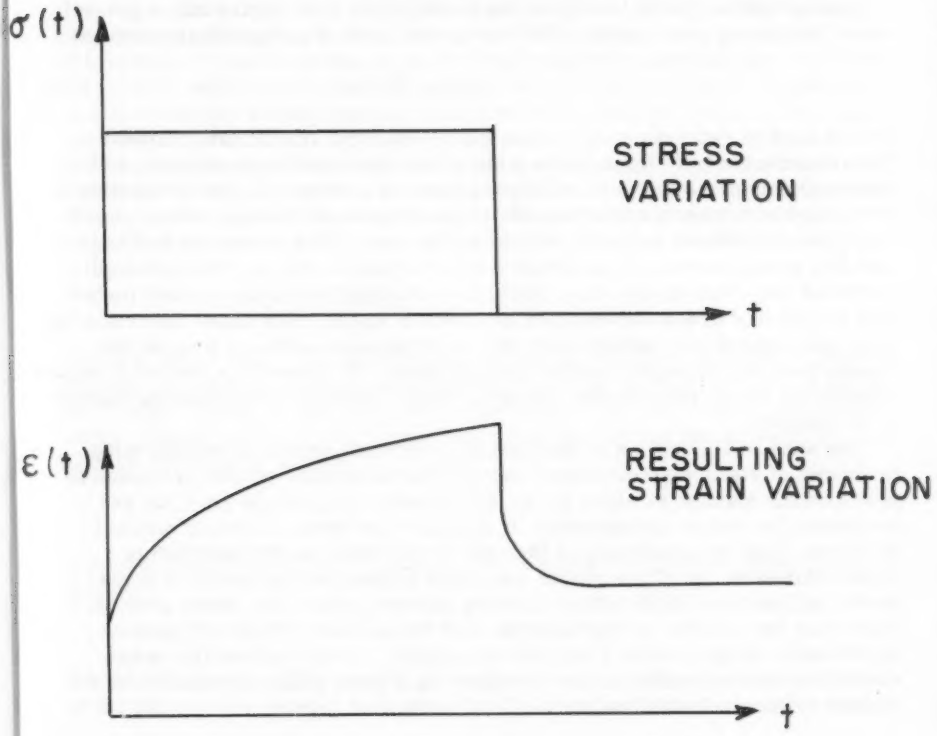

FIG. 2

where σ is the stress, ϵ the strain, and P is a differential operator of the form $\sum_{r=0}^{p} p_r \frac{\partial^r}{\partial t^r}$, the p_r being material constants and t the time, and Q is of similar form: $\sum_{r=0}^{q} q_r \frac{\partial^r}{\partial t^r}$. Relation (1.1) is written for uniaxial response to stress; in the case of combined stresses analogous relations apply for stress components. For an isotropic viscoelastic material, two such laws are needed, one for shear effects and one for average hydrostatic tension and associated dilatation. In general the response of such materials to stress can be considered by replacing the elastic constants of an elastic body by the quotient of such rate operators. Relation (1.1) includes the behavior of materials represented by the commonly used viscoelastic models of springs and dashpots. In particular the Kelvin delayed elastic material and the Maxwell material correspond to operators Q of first order, and operators P of zero and first order respectively. The four element model, which is the simplest relation to exhibit the three main qualitative aspects of viscoelastic behavior—instantaneous elastic response, delayed elastic response, and viscous flow as depicted in Fig. 2—is represented by quadratic operators.

Linear visco-elastic theory as expressed by (1.1) or by the more general use of the creep or relaxation function in the form of an hereditary integral:

$$\varepsilon = \int_{-\infty}^{t} J(t-\tau)\frac{d\sigma}{d\tau}\, d\tau \qquad (1.2)$$

can be used to reproduce any measured creep or relaxation law. However, linear viscoelasticity implies the truth of the superposition principle, so that unless this is exhibited to a sufficient degree of accuracy by the properties of the subgrade material under consideration, non-linear theory, and an inordinately more difficult analysis, will be necessary. This constraint demands that if a creep curve $\epsilon_o(t)$ is obtained at a certain stress σ_o, then the application of twice the stress, $2\sigma_o$, would have doubled the strain at each instant, that is, the new creep curve would be given by $2\epsilon_o(t)$. For many materials this principle applies to a satisfactory degree of approximation as long as the stress does not exceed a certain critical value. (7) presents a review of stress analysis in linear viscoelastic materials and of methods of measuring material properties.

The ease of application of the method mentioned above, of transforming problems of visco-elastic stress analysis into analogous elastic problems depends on the manner in which the elastic constants appear in the final expressions for stress components. If this is in the form of simple rational functions, then the evaluation of the equivalent visco-elastic problem is straightforward, but if the elastic constants appear as arguments in transcendental functions, difficulties of interpretation arise. For some problems there may be a choice of representation of the solution which will provide appreciable simplification from this standpoint. In the next section some elastic foundation problems are discussed in a form which is suitable for extension to visco-elastic analysis.

2. Elastic Foundation Problems

We will be concerned with axially symmetric loading problems in foundations for which edge effects can be disregarded, so that the foundation and surface are effectively infinite in extent. We will consider loading problems in which inertia forces due to the deformation are negligible so that quasi-static analysis will be applied. This will introduce no restriction for most foundation problems, although there will be a limiting speed for a moving vehicle, or for the build-up of a dynamically applied load beyond which inertia forces will have an appreciable influence on subgrade stresses.

For axially symmetrical problems both in three dimensional elasticity theory, and in plate theory, stress components which vary radially in proportion with the Bessel function $J_o(mr)$, where r is the radius and m a constant, play a particularly significant role. For elasticity theory in cylindrical coordinates, this distribution produces separation of the axial coordinate z, and the radial coordinate r in the basic equations and so generates simple solutions in closed form. For example, for a load distribution $q(r) = J_o(mr)$ on the surface of a semi-infinite homogeneous elastic half-space, the deflection of the surface is given by:

$$w(r) = \frac{1-\mu}{Gm} J_o(mr) \qquad (2.1)$$

where μ is Poisson's ratio and G the shear modulus (see (1) p. 20, the original reference being Lamb (8)). Burmister[3] has shown that loading on several layers of different elastic media can be treated in a similar way, and that the surface deflection is given by an expression analogous to (2.1), with the coefficient of the Bessel function a more complicated, but rational function of the elastic constants.

The analysis for a single elastic layer resting on an elastic half-space of different material properties is more simply treated if the dimensions of the surface layer permit thin plate theory to be used to represent the layer. The plate theory equation for lateral deflection w of this layer is (see for example (1) p. 13):

$$D\nabla^2\nabla^2 w(r) + s(r) = q(r) \tag{2.2}$$

where D is the plate flexural rigidity, s(r) is the reactive pressure applied to the plate's lower surface by the foundation, and q(r) is the intensity of the applied load. Owing to the radial symmetry present in the class of problems under consideration, w, s and q are functions only of the radial coordinate r, and the Laplacian operator is given by

$$\nabla^2 = \frac{d^2}{dr^2} + \frac{1}{r}\frac{d}{dr}$$

The particular convenience of the Bessel function distribution arises from the identity

$$\nabla^2 J_o(mr) = -m^2 J_o(mr) \tag{2.3}$$

The combination of (2.1) with (2.2) and the identity (2.3), gives the deflection of the plate on the elastic half space for the surface loading $q(r) = J_o(mr)$:

$$w(r) = \frac{1}{Dm^4 + \frac{Gm}{1-\mu}} J_o(mr) \tag{2.4}$$

A similar result is obtained if the elastic half space is replaced by the simplest type of elastic foundation first suggested by Hertz which consists of a series of closely spaced uncoupled springs each of the same stiffness (Fig. 3). Here the appropriate stress deflection relation is:

$$s = kw \tag{2.5}$$

where k is a material constant for the foundation. Such a foundation is commonly termed the dense liquid type, since it represents the flotation which a dense liquid would produce, although the value of k normally associated with foundation problems is much larger than the density of the material displaced. Most of the formulae used for the rational design of concrete pavements have been obtained by assuming this type of foundation response. For this case (2.2), (2.3), and (2.5) determine the deflection of the plate under the load $q(r) = J_o(mr)$ to be:

$$w(r) = \frac{1}{Dm^4 + k} J_o(mr) \tag{2.6}$$

Reissner[12] has developed a theory of subgrade action which is intermediate between the above two assumptions. It is simpler than the continuum

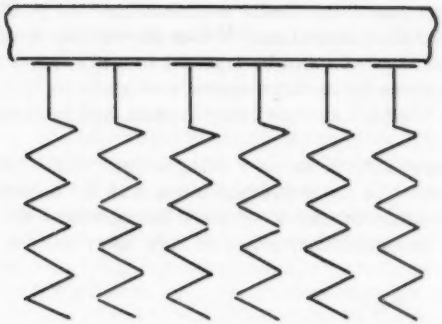

FIG. 3 SIMPLE ELASTIC FOUNDATION

theory, and supplies some of the shear coupling which is absent in the liquid subgrade assumption. Since the equations relating pressure and deflection contain space derivatives only in the form of ∇^2 in the surface, the use of the Bessel function pressure distribution will achieve separation of the space and time variables also in this case.

Thus for all the foundation representations considered, the application of the Bessel function loading distribution leads to simple deformation expressions, and incidentally, expressions in which the elastic constants appear as simple, multiplying factors; these lend themselves readily to generalization for visco-elastic materials. However this load function introduces certain difficulties. $J_o(mr)$ represents a damped oscillatory load with maximum intensity at the origin. The amplitude of the oscillations decrease to zero with increasing radius, and in fact the function is represented asymptotically for large r by:

$$J_o(mr) \sim \sqrt{\frac{2}{\pi mr}} \cos(mr - \tfrac{1}{4}\pi) \tag{2.7}$$

This ensures that the plate deflection and its derivatives approach zero as r increases, so that all moments and stress components do likewise. However, the total load on the surface is not defined. The total load to the radius b is given by

$$\int_0^b 2\pi r\, J_o(mr)dr = \frac{2\pi b}{m} J_1(mb) \sim 2\sqrt{\frac{2\pi b}{m^3}} \cos(mb - \tfrac{3}{4}\pi) \tag{2.8}$$

As b increases this oscillates with an amplitude that approaches infinity, so that the total load on the infinite plate is not defined. This difficulty can be overcome by considering an integral of terms of this type over varying m, and for example, a distribution of load that is of uniform intensity q_o over an area of radius a, but which is zero outside this area (as depicted in Fig. 1) can be represented in the form:

$$q(r) = q_o a \int_0^\infty J_o(mr) J_1(ma)dm \tag{2.9}$$

Since r appears only in the term $J_0(mr)$, the analysis detailed above for deflection of a flexible surface supported by certain types of foundation, can be applied directly to the integrand of (2.9), resulting in an infinite integral over m for the deflection and other quantities which may be of interest. For example, the deflection of a plate resting on an elastic half-space for this loading is given from (2.4) by the integral:

$$w(r) = q_o a \int_0^\infty \frac{1}{Dm^4 + \frac{Gm}{1-\mu}} J_o(mr) J_1(ma) dm \qquad (2.10)$$

The numerical evaluation of an integral of this type is carried out in the example given later.

In spite of the difficulty of not being able to define the total load on an infinite plate for the load distribution $J_0(mr)$, it may still be useful to use a finite sum of such terms to represent prescribed radially symmetric load distributions adjacent to the origin. Again the total load for the infinite surface will not be defined, but since the deformation under the load is effectively a local phenomenon, and the stresses at infinity approach zero, it is reasonable to expect that if the series of Bessel terms represents the load distribution satisfactorily around the origin, it will be a usable representation for the determination of deflections and stresses in this neighborhood. The reason for suggesting this, when an integral representation of the type (2.9) is available which avoids these complications, is associated with the simplicity of evaluating a finite sum rather than an infinite integral. If an elastic layer analysis of the type developed by Burmister[3] is used, the complexity of the displacement expression for a single $J_0(mr)$ loading term may dictate the use of a finite series to achieve a solution within practicable computing limits.

An expression of the type (2.9) is developed from the orthogonality of Bessel functions in a manner similar to the development of the Fourier integral for trigonometric functions. Corresponding to the Fourier series, which represents an arbitrary function over a finite interval, the Fourier-Bessel series of Bessel functions also achieves this. It is developed in an analogous manner (see for example (9) Chap. VIII) by means of orthogonality relations over a finite interval. Whereas the Fourier series represents a periodic function which repeats itself outside the chosen interval, the Fourier-Bessel series in terms of $J_0(mr)$ also introduces a continuing contribution with increasing radius, but this is attenuated as the radius increases and approaches zero for large radius as does the Bessel function itself. Fig. 4 shows the representation by a finite number of terms of a Fourier-Bessel expansion of a uniform distribution of pressure of the type depicted in Fig. 1 of magnitude 2.5 over a circle of radius 0.2. Fig. 4a shows the result of summing five terms, and Fig. 4b, thirty terms. In each figure the broken line shows the distribution to which the finite series is an approximation. The basic interval for choosing the coefficients of the terms of the series was from r = 0 to 1. The figures show that these series introduce a ring of negative pressure in the neighbourhood of r = 2, and such rings of decreasing amplitude will appear for larger values of the radius. These distributions suggest that the finite series will provide a satisfactory representation of the single region of uniform pressure, as long as the deflection solutions associated with the separate rings of pressure introduced by the finite series do not interact appreciably. This can readily be checked by computing the deflection distributions. For viscoelastic behaviour, such representations by finite series may be

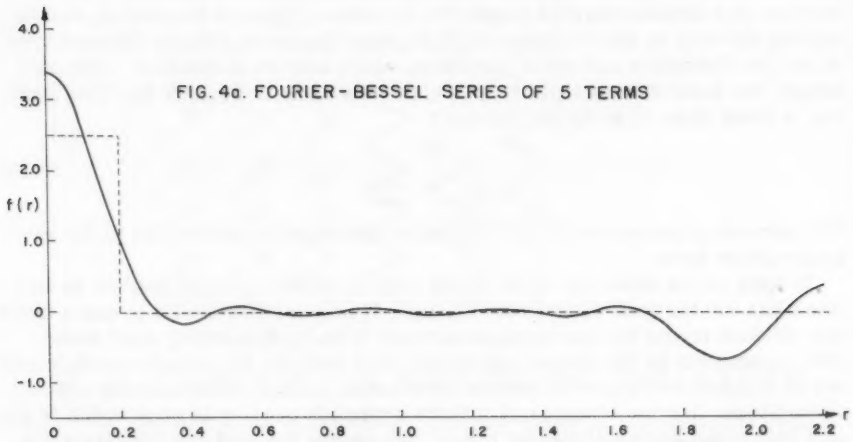

FIG. 4a. FOURIER-BESSEL SERIES OF 5 TERMS

satisfactory for a limited time duration, after which the deflection distribution spreads out and introduces interaction between the separate pressure regions. The finite series representations depicted in Fig. 4 were based on the interval $0 \leq r \leq 1$. A larger interval would displace the first negative pressure ring to a larger radius, but would call for a larger number of terms to achieve adequate representation of the shape of the pressure distribution in the region of the origin. A compromise must be chosen in these two respects, and Figs. 4 show examples with five and thirty terms, respectively. In assessing the accuracy needed for the approximation to the desired load distribution, it should be born in mind, as shown by Reissner,(2) that in the range of loading areas and surface plate thicknesses for which the subgraded pressure is appreciably less than the load intensity, that is the practical design range, the deflection and subgrade pressure functions are insensitive to the detail of the form of the load distribution. Thus the approximation shown in Fig. 4a is likely to be quite adequate for computing foundation properties. Although for the particular problem solved in detail in this report numerical integration using a Fourier-Bessel integral relation of the type (2.9) was utilized, aspects of the application of finite series have been discussed since, as mentioned above, the simplification achieved may be worthwhile when more complicated foundation situations are analysed.

3. Analysis for Viscoelastic Materials

The previous section dealt with stress and deflection solutions for elastic flexible surfaces and subgrades. When there are components which respond to stress in a viscoelastic manner, corresponding laws must be introduced, and the resulting stresses and deflections will be found to vary with time even when the applied loads remain constant. The shape of the distributions of stress and deformation will in general also vary. A convenient method of analysing this situation is to apply the Laplace transformation with respect to time to the basic equations and boundary and initial conditions.(6) Writing in general

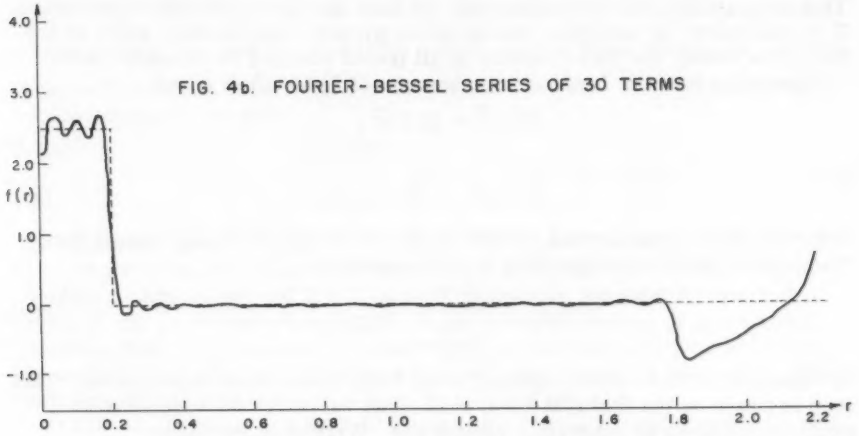

FIG. 4b. FOURIER-BESSEL SERIES OF 30 TERMS

$$\bar{f}(r,p) = \int_0^\infty f(r,t)e^{-pt}\,dt \tag{3.1}$$

where p is a parameter, it is well known (see for example (10) Chap. 1) that the Laplace transform of the time derivative of a function is simply p times the Laplace transform of the function itself if the function is zero initially:

$$p\bar{f}(r,p) = \int_0^\infty \frac{\partial}{\partial t}[f(r,t)]\, e^{-pt}\,dt \tag{3.2}$$

Thus, with this transformation, viscoelastic laws of the form (1.1) become equivalent to elastic laws with the elastic constants in the form of rational functions of the parameter p. Thus the determination of transformed variables, of say stress or deflection, becomes an elastic problem of the type discussed in the previous section, and standard methods of inversion of the Laplace transform determine the stresses and deflections as functions of the time.

Consider, for example, Eq. (2.1) for the deflection of the surface of an elastic half-space subjected to the load distribution $q(r) = J_0(mr)$. Let us suppose the material to be viscoelastic with the shear modulus G replaced by the viscoelastic relation:

$$P\left(\frac{\partial}{\partial t}\right)(\tau) = Q\left(\frac{\partial}{\partial t}\right)(\gamma) \tag{3.3}$$

where τ and γ are shear stress and shear strain respectively. Further, let us suppose that the operator for the visco-elastic body which corresponds to Poisson's ratio μ for the elastic material, is a constant, which means that in a simple tension test of the viscoelastic material, the ratio of lateral to longitudinal strain remains constant throughout the test. This would be the case, for example, were the material incompressible, corresponding to $\mu = 1/2$.

For a viscoelastic problem, loads varying with time must usually be considered, and so let us take:

$$q(r,t) = \varphi(t)J_0(mr) \tag{3.4}$$

This is a special type of loading with the time and space variables separated. It is convenient for analysis, and is called proportional loading, since at any two given times, the load intensity at all points changes in the same ratio.

Operating with the Laplace transform on (3.3) and (3.4) gives:

$$P(p)\bar{\tau} = Q(p)\bar{\gamma} \tag{3.3}$$

$$\bar{q}(r,p) = \bar{\varphi}(p)J_o(mr) \tag{3.4}$$

In terms of the transformed variables, the deflection of the surface of the viscoelastic solid corresponding to (2.1) becomes:

$$\bar{w}(r,p) = \frac{1-\mu}{\frac{Q(p)}{P(p)}\,m}\,\bar{\varphi}(p)J_o(mr) \tag{3.5}$$

by replacing in (2.1) elastic quantities by their viscoelastic equivalents. This step is based on the fact that for transformed variables the viscoelastic problem becomes an equivalent elastic one. Written in the form:

$$P(p)\left[\frac{1-\mu}{m}\,\bar{\varphi}(p)J_o(mr)\right] = Q(p)[\bar{w}(r,p)] \tag{3.6}$$

or after application of the inverse Laplace transform:

$$P\left(\frac{\partial}{\partial t}\right)\left[\frac{1-\mu}{m}\,\varphi(t)J_o(mr)\right] = Q\left(\frac{\partial}{\partial t}\right)[w(r,t)] \tag{3.7}$$

and bearing in mind the linearity of all operators, so that constants or functions of space variables can be taken outside the rate operators, we see that there is a direct correspondence between the shear strain response to the applied stress variation for uniform shear, and the deflection response $w(r, t)$ to the time varying load $\phi(t)\,J_o(mr)$ for any value of the radius of the surface loading problem. One could, for example, measure the shear strain for a certain history of stress application in uniform shear, and deduce the surface deflection for a proportional variation of surface loading. In this case the additional factor which arises is expressed in terms of μ and m, which will be known constants for a specific problem. In this application only the single operator quotient Q/P appears as a multiplying factor, so that the solution can be determined from direct measurement of a related situation under homogeneous stress conditions. This is even true for arbitrary radially symmetric proportional loading on the surface of a homogeneous half space. Such an arbitrary distribution can be represented by the Fourier-Bessel integral:

$$q(r,t) = \varphi(t)\int_0^\infty A(m)J_o(mr)\,dm \tag{3.8}$$

The spectral function A(m) determines the shape of the load distribution, and $\phi(t)$ the variation with time which must have the same form at all surface points. Eq. (2.9) gave an integral of this type for a cylindrical distribution of uniform pressure of radius a and intensity q_o, for which $A(m) = q_o a J_1(ma)$, and no variation with time was considered. Using the Laplace transform procedure, and the solution of the associated elastic problem in the form (2.1), we obtain for the loading of a general viscoelastic half-space the transform of the deflection:

$$\bar{w}(r,p) = \frac{1-\mu(p)}{G(p)}\,\bar{\varphi}(p)\int_0^\infty \frac{A(m)}{m}\,J_o(mr)\,dm \tag{3.9}$$

where $\mu(\frac{\partial}{\partial t})$ and $G(\frac{\partial}{\partial t})$ are the viscoelastic operators corresponding to the elastic constants μ and G. The term $\frac{1-\mu(p)}{G(p)}$ can be taken outside the integral because it does not contain m, the integration variable. Applying the inverse Laplace operator we have

$$w(r,t) = \frac{1-\mu(\frac{\partial}{\partial t})}{G(\frac{\partial}{\partial t})} \varphi(t) \int_0^\infty \frac{A(m)}{m} J_o(mr)dm \qquad (3.9)$$

The combined operator $(1-\mu(\partial/\partial t))/G(\partial/\partial t)$ cannot now be directly related to a simple loading problem in homogeneous stress as was the case for constant μ, and in general it will have to be treated for specific operators $G = Q/P$ and μ. If these correspond to the common models of springs and dashpots, which implies that the operators are rational functions of $(\partial/\partial t)$, the method of partial fractions can be used to deduce $w(r, t)$ from $\phi(t)$. Simple examples of this procedure are given in the next section.

It will be observed that in (3.9) the rate operators can be combined into a single operator which is a factor of one side of the equation. This means that to each particular shape of load distribution determined by A(m), a unique shape of surface displacement will correspond, being proportional to

$$\int_0^\infty \frac{A(m)}{m} J_o(mr)dm \qquad (3.10)$$

This shape will be retained throughout the motion, so that points at different radii will be displaced proportionately, and this will take place independently of the particular form of the viscoelastic operators or the force variation $\phi(t)$. This situation is extremely special for visco-elastic deformation problems for which in general the space and time distribution of stress and strain both differ in form from each other and at different points in the body. For example, a constant applied load can produce differing stress variations inside the body at different times.

If we now consider a viscoelastic foundation with a flexible surface, we consider the transformed equivalent of (2.4):

$$\bar{w}(r,p) = \frac{1}{D(p)m^4 + \frac{G(p)m}{1-\mu(p)}} \bar{\varphi}(p) J_o(mr) \qquad (3.11)$$

if the load distribution is given by:

$$q(r,t) = \varphi(t) J_o(mr) \qquad (3.12)$$

The plate flexural rigidity D is considered as a function of p to permit visco-elastic surface layers to be treated, as well as viscoelastic subgrades. This may be needed to provide a satisfactory analysis for chemically treated surface soil layers. In this case the rate operators cannot be separated out as a factor apart from the parameter m, even for constant D, so that when an arbitrary load distribution (3.8) is considered, the transform of the resulting deflection is given by:

$$\bar{w}(r,p) = \int_0^\infty \frac{1}{D(p)m^4 + \frac{G(p)m}{1-\mu(p)}} J(mr)dm\ \bar{\varphi}(p) \qquad (3.13)$$

The combination of the operators and m in the integrand indicates that for a fixed shape of load distribution, the shape of the displacement distribution will in general vary with time. A similar situation arises if the heavy liquid subgrade assumption is used as in (2.6).

The combination of the application of the Laplace transform and the solutions of associated elastic problems already used in foundation analysis and reviewed briefly in the previous section, permits the stress and deformation analysis of a variety of foundation problems involving viscoelastic components. The complexity of the analysis depends on the particular operators needed to represent the materials, and in general this increases markedly with the order of the operators. If Burmister's[3] elastic solutions are used for two or more layers, any one of which could be considered viscoelastic, much more involved operators are encountered than in (3.13), and use of a finite series of Bessel functions may be indicated in place of the integral as discussed in the previous section. Simple examples of the method are detailed below.

It will be noted that the interpretation of elastic solutions to generate viscoelastic solutions depends on the elastic constants appearing in a simple manner, preferably as coefficients of space functions. This is the situation for all cases cited above, for which the elastic constants appear as a factor of the Bessel function with radius in the argument. For the evaluation of elastic solutions, manipulation has been successful in avoiding integral expressions, for example, the deflection of a plate on a heavy liquid type subgrade with a cylindrical region of uniform pressure of radius a and intensity q_o can be expressed in closed form using the Hankel functions $H_o^{(1)}$, $H_1^{(1)}$ as follows:[2]

$$w(r) = \frac{q_o}{k}\left[1 + \frac{\pi}{2}\,\mathrm{Im}\left\{\mu H_1^{(1)}(\mu) J_o\left(\frac{\mu r}{a}\right)\right\}\right], \qquad r \le a$$

$$= \frac{q_o}{k}\,\frac{\pi}{2}\,\mathrm{Im}\left\{\mu J_1(\mu) H_o^{(1)}\left(\frac{\mu r}{a}\right)\right\}, \qquad r > a \tag{3.14}$$

where $\mu = \sqrt[4]{\frac{k}{D}}\, a e^{i\pi/4}$. This is equivalent to (2.6) integrated with respect to m over the range 0 to ∞ with the spectral function $q_o a J_1(ma)$. Clearly (3.14) would be difficult to interpret as a viscoelastic problem with the elastic constants appearing in such a complicated fashion in the Bessel function arguments. Thus in developing elastic solutions for viscoelastic applications special considerations arise which may dictate the suitable form of solution different from that for most convenient elastic analysis.

4. Particular Solutions

We consider a subgrade covered by a flexible elastic plate, initially undisturbed. At time t = 0, a load distribution is suddenly applied, and subsequently it remains constant. Thus

$$q(r,t) = H(t) q_1(r) \tag{4.1}$$

where H(t) is the Heaviside step function, and $q_1(r)$ specifies the purely spatial distribution of load.

We will consider a heavy liquid type subgrade, with its response to load governed by the Maxwell viscoelastic law. Thus each of the springs shown in

Fig. 3 must be considered as replaced by a spring and dashpot in series (Fig. 5). The stress deflection law for this foundation is:

$$\frac{\partial w}{\partial t} = A\frac{\partial s}{\partial t} + Bs \tag{4.2}$$

using the notation of Eq. (2.2), A and B being subgrade constants. The Maxwell law represents a material which exhibits instantaneous elasticity combined with viscous flow if the load is maintained as is apparent from the model representation, Fig. 5. Under constant deformation, such a material exhibits relaxation of the stress.

The Laplace transform of the plate deformation Eq. (2.2) for the load distribution (4.1) and zero initial deflection is:

$$D\nabla^2\nabla^2\,\bar{w}(r,p) + \bar{s}(r,p) = \frac{1}{p}\,q_1(r) \tag{4.3}$$

The transform of (4.2) gives:

$$p\bar{w} = (Ap + B)\bar{s} \tag{4.2}$$

and combining these we have the associated elastic plate deformation problem:

$$D\nabla^2\nabla^2\,\bar{w}(r,p) + \frac{p}{Ap+B}\,\bar{w}(r,p) = \frac{1}{p}\,q_1(r) \tag{4.4}$$

We consider the spatial distribution of applied load to be of uniform intensity q_o over a circular region of radius a about the origin and zero elsewhere. Representing this by the integral of Bessel functions (2.9), the solution of (4.4) is given by an integral over solutions of the type (2.6):

$$\bar{w}(r,p) = q_o a\int_0^\infty \frac{J_o(mr)J_1(ma)}{Dm^4 + \frac{p}{Ap+B}}\,dm \tag{4.5}$$

This expression can be inverted in an elementary fashion using partial fractions and on performing this inversion it is found that

$$w(r,t) = \frac{q_o a}{D}\int_0^\infty \frac{J_o(mr)J_1(ma)}{m^4}\left[1 - \frac{1}{ADm^4+1}\exp\left\{-\frac{BDm^4 t}{ADm^4+1}\right\}\right]dm. \tag{4.5}$$

The corresponding foundation reactive pressure can be found most conveniently by substituting (4.5) in (4.2) and then inverting. The result is

$$s(r,t) = q_o a\int_0^\infty \frac{J_o(mr)J_1(ma)}{ADm^4 + 1}\exp\left\{\frac{-BDm^4 t}{ADm^4+1}\right\}dm. \tag{4.6}$$

The bending moments in the plate can be determined from (4.5) by the standard formulae of thin plate theory, the time being merely a parameter for this determination. For instance the radial bending moment per unit length, $M^{(r)}(r,t)$ is given by

$$M^{(r)}(r,t) = -D\left(\frac{\partial^2 w}{\partial r^2} + \frac{\nu}{r}\frac{\partial w}{\partial r}\right),$$

where ν is Poisson's ratio for the plate material. Hence

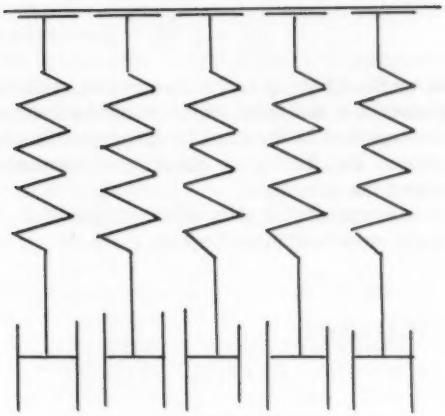

FIG. 5 SIMPLE MAXWELL VISCO-ELASTIC FOUNDATION

$$M^{(r)}(r,t) = -q_o a \int_0^\infty (J_o''(mr) + \frac{\nu J_o'(mr)}{mr}) \frac{J_1(ma)}{m^2} \times \left[1 - \frac{1}{ADm^4+1} \exp\left\{ \frac{-BDm^4 t}{ADm^4+1} \right\} \right] dm \qquad (4.7)$$

the dashes denoting differentiations.

For numerical work it is convenient to introduce the parameters

$$\rho = \frac{r}{a} ,$$

$$\lambda = \frac{a}{\sqrt[4]{AD}} ,$$

and $\tau = Bt/A$. With this notation (4.5) and (4.6) become

$$\frac{w(\rho,\tau)}{q_o A} = \lambda^4 \int_0^\infty \frac{J_o(m\rho)J_1(m)}{m^4} \left[1 - \frac{1}{(\frac{m}{\lambda})^4 + 1} \exp\left\{ \frac{-\tau}{1 + (\frac{\lambda}{m})^4} \right\} \right] dm \qquad (4.8)$$

and

$$\frac{s(\rho,\tau)}{q_o} = \lambda^4 \int_0^\infty \frac{J_o(m\rho)J_1(m)}{1 + (\frac{m}{\lambda})^4} \exp\left\{ \frac{-\tau}{1 + (\frac{\lambda}{m})^4} \right\} dm \qquad (4.9)$$

Similarly, (4.7) can be written

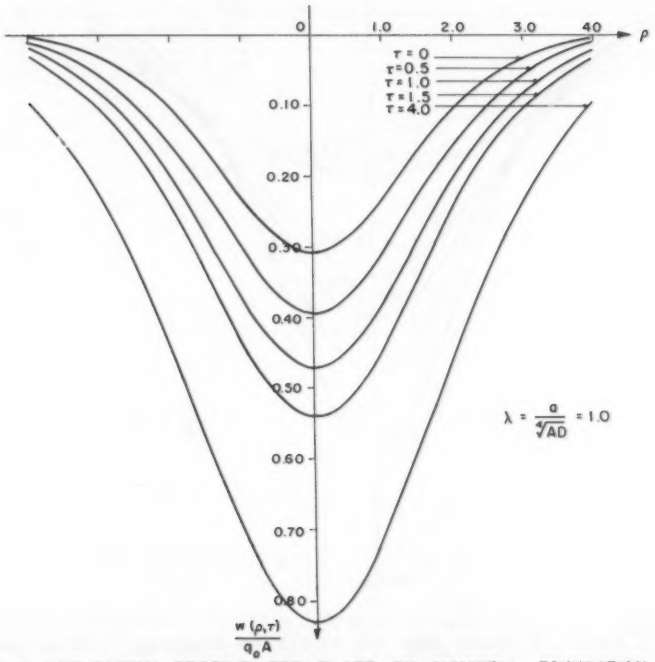

FIG. 6. DEFLECTION PROFILE FOR PLATE ON MAXWELL FOUNDATION

$$\frac{M^{(r)}(\rho,\tau)}{q_o a^2} = \frac{1+\nu}{2}\int_0^\infty \left\{J_o(m\rho) - J_2(m\rho)\frac{1-\nu}{1+\nu}\right\}\frac{J_1(m)}{m^2}\left[1 - \frac{1}{(\frac{m}{\lambda})^4+1}\right.$$

$$\left.\exp\left\{\frac{-\tau}{1+(\frac{\lambda}{m})^4}\right\}\right] dm \qquad (4.10)$$

where use has also been made of the Bessel function relations

$$J_o'' = \frac{J_2 - J_o}{2}$$

$$\frac{J_o'(x)}{x} = -\frac{J_2(x) + J_o(x)}{2}$$

These integrals were evaluated numerically by means of Simpsons rule. The m^4 in the denominator of (4.8) calls for a limit evaluation for small m. For large m, the integrals converge rapidly because of the properties of Bessel functions, and the inverse powers of m appearing. If the convergence for large m is not sufficiently rapid, the well known asymptotic expansions for Bessel functions can be employed to provide integrals which can be evaluated in closed form beyond a particular value of m.

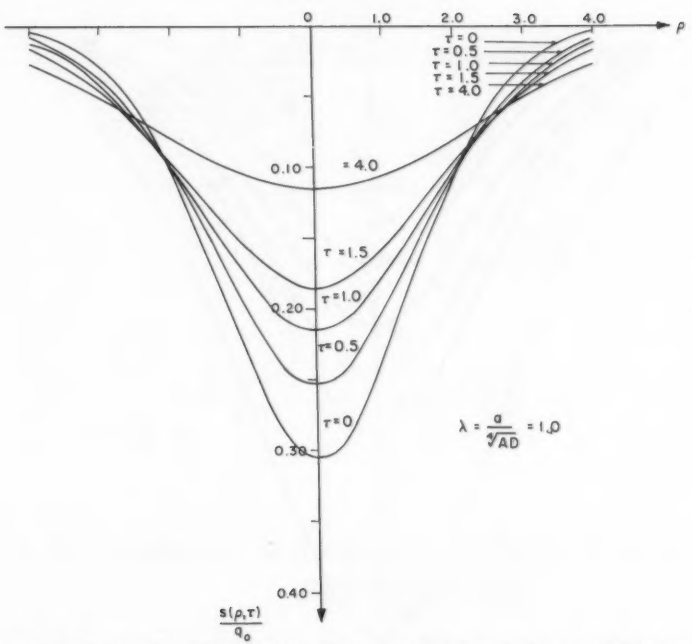

FIG. 7. REACTIVE PRESSURES FOR PLATE ON MAXWELL FOUNDATION

Profiles of the deflection and foundation reactive pressure at various times are shown in Figs. 6 and 7, for a system characterised by $\lambda = 1$. The variation with time of the bending moment in the plate at the centre of the loaded region, i.e. $\rho = 0$, is shown in Fig. 8 for this same system. The particular value unity was chosen for the parameter λ since, as pointed out by Reissner,(2) this represents the approximate limit of effectiveness of the flexible surface. As shown in Fig. 7, the maximum subgrade pressure induced is about 30% of the applied load intensity. For larger values of λ, that is either a larger area of applied load or a thinner surface plate, worthwhile reduction of the pressure on the subgrade is not achieved. The subgrade pressure decreases with decreasing λ for a fixed load intensity, but for $\lambda << 1$, the analysis becomes unreliable because the region of loading is too small compared with the plate thickness to permit plate theory to be applicable. For small λ, Burmister's solution(3) based on three dimensional elastic analysis would have to be employed.

The influence of the viscoelastic property of the subgrade is clearly evident in Figs. 6, 7 and 8 in comparison with elastic subgrade analysis, which, for the constant load distribution applied, would predict a constant deflection and constant subgrade pressure distribution. Fig. 6 shows that the deflection pattern gradually spreads out, for while the central deflection doubles in the interval from $\tau = 0$ to 4, the deflection at $\rho = 4$ increases manyfold. Under the more intense central peak of subgrade pressure, the deflection at the centre of the plate increases rapidly, causing an increase in plate curvature there, which is reflected in the monotonically increasing central bending moment shown in Fig. 8.

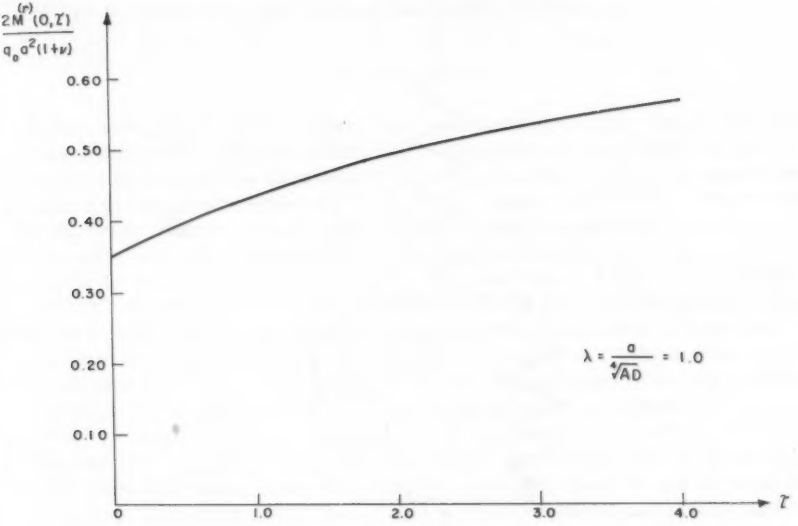

FIG. 8. BENDING MOMENT AT CENTER OF PLATE ON MAXWELL FOUNDATION

The initial response of the Maxwell type subgrade is purely elastic before the dashpots have had time to deform. This determines the subgrade pressure distribution denoted by $\tau = 0$ in Fig. 7. Since τ represents dimensionless time in terms of the relaxation time, $t_o = A/B$, of the Maxwell type subgrade, for $t << t_o$ the situation is closely approximated by the elastic solution. Thus for large t_o, elastic analysis will be satisfactory for moderate loading times. As τ increases, the increased flow of the central part of the subgrade relieves the pressure there and the subgrade pressure distribution spreads out. The applied load is thus supported over an increasing area of subgrade at reduced pressure. The effective increase in span of the plate carrying the load causes the increased bending moment mentioned above.

With increasing time, this effect will continue and will approach the analogous situation to the floating beam mentioned by Freudenthal and Lorsch,[5] when in the limit the subgrade pressure will approach zero, as a large area of the plate transmits deformation to the foundation at a uniform rate which approaches zero. In practice this limit will not be reached since no practical subgrade system can permit unrestricted flow as does the Maxwell body, and moreover, plate edge effects may become important as the deformed area spreads. In order to represent a practical foundation, the material properties must be changed so that the deformation is in effect restricted by a spring in parallel with the dashpot to transform the viscous flow to delayed elastic deformation. However, in such a case, the solution detailed above will provide a good approximation for a limited time of load application.

Consider now material properties which correspond to restricting the flow of the Maxwell type foundation by, in effect, inserting a spring across the dashpot and thus transforming the viscous flow to delayed elasticity. The foundation elements of Fig. 5 are thus replaced by the type depicted in Fig. 9. A material responding in this manner to stress is known as the standard

FIG. 9

linear solid, and Freudenthal and Lorsch[5] gave an example of how this can approximate soil behaviour. The stress deflection relation for this foundation is

$$\frac{\partial w}{\partial t} + C_1 w = A_1 \frac{\partial s}{\partial t} + B_1 s \qquad (4.11)$$

where A_1, B_1 and C_1 are subgrade constants. Using this relation in place of (4.2) of the previous problem leads to a solution by an analogous procedure. (4.2) becomes:

$$\bar{s} = \frac{p+C_1}{A_1 p+B_1} \bar{w} \qquad (\overline{4.11})$$

and the final expression for plate deflection corresponding to (4.5) is

$$w(r,t) = q_o a \int_0^\infty \frac{J_o(mr)\, J_1(ma)}{(A_1 Dm^4+1)(B_1 Dm^4+C_1)} \left[B_1(A_1 Dm^4+1) - (B_1-A_1 C_1) \exp\left\{ \frac{-(B_1 Dm^4+1)}{A_1 Dm^4+1} t \right\} \right] dm \qquad (4.12)$$

The other quantities of interest may be derived as before.

5. Discussion

It has been shown in this report that a variety of elastic stress and deformation distribution analyses which have been used in the consideration of foundation problems can be extended to materials with a time dependent response to stress represented by linear viscoelastic behaviour. Thus if rate effects, creep and relaxation behaviour of foundation and subgrade materials can be satisfactorily represented by linear viscoelastic laws, analyses are available to include these effects in the consideration of foundation design problems. It may be that if linear viscoelasticity does not represent these effects in foundations and subgrades quantitatively, qualitative information derived from such analyses will be valuable to supplement information derived from elastic solutions, from which such rate influences are entirely absent.

Throughout the analyses it has been assumed that no separation between the flexible surface and the subgrade occurs, even though negative subgrade pressures are exhibited by certain solutions. In general this is unlikely to be a significant difficulty, since the complete solution involves the superposition of a uniform pressure due to the weight of the foundation materials, and this will tend to eliminate the negative reaction pressures. Because of the linearity of the analysis, such superposition is allowable without violating any of the equations used. Another aspect of this question which has been discussed by Holl,[11] is that the oscillatory solution with negative subgrade pressures occurs with the heavy liquid type subgrade behaviour which is less likely to represent detailed aspects of foundation action than the homogeneous material subgrade. The latter does not lead to oscillatory variations of displacement and pressure.

Reference (1) gives solutions for finite circular plates on subgrades using similar Fourier-Bessel series to those treated in this report. Also non-symmetrical loading is considered by expanding in series of Bessel functions of higher order of the radius and trigonometric functions of the angle in polar coordinates. The results are much more elaborate than those presented here, but in principle the present viscoelastic method of analysis can be applied without change. Individual cases would need to be studied to assess whether the computing task involved makes the final numerical evaluation feasible.

The particular examples treated in this report analyse loads suddenly applied at t = 0, and held constant thereafter. Varying loads can be treated in a similar manner by modifying (4.1) to include a function of t other than the step function, and by including the corresponding transform in (4.3). Alternatively the solution already obtained for step function loading can be used directly in a Duhamel integral to give results for varying load. For example, any quantity determined for the steady load (4.1), can be generalized for an applied load given by:

$$q(r,t) = f(t)H(t)q_1(r) \tag{5.1}$$

Suppose that we are concerned with, say, displacement $w(r,t)$. If $w_1(r,t)$ is known for the loading (4.1), the displacement function for the loading (5.1) is given by:

$$w(r,t) = \int_0^t \frac{\partial f(\tau)}{\partial \tau} w_1(r,t-\tau)\,d\tau \tag{5.2}$$

This relation arises from the linearity of the analysis, and applies for other quantities such as stress and bending moment.

REFERENCES

1. Pickett, Gerald; Raville, Milton E.; Janes, William C. and McCormick, Frank J., Deflections, Moments and Reactive Pressures for Concrete Pavements, Kansas State College, Engineering Experiment Station Bulletin No. 65, Oct. 1951.
2. Reissner, Eric, Stresses in Elastic Plates over Flexible Subgrades, Proc. ASCE, vol. 81, Separate No. 690, May 1955.
3. Burmister, D. M., The General Theory of Stresses and Displacements in Layered Systems. I, II and III. J. Appl. Phys. 16, 89-94, 126-127, 296-302, 1945.
4. Hoskin, B. C. and Radok, J. R. M., Elastic Plates on Viscoelastic Subgrades with Applications to Pavement Design, Div. Applied Math., Brown University, T. R. DA-3648/1, Mar. 1956.
5. Freudenthal, Alfred M. and Lorsch, Harold G., The Infinite Elastic Beam on a Linear Visco-elastic Foundation, Jour. of Eng. Mech. Div., Proc. ASCE, vol. 83, p. 1158, Jan. 1957.
6. Lee, E. H., Stress Analysis in Visco-elastic Bodies, Quart. Appl. Math., vol. 13, No. 2, p. 183, 1955.
7. Lee, E. H., Stress Analysis in Viscoelastic Materials, J. Appl. Phys. 27, 665-672, 1956.
8. Lamb, H., On Boussinesq's Problem. Proc. London Math. Soc. 34, 276, 1902.
9. Gray, A., Mathews, G. B., and Macrobert, T. M., A treatise on Bessel Functions and Their Application to Physics. Macmillan, 1931.
10. Carslaw, H. S., and Jaeger, J. C., Operational Methods in Applied Mathematics. Oxford, 1953.
11. Holl, D. L., Thin Plates on Elastic Foundations. Proc. 5th Int. Congr. for Appl. Mech., p. 71, Wiley, 1939.
12. Reissner, E., A note on deflections of plates on a viscoelastic foundation. Jl. Appl. Mech., 25, 144, 1958.

Journal of the
ENGINEERING MECHANICS DIVISION
Proceedings of the American Society of Civil Engineers

SOLUTIONS FOR ONE-DIMENSIONAL STRUCTURAL LATTICES

Donald L. Dean,[1] M. ASCE and Selmo Tauber[2]

ABSTRACT

A brief argument is presented on the advantages of using closed form solutions to difference equations as a tool for structural analysis. In solving directly the difference equations obtained by substituting standard force-joint deformation relations into the general joint equilibrium equations, complete solutions are obtained for regular parallel chord Vierendeel and triangulated trusses with n panels.

INTRODUCTION

It seems that methods familiar to persons conversant with the calculus of finite differences(1) are seldom used as an analytical tool by stress analysts and structural engineers practicing today. Although in recent years this branch of mathematics has been applied most extensively by statisticians, it is interesting to note that one of the near-classics(2) on the subject deals primarily with applications to the field of structural analysis. Portions of this work have appeared in recent texts,(3,4) but there have been very few published attempts to extend it. This is unfortunate, as modern operational methods in the calculus of finite differences may readily be used to obtain complete practical solutions to a rather broad class of interesting structural problems. This is especially true in the area of structural lattices, i.e. structural systems composed of a large number of members or units which are identical or have properties which vary in a regular manner. Considerable generality in regard to loading can be dealt with routinely. An elementary load distribution is selected for the problems here with the hope that they will

Note: Discussion open until March 1, 1960. To extend the closing date one month, a written request must be filed with the Executive Secretary, ASCE. Paper 2196 is part of the copyrighted Journal of the Engineering Mechanics Division, Proceedings of the American Society of Civil Engineers, Vol. 85, No. EM 4, October, 1959.

1. Associate Prof., Dept. of Civ. Eng., Univ. of Kansas, Lawrence, Kans.
2. Assistant Prof., Dept. of Mathematics, Univ. of Kansas, Lawrence, Kans.

thereby serve as heuristic samples of the approach. Load variations expressible as algebraic polynomials can usually be solved and, at least in the case of systems represented by difference equations with constant coefficients, transcendental variations in the loading are tractable. The step function (loading begins at an arbitrary location) and the delta distribution (a single load arbitrarily located) are examples of the latter. The dynamic analysis of structural lattices also can be accomplished by direct solution of the governing difference equations.

The usefulness of their direct solutions in the design and/or analysis of lattice structures leads the writers to recommend that consideration be given to the inclusion of a study of difference equations in the undergraduate curriculum of students specializing in structural design. To their knowledge, such a program does not exist currently. The modern curriculum regularly includes a study of differential equations, which are a limiting case of difference equations. The methods for solving the more general case involve enough analogies to the approach used in differential equations so that one or two additional lectures will enable the student to solve elementary difference equations. Preliminary experiments with the introduction of such material into a second course in indeterminate structures have been successful. Since in the first course he has learned a number of methods convenient for solving the coarse lattice (less than 20 joints or units), the student readily grasps the significance of a tool with which he can handle finer structural lattices. The simpler solutions for regular lattices are often useful for an approximate analysis of more irregular systems.

In the two examples given here, a general solution is obtained which contains enough arbitrary constants to satisfy any given set of boundary conditions. For the Vierendeel truss, the constants number three for θ_x and four for $\bar{Y}_x$. This is a generalization of the results presented in reference (2) where the shear rather than the load was used as a starting point. The solution for example two seems to be new. Only energy due to bending is considered for the Vierendeel truss and direct or primary stresses are the sole consideration in the case of the triangulated truss. The loading is limited to statically applied joint forces.

The Regular Vierendeel Truss

An unknown deformation (slope-deflection) method is used. The adimensional unknowns are: θ_x, rotation of joint x and $\bar{Y}_x$, lateral deflection of joint x divided by h (see Fig. 1 at end of paper). The effects of axial forces on curvature are ignored so that typical moments in terms of unknown deformations are:

Web Moments $\quad M_{x,x'} = 6K_w \theta_x$

Chord Moments $\quad M_{x,x+1} = K_c (4\theta_x + 2\theta_{x+1} + 6\bar{Y}_x - 6\bar{Y}_{x+1})$

The two necessary difference equations are obtained by substituting these relations into the two equilibrium equations expressing: 1. The summation of moments on joint x equals zero and 2. the summation of lateral forces on joint x equals zero.

$$\theta_{x+1} + (4+3\alpha)\,\theta_x + \theta_{x-1} - 3\,(\bar{Y}_{x+1} - \bar{Y}_{x-1}) = 0 \qquad (1)$$

$$\theta_{x+1} - \theta_{x-1} - 2(\bar{Y}_{x+1} - 2\bar{Y}_x + \bar{Y}_{x-1}) = \alpha C_o \bar{p}_x \qquad (2)$$

The symbols are defined as follows:

Chord Stiffness, $K_c = EI/h)_{chord}$;

Web Stiffness, $K_w = EI/\ell\,)_{web}$;

Stiffness Ratio, $\alpha = K_w/K_c$;

Load Intensity Constant, $C_o = \dfrac{ph}{12K_w}$;

Adimensional Load Variation Function - $\bar{p}_x$.

Eqs. (1) and (2) are transformed to a standard form by introducing the Boole displacement operator E, where $E\,f(x) = f(x+1)$ and $E^m f(x) = f(x+m)$, and operating on each equation with E.

$$\left[E^2 + (4+3\alpha)E + 1\right] \theta_x - 3(E^2-1)\bar{Y}_x = 0 \qquad (1a)$$

$$(E^2-1)\theta_x - 2(E^2-2E+1)\bar{Y}_x = \alpha C_o E\bar{p}_x \qquad (2a)$$

The problem will now be made more specific by selecting $\bar{p}_x = 1$, i.e. a concentrated lateral load of p on each joint. (1a) and (2a) are then reduced to two independent equations by using determinants, as with algebraic equations.

$$(E-1)^2\,\phi(E)\,\theta_x = 3(E^2-1)\alpha C_o \qquad (1'b)$$

$$\text{or} \quad (E-1)\,\phi(E)\,\theta_x = 6\alpha C_o \qquad (1b)$$

$$\text{and} \quad (E-1)^2\,\phi(E)\,\bar{Y}_x = 3(2+\alpha)\alpha C_o \qquad (2b)$$

$$\text{where } \phi(E) = \begin{vmatrix} \left[E^2 + (4+3\alpha)E + 1\right] & -3(E+1) \\ (E+1) & -2 \end{vmatrix}$$

$$\text{or } \phi(E) = E^2 - 2(1+3\alpha)E + 1$$

The formulas needed to solve difference Eqs. (1b) and (2b) are summarized in the following for convenient reference. The given difference equation,

$$\psi(E)\,f(x) = Ca^x,$$

where $\psi(E)$ is a polynominal of E, has a solution,

$$f(x) = \frac{Ca^x}{\psi(a)} + C_1 r_1^x + C_2 r_2^x + \cdots C_n r_n^x,$$

where $r_1, r_2, \ldots r_n$ are simple roots of ψ, and "a" is not a root of ψ. The particular solution,

$$f(x)_p = \frac{Cxa^{x-1}}{D\,\psi(a)}$$

if "a" is simple root of ψ, and

$$f(x)_p = \frac{Cx(x-1)a^{x-2}}{D^2\psi'(a)} ,$$

if "a" is a double root of ψ. If r_1 is equal to r_2, the first and second terms of the homogeneous solution are $(C_1+C_2x)r_1^x$.

These formulas are applied to (1b) and (2b) to yield the complete solutions.

$$\Upsilon_x = -\frac{2+\alpha}{4}C_o x^2 + C_1 + C_2 x + C_3' B^x + C_4' B^{-x} \tag{1c}$$

$$\Theta_x = -C_o x + C_1' + C_3'' B^x + C_4'' B^{-x} \tag{2c}$$

Where B and 1/B are the roots of ϕ.

$$B = 1 + 3\alpha + \left[3\alpha(2+3\alpha)\right]^{1/2}.$$

The arbitrary constants in (1c) and (2c), C_1, C_2, . . . C_4'', represent only four independent constants as may be determined by substituting the solutions into (1a) and (2a). In matching coefficients of like terms, it is seen that

$$C_3'' = 2\frac{B-1}{B+1}C_3' , \quad C_4'' = -2\frac{B-1}{B+1}C_4' \quad \text{and} \quad C_1' = \frac{2}{2+\alpha}C_2$$

In many instances, depending upon the type of boundary conditions used to evaluate the constants, it is more convenient to express the solution in terms of hyperbolic rather than exponential functions. Proceeding in this manner for problem considered, one obtains

$$\Upsilon_x = -\frac{2+\alpha}{4}C_o x^2 + C_1 + C_2 x + C_3 \cosh Ax + C_4 \sinh Ax \tag{1d}$$

$$\Theta_x = -C_o x + \frac{2}{2+\alpha}C_2 + 2\tanh\tfrac{1}{2}A\,(C_4 \cosh Ax + C_3 \sinh Ax) \tag{2d}$$

$$\text{Shear} \quad \frac{h}{6k_w}V_{x,x+1} = \tfrac{1}{2}C_o(2x+1) - \frac{2}{2+\alpha}C_2 \tag{3}$$

$$\text{Moment} \quad \frac{1}{6k_w}M_{x,x+1} = \tfrac{1}{4}C_o\left(2x+1+\frac{2}{3\alpha}\right) - \frac{1}{2+\alpha}C_2 - (C_3+C_4\tanh\tfrac{1}{2}A)\cosh Ax - (C_3\tanh\tfrac{1}{2}A + C_4)\sinh Ax \tag{4}$$

where $C_3 = C_3' + C_4'$; $C_4 = C_3' - C_4'$; $e^A = B$ or

$\cosh A = 1+3\alpha$, $\sinh A = \left[3\alpha(2+3\alpha)\right]^{1/2}$ and

$\coth\tfrac{1}{2}A = \frac{1}{3\alpha}\left[3\alpha(2+3\alpha)\right]^{1/2}$

Eqs. (1d), (2d), (3), and (4) comprise a complete solution for a regular Vierendeel truss uniformly loaded at the joints. The constants C_1, C_2, C_3, and C_4 are determined by substituting the given boundary conditions into this solution.

The constants will now be evaluated for a specific set of boundary conditions to complete the example and furnish working formulas. The mixed boundary conditions of a cantilevered structure will be used (see Fig. 1 at end of paper).

$$\theta_o = Y_o = M_{n,n+1} = V_{n,n+1} = 0$$

These conditions substituted into (1d) . . . (4) yield expressions for C_1 . . . C_4. For this specific case then, Eqs. (1d) . . . (4) can be written:

$$V_{x,x+1} = -\frac{p}{2}(n-x) \tag{3a}$$

$$\frac{1}{C_o K_c} M_{x,x+1} = 1-3\alpha(n-x) - C_5\left[(2n+1)\tanh\tfrac{A}{2}\sinh An + 1\right]\cosh Ax \tag{4a}$$

$$+ \tanh\tfrac{A}{2}\, C_5\left[(2n+1)\cosh An - 1\right]\sinh Ax$$

$$\frac{2}{C_o}\theta_x = -2x -(2n+1)(\cosh Ax - 1) + C_5 C_6 \frac{\sinh Ax}{\sinh A} \tag{2e}$$

$$\frac{4}{C_o} Y_x = (2+\alpha)\left[(2n+1)x - x^2\right] - \frac{2n+1}{\tanh\frac{1}{2}A}\sinh Ax + C_5 C_6 \frac{\cosh Ax - 1}{3\alpha} \tag{1e}$$

where $1/C_5 = \tanh\frac{A}{2}\sinh An + \cosh An$ and

$$C_6 = 2 + (2n+1)(\sinh A)(\tanh\tfrac{A}{2}\cosh An + \sinh An)$$

A convenient check may be made by comparing results with those obtained by one of the "coarse lattice" methods for small values of n.

For example, when n = 1

$$\theta_1 = \frac{3\alpha}{1+6\alpha} C_o \; ; \quad Y_1 = \frac{2+3\alpha}{1+6\alpha}\alpha C_o \; ; \quad M_{01} = -\frac{ph}{2}\frac{1+3\alpha}{1+6\alpha}$$

or when n = 2 and $\alpha = 2/3$

$$\theta_1 = 1.1035\, C_o \; ; \quad \theta_2 = .6207\, C_o \; ; \quad Y_1 = 1.2184\, C_o \; ;$$

$$Y_2 = 2.4138\, C_o \; ; \quad M_{01} = -5.103\, C_o K_c \text{ or } -.638\, ph \; ;$$

$$M_{12} = -1.517\, C_o K_c \text{ or } -.190\, ph.$$

The Regular Triangulated Truss

Again, an unknown deformation method will be used. The governing difference equations will be obtained by substituting into the joint equilibrium

equations expressions which give the member force components in terms of the unknown joint deformations. Although readily available,[5] these equations are not so well known as the slope deflection equations and will be explained in more detail. For either plane or space trusses, depending upon whether the indices assume two or three values, the equations written in compacted form, are:

$$\sum_j \sum_m Q_{km} U_k^j X_{km}^j X_{km}^i - \sum_j \sum_m Q_{km} U_m^j X_{km}^j X_{km}^i = F_k^i \qquad (5)$$

Where (see Fig. 2 at end of paper): the indices i and j indicate components parallel to one of the axes of the reference frame, here assuming values 1 and 2; (readers accustomed to the tensor notation, where a repeated index denotes summation, will find the first summation redundant). k indicates the joint for which equations are written; m refers to each joint connected with k by a structural member; Q_{km} is an elastic constant equal to AE/ℓ^3 for member km; F_k^i are the components of external forces applied to joint k; the projections of length $X_{km}^i = x_k^i - x_m^i$; and U_k^i are the components of deformation for joint k. (For convenience in writing the difference equations below, the subscript k is replaced by a subscript and a variable, for example, the horizontal movement of the 3rd joint on the top chord is written U_t^1 (3) and the vertical deformation of the r^{th} joint on the bottom chord is denoted $U_b^2(r)$.)

The member forces and force components, in terms of the joint deformations are:

$$S_{km} = \sum_j (\ell Q)_{km} (U_k^j - U_m^j) X_{km}^j \qquad (6)$$

$$S_{km} = \sum_j Q_{km} (U_k^j - U_m^j) X_{km}^j X_{km}^i \qquad (6a)$$

Here, the four difference equations needed to solve for unknowns $U_t^1(r)$, $U_b^1(r)$, $U_b^2(r)$ and $U_t^2(r)$ are obtained by substituting the indicated physical quantities into Eqs. (5) for the r^{th} top and bottom joints.

$$-U_t^1(r+1) + 2(1+a_2)U_t^1(r) - U_t^1(r-1) - a_2 U_b^1(r+1) - a_2 U_b^1(r) - a_4 U_b^2(r+1) + a_4 U_b^2(r) = a_6 \bar{p}^1(r) \qquad (7)$$

$$-a_3 U_t^1(r) - a_3 U_t^1(r-1) - U_b^1(r+1) + 2(1+a_3)U_b^1(r) - U_b^1(r-1) + a_5 U_t^2(r) - a_5 U_t^2(r-1) = a_7 \bar{q}^1(r) \qquad (8)$$

$$a_1 U_t^1(r) - a_1 U_t^1(r-1) + 2U_b^2(r) - U_t^2(r) - U_t^2(r-1) = a_0 \bar{q}^2(r) \qquad (9)$$

$$-a_1 U_b^1(r+1) + a_1 U_b^1(r) - U_b^2(r+1) - U_b^2(r) + 2U_t^2(r) = a_0 \bar{p}^2(r) \qquad (10)$$

Where:

$$a_2 = 2A_1E_1\frac{\cos^3\gamma}{A_2E_2}\ ;\quad a_4 = 2A_1E_1\frac{\cos^2\gamma\sin\gamma}{A_2E_2}\ ;\quad a_6 = \frac{p\ell}{A_2E_2}\ ;$$

$$a_3 = 2A_1E_1\frac{\cos^3\gamma}{A_oE_o}\ ;\quad a_5 = 2A_1E_1\frac{\cos^2\gamma\sin\gamma}{A_oE_o}\ ;\quad a_7 = \frac{p\ell}{A_oE_o}\ ;$$

$$a_1 = \cot\gamma\ ;\quad a_o = p\ell_1\frac{\csc^2\gamma}{A_1E_1}\ ;\quad a_2 = a_1a_4;\ a_3 = a_1a_5;$$

$p^{-1}(r)$ and $p^{-2}(r)$ are adimensional functions of (r) describing variations of horizontal and vertical components of top chord joint loads and $q^{-1}(r)$ and $q^{-2}(r)$ are similar functions for the lower chord joint loads. For example,

$$F_b^1(r) = p\bar{q}^1(r).$$

The sample problem here will be the regular triangulated truss with uniform vertical joint loads at the upper chord level. Therefore,

$$\bar{q}^1(r) = \bar{q}^2(r) = \bar{p}^1(r) = 0 \text{ and } \bar{p}^2(r) = 1.$$

Then Eqs. (7), (8), (9), and (10), in operator notation, become:

$$\left[\bar{E}^2-2(1+a_2)E+1\right]U_t^1(r)+a_2(E^2+E)U_b^1(r)+a_4(E^2-E)U_b^2(r) = 0 \qquad (7a)$$

$$a_3(E+1)U_t^1(r)+\left[\bar{E}^2-2(1+a_3)E+1\right]U_b^1(r)-a_5(E-1)U_t^2(r) = 0 \qquad (8a)$$

$$a_1(E-1)U_t^1(r) + 0 + 2EU_b^2(r) - (E+1)U_t^2(r) = 0 \qquad (9a)$$

$$0 + a_1(E-1)U_b^1(r) + (E+1)U_b^2(r) - 2U_t^2(r) = -a_o \qquad (10a)$$

As in example one, these equations are subjected to the usual algebraic operations (determinants were used here) to yield four equations each with only one unknown.

$$(E-1)^6U_t^1(r) = a_4E(E+1)(E-1)^3a_o \qquad (7b)$$

or $$(E-1)^3U_t^1(r) = a_4E(E+1)a_o \qquad (7c)$$

$$(E-1)^6U_b^1(r) = -2a_5E(E-1)^3a_o \qquad (8b)$$

or $$(E-1)^3U_b^1(r) = -2a_5Ea_o \qquad (8c)$$

$$(E-1)^6U_b^2(r) = -(E+1)(E-1)^2\left[\bar{E}^2-2(1+a_2+a_3)E+1\right]a_o \qquad (9b)$$

or $$(E-1)^4U_b^2(r) = -(E+1)\left[\bar{E}^2-2(1+a_2+a_3)E+1\right]a_o \qquad (9c)$$

$$(E-1)^6U_t^2(r) = -E(E-1)^2\left[(2-a_2)E^2-2(2+a_2+2a_3)E+2-a_2\right]a_o \qquad (10b)$$

or $$(E-1)^4 U_t^2(r) = -E\left[(2-a_2)E^2-2(2+a_2+2a_3)E+2-a_2\right] a_o \qquad (10c)$$

The solutions to (7c), (8c), (9c), and (10c) may be written as algebraic polynominals of the third and fourth degrees containing three or four arbitrary constants respectively depending on the order of the governing difference equation. In this particular case, however, it is more convenient to work with factorials and the final result is just as easily used numerically as if ordinary polynominals had been used. A factorial of the m^{th} degree is written $(r)_m$ and is equal to $r(r-1)(r-2)\ldots(r-m+2)(r-m+1)$. If it is desired to transform a result which appears as a polynominal of factorials to its equivalent as an algebraic polynominal, a table of coefficients called Stirling[1] numbers is used. The convenience of factorials is understood if one remembers that difference equations are sometimes more easily used if written with operators other than E. For example, Eqs. (7c)-(10c) are more compactly written with the forward difference operator Δ where $\Delta f(x) = f(x+1) - f(x)$ or $\Delta = (E-1)$. An advantage of transforming difference equations from the E to the Δ notation is that one may then use the difference formula $\Delta^n(r)_m = (m)_n(r)_{m-n}$ which is analogous to the well known derivative formula for an operation on the power form in infinitesimal calculus $D^n(r)^m = (m)_n(r)^{m-n}$. The solutions to (10c)-(7c) are written:

$$\frac{1}{a_o} U_t^2(r) = C_1 + C_2(r) + C_3(r)_2 + C_4(r)_3 + \tfrac{1}{6}(a_2+a_3)(r+2)_4 - \tfrac{1}{2}(2-a_2)(r+1)_2 \qquad (10d)$$

$$\frac{1}{a_o} U_b^2(r) = C_5 + C_6(r) + C_7(r)_2 + C_8(r)_3 + \tfrac{r}{6}\left[(a_2+a_3)(r+1)_3 - 6\right] \qquad (9d)$$

$$\frac{1}{a_o} U_b^1(r) = C_9 + C_{10}(r) + C_{11}(r)_2 - \tfrac{1}{3}a_5(r+1)_3 \qquad (8d)$$

$$\frac{1}{a_o} U_t^1(r) = C_{12} + C_{13}(r) + C_{14}(r)_2 + \tfrac{1}{6}a_4(2r+1)(r+1)_2 \qquad (7d)$$

It will be noted that certain terms are retained in the particular solution which apparently could have been grouped with similar terms in the complementary solution by a simple change of constants. This was done for algebraic convenience in obtaining relations between the arbitrary constants. Also, one must exercise care in selecting particular solutions to the independent equations, (7c)-(10c), to avoid the difficulty of terms which will not satisfy the dependent Eq. (7a)-(10a).

Inspection of the four independent Eqs. (7b)-(10b) reveals that the operator determinant of the four simultaneous Eqs. (7a)-(10a) is of degree six. Therefore, the solutions (10d)-(7d) contain only six independent constants which can be used to satisfy the boundary conditions. The remaining eight can be expressed in terms of the six independent constants. Such expressions, eight in number, are obtained by substituting the general solutions (10d)-(7d) into the original equations (7a)-(10a) and matching like terms. For convenience in carrying out these operations, the original equations were transformed to the Δ notation. For example,(8a) was rewritten as:

$$a_3\left[\Delta+2\right]U_t^1(r) + \left[\Delta^2-2a_3(\Delta+1)\right]U_b^1(r) - a_5\Delta U_t^2(r) = 0$$

and (10a) as:

$$a_1\Delta U_b^1(r) + (\Delta+2)U_b^2(r) - 2U_t^2(r) = -a_o$$

The result of this substitution and term matching is:

$$C_6 = C_2 - C_3 + \frac{3}{2(a_2+a_3)}(a_2+2a_3)C_4$$

$$C_7 = C_3 - \tfrac{3}{2}C_4$$

$$C_8 = C_4$$

$$C_{10} = \frac{1}{a_1}(2C_1 - 2C_5 - C_6)$$

$$C_{11} = \frac{-3}{2(a_2+a_3)}(a_5C_4)$$

$$C_{12} = \frac{1}{a_1}(C_1 - C_5 + a_1C_9 + \frac{3}{2(a_2+a_3)}C_4)$$

$$C_{13} = \frac{1}{a_1}(2C_1 + C_2 - 2C_5 - 2C_6)$$

$$C_{14} = \frac{3}{2(a_2+a_3)}(a_4C_4)$$

The general solution is now complete. Working formulas may be obtained by inserting the boundary conditions for a specific problem into the general solution. Some care is required for this step. Therefore, the constants will be evaluated for a particular problem to illustrate the method and give results for a popular structural system (see Fig. 2). The ordinary simply supported truss is a mixed boundary value problem. Three conditions are specified deformations and the other three are specified forces which "tell" the solution that the truss has been discontinued. They may be written:

I $S_{b\,b}(1,0) = 0 = \Delta U_b^1(0)$ or $C_{10} = 0$

II $S_{b\,b}(n,n+1) = 0 = \Delta U_b^1(n)$ or $C_{11} = \frac{1}{2}a_5(n+1)$

III $S_{t\,t}(n,n+1) + \cos\gamma\, S_{t\,b}(n,n+1) = 0 = \Delta U_t^1(n) - \frac{1}{2}(n+1)a_4a_o$
or $C_{13} = -\frac{1}{2}(n+1)a_4$

IV $U_t^2(0) = 0$ or $C_1 = 0$

V $U_t^1(0) = 0$ or $C_{12} = 0$

VI $U_t^2(n) = 0$ or $nC_2+n_2C_3 = \frac{1}{6}(a_2+a_3)(n-6)(n+1)_3$

The relations between constants yield:

$$C_2 = \tfrac{1}{6}(a_2+a_3)(n+1)_3 + \tfrac{1}{2}(2-a_2)(n+1)$$

$$C_3 = -(a_2+a_3)(n+1) \; ; \quad C_4 = C_8 = -\tfrac{1}{3}(a_2+a_3)(n+1)$$

$$C_5 = -\tfrac{1}{2}C_6 = -\tfrac{1}{12}(a_2+a_3)(n+1)_3 - \tfrac{1}{2}(n+1)$$

$$C_7 = -\tfrac{1}{2}(a_2+a_3)(n+1) \; ; \quad a_1C_9 = -\tfrac{1}{12}(a_2+a_3)(n+1)_3$$

$$C_{14} = -\tfrac{1}{2}a_4(n+1)$$

These results are checked by calculating deflections for a short truss which can also be analyzed by coarse lattice methods. For example, with n = 5:

$$U_t^1(2) = -7\tfrac{3}{4}a_o \; ; \quad U_t^1(4) = -18\tfrac{3}{4}a_o \; ; \quad U_b^1(1) = -10(a_4+a_5)a_o$$

$$U_b^1(3) = -10a_4a_o \; ; \quad U_t^2(1) = (4+18a_2+20a_3)a_o \; ;$$

$$U_t^2(3) = (6+29a_2+32a_3)a_o \; ; \quad U_b^2(1) = (2+10a_2+10a_3)a_o \; ;$$

$$U_b^2(3) = (6+32a_2+32a_3)a_o$$

CONCLUSIONS

The use of a closed form solution to the governing difference equation as a tool for the structural analyst has been illustrated in two cases. The reader will readily perceive that the two practical (but rather prosaic) examples presented here do not fully exploit the use of the method in solving one-dimensional lattices. Rather it is hoped that the two cases here, chosen from different structural classes, will serve as heuristic illustrations which might interest others in working more interesting problems such as lattices which are curved in space and have unusual basic units or carry loads in a different manner.

ACKNOWLEDGMENTS

The writers wish to acknowledge the help given by Willard Strode of the University of Kansas, Architectural Engineering Department, in preparing the illustrations.

BIBLIOGRAPHY

1. Jordan, C., Calculus of Finite Differences, Chelsea Publishing Company, New York, 1950.
2. Bleich, F. and Melan, E., Die gewöhnlichen und partiellen Differenzengleichungen der Baustatik, Julius Springer, Berlin, 1927.

3. V. Kármán, T., Mathematical Methods in Engineering, McGraw-Hill Company, New York, 1940, pp. 437-451.

4. Bleich, F., Buckling Strength of Metal Structures, McGraw-Hill Company, New York, 1952, pp. 260 and 275.

5. Maugh, L. C., Statically Indeterminate Structures, John Wiley & Sons, New York, 1946, pp. 300.

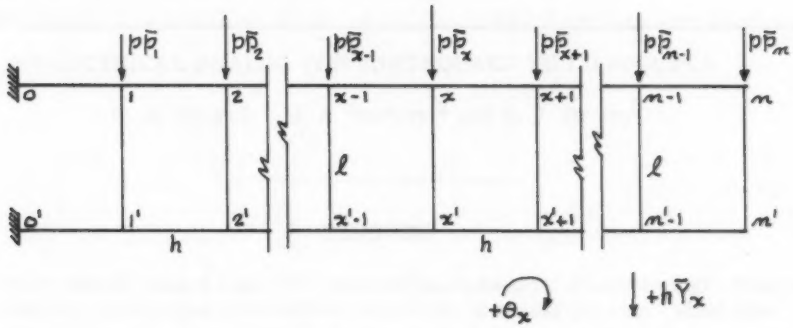

Fig. 1

Cantilevered Vierendeel Truss Of n Panels

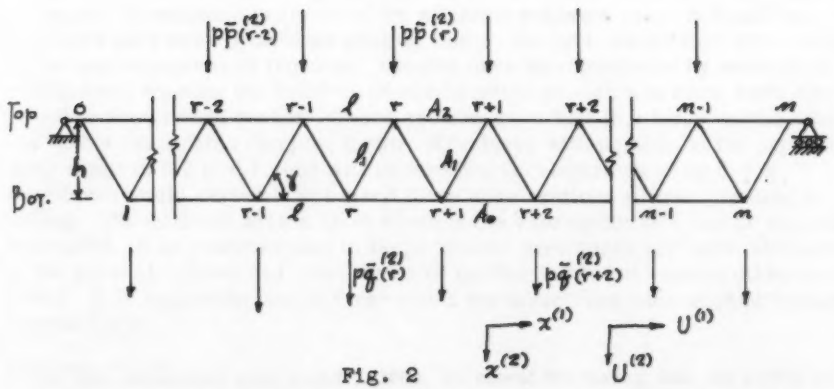

Fig. 2

Simply Supported Triangulated Truss Of n Panels

Journal of the
ENGINEERING MECHANICS DIVISION
Proceedings of the American Society of Civil Engineers

ELECTRICAL ANALOG FOR EARTHQUAKE YIELD SPECTRA

G. N. Bycroft,[1] M. J. Murphy,[2] and K. J. Brown[3]

SYNOPSIS

An electrical analog has been designed to simulate a damped single degree of freedom, elasto-plastic structure subjected to an earthquake. Yield displacement spectra of the 1940 El Centro earthquake are shown. It is suggested that this approach be the basis of a more relevant analysis.

INTRODUCTION

Earthquake resistant design of structures still rests largely on an empirical basis. A complete analysis of the situation presents great difficulties. Buildings have been treated as simple, linear, damped, oscillatory systems of one or more degrees of freedom. Spectra have been produced by several investigators, showing the build-up of acceleration in such a system when subjected to actual earthquakes. These spectra show that in a large earthquake and with a reasonable damping factor, structures with periods in the approximate range of 0.2 to 0.5 secs will experience accelerations of up to 1 g. Structures would certainly not stand these accelerations without yielding or failing. The question arises as to whether the assumption of a linear analysis is tenable. It is observed that in large 'quakes structures are often stressed to the point of cracking of concrete or of mortar joints but remain otherwise sound. It is suggested that in these cases the structures have worked through a yield cycle.

Note: Discussion open until March 1, 1960. To extend the closing date one month, a written request must be filed with the Executive Secretary, ASCE. Paper 2197 is part of the copyrighted Journal of the Engineering Mechanics Division, Proceedings of the American Society of Civil Engineers, Vol. 85, No. EM 4, October, 1959.

1. Senior Scientific Officer, Eng. Seismology Section, Dominion Physical Lab., Lower Hutt, New Zealand. Now Research Officer, Bldg. Physics Section, Div. of Bldg. Research, National Research Council, Ottawa, Canada.
2. Chief Mech. Engr., Dominion Physical Lab., Lower Hutt, New Zealand.
3. Technical Officer, Eng. Seismology Section, Dominion Physical Lab., Lower Hutt, New Zealand.

A building code consistently based on the linear spectrum is impracticable because of the cost of designing for such large accelerations. It may well be that codes used in practice which design for accelerations much lower than those predicted on a linear basis already implicitly allow for yielding of the structure without explicitly stating so. It is proposed that we accept yield and base our code on a consideration of the safe extent and implications of this yield.

This paper is concerned with the preparation of yield displacement spectra of a simple damped oscillator subjected to the N-S component of the El Centro earthquake, May 18, 1940—the worst earthquake so far recorded.

Mechanical System

The mechanical system considered is that of a mass and a stiffness member having an elasto-plastic restoring force. The restoring force is proportional to displacement up to the yield point and then stays constant. If the velocity now changes sign the force displacement characteristic decreases along a line parallel to the initial linear portion. The hysteresis loop is thus a parallelogram. The system is also damped both in the elastic and inelastic ranges. It is assumed that whatever causes the damping continues to do so after yield takes place. When such a system is subjected to an impulsive exciting force of the nature of an earthquake, the initial impulses set the oscillator swinging in its elastic range. At some stage an impulse from the earthquake may force it beyond the elastic range into the plastic range. It now oscillates about a new zero. Further impulses may increase or decrease this "permanent set".

The number of yield displacements, their extent and the final permanent set of such a system is a function of period, damping, yield value, and the particular earthquake considered.

The Analogy

An electrical analog has been set up to measure the maximum yield displacement, the total energy dissipation and final permanent set of this mechanical system. This analog is basically the same as that used by Murphy, Bycroft and Harrison[1] for finding stresses in multi-storey structures. It has been modified in that biased diodes have been placed in parallel across the active condenser to produce the analogy of the mechanical hysteresis loop. The basic circuit is shown in Fig. 1. The condenser diode branch behaves as a condenser as long as the applied voltage is less than the biasing voltage.

If an attempt is made to raise the voltage above the biasing voltage current flows through one or other of the diodes.

The following notation is used:

m = mass of the structure

k = stiffness between the mass and ground

$w = \sqrt{k/m}$ = angular frequency of the mechanical system

c = viscous damping coefficient

x = displacement of the mass relative to the ground

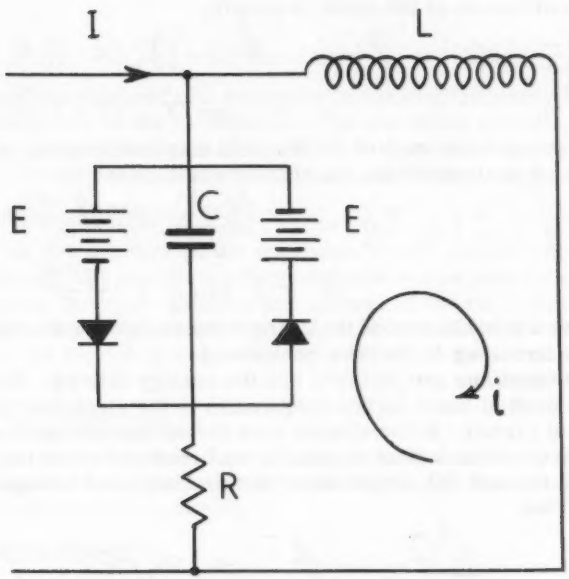

FIG. 1. ELECTRICAL ANALOG.

x_o = displacement at which the structure yields

kx_o = F = yield force

w^2xo/g = G = fraction of gravity at the yield point and will be called the yield value

$\alpha(t)$ = the ground acceleration

λ-$\mathscr{C}$ = C/2wm = fraction of critical damping

L = inductance

C = capacitance

p = $\sqrt{\frac{1}{LC}}$ = angular frequency of the electrical circuit

R = resistance

τ = R/2pl = fraction of critical damping

I = current fed into circuit

i = loop current

E = bias volts on the diodes

q = charge corresponding to current i

Q = charge corresponding to current I

The equation of motion of the mass is simply,

$$m\{\ddot{x} + \alpha(t)\} + b\dot{x} = -k(x-Y),\ (x-Y) \leq x_0$$
$$= -F \operatorname{sgn} \dot{x},\ (x-Y) \geq x_0 \qquad (1)$$

where Y is the algebraic sum of all the yield displacements up to the time considered. A loop analysis of the electrical circuit gives

$$L(\ddot{q} + \ddot{Q}) + R\dot{q} = -\frac{(q-e)}{C},\ \frac{(q-e)}{C} \leq E$$
$$= -E \operatorname{sgn} \dot{q},\ \frac{(q-e)}{C} \geq E \qquad (2)$$

where e is the algebraic sum of the charges which have flowed in the diode branch of the circuit up to the time considered.

These two equations are identical and the analogy follows. However, it is necessary to work at much higher frequencies in the electrical circuit than in the mechanical circuit. In the system used the earthquake accelogram $\alpha(t)$ was scanned ρ times as fast as it actually occurred and the resulting voltage integrated. A current I(t), proportional to this integrated voltage, was fed into the circuit. Thus

$$\frac{d^2Q}{dt^2} = \frac{dI}{dt} \equiv \alpha(\rho t). \qquad (3)$$

Eqs. (1) and (2) may now be rewritten to give

$$\ddot{x} + \alpha(t) + 2\omega\lambda\dot{x} = -\omega^2(x-Y),\ (x-Y) \leq x_0$$
$$= -Gg \operatorname{sgn} \dot{x},\ (x-Y) \geq x_0 \qquad (4)$$

$$\ddot{q} + \alpha(\rho t) + 2p\tau\dot{q} = -p^2(q-e),\ \frac{(q-e)}{C} \leq E$$
$$= \frac{-E}{L} \operatorname{sgn} \dot{q},\ \frac{(q-e)}{C} \geq E. \qquad (5)$$

Put $\rho t = T$ and Eq. (5) becomes,

$$\frac{d^2q}{dT^2} + \frac{\alpha(T)}{\rho^2} + \frac{2p\tau}{\rho}\frac{dq}{dT} = \frac{-p^2}{\rho^2}(q-e),\ \frac{(q-e)}{C} \leq E$$
$$= \frac{-E}{\rho^2 L} \operatorname{sgn} \dot{q},\ \frac{(q-e)}{C} \geq E \qquad (6)$$

Eqs. (4) and (6) show that if

$$\lambda = \tau \qquad (7)$$

i.e. same damping factor in both systems and

$$\omega\rho = p \qquad (8)$$

then

$$x \propto q\rho^2. \tag{9}$$

This permits the analysis of a structure of varying frequency by changing only the scanning rate of the earthquake in the electrical circuit.

The displacement of the mass at any time is the sum of elastic and yield components. The following displacements are considered.

(a) Maximum Yield Displacement

This is defined here as the maximum elastic displacement x_0 subtracted from the maximum over-all displacement measured from the initial zero that occurs during the passage of the earthquake. It is the maximum value of the algebraic sum of the yield displacements where signs of the yield displacements are taken to be the same as the velocities.

(b) Total Yield Excursion

This is the sum of all the yield displacements added irrespective of their sign and is a measure of the plastic energy dissipated during the passage of the earthquake.

(c) Permanent Set

The residual displacement remaining after the passage of the earthquake will be known as the permanent set.

General Arrangement

The reader is referred to Murphy, Bycroft and Harrison[1] for a more detailed account of the driving and recording parts of the analog.

Briefly, the earthquake accelogram is mounted on the outside of a 30 in. diam. revolving drum. One side of the accelogram is blacked out and the whole scanned by a light slit and photocell. The resulting voltage, proportional to acceleration, is amplified and integrated. A current I proportional to this voltage is fed from a pentode into the yield circuit and the voltage on the respective measuring condensers is photographed on a cathode ray oscilloscope (C.R.O.). The wheel is speeded up to 600 r.p.m. and allowed to decay under an eddy current brake. The response of the circuit for each passage of the earthquake is photographed on the C.R.O. The film is moved forward each revolution of the wheel by a uni-selector switch driven from a timing mark on the drum. The slowing down of the drum changes the parameter ρ and permits an analysis of structures of different periods. The decay of the wheel is slow and a very detailed spectrum is obtained.

A few modifications to the original analog have been made. A phase inversion and switching stage has been incorporated so that for certain of the measurements needed here every alternatate earthquake impulse is inverted. In order to make quite sure that the circuit is in a quiescent condition before the next presentation of the earthquake, the measuring side of the condenser is shorted to the high tension (H.T.) by relays after each passage of the earthquake.

A cathode follower stage has been inserted between the measuring point and the oscilloscope so that the oscilloscope presents an impedance somewhat

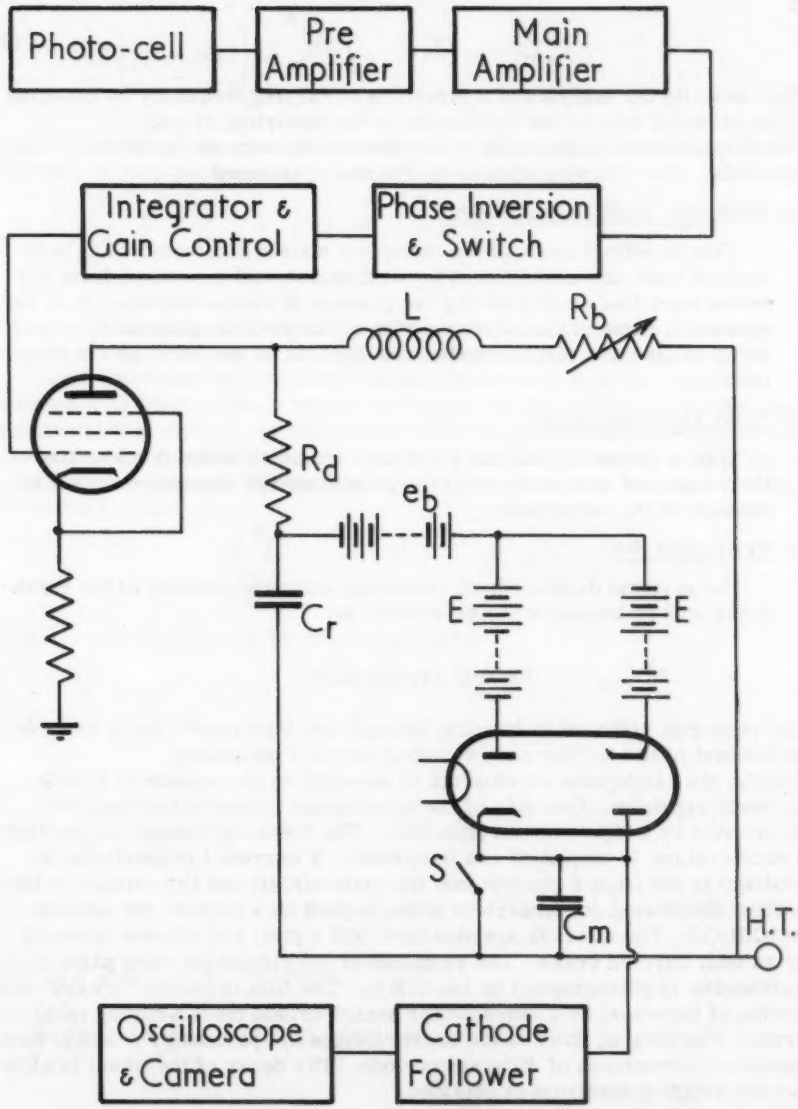

FIG. 2. MAXIMUM YIELD DISPLACEMENT CIRCUIT

greater than sixty megohms. A photocell operated from a timing mark on the wheel triggers the relays and the camera drive. As in the previous analog, minute marks appear on the film from the second beam of the C.R.O. The distance between these minute marks on the film gives the period of the structure at the middle point of the marks.

Fig. 2 shows the circuit for measuring the maximum yield displacement. Each alternate earthquake signal is reversed by the phase inverter and fed into the circuit.

A D.C. current flows from the plate of the pentode through the coil to H.T. and as the coil has a sensible resistance the D.C. voltage drop across it is balanced by a battery. Final balance is secured by the small variable balancing resistance. This ensures that the diodes are equally biased.

L = coil of inductance, 17.24 henries

R_d = damping resistor, 100 ohm to 30 kohm

e_b = balancing battery of 12 volts

R_b = balancing resistor 0 - 500 ohm (10)

C_r = resonant condenser of 0.003 μf to 0.05 μf

C_m = measuring condenser 0.1 μf to 16 μf

S = shorting switch on measuring condenser

E = biasing voltage

The measuring condenser C_m consists of a bank of condensers, a particular condenser being selected in any particular circumstances so that the voltage drop across it is small compared to the biasing voltage. Its position in the circuit is such that it measures the total charge that has flowed in the diode branch and thus is a measure of the yield displacement at any instant. Fig. 3 shows the arrangement for measuring the total yield excursion and the residual permanent set.

The earthquake is fed in the same way all the time and the switching stage S_3 is used to switch alternately between the measuring condensers C_m. As these condensers measure respectively the current through each diode they add up the total yield in one or other direction. The switching stage adds them positively on the oscilloscope and gives the total yield distance irrespective of sign. Subtraction of the yields in the two directions gives the permanent set. Switches S_1 and S_2 discharge the measuring condensers after each passage of the signal.

Setting-Up and Calibration

Before each run the resistance R_b and battery e_b were adjusted so that the resistive drop in the inductive branch was balanced by e_b. An infinitely stiff structure will yield when the base acceleration is equal to the equivalent yield point acceleration Gg. This may be used to set up the gain control.

Fifty-nine volts were chosen to represent the maximum acceleration of the El Centro earthquake i.e. 0.32g. This infinitely stiff structure is simulated by removing the resonant condenser C_r. The diodes are then biased at 59 volts and the gain of the amplifier increased until the diodes just fire. This

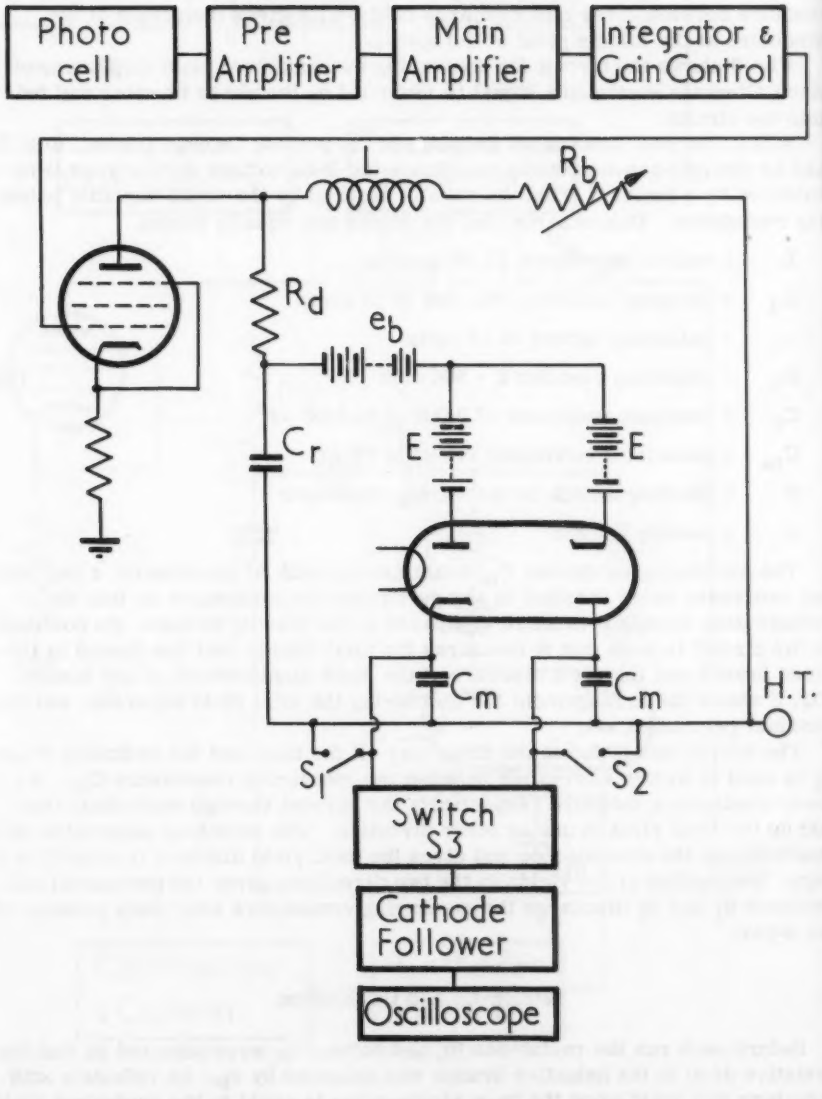

FIG. 3. TOTAL YIELD EXCURSION AND PERMANENT SET CIRCUIT.

is the required gain setting. The bias voltage is then changed to 59G/0.32 volts to represent the particular yield value G required.

Calibration is effected by measuring the voltage across the inductance L with the diodes and resonant condenser C_r removed. This is photographed at the beginning of each run.

It is necessary to determine the relation of voltage on a measuring condenser with displacement in the structure. Imagine the resonant condenser C_r to be very small, i.e., C_o. This corresponds to a building being very rigid—the conditions of calibration. If k_o is the stiffness of this very rigid building and Ag the maximum earthquake acceleration, the maximum relative mechanical displacement is given by

$$S = \frac{mAg}{k_o} \tag{11}$$

and this displacement is shown as the calibration height Z on the film. On a bigger measuring condenser C_m the displacement S would show as a calibration height of $\frac{z\,C_o}{C_m}$. Using

$$k_o C_o = k_r C_r \tag{12}$$

it follows that a height y on the film represents a mechanical displacement of

$$\frac{y\,C_m\,m\,A}{z\,C_r\,k_r} = \frac{y\,C_m\,A\,g\,T^2}{z\,C_r\,4\pi^2} \tag{13}$$

where T is the structure period.

Checking

All components are accurate to within 1% and the over-all linearity of the amplifiers is within 3% from 40 cs/sec to 10,000 cs/sec. The behavior of the analog was checked by measuring the yield taking place when a single square wave is applied to the system and comparing this with the theoretical value. The results are shown in Fig. 4. The theoretical and experimental ratios of yield displacement to elastic displacement are shown as $\sqrt{t}$ and $\sqrt{e}$ plotted against μ the ratio of pulse length to the period of the oscillator. Two values of the ratio of pulse height A to yield value G were taken.

Results

Typical shapes of the yield displacement during the passage of the earthquake are shown in Fig. 5 for two structure periods. These are photographs taken directly from the C.R.O. displayed on a time base. They show yield taking place in both directions and a change of configuration with period.

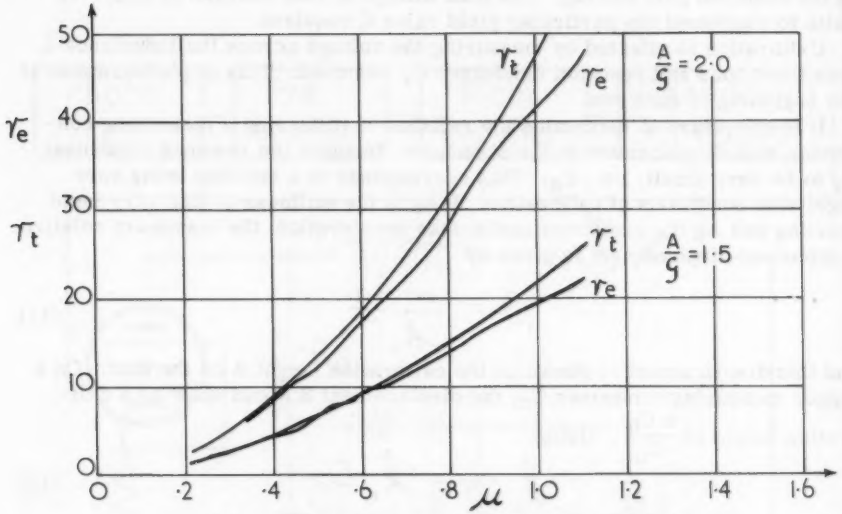

FIG. 4 SQUARE WAVE CHECK OF ANALOG.

Figs. 6, 7, 8, and 9 show the maximum yield displacement taking place for various yield values G damping coefficients λ and periods T. The maximum elastic displacement x_0 corresponding to the particular yield value is also shown. An addition of the two displacements gives the maximum over-all displacement from the initial zero. Figs. 10, 11 and 12 give the total yield excursion and if this distance is multiplied by m G it gives the value of the plastic energy dissipated in the structure. The permanent sets are given in Figs. 13, 14, 15.

These results have several interesting features. It is, of course, to be expected that increasing the damping and yield values will greatly decrease the yield displacements. If a building is designed to the common rule of withstanding one tenth of its weight horizontally, safety factors will determine its yield value probably between G = 0.175 and G = 0.24. Practical damping ratios λ generally lie between 0.1 and 0.2. Figs. 8 and 9 show that the upper and lower limits of the maximum yield displacement occurring in this range of parameters are 1.2 inches and 0.2 inches. However, these limits occur at periods between 0.5 and 0.7 seconds. As single degree of freedom structures will generally have periods rather less than these, the significant maximum yield displacements will be smaller.

It may be seen from the figures that the period corresponding to the largest of the maximum yield displacements depends on the yield value. This period becomes shorter with increasing yield value. With the small yield value of 0.06 the largest yield occurs at about 2.5 seconds and is large. However, single degree of freedom structures almost invariably have periods shorter than 0.5 secs, and the yield displacement of up to ten inches is irrelevant. The relevant maximum yield displacements for G = 0.06 will be less than two inches. If one considers the case of G = 0.12 it is seen that the maximum yield displacements will be less than one inch. A typical single degree of freedom structure will have a period of about 0.3 secs and damping ratio

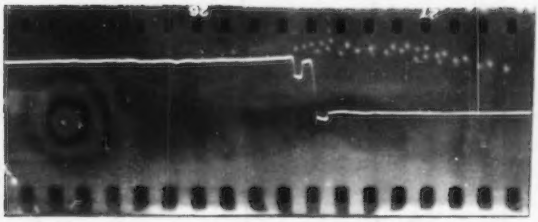

T = 0·36 secs, λ = 0·10, ς = 0·2

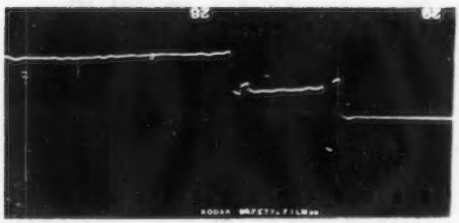

T = 0·5 secs, λ = 0·10, ς = 0·2

FIG. 5. YIELD DISPLACEMENT SHAPES

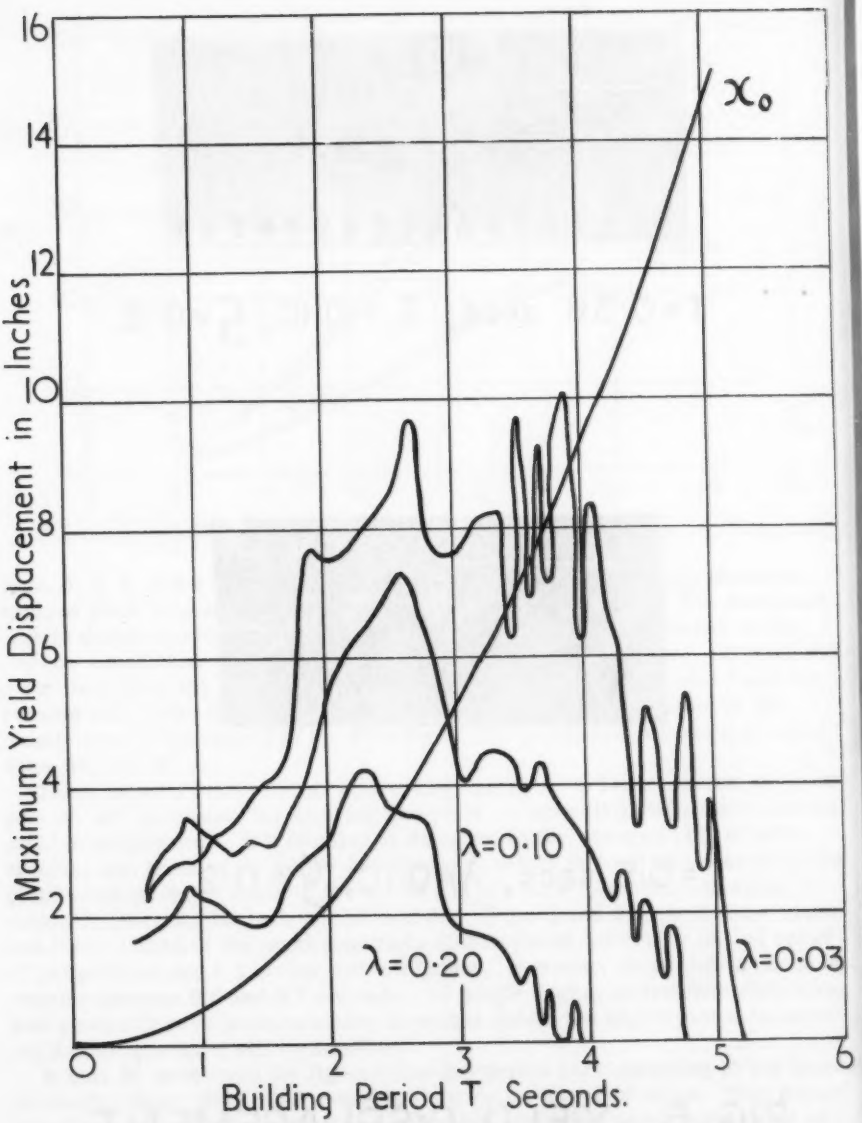

FIG. 6. MAXIMUM YIELD DISPLACEMENTS
$\zeta = 0{\cdot}06$

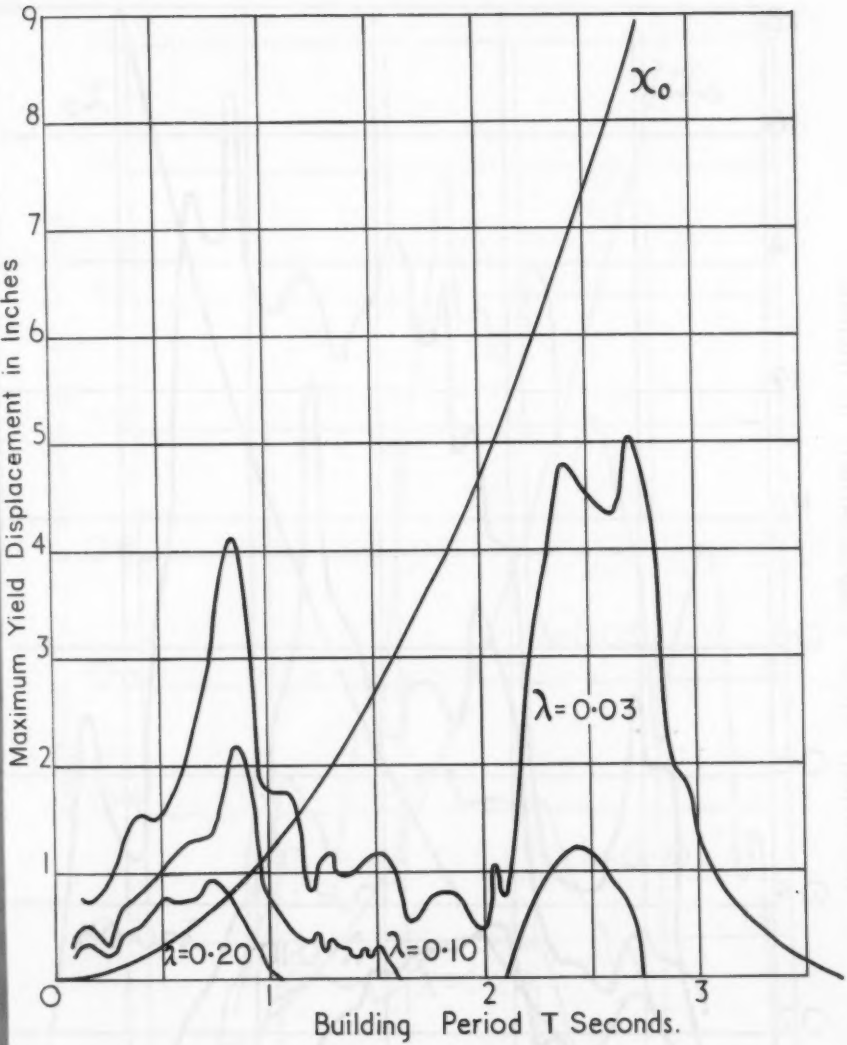

FIG. 7. MAXIMUM YIELD DISPLACEMENTS
$\varsigma = 0{\cdot}12$

of 0.10. The maximum yield displacement in this case for yield values of 0.06, 0.12, 0.175, and 0.24 is respectively 1.6, 0.6, 0.3, and 0.24 inches. Intuitively, one feels that even a yield of 1.6 inches in a storey height of, say, fifteen feet is not excessive.

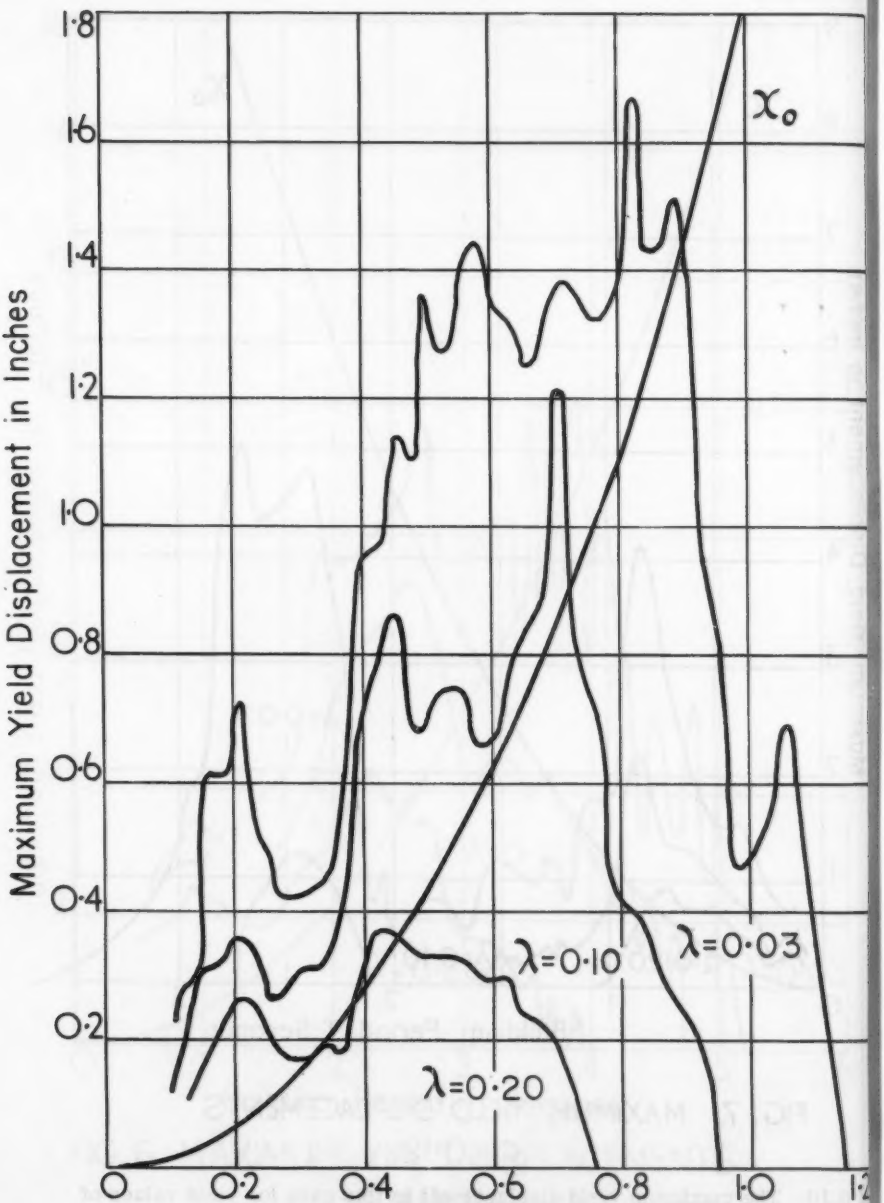

FIG. 8. MAXIMUM YIELD DISPLACEMENTS
$\zeta = 0{\cdot}175$

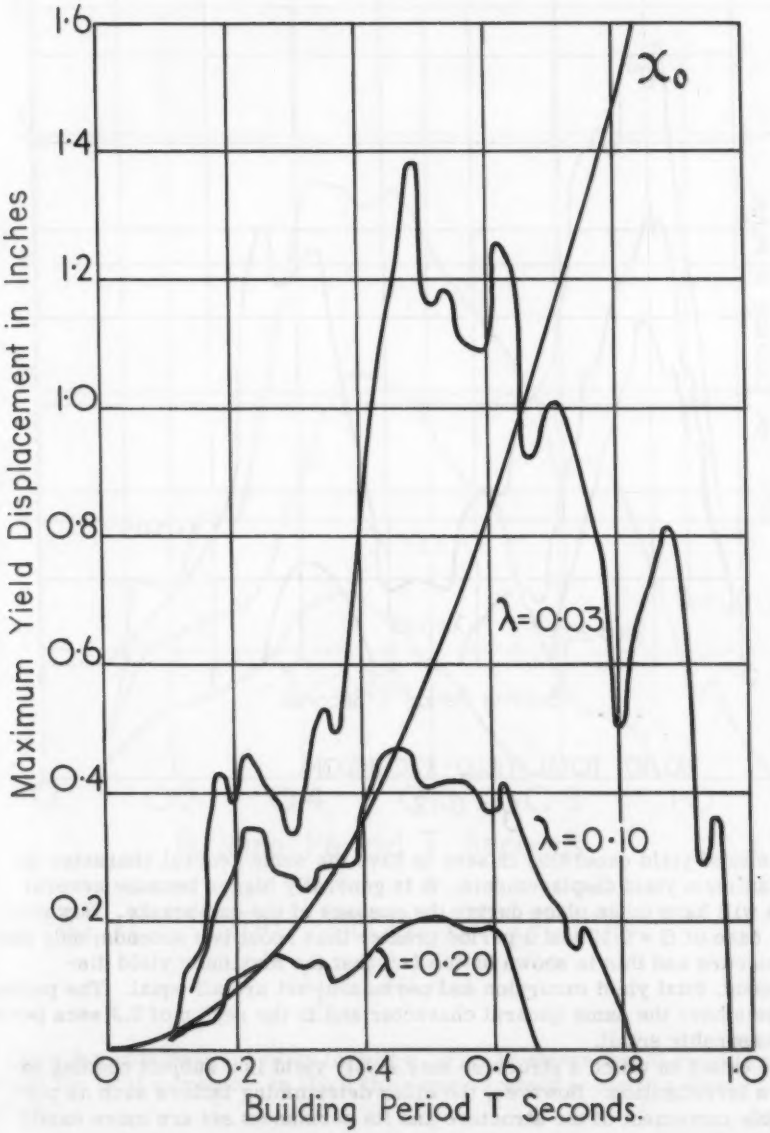

FIG. 9. MAXIMUM YIELD DISPLACEMENTS

$\zeta = 0{\cdot}24$

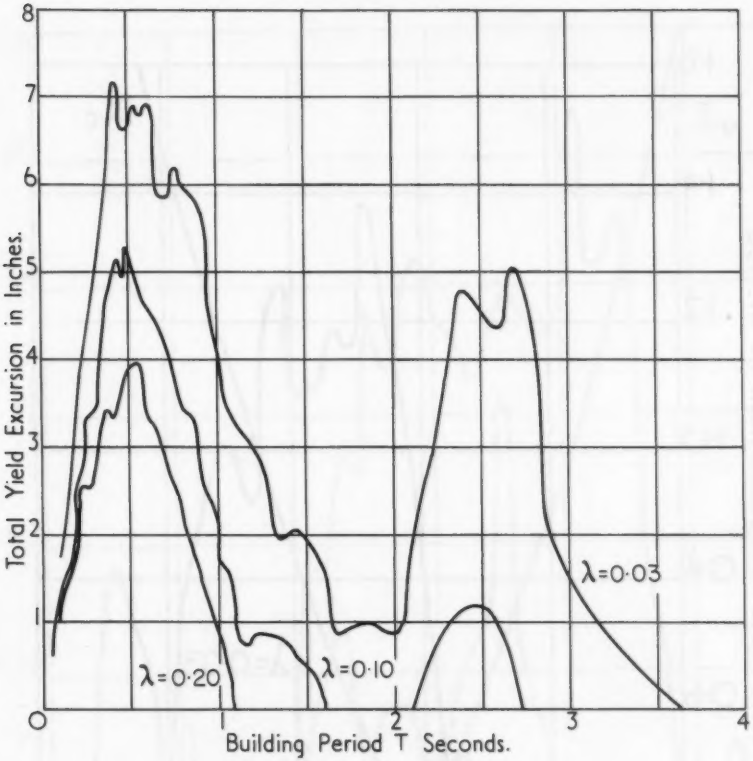

FIG. 10. TOTAL YIELD EXCURSION.
$G = 0.12$

The total yield excursion is seen to have the same general character as the maximum yield displacements. It is generally bigger because several yields will have taken place during the passage of the earthquake. However, in the case of G = 0.12 and a period greater than about two seconds, only one yield occurs and this is shown by the fact that the maximum yield displacement, total yield excursion and permanent set are all equal. The permanent sets have the same general character and in the region of 0.3 secs period are reasonably small.

The extent to which a structure may safely yield is a subject needing extensive investigation. However, the other determining factors such as permissible movement of the structure and its permanent set are more easily decided on.

Figs. 16 and 17 compare elastic and elasto-plastic designs.

Two yielding designs of $\lambda = 0.10$, G = 0.175 and $\lambda = 0.20$, G = 0.2, have been chosen to represent the probable upper and lower limits of these parameters. The figures compare the accelerations built up in the elastic case with the yield value acceleration Gg of the inelastic case and also the resulting displacements. Fig. 16 shows that a logical design on a linear basis would have

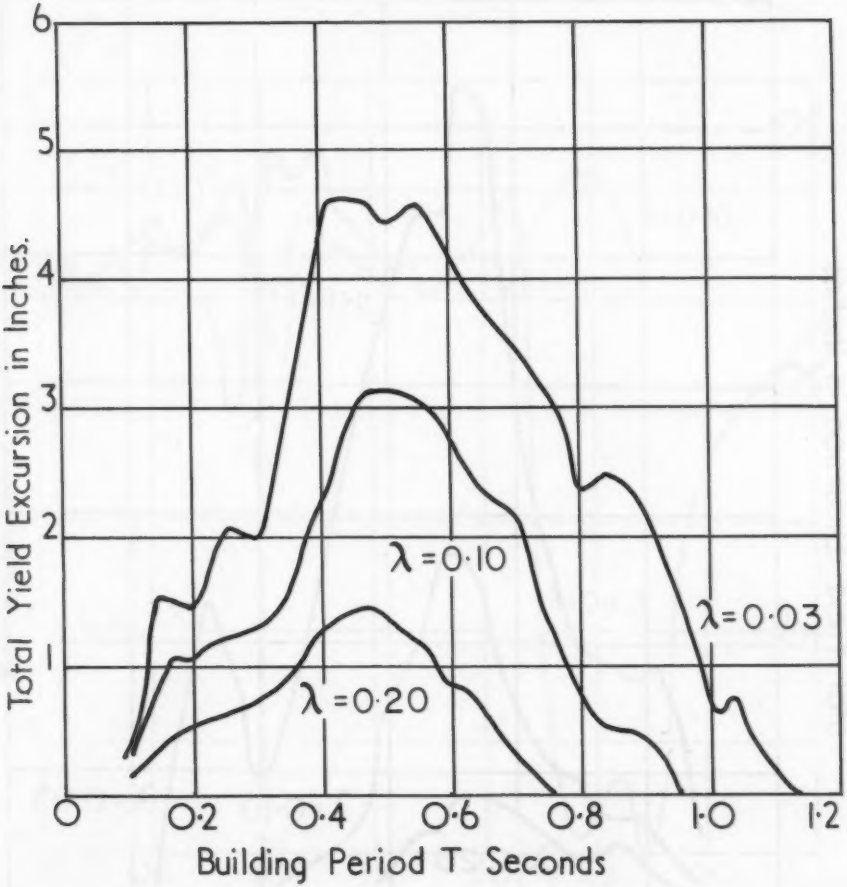

FIG. 11. TOTAL YIELD EXCURSION.
$\zeta = 0{\cdot}175$

to allow for accelerations of up to 0.52 g. Fig. 17 shows that if yield is permitted the total movement is about the same as would occur in a linear system.

CONCLUSION

Research is needed to determine permissible yielding of plastic hinges. When this is decided an analysis of the type described may be used to design a structure in a consistent manner. The paper attempts to show that many

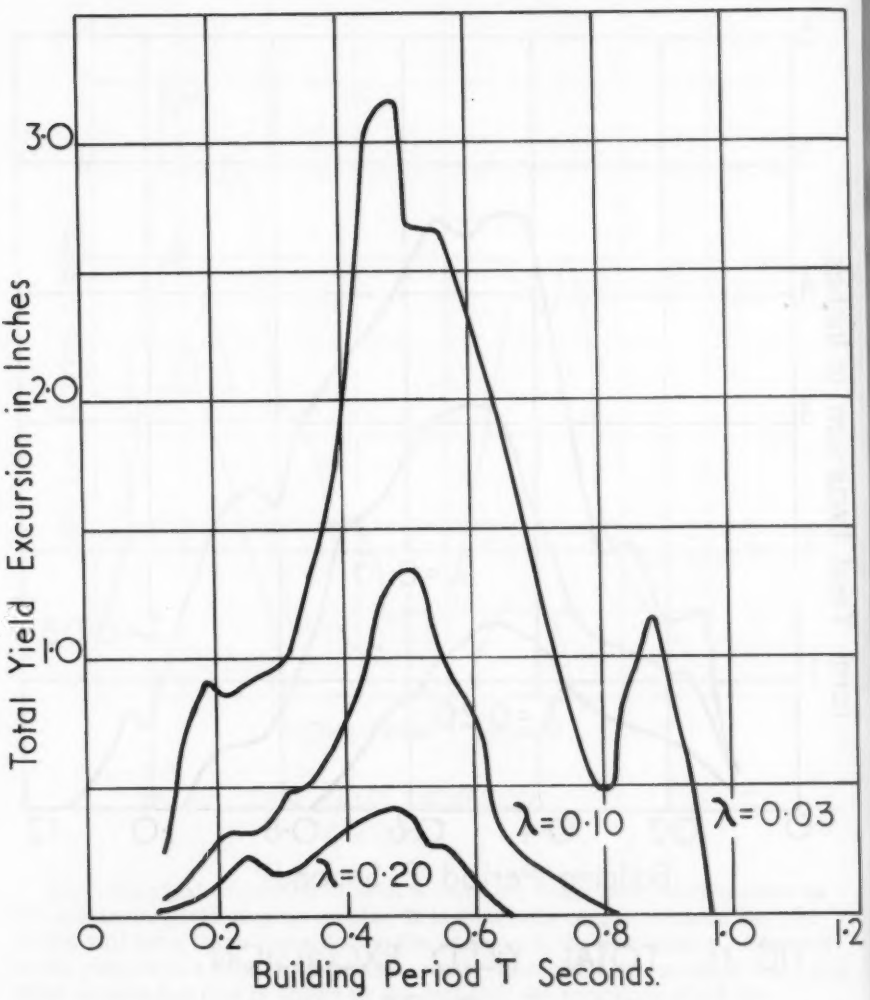

FIG. 12. TOTAL YIELD EXCURSION
$\zeta = 0{\cdot}24$

structures designed to the basis of 0.1 g acceleration must yield in large earthquakes but that the consequences of this are not particularly serious. The total movement is often less than if the structures had been designed linearly up to 0.52 g. The extent of the yield displacements is generally less than an inch, and an inch yield movement of one floor to another represents an extremely small plastic strain in the plastic hinges. The permanent sets

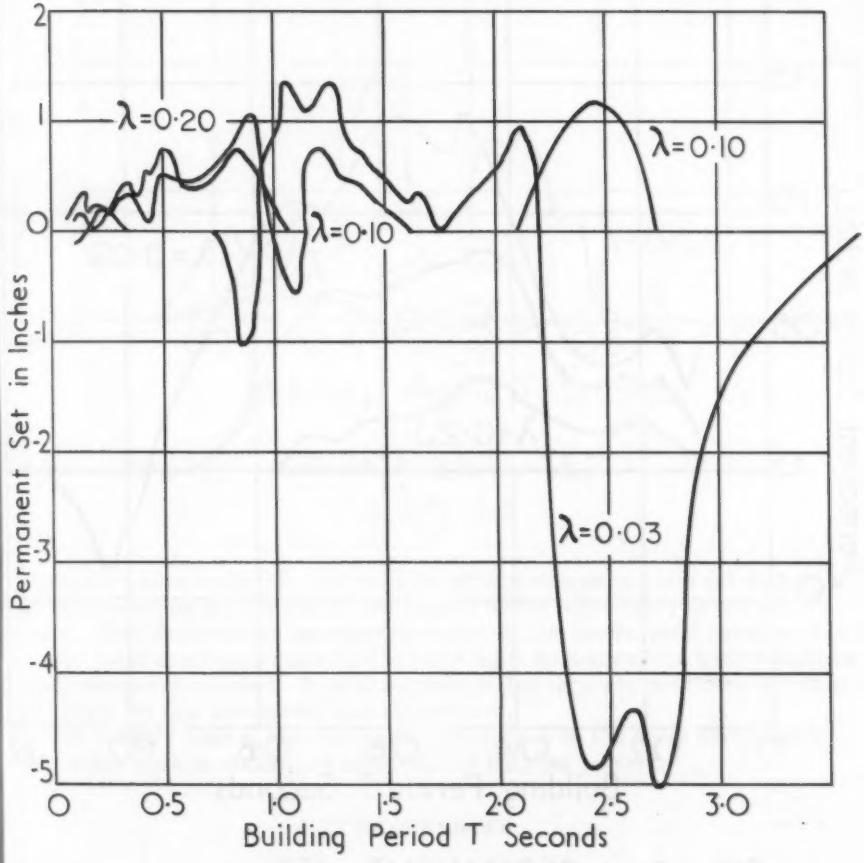

FIG. 13 PERMANENT SET.

$\zeta = 0{\cdot}12$

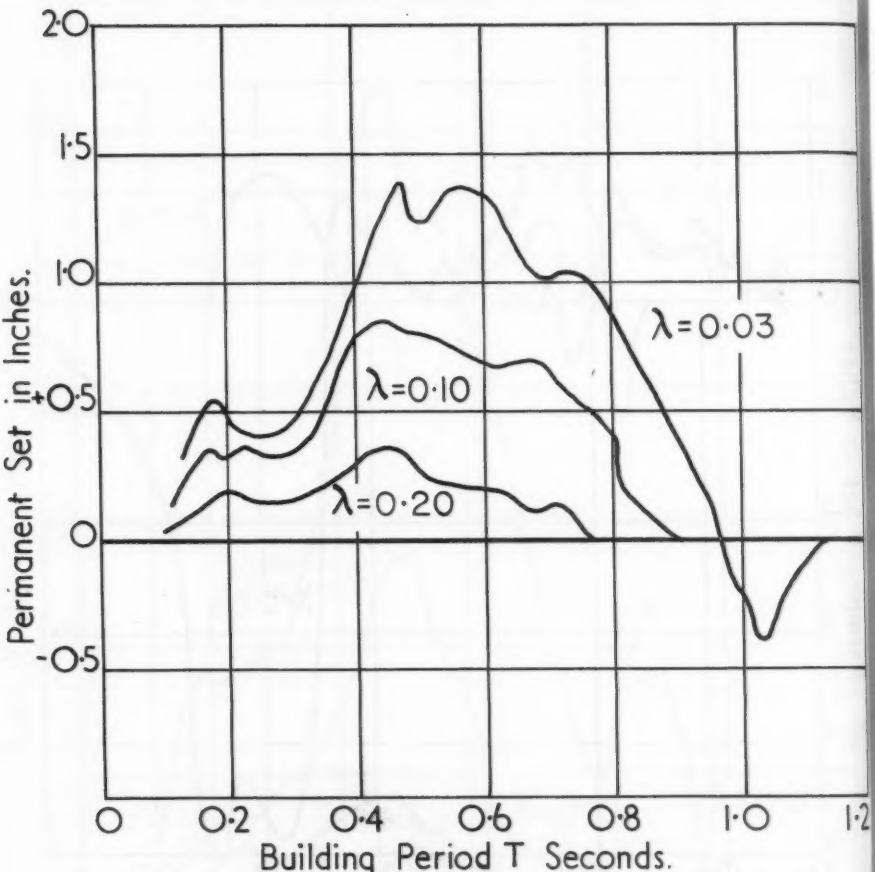

FIG. 14. PERMANENT SET.
$\zeta = 0{\cdot}175$

are in general small and would be within the building tolerances. It seems very likely that design coefficients could be safely lowered in buildings where plastic hinges are available. This applies particularly to steel framed structures. However, if the yield value was lowered too much the resulting increased displacements would probably be the limiting factor.

Other building types such as bearing wall buildings or buildings involving pre-stressing do not fall into this category. It would appear logical that these types should be designed for accelerations of up to half that of gravity.

Dr. B. W. Faulkner[2] kindly pointed out to the authors one result of allowing dynamic yields to take place. Where any of the plastic hinges have a static

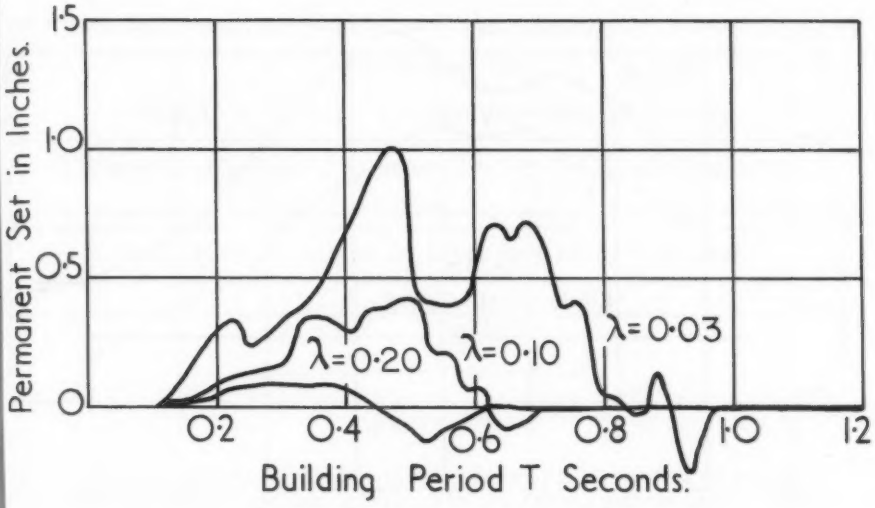

FIG. 15 PERMANENT SET.
$\zeta = 0{\cdot}24$

bending moment due to the weight of the structure a permanent set will arise superimposed on the permanent set caused by the asymmetry of the earthquake. This feature may increase or decrease the fundamental permanent set.

The yield spectra of more earthquakes must be determined before definite conclusions are reached. It is likely though that they will not differ substantially from the one earthquake considered here.

The authors hope to analyse more earthquakes on the same basis and to extend the work to yielding of multi-storey building frames.

REFERENCES

1. "Electrical Analog for Shear Stresses in a Multi-storied Building", by M. J. Murphy, G. N. Bycroft, L. W. Harrison, Proceedings of the World Conference on Earthquake Engineering, Berkeley, California, June 1956.

2. Dr. B. W. Faulkner, Design Engineer, Ministry of Works, Wellington, New Zealand.

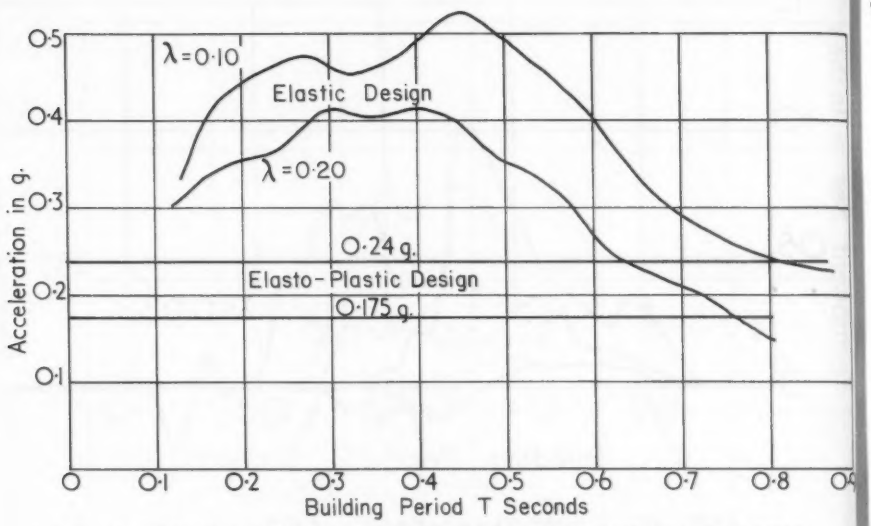

FIG. 16. COMPARISON OF DESIGN ACCELERATIONS IN ELASTIC AND ELASTO-PLASTIC STRUCTURES

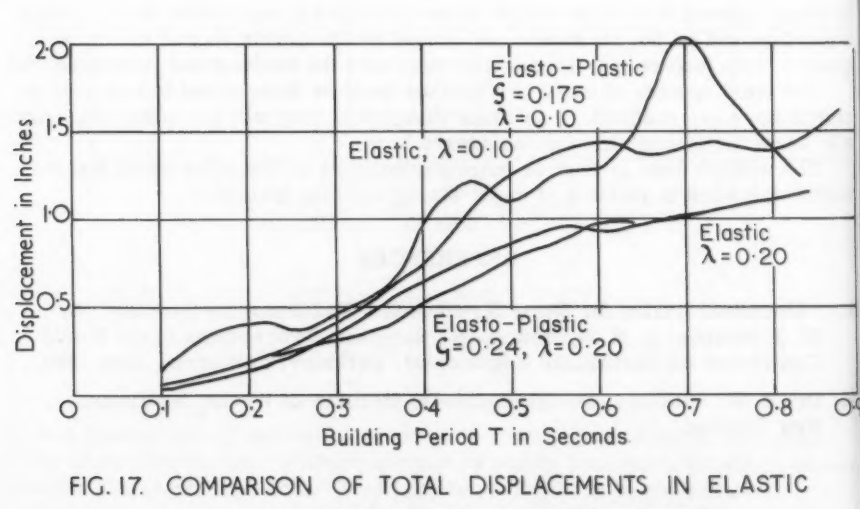

FIG. 17. COMPARISON OF TOTAL DISPLACEMENTS IN ELASTIC AND ELASTO-PLASTIC DESIGNS

Journal of the
ENGINEERING MECHANICS DIVISION
Proceedings of the American Society of Civil Engineers

THE NEUTRAL AXIS IN PLASTIC BENDING OF BEAMS[a]

Aris Phillips,[1] F. ASCE

ABSTRACT

The motion of the neutral axis in symmetrical pure bending of beams in plasticity is discussed. Both perfectly plastic beams and beams with linear strain hardening are considered. A method is given by means of which it is possible to correlate in a simple manner the motion of the neutral axis with the motion of the elastic-plastic boundaries. Formulas are found for the motion of the neutral axis with increasing curvature. Conditions are established for reversal of direction of motion of neutral axis.

INTRODUCTION

The purpose of this paper is to discuss the motion of the neutral axis with increasing curvature in plasticity, and the relation between the motion of the neutral axis and the corresponding motion of the elastic-plastic boundaries. This discussion will be restricted to symmetrical pure bending of beams. Specifically, it is assumed that the cross section has only one axis of symmetry which lies in the plane of the external forces, and it is also assumed that the stress-strain curves for tension and for compression are identical and that they have the form shown in Fig. 1. On the basis of the elementary theory of bending of beams in plasticity(1) a simple graphical method will be outlined by means of which it is possible to find the elastic-plastic boundaries corresponding to a given position of the neutral axis. In the last part of the paper certain conclusions will be drawn concerning the motion of the neutral axis and the motion of the elastic-plastic boundaries for increasing value of the curvature, and formulas will be found expressing the rate of motion of the

Note: Discussion open until March 1, 1960. To extend the closing date one month, a written request must be filed with the Executive Secretary, ASCE. Paper 2198 is part of the copyrighted Journal of the Engineering Mechanics Division, Proceedings of the American Society of Civil Engineers, Vol. 85, No. EM 4, October, 1959.

a. This investigation is part of a research program sponsored by the National Science Foundation.

1. Associate Prof. of Civ. Eng., Yale University, New Haven, Conn.

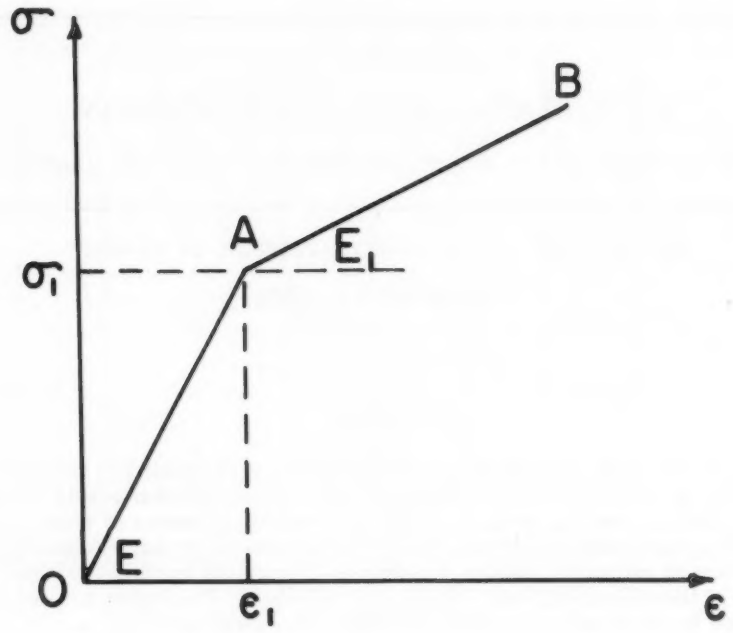

Fig. 1

neutral axis as a function of the curvature and of the position of the neutral axis. Also conditions will be given for the reversal of the direction of motion of the neutral axis.

In Figs. 2a and 2b a general cross section has a plastic region on only one side of the neutral axis. In Fig. 2c the cross section has plastic regions on both sides of the neutral axis. The corresponding strain distributions and stress distributions are shown in the same Figs. 2a to 2c.* Because of symmetry the neutral axis is always normal to the axis of symmetry.

For a small bending moment the entire cross section is elastic and the neutral axis passes through the centroid of the cross section. The fibers which lie at the greatest distance from the neutral axis will always have the maximum strain and as the bending moment increases they will finally be strained to the yield strain ϵ_1; then a plastic region will start forming beginning from these fibers. These fibers will be either the lowest or the highest fibers of the cross section taking the axis of symmetry of the cross section to be vertical. If the highest and lowest fibers have the same distances from the elastic neutral axis then they will all become plastic simultaneously. If the highest and lowest fibers are at different distances from the elastic neutral axis plasticity will start at the fibers which are situated at the greatest

*Fig. 2 is only a schematic representation of different cases of discussion; it does not represent results of actual calculations.

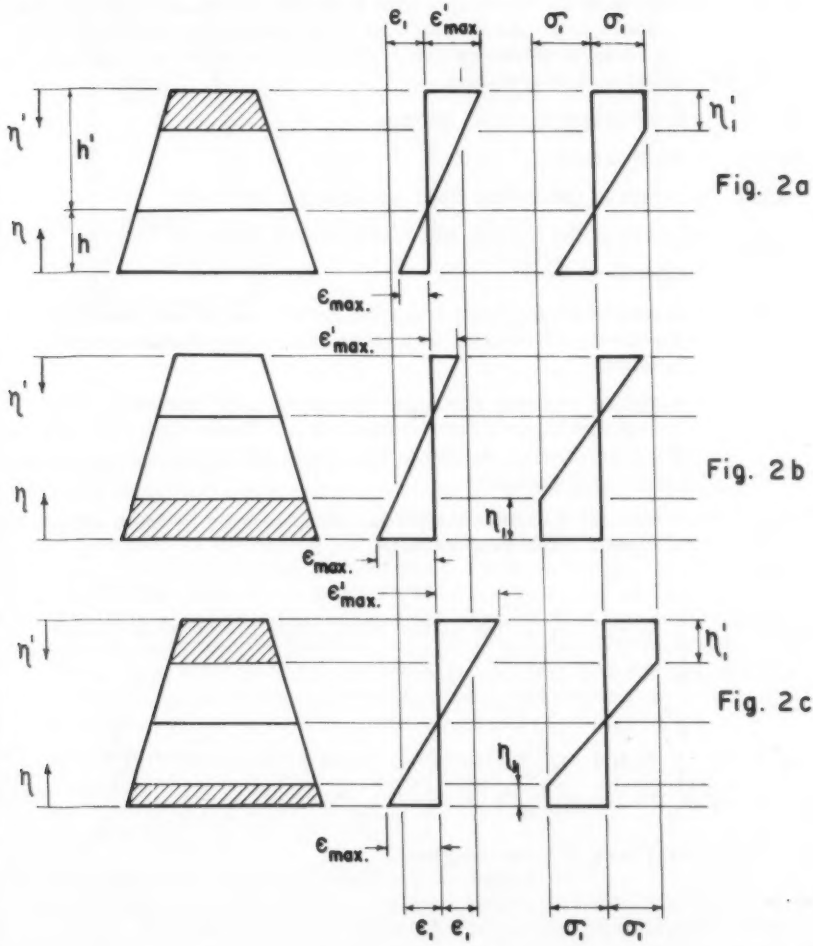

distance from the elastic neutral axis. In what follows it will be assumed that the fibers situated at the greatest distance are the highest fibers; hence the cases given in Figs. 2a and 2c will be considered. Obviously, a rotation of the cross section by 180° produces the case 2b from the case 2a. Thus by restricting our considerations to Figs. 2a and 2c we do not restrict the validity of the argument to these two cases only.

The following notations will be introduced:

E = slope of the line OA in Fig. 1. This is the modulus of elasticity of the material.

E_1 = slope of the line AB in Fig. 1. This is the modulus of linear strain hardening of the material.

h, h' = distances of the neutral axis from the lowest and highest fibers respectively. As the position of the neutral axis changes with increasing curvature (once plasticity has started) it follows that h and h' are variables.

H = total height of cross section

ϵ_1 = yield strain

ϵ_{max} = strain of the lowest fiber (considered positive)

ϵ'_{max} = strain of the highest fiber (considered positive)

k = curvature

η, η' = distances of any fiber from the lowest and highest fibers respectively. Referring to a given fiber these distances are constant.

η_1, η_1' = distances of lower and upper elastic-plastic boundary from lowest and highest fiber respectively. These distances are variable; they are respectively zero wnen the lower and upper plastic region is nonexistent.

$B(\eta)$, $B(\eta')$ = width of the cross section at distance η or η' from the lowest or highest fiber respectively.

$$A(\eta) = \int_0^{\eta} B(\eta)\, d\eta = \text{area of the cross section between } \eta = 0 \text{ and } \eta = \eta$$

$$A'(\eta') = \int_0^{\eta'} B(\eta')\, d\eta' = \text{area of the cross section between } \eta' = 0 \text{ and } \eta' = \eta'$$

A = total area of cross section.

$$A_2(\eta) = \int_0^{\eta} A(\eta)\, d\eta$$

$$A_2'(\eta') = \int_0^{\eta'} A'(\eta')\, d\eta'$$

The expressions for $A_2(\eta)$ and $A_2'(\eta')$ have been calculated for some cross sections and are given in reference (1). For example, for a rectangular cross section of width B and height H we find

$$A_2(\eta) = \frac{BH}{2}(2\eta - H), \qquad A_2'(\eta') = \frac{BH}{2}(2\eta' - H)$$

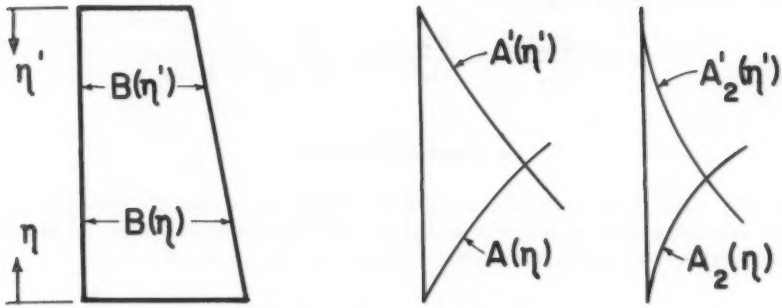

Fig. 3

In Fig. 3 the graphs for the six functions $B(\eta)$, $B(\eta')$, $A(\eta)$, $A'(\eta')$, $A_2(\eta)$, $A_2'(\eta')$ are shown for a general cross section. The slope of curve $A_2(\eta)$ at $\eta = \alpha$, with respect to the vertical is equal to the ordinate A(a) and to the area of the cross section between $\eta = 0$ and $\eta = \alpha$. Similarly, the slope of the curve $A_2'(\eta')$ at $\eta' = \alpha'$, with respect to the vertical is equal to the ordinate $A'(\alpha')$ and to the area of the cross section between $\eta' = 0$ and $\eta' = \alpha'$. Remark also that as η (or η') increases, the value of $A(\eta)$ (or of $A_2'(\eta')$) increases also and thus also the slope of $A_2(\eta)$ (or of $A_2'(\eta')$) increases. For a = 0 the area is zero; hence the curve $A_2(\eta)$ is tangent to the vertical at $\eta = 0$. Similarly, the curve $A_2'(\eta')$ is tangent to the vertical at $\eta' = 0$.

The position of the neutral axis will be given by the expression

$$\frac{E}{E-E_1}\left[A_2'(h') - A_2(h)\right] = A_2'(\eta_1') - A_2(\eta_1) \qquad (1)$$

which follows from formulas (4-19) in reference (1).*

As it is seen from Fig. 2c, when plastic regions exist on both sides of the neutral axis, the distance of the upper elastic-plastic boundary from the neutral axis is equal to the distance of the lower elastic-plastic boundary from the neutral axis. From Fig. 2 it is seen also that the following formulas are valid

$$\frac{\varepsilon_1}{\varepsilon_{max}} = \frac{h-\eta_1}{h} \qquad (2)$$

$$\frac{\varepsilon_1}{\varepsilon'_{max}} = \frac{h'-\eta_1'}{h'} \qquad (3)$$

*Expression (1) follows from formulas (4-19) in reference (1) by writing $N_b = N_a$ and noting that in the present case there exist two materials only with $G_1 = G_1' = E - E_1$ and $G_2 = G_2' = E_1$.

Hence, the curvature is given by

$$\chi = \frac{\varepsilon_{max}}{h} = \frac{\varepsilon'_{max}}{h'} = \frac{\varepsilon_1}{h-\eta_1} = \frac{\varepsilon_1}{h'-\eta'_1} \qquad (4)$$

A Graphical Method

In Fig. 4 the lines $A_2(\eta)$ and $A'_2(\eta')$ are drawn for a specific cross section. These two lines meet at N'_1 where $A_2(\eta) = A'_2(\eta')$. Note that when no plastic regions exist—that is, in the elastic region—Eq. (1) becomes

$$A_2(h) = A'_2(h')$$

because then $A_2(\eta_1) = A'_2(\eta'_1) = 0$. Hence the elastic position NN'_1 of the neutral axis passes through the intersection N'_1 of the two lines $A_2(\eta)$ and $A'_2(\eta')$.

Next the line NM with equation

$$\frac{E}{E-E_1}\left[A'_2(h') - A_2(h)\right] = (ab)$$

is drawn in Fig. 4. This line starts at the intersection N between elastic neutral axis and vertical base 00' and is drawn toward the boundary which is at the shortest distance from NN'_1. Hence, in Fig. 4 this line NM is drawn toward the lower boundary. It is seen that

$$(ab) = \frac{E}{E-E_1}(a'b')$$

because $(a'b') = A'_2(h') - A_2(h)$. Therefore $ab \geqq a'b'$, with the equality sign being valid when $E_1 = 0$, that is for a perfectly plastic material. On the other hand $E_1 = E$ for a purely elastic material; hence for an elastic material $ab = \infty$ in which case the curve MN coincides with the line NN'_1.

The first appearance of a plastic region will be at the boundary of the cross section which is at the greatest distance from the elastic position of the neutral axis; in Fig. 4 this is the upper boundary. When a plastic region exists on only one side, for example above the neutral axis, then in Eq. (1) we have $A_2(\eta_1) = 0$. Hence in this case Eq. (1) simplifies to

$$\frac{E}{E-E_1}\left[A'_2(h') - A_2(h)\right] = A'_2(\eta'_1) \qquad (5)$$

Let nn' be a neutral axis in Fig. 4. Then the left hand member in Eq. (5) is equal to length ns and the right hand member will be found by drawing a vertical line from s until it intersects the $A'_2(\eta')$ line; then the right hand member of (5) is equal to length pr. It is seen that as long as a plastic region exists only on one side of the cross section the corresponding values of h' and η'_1 will be determined by drawing vertical lines and finding the intersections of these vertical lines with the lines NM and $O'N'_1$. The intersection of the vertical line with the line NM gives the position of the neutral axis while the

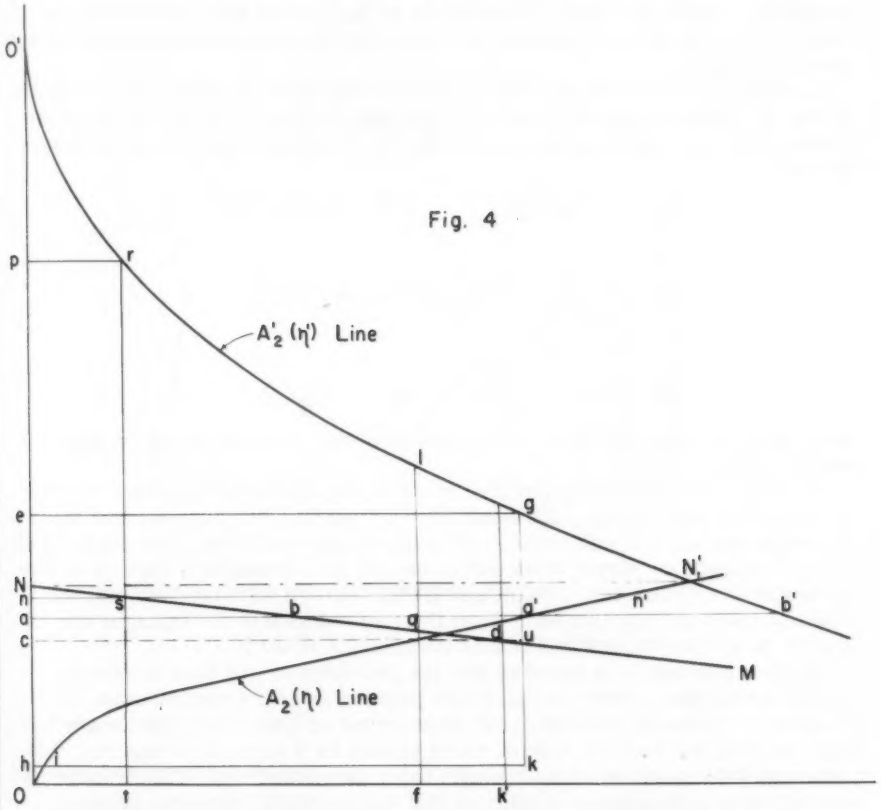

Fig. 4

intersection of the vertical line with the line $O'N_1'$ gives the corresponding elastic-plastic boundary.

We remark that length $O'p = \eta_1'$, length $O'n = h'$, and length $On = h$. As η_1' increases it is seen that h' increases also but at a slower rate because the slope of NM with respect to the vertical is greater than the corresponding slope of $O'N_1'$. It appears as if the neutral axis tries to avoid the plastic regions as this plastic region spreads downward but that it does not succeed to keep the distance from the elastic plastic boundary constant. From formula (4) we also see that

$$h' - \eta_1' = \frac{\varepsilon_1}{\varkappa} \tag{6}$$

which shows that the distance between the elastic-plastic boundary and the neutral axis is inversely proportional to the curvature k. Expression (6) can be used for finding the curvature k which corresponds to a given position of the neutral axis.

The plastic region will be restricted to the upper side as long as length $sr \geqq$ length st. Suppose that for the position mq of the neutral axis it is

length ql = length qf.* Then for positions of the neutral axis below line mq there will be two plastic regions, one above the neutral axis and another below the neutral axis.

Consider now a position cd of the neutral axis below position mq, as shown in Fig. 4. Suppose also that line eg is the elastic-plastic boundary above the neutral axis and line hi is the elastic-plastic boundary below the neutral axis. We have

$$\left.\begin{aligned} eg &= A_2'(\eta_1') \quad , \quad hi = A_2(\eta_1) \\ cd &= \frac{E}{E-E_1}\left(A_2'(h') - A_2(h)\right) \\ ch &= ce \quad , \quad hi + cd = eg \end{aligned}\right\} \tag{7}$$

Thus we have three points, h, c, e on 00' such that the last two of the Eqs. (7) will be valid.

Consider now the line kg parallel to 00' in Fig. 4 and the extensions of line hi to k and of line cd to u. Obviously ku = ug and ik = cd. Suppose that kg and ik are the two normal sides of a right angle triangle with the right angle (gkh). Let this triangle be moved down and to the left in a translatory motion so that the length ik will remain constant and let this motion be continued until the length ik takes the position 0k'. Then the vertical side of the triangle will pass by d, so that the new position of the triangle is 0k'd.

Suppose now that it is asked to find the positions eg and hi of the elastic plastic boundaries corresponding to the position cd of the neutral axis. The translatory motion mentioned above is reversed so that now a right angle triangle is used, the vertical side of which passes by d while its horizontal side passes by 0 the position of the triangle being therefore 0k'd. This triangle is now moved in a translatory motion so that the length 0k' remains constant until at some position (ikg) there is ku = ug. At this position hk and eg are the two elastic plastic boundaries and Eq. (6) gives the corresponding curvature. Fig. 5 shows the procedure and in Fig. 6 a complete determination of the elastic plastic boundaries is given for several positions of the neutral axis for a given cross section and a given material.

Discussion

Referring to Fig. 4 we note that the slope to the vertical of the line MN at any point s is always greater than the slope of the line $0'N_1'$ at the corresponding point r. Hence when only one plastic region exists the neutral axis moves always downward. When the neutral axis intersects the MN line at q the lower elastic plastic boundary is at 0. But the slope of $0N_1'$ is zero at 0; hence it is smaller than the slope of $0'N_1'$ at 1. Therefore, when the second plastic region first appears the neutral axis continues to move upward.

The motion of the neutral axis as the curvature increases can be related to the motion of the elastic-plastic boundaries as follows. From Eq. (4) we find

*Here q is the intersection of line lf with line NM, and line mq is a neutral axis—not shown in the figure—which passes by the point q.

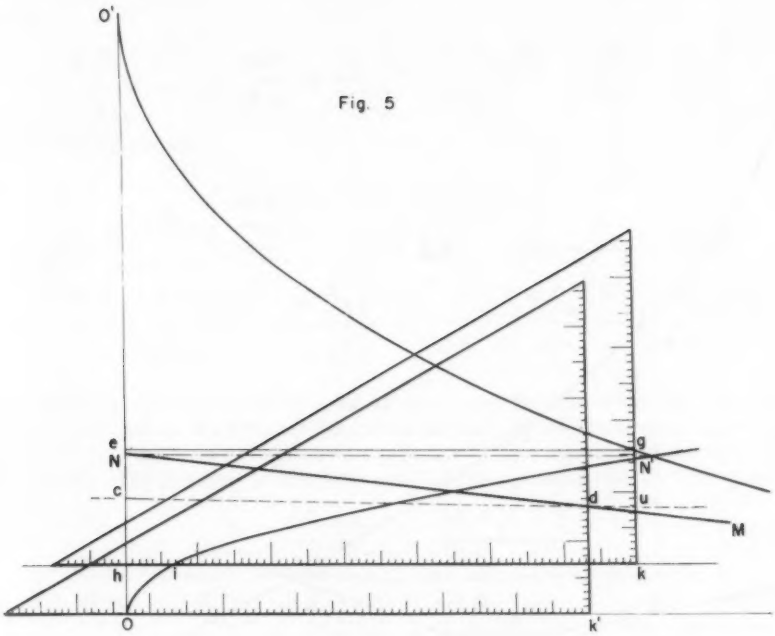

Fig. 5

$$\eta_1 = h - \frac{\varepsilon_1}{\kappa} \quad , \quad \eta_1' = h' - \frac{\varepsilon_1}{\kappa} = H - h - \frac{\varepsilon_1}{\kappa} \tag{8}$$

Differentiating we obtain

$$\frac{d\eta_1}{d\kappa} = \frac{dh}{d\kappa} + \frac{\varepsilon_1}{\kappa^2} \quad , \quad \frac{d\eta_1'}{d\kappa} = -\frac{dh}{d\kappa} + \frac{\varepsilon_1}{\kappa^2} \tag{9}$$

from which

$$\frac{dh}{d\kappa} = \frac{1}{2}\left(\frac{d\eta_1}{d\kappa} - \frac{d\eta_1'}{d\kappa}\right) \tag{10}$$

Eq. (10) gives the rate of motion of the neutral axis in terms of the rates of motion of the elastic-plastic boundaries. It is seen that for the neutral axis to remain stationary the rates of motion of the two boundaries must be equal. It is seen also that the neutral axis moves toward the elastic-plastic boundary which has the slowest motion.

Eq. (10) is not sufficient to give the rate of motion of the neutral axis because the quantities $d\eta_1/dk$ and $d\eta_1'/dk$ are not known. Curves $A(\eta)$ and $A(\eta')$ can now be used for determining the rate of motion of the neutral axis. Eq. (1) gives

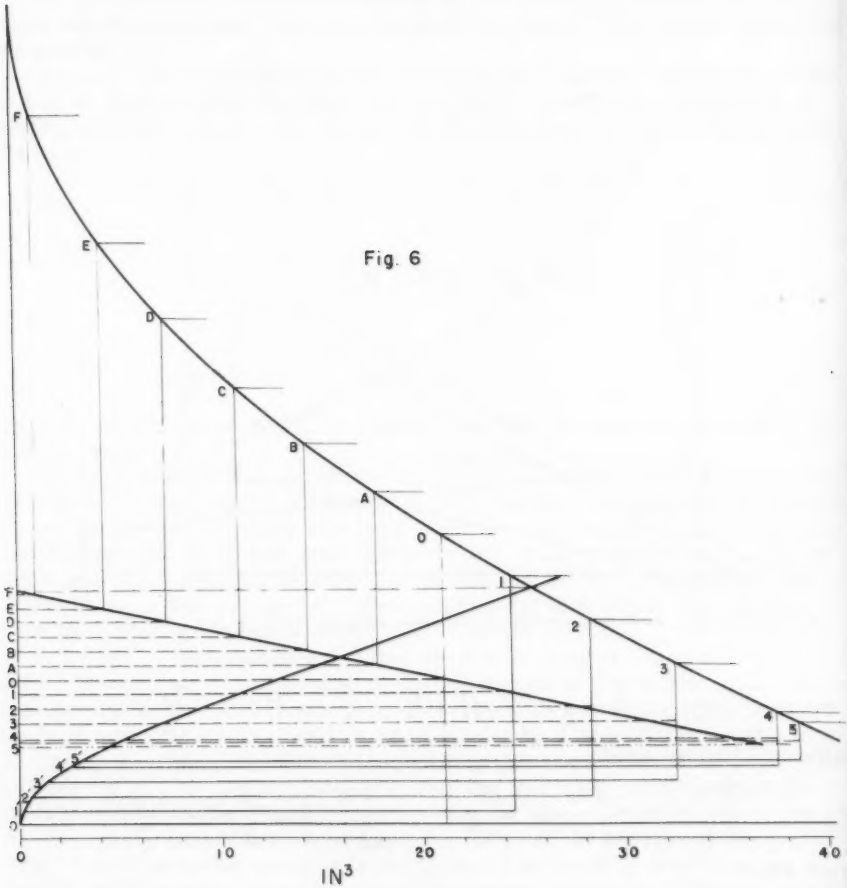

Fig. 6

$$\frac{E}{E-E_1}\left[\frac{dA_2'(h')}{dh'}\frac{dh'}{dx}-\frac{dA_2(h)}{dh}\frac{dh}{dx}\right]= \tag{11}$$

$$=\frac{dA_2'(\eta_1')}{d\eta_1'}\frac{d\eta_1'}{dx}-\frac{dA_2(\eta_1)}{d\eta_1}\frac{d\eta_1}{dx}$$

But

$$h'=H-h$$

Hence, the left hand member of Eq. (11) becomes

$$-\frac{E}{E-E_1}\frac{dh}{dx}\left[\frac{dA_2'(h')}{dh'}+\frac{dA_2(h)}{dh}\right]$$

while the right hand member of Eq. (11), with the help of expressions (9), becomes

$$\frac{dA_2'(\eta_1')}{d\eta_1'}\left[-\frac{dh}{dx}+\frac{\varepsilon_1}{x^2}\right]-\frac{dA_2(\eta_1)}{d\eta_1}\left[\frac{dh}{dx}+\frac{\varepsilon_1}{x^2}\right]$$

Eq. (11) becomes now

$$\frac{dh}{dx}=\frac{\frac{\varepsilon_1}{x^2}\left[\frac{dA_2'(\eta_1')}{d\eta_1'}-\frac{dA_2(\eta_1)}{d\eta_1}\right]}{\frac{dA_2(\eta_1)}{d\eta_1}+\frac{dA_2'(\eta_1')}{d\eta_1'}-\frac{E}{E-E_1}\left[\frac{dA_2'(h')}{dh'}+\frac{dA_2(h)}{dh}\right]} \tag{12}$$

Recalling that dA_2/dh is the area of the cross section below the neutral axis and dA_2'/dh' is the area of the cross section above the neutral axis it is concluded that the sum of these two quantities which appears in the denominator of Eq. (12) is equal to the total area of the cross section. Therefore

$$\frac{dh}{dx}=\frac{\varepsilon_1}{x^2}\,\frac{\frac{dA_2'(\eta_1')}{d\eta_1'}-\frac{dA_2(\eta_1)}{d\eta_1}}{\frac{dA_2'(\eta_1')}{d\eta_1'}+\frac{dA_2(\eta_1)}{d\eta_1}-\frac{EA}{E-E_1}} \tag{13}$$

It is recalled that $dA_2/d\eta_1$ is the lower plastic area of the cross section and that $dA_2'/d\eta_1'$ is the upper plastic area. As $EA/(E - E_1)$ is always larger or equal to A it follows that the denominator of the right hand member of Eq. (13) is always negative. Therefore dh/dk has always a sign opposite to that of the numerator of the right hand member of Eq. (13). It follows therefore that the neutral axis moves upward, remains stationary, or moves downward when $dA_2'/d\eta_1'$ is smaller, equal, or larger than $dA_2/d\eta_1$, respectively, that is, when the upper plastic area is smaller, equal, or larger than the lower plastic area respectively.

When plasticity first appears the upper plastic area is the only existing one; hence, the neutral axis moves downward. This downward motion of the neutral axis continues even after the lower plastic area appears. As the lower plastic region increases in size it is possible that this region may become equal in size to the upper plastic region in which case the neutral axis stops moving. When the lower plastic region becomes larger than the upper plastic region the neutral axis moves upward thus reversing its direction of motion.

Consider also the positions (cd), (eg), and (hi) of the neutral axis and of the two corresponding elastic-plastic boundaries in Fig. 4. For the neutral axis to remain stationary as the curvature increases it is necessary that the slopes (with respect to the vertical) at i of $A_2(\eta)$ and at g of $A_2'(\eta')$ be equal. If the slope at i is smaller than the slope at g then the neutral axis moves downward. If the slope at i is greater than the slope at g then the neutral axis moves upward.

Eq. (13) together with Eqs. (8) are sufficient for determining the rate of motion of the neutral axis. Indeed $A_2(\eta_1)$ and $A_2'(\eta_1')$ are known functions and therefore the derivatives $dA_2/d\eta_1$ and $dA_2'/d\eta_1'$ can be determined. Let these two derivatives be denoted by $f_1(\eta_1)$ and $f_2(\eta_1')$. Eqs. (13) and (8) give

$$\frac{dh}{dx} = \frac{\xi_1}{x^2} \frac{f_2\left(h' - \frac{\xi_1}{x}\right) - f_1\left(h - \frac{\xi_1}{x}\right)}{f_2\left(h' - \frac{\xi_1}{x}\right) + f_1\left(h - \frac{\xi_1}{x}\right) - \frac{EA}{E - E_1}} \tag{14}$$

Thus, at each value of x and h we find from (14) the value of dh/dx, from which the new set of values h + dh and x + dx can be determined. Thus, a step by step integration of the differential Eq. (14) can be performed. The graphical construction given in this paper seems, however, much simpler to use than the analytical method just outlined.

Strain hardening influences the motion because of the factor $E/(E-E_1)$ in Eq. (1). For $E_1 = 0$ there is no strain hardening. For $E = E_1$ there is linear elasticity. As strain hardening increases $E-E_1$ becomes smaller and the middle line NM in Fig. 4 tends toward the horizontal position. Hence as strain hardening increases the motion of the neutral axis tends to slow down for the same amount of motion of the elastic plastic boundaries. It is also seen that two materials with the same ratio $E/(E-E_1)$ have the same relationship between the two motions.

Once the functions A_2 and A_2' have been determined for a cross section it is comparatively easy to find the relationship between the two motions for any value of $E/(E-E_1)$. Compared to the well known method of Saint-Venant described in reference (2) the method presented in this paper has the advantage that in order to find the position of the elastic plastic boundaries corresponding to a given neutral axis now only a comparison of lengths is necessary while in Saint-Venant's method a comparison of areas is necessary.

In order to find the relationship between the motion of the neutral axis and the motion of the elastic-plastic boundaries it is necessary to repeat a given procedure a number of times. Such a repetitive procedure is much easier accomplished by means of the present method than by means of a method in which it necessary to compare areas.

REFERENCES

1. Phillips, A. "Introduction to Plasticity", The Ronald Press Company, New York, 1956, Chapter IV.

2. Timoshenko, S., "Strength of Materials", vol. II, Third Edition, D. Van Nostrand Company, New York, 1956, p. 366.

Journal of the
ENGINEERING MECHANICS DIVISION
Proceedings of the American Society of Civil Engineers

LATERALLY LOADED THIN FLAT PLATES

William A. Bradley,[1] M. ASCE

SUMMARY

In the work reported in this paper, certain laterally loaded thin plates were studied experimentally, using the Moiré method, and analytically, by finite differences. The procedures followed in the study are summarized, the results are presented, and possible sources of error in the Moiré technique are discussed. In general, the agreement of deflections and moments as found by the two methods is good, maximum variations being about ten percent.

It is concluded that the Moiré method, with possible improvements in technique, offers a useful tool, along with numerical methods, for the future study of plates.

INTRODUCTION

In the formal analysis for moments and deflections in laterally loaded thin plates, the formulation of the boundary conditions and the solution of the partial differential equations, except for certain of the simpler cases, become difficult. Two of the alternate procedures which may then be employed to obtain values of these quantities suitable for design purposes are:

a. Experimental methods—in which the boundary conditions are satisfied directly by a model, and measurements made on the loaded model can be used to determine expressions for moments and deflections.

b. Numerical solutions of the differential equations—in which the differential equation can be approximated at a finite number of points in the plate by finite difference expressions. This procedure leads to the solution of systems of linear algebraic equations—a routine which can be performed by digital computer or by the use of the desk calculator.

Note: Discussion open until March 1, 1960. To extend the closing date one month, a written request must be filed with the Executive Secretary, ASCE. Paper 2199 is part of the copyrighted Journal of the Engineering Mechanics Division, Proceedings of the American Society of Civil Engineers, Vol. 85, No. EM 4, October, 1959.

1. Associate Prof. of Applied Mechanics, Michigan State Univ., East Lansing, Mich.

In this study, certain problems have been solved by each of the two above methods and the results compared. The experimental procedure used was the Moiré method, a photographic interference method first described by Ligtenberg,(1) and later applied by Bradley(2) in the study of clamped plates with cutouts.

The principal objectives of this research were:

a. To study the application of the Moiré method to plates, particularly those with simple supports, in order to determine its accuracy.

b. To determine the deflections and the distribution of moments in certain plates by both the Moiré method and by finite differences. The comparison of the results by the two methods serves as a check on both.

Some of the results obtained in this study have been reported by B. Raju in his master's thesis.(3)

Theoretical Considerations

Differential Relationships for Thin Plates

A thin elastic plate, when laterally loaded, is subject to bending moments, twisting moments, and shears, as shown in Fig. 1. The relationships between the shape of the deflected neutral plane of the plate and these quantities are:

$$M_x = -D\left(\frac{\partial^2 w}{\partial x^2} + \mu \frac{\partial^2 w}{\partial y^2}\right) \tag{1}$$

$$M_y = -D\left(\frac{\partial^2 w}{\partial y^2} + \mu \frac{\partial^2 w}{\partial x^2}\right) \tag{2}$$

$$M_{xy} = -D\,(1 - \mu)\,\frac{\partial^2 w}{\partial x \partial y} \tag{3}$$

$$Q_x = -D\,\frac{\partial}{\partial x}\left(\frac{\partial^2 w}{\partial x^2} + \frac{\partial^2 x}{\partial y^2}\right) \tag{4}$$

and

$$Q_y = -D\,\frac{\partial}{\partial y}\left(\frac{\partial^2 w}{\partial x^2} + \frac{\partial^2 w}{\partial y^2}\right) \tag{5}$$

with the shape of the deflected plate being given by the solution of the plate equation,

$$\frac{\partial^4 w}{\partial x^4} + 2\,\frac{\partial^4 w}{\partial x^2 \partial y^2} + \frac{\partial^4 w}{\partial y^4} = \frac{q}{D} \tag{6}$$

in which D, the plate constant, is equal to $\frac{Et^3}{12\,(1 - \mu^2)}$, μ being Poisson's ratio and E the modulus of elasticity.

The derivation of these formulae assumes that no normal stress acts in the middle plane of the plate; i.e., no membrane stresses exist. For small deflections, this assumption is acceptable, but if the deflection is of the order of half the plate thickness, these membrane stresses cannot be neglected.

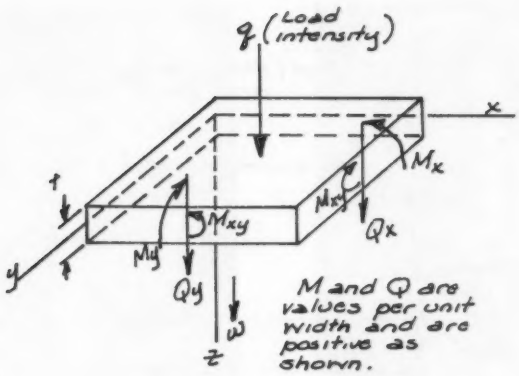

Fig. 1. Plate notations.

In the mathematical solution of a plate bending problem, it is necessary to find $w = f(x,y)$ such that equation (6) and the boundary conditions of the plate are satisfied. Knowing the function, w, throughout the plate, equations (1) through (5) can then be used to calculate the moments and shears.

If the solution of equation (6) was unobtainable, it would also be possible to determine M_x and M_y at any point in the plate if the curvatures, $\frac{\partial^2 w}{\partial x^2}$ and $\frac{\partial^2 w}{\partial y^2}$, the plate constant, and Poisson's ratio were known. These curvatures were experimentally determined in this study by the Moiré method, which gives the slopes of the plate at every point in any desired direction; from these slopes, it is then possible to determine the curvatures. Another experimental method, in which curvatures are directly measured, is applied commercially by the Presan Corporation in the analysis of floor slabs.(4)

The Moiré Method

The Moiré method is explained in detail in both references 1 and 2, and is summarized in reference 3. The essential items required are those shown in Fig. 2—the model having a reflecting surface, a finely lined grid of alternate dark and light lines of equal width, and the camera, located behind a small hole in the grid; the test setup is shown also in Figs. 3a and 3b. An exposure is first made on the negative with the plate model unloaded, or with a small initial load; next, the final load is applied, and a second exposure is made on the same negative. The interference of the reflections of the grid produces patterns as shown in Fig. 4. These patterns give the slopes at all points in the plate model; for example, in Fig. 4a, which was taken with the grid lines in a vertical position, the fringes are those for slopes of the loaded plate in the horizontal, or x, direction. Since the top edge is clamped, the slope along this edge is zero, and the fringe is of zero order; at each point along the next fringe, the slope in the x direction ($\frac{\partial w}{\partial x}$) will be unity

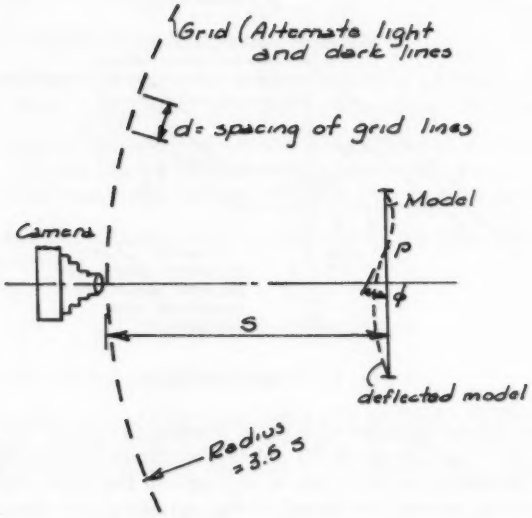

Fig. 2. Schematic side view of test set-up.

multiplied by a constant which is shown in reference 2 to be equal to $\frac{d}{2s}$, where d is the spacing of the grid lines and s is the distance from the model to the grid. Thus, in Fig. 4a, the maximum slope of the model in the x direction is (6-1/2 ($\frac{d}{2s}$) at the lower right hand corner, and in Fig. 4b, the maximum slope of the model in the y direction is (13-1/2)($\frac{d}{2s}$) at the lower right hand corner.

After the slopes in a given direction are found, it is then possible to plot curves of the slope along a given line, as shown in Fig. 5. Then, the slope of the $\frac{\partial w}{\partial x}$ vs x curve at a given point, p, in the plate will give the $\frac{\partial^2 w}{\partial x^2}$ value for this point. A similar curve of $\frac{\partial w}{\partial y}$ vs y would give $\frac{\partial^2 w}{\partial y^2}$. Further, if the values of $\frac{\partial w}{\partial y}$ are plotted against x, the slope of this curve at p will be $\frac{\partial^2 w}{\partial x \partial y}$, the twist; from this value and equation (3), the twisting moment, M_{xy}, can be determined.

It is also possible to plot values of ($\frac{\partial^2 w}{\partial x^2} + \frac{\partial^2 w}{\partial y^2}$) along a given line, and the slope of this curve will give the derivative required in equation (4) or (5) for computation of the shear. It should be noted, however, that this has certain practical limitations, since graphical differentiation produces errors and the results may not be very accurate.

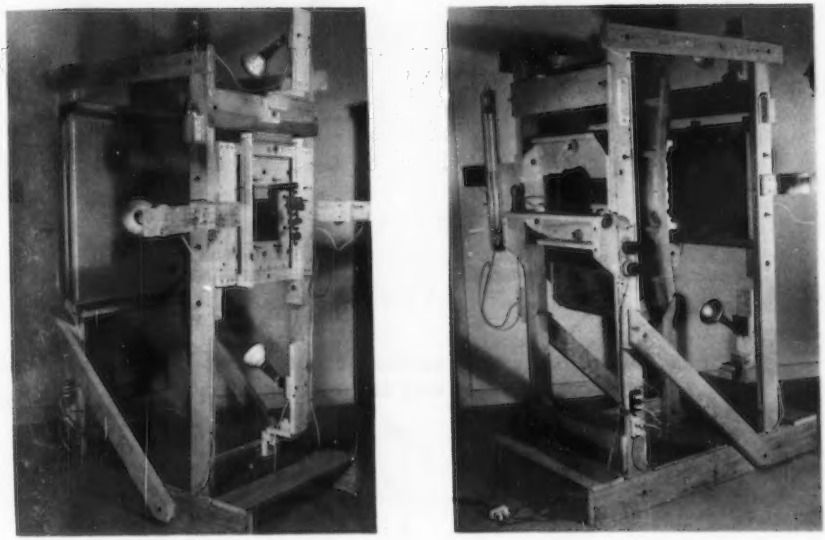

Fig. 3. Test set-up.

The deflections may be found by integration of the area under the slope curves, using the relation,

$$w_{a'} = w_a + \int_a^{a'} \frac{\partial w}{\partial x}\, dx \tag{7}$$

Diagonal Relationships

The relationships between the slopes, curvatures, and moments in various directions at a point in a deflected plate may, in some cases, be useful. Using the notation in Fig. 6, the following relations exist:

Slopes—

$$\frac{\partial w}{\partial n} = \frac{\partial w}{\partial x} \cos\theta + \frac{\partial w}{\partial y} \sin\theta \tag{8}$$

$$\frac{\partial w}{\partial t} = \frac{\partial w}{\partial y} \cos\theta - \frac{\partial w}{\partial x} \sin\theta \tag{9}$$

$$\left(\frac{\partial w}{\partial n}\right)^2 + \left(\frac{\partial w}{\partial t}\right)^2 = \left(\frac{\partial w}{\partial x}\right)^2 + \left(\frac{\partial w}{\partial y}\right)^2 \tag{10}$$

Curvatures—

$$\frac{\partial^2 w}{\partial n^2} = \frac{\partial^2 w}{\partial x^2} \cos^2\theta + 2\frac{\partial^2 w}{\partial x \partial y} \sin\theta \cos\theta + \frac{\partial^2 w}{\partial y^2} \sin^2\theta \tag{11}$$

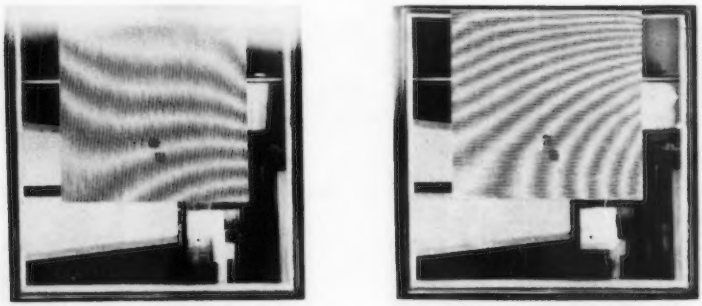

Fig. 4. Moiré fringes for cantilever plate clamped at top and with concentrated load at lower right hand corner.

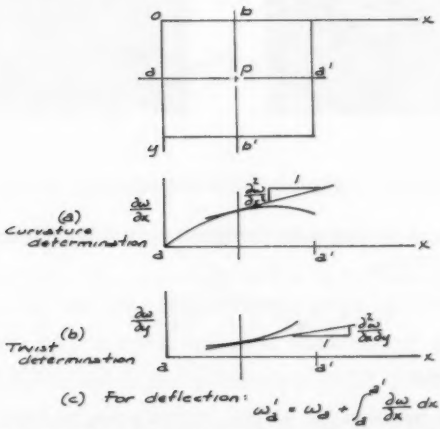

Fig. 5. Determination of curvature and twist.

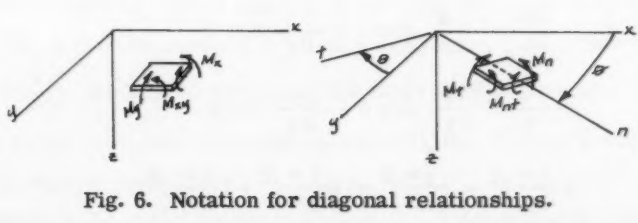

Fig. 6. Notation for diagonal relationships.

$$\frac{\partial^2 w}{\partial t^2} = \frac{\partial^2 w}{\partial x^2} \sin^2 \theta - 2\frac{\partial^2 w}{\partial x \partial y} \sin \theta \cos \theta + \frac{\partial^2 w}{\partial y^2} \cos^2 \theta \qquad (12)$$

$$\frac{\partial^2 w}{\partial n^2} + \frac{\partial^2 w}{\partial t^2} = \frac{\partial^2 w}{\partial x^2} + \frac{\partial^2 w}{\partial y^2} \qquad (13)$$

Moments—

$$M_n = \frac{M_x + M_y}{2} + \frac{M_x - M_y}{2} \cos 2\theta + M_{xy} \sin 2\theta \qquad (14)$$

$$M_{nt} = \frac{M_x - M_y}{2} \sin 2\theta + M_{xy} \cos 2\theta \qquad (15)$$

$$M_n + M_t = M_x + M_y \qquad (16)$$

Principal moments—

$$\left.\begin{matrix} M_1 \\ M_2 \end{matrix}\right\} = \frac{M_x + M_y}{2} \pm \sqrt{\left(\frac{M_x - M_y}{2}\right)^2 + M_{xy}^2} \qquad (17)$$

$$\tan 2\theta_1 = \frac{2M_{xy}}{M_x - M_y} \qquad (18)$$

A series of fringe photos for a uniformly-loaded plate is shown in Fig. 7; the fringe patterns for $\frac{\partial w}{\partial x}$ become somewhat obscure along the side edges. However, the diagonal fringes are well defined along these edges; thus, the curvatures in the diagonal directions could be used along with $\frac{\partial^2 w}{\partial y^2}$ (which, in this case, is zero) to determine the x curvature ($\frac{\partial^2 w}{\partial x^2}$) by application of equation (11) or (13). The use of these diagonal relations is also helpful as a check on the work.

Finite Difference Approximations

The solutions of differential equations—both ordinary and partial—can often be approximated by the use of finite differences. This procedure is discussed in detail by Salvadori[5] and others, and its application to plate problems is reviewed in reference 2; in reference 2, also, the difference operators for points near various types of boundaries are summarized. The systems of algebraic linear equations which result from the application of the difference operators were solved largely by the Michigan State University digital computer—the MISTIC; a few of the simpler systems were solved by the Gauss-Doolittle reduction scheme,[6] using a desk calculator.

For most of the cases given here, difference solutions have been carried out with two different grid spacings, and Richardson's extrapolation used to produce improved results.

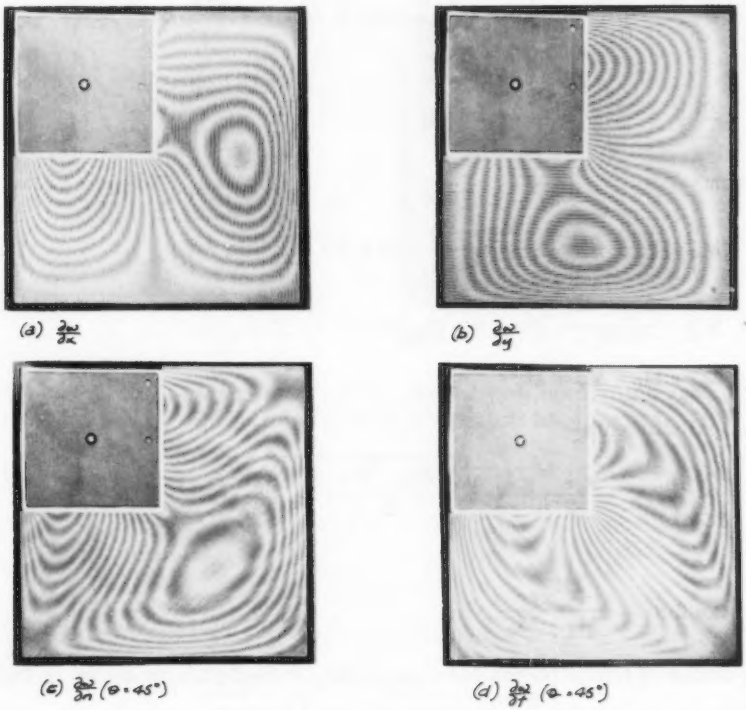

Fig. 7. Moiré fringes for clamped, uniformly loaded square plate with cutout. Plate mode, 9" × 9" square and 1/8" thick.

Experimental Considerations

The test frame—supporting the model, grid, lights, camera, and loading arrangements—is shown in Fig. 3. The setup is described in detail in references 2 and 3, but certain features are reviewed here.

The Model

Both plastic and metal sheet material has been used for the models. Advantages of the plastic materials are;

a. Smaller stiffness—thus making it possible to use thicker plates with small loads and to allow greater deflections, with the corresponding finer fringe patterns, without deflecting the plate to the extent that large membrane stresses occur. The relatively small modulus of elasticity of most plastics also makes it possible to obtain clamped edge conditions more easily. Also, since small loads can be applied, the stiffness of the supporting framework does not need to be as great to prevent deflections of the frame.

b. Surface smoothness—many plastic sheets are poured on plate glass, thus giving a very smooth surface, which is necessary for faithful reflection of the grid. In rolled metal sheets, very slight roughness in the roller surface is transferred to the sheet.

c. Machinability—plastics may be easily and accurately cut and shaped with common shop tools.

The advantages of the metal models are:

a. Thickness uniformity—this is helpful, since any large variation in thickness will change the distribution of moments in the plate. Also, as shown in Equations (1) and (5), the moments and shears at a point in the plate are dependent on D, which in turn varies as the cube of the thickness. This makes it necessary to accurately measure the thickness of the plastic sheet in order to know the D values at all points.

b. Physical properties—the values of modulus of elasticity may be taken as constant for metals, but E for plastics varies materially with both temperature and humidity and somewhat from sheet to sheet. This makes it necessary to calibrate the model each time a test is run. In addition, in an experimental study of elastic plates, it is best to use an elastic material. In using plastics, the creep tendencies of the material must be considered in planning the experimental routine.

In view of the advantages of the metals, which it was felt would result in more accurate results, considerable effort was directed toward the use of various types of metal plates—copper, brass, aluminum and steel, both plated and polished. It was found that most surfaces which appeared smooth to the eye still possessed enough grain to cause distortion of the grid reflection. This, along with the consideration of the other listed factors, led to the adoption of the plastic for most tests. The material used was Perspex, a methyl methacrylate; the transparent material can be used, but requires mirroring of the reflecting surface; to avoid this added step, the black opaque sheet was used, and it yielded good fringe patterns. All results given here were obtained using the Perspex model unless specifically stated otherwise.

The Grid

The number of fringes appearing for a given deflected plate depends on the spacing of the alternate black and white lines of the grid. In most of the work so far done, the line width is 0.05 inches, giving a d of .10". Since the distance from screen to model, s, for the setup used is 25", the difference in slope between two adjacent fringes is $d/2s = 0.002$. An alternate grid was used, with d = .05", but it was found that the definition between fringes was reduced in some cases, and there appeared to be little advantage.

Support of the Model

In this study, the plates have been either clamped, simply supported, or with free edges. In all cases, the clear unsupported length, a, was 9.05 inches.

The clamped edge condition was provided as shown in Fig. 8; the model was placed between the two 3/4" thick steel plates and the assembly clamped together with twenty 5/16" bolts. This assembly was mounted into the frame as shown in Fig. 3.

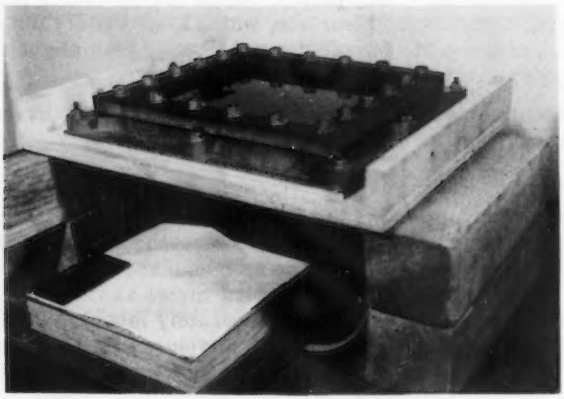

Fig. 8. Clamped edge fixture; below is the air cell used for applying distributed load.

For the simply supported edge, the fixture was as shown in Fig. 9; the model was held vertically between the knife edges by two fine threads. The bolts were tightened only enough to lightly draw the assembly together. On testing, a small initial load was applied to the model in order to seat it against the front knife edge.

Loading

Concentrated loads were applied to the model by means of a lever system, which appears at the rear of the model in Fig. 3.

The uniform loads were applied through air cells placed against the back surface of the model; one of these cells ready to be put into place is shown in Fig. 8. The load pressure was read, in inches of water, from the manometer mounted on the frame as shown in Fig. 3.

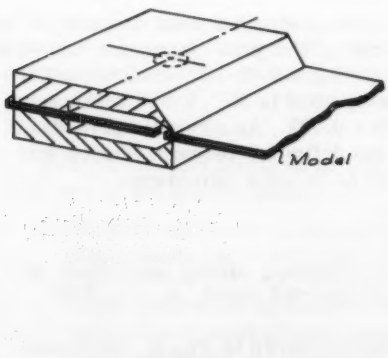

Fig. 9. Arrangement for simple support condition.

Calibration of the Material

Since the modulus of elasticity of Perspex varies with both the temperature and the humidity, it is necessary to determine it during each test. This can be done by measuring the deflection, slope, or curvature of a plate of known dimension under a known load, and, using the theoretical relation between these quantities, calculating D. In this study, the calibration plate was cut from the same sheet of material as the model, thus avoiding the variation in material which may occur between different batches.

Two simple cases of plates which may be used for calibration are discussed below.

a) Square plate supported at three corners and with concentrated load at the fourth. (Fig. 10)

For this plate[7] the curvature in the x direction is constant throughout, and

$$D_c = \frac{-P}{2(1-\mu)\left(\frac{\partial^2 w}{\partial x^2}\right)} \quad ; \tag{19}$$

but, since between two successive fringes, $\frac{\partial w}{\partial x}$ changes by $\frac{d}{2s}$,

$$\frac{\partial^2 w}{\partial x^2} = \frac{-d}{(2s)\,(\text{spacing of fringes})} \quad ,$$

and substituting in equation (19),

$$D_c = \frac{P\,(2s)\,(\text{spacing of fringes})}{2\,(1-\mu)\,d} \tag{20}$$

Thus, knowing d and s (which are constants), the applied load, and Poisson's ratio, it is possible to measure the fringe spacing from the Moire photo, as in Fig. 10b, and compute D.

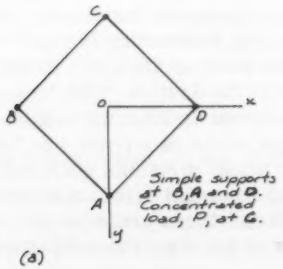

(a)

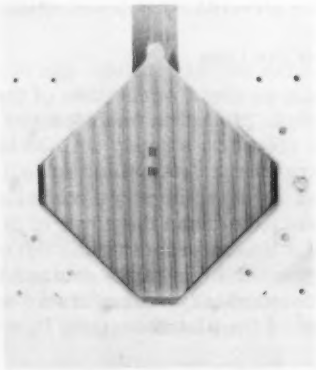

(b) Fringe pattern; P = ½"; 6" square model of green opaque Plexiglas.

Fig. 10. Alternate calibration arrangement.

EM 4

This procedure requires, however, that the calibration plate be mounted in the test frame and that photos be taken during each test. To avoid this, the method of b) was adopted.

b) Circular clamped plate.

For a uniformly loaded clamped circular plate of radius, a, the center deflection,

$$w = \frac{q\,a^4}{64\,D_c} \tag{21}$$

Thus, after loading the plate and measuring the center deflection, the plate constant can be computed. This measurement was made using the setup shown in Fig. 11.

As a partial check on this procedure, the Moiré fringes were obtained for this plate, as shown in Fig. 12. From these fringes, the center deflection was computed as 0.0111 inches, and using equation (21), $D_c = 82.3$ lb.-in. The curvature was also found, and using equation (2), the center moment, M_y, was calculated as 0.549 in.-lbs. per inch, using Poisson's ratio as 1/3. This compares with the theoretical value of center moment,

$$M = \frac{1+\mu}{16}\,q\,a^2 = 0.542\ \frac{\text{in. lbs.}}{\text{in.}}$$

To complete the check, the dial gage deflection was then read for the same load, with readings of 0.0113" and 0.0110", or an average of 0.01115".

For all cases, the calibration plate was chosen from the large Perspex sheets so that the thickness variation would be as small as possible.

The Test Procedure

Since the model materials used are plastics and subject to time effects, the accuracy of the results probably depends somewhat on the time intervals during the test. The procedure followed in this study was essentially that described in reference 2, with a four minute interval between successive photos to allow recovery of the material.

All fringe pictures were taken using Royal Pan sheet film.

Reduction of the Data

After enlargements were made of the fringe patterns for slopes, curves of the slopes were plotted in each desired direction by locating the half-fringes, since these are more sharply defined than the integral fringes. From these, the curvatures were determined as indicated in the Section "The Moire Method" and Fig. 5. The slope curves were drawn on 20 square-to-the-inch cross section paper, and the slope of the slope curve at a point was taken as the slope of a line intersecting the curve two small divisions each side of the point. To speed the curvature determination, a special protractor-like device was constructed which was calibrated so that curvature could be read directly.

The value of the plate constant, D, was found for a particular point from

$$D = D_c\left(\frac{t}{t_c}\right)^3 \tag{22}$$

where D_c is the value for the calibration plate,

Fig. 11. Set up for calibration of material. The box appearing in background houses an air reservoir used to cushion impact effect of load application.

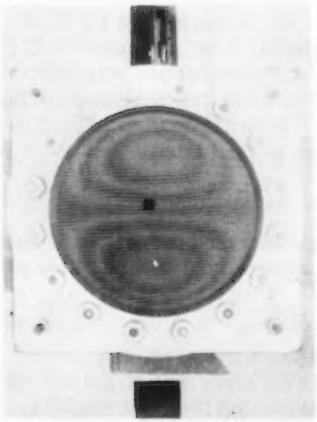

Fig. 12. Moiré pattern for uniformly loaded clamped calibration plate.
Radius = 3" q = 20" of water = .722 psi.
Plate thickness = .1275"

t_c was taken as the average thickness of the calibration plate, and

t was the thickness of the model at the point.

The moments were computed from equations (1), (2) and (3), using Poisson's ratio as one-third for Perspex, and equation (7) was used for determining deflections, with the integrations being carried out by totaling the areas under the slope curves.

EM 4

Results

Square, Uniformly Loaded, Clamped Plate

The fringe patterns for this plate are shown in Fig. 13. Figs. 13a and 13b show the slope fringes for a load of q = 0.2167 psi.; from enlargements of these two photos, the moments were computed at intervals of 0.1a, a being the side dimension of the plate; deflections along the center lines were also computed. In Fig. 14, the moment values are given, as computed by the Moiré method and also by finite differences, using a grid spacing of $\lambda = a/10$. In the case of the Moiré moments, the four values given are those obtained at symmetrical points in the plate and are presented to give an idea of the range of values. The difference results for $\lambda = a/10$ are slightly lower than the actual, or extrapolated, values, as shown in Fig. 15, where the moments along a center-line are plotted; this figure shows values for $\lambda = a/8$ and $\lambda = a/10$, the extrapolated value, and the Moiré value. Fig. 15 also shows a comparison of deflections along a center-line. In Figs 13c and 13d, the fringe patterns for larger loads are shown, and Fig. 13e gives the fringes for diagonal slopes.

The curves of Figs. 14 and 15 show that the Moire and difference results are in very close agreement; it might also be noted that the maximum deflection is 0.0233" for the smaller load, or about 0.182 times the plate thickness. When the load was doubled, the deflection was 0.0450", not quite double the previous deflection; for this load, the maximum deflection was 0.350 times the plate thickness. For the larger load, a part of the load is apparently resisted by membrane action of the plate.

Square, Uniformly Loaded, Simply Supported Plate

Fig. 16 shows the fringe patterns for this case, and Fig. 17 compares the moments and deflections along a center-line of the plate as determined by the Moiré method and by finite differences. The complete distribution of M_x, M_y and M_{xy} is given in reference 3, along with the finite difference results using grid spacings of both a/8 and a/16.

One of the purposes of this study was to determine whether simple support conditions could be obtained using the knife edge arrangement shown in Fig. 9. The boundary condition at the simply supported edge leads to the requirement that the curvature be zero in the direction of the edge and also perpendicular to it. For the first requirement to be met, it is necessary that the slope in the direction of the edge be zero; looking at Fig. 16, it is seen that this is particularly the case. To meet the requirement that curvature be zero perpendicular to an edge, it is necessary that the slope perpendicular to the edge be constant; that this is true is indicated by the fact that the fringes (lines of constant slope) are indeed perpendicular to the edges at the intersection points.

The moment results obtained by the Moiré method were, in general, five to ten percent less than those obtained by differences (which, for this case, agree very closely with theoretical values). The Moiré deflection results were also about ten percent below the exact values. Most of this difference can be accounted for by considering the membrane action of the plate.

Membrane action of plate

When a plate is deflected by lateral loading, a portion of the load is resisted by the flexure of the plate and a portion of the membrane stresses in

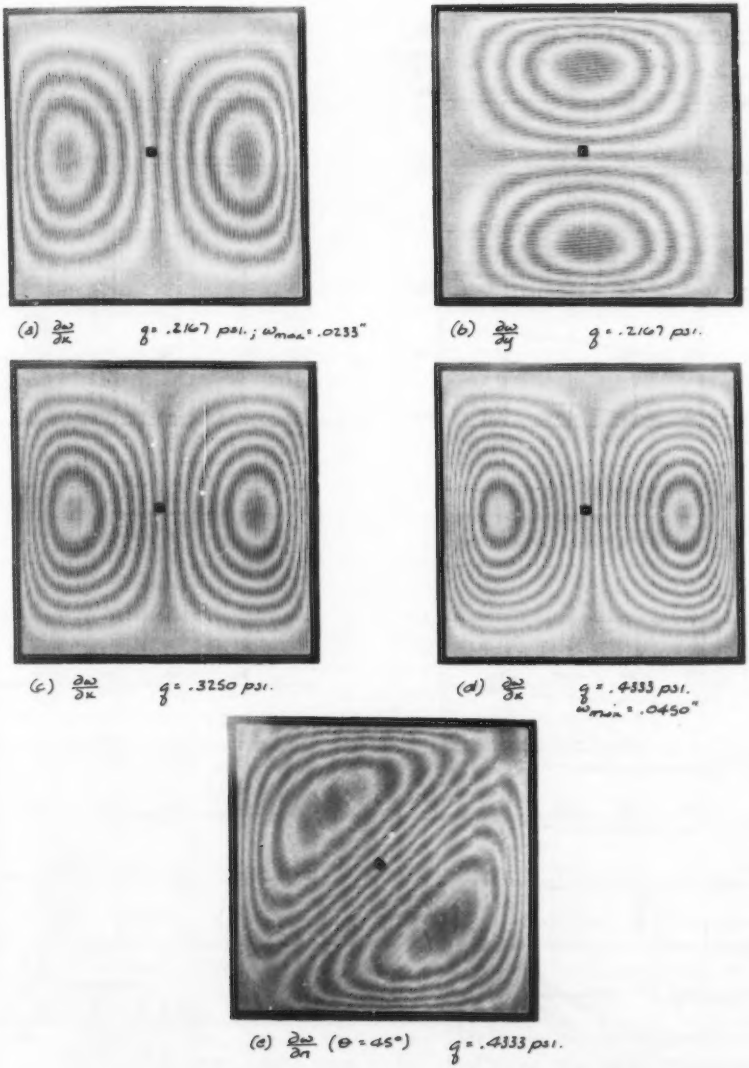
(a) $\frac{\partial \omega}{\partial x}$ $q = .2167$ psi.; $\omega_{max} = .0233"$
(b) $\frac{\partial \omega}{\partial y}$ $q = .2167$ psi.
(c) $\frac{\partial \omega}{\partial x}$ $q = .3250$ psi.
(d) $\frac{\partial \omega}{\partial x}$ $q = .4333$ psi. $\omega_{max} = .0450"$
(e) $\frac{\partial \omega}{\partial n}$ $(\theta = 45°)$ $q = .4333$ psi.

Fig. 13. Moiré patterns for uniformly loaded square clamped plate. Plate 9" square; average thickness = .1281".

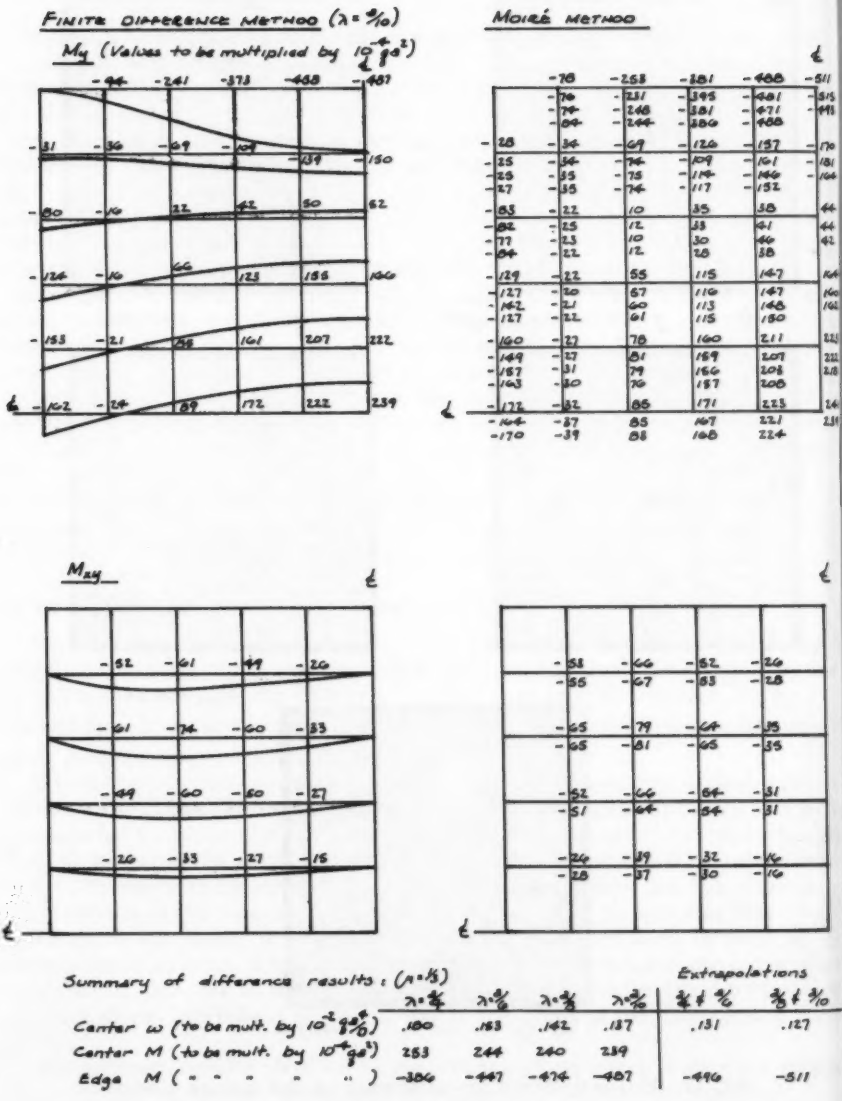
FINITE DIFFERENCE METHOD (λ = 1/10)
My (Values to be multiplied by 10⁻⁴ qa²)
MOIRÉ METHOD
Mxy
Summary of difference results: (ν = 1/3)
λ = 1/10
λ = 1/8
λ = 1/6
λ = 1/4
Extrapolations
1/8 & 1/6
1/6 & 1/10
Center ω (to be mult. by 10⁻² qa⁴/D) .180 .163 .142 .137 .131 .127
Center M (to be mult. by 10⁻⁴ qa²) 253 244 240 239
Edge M (" " " " ") -386 -447 -474 -487 -496 -511

Fig. 14. Moment distribution in uniformly loaded clamped square plate. Comparison of Moiré and difference results.

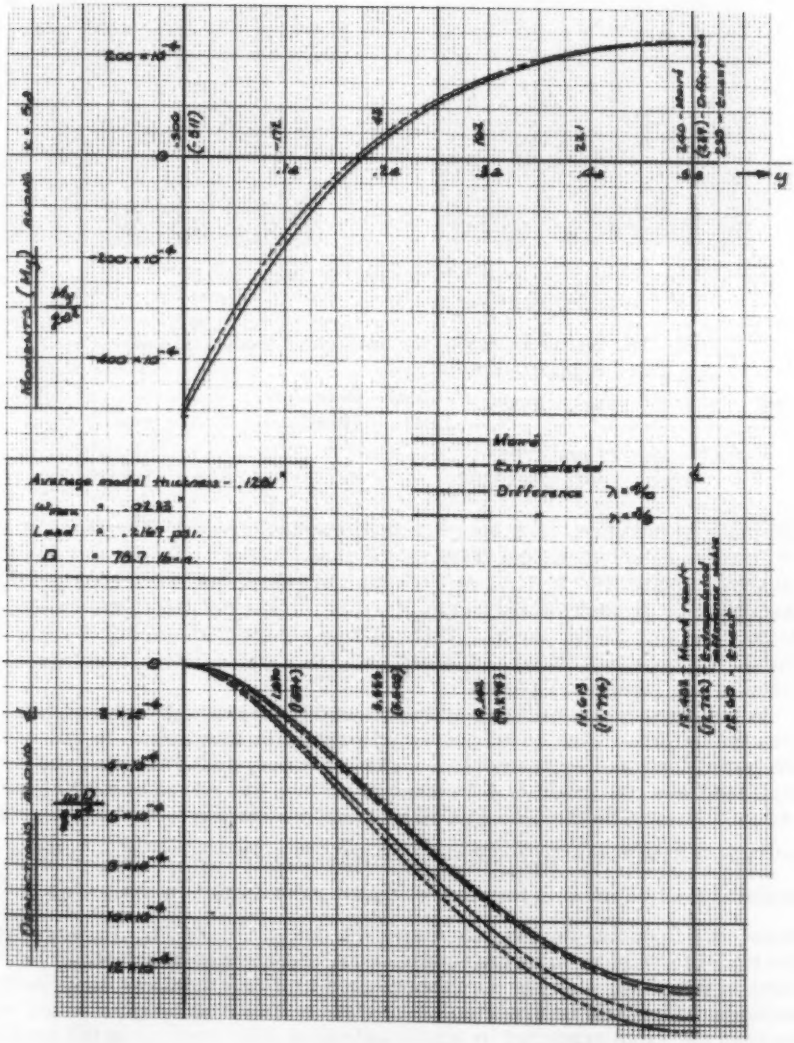

Fig. 15. Moments and deflections along centerline of square, uniformly loaded clamped plate.

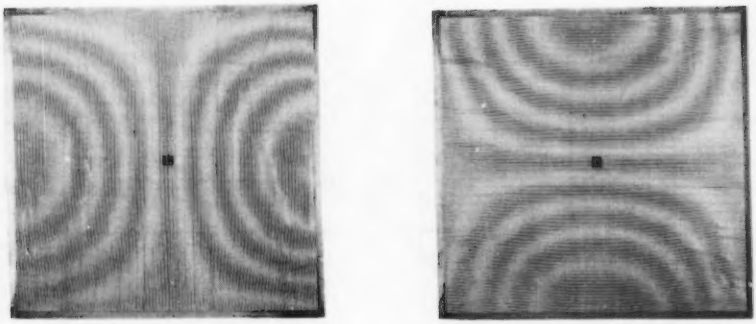

(a) $\frac{\partial w}{\partial x}$ (b) $\frac{\partial w}{\partial y}$

Fig. 16. Moiré patterns for uniformly loaded, simply-supported plate.

$q = .09028 \begin{cases} \text{initial} & .07222 \text{ psi.} \\ \text{final} & .16250 \text{ psi.} \end{cases}$

$t_{ave} = .1337''$

$w_{max} = .0230''$

the plane of the plate. For small deflections, the effect of membrane stresses is usually neglected and the deflection is taken to vary linearly with the load, as shown in Fig. 18. If, however, the membrane stresses are considered, as discussed by Timoshenko[7] and by Prescott,[8] the relation between load and deflection is no longer linear. This relation for the plate of Fig. 16 was computed, and is plotted in Fig. 18, along with the approximate percentage of load taken by the membrane action.

In the procedures followed, an initial load was always put on the plate before the initial—or "unloaded condition"—exposure was made. In this case, the initial load was equivalent to 2 inches of water, or 0.0722 psi., and the final load was equivalent to 4.5 inches of water. For a load of 4.5" of water, the calculated deflection, considering membrane stresses, is 0.041" and for 2" load, 0.0194"; the difference is 0.0216", or $34.6 \times 10^{-4} \frac{qa^4}{D}$. The actual model deflection for this increment of load was 0.0230" or $36.7 \times 10^{-4} \frac{qa^4}{D}$. Prescott's formula, used in calculating the deflections of Fig. 18, assumes the model to be held, allowing rotations but no edge displacements in the plane of the plate, whereas the support used probably did allow some such movement. It would be expected, then, that the model deflections would be between the value predicted by small deflection plate theory and the modified theory in which membrane stresses are considered; this was the case.

In the clamped plate of the Section, "Square, Uniformly Loaded, Clamped Plate," smaller initial load (1" of water) was used, since it was not necessary to seat the model against the supports; the increment of loading was 6" of water (0.2167 psi.) and the deflection due to this increment was 0.0233" or about one-sixth of the plate thickness; the maximum deflection due to the total load was about 0.027", or 0.21 times the thickness. The greater deflection, coupled with the fact that membrane action is greater in the unclamped

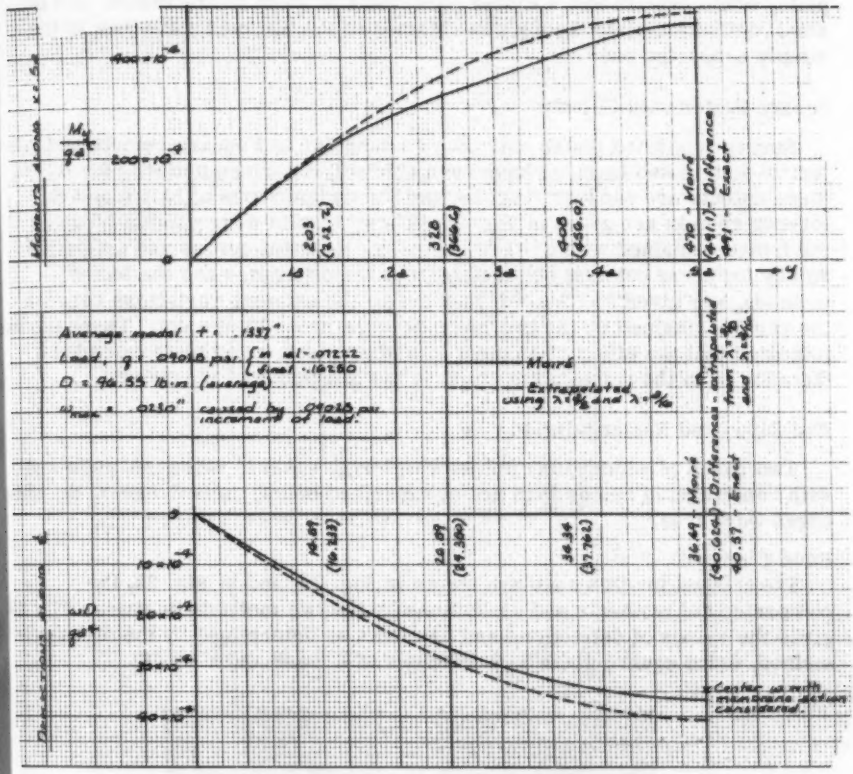

Fig. 17. Moments and deflections along centerline of square, uniformly loaded, simply-supported plate.

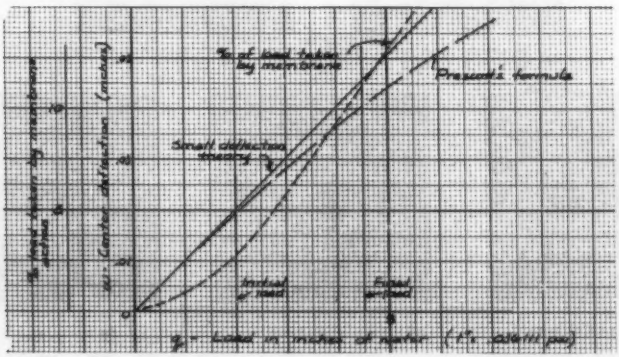
% of load taken by membrane
Pressure, psi
Pressure's formula
Small deflection theory
% of load taken by membrane
w, Center deflection (inches)
Initial crack
Failure load
q = Load in inches of water (1" = .036 psi)

Fig. 18. Effect of membrane stresses on plate action.

plate, would explain why a closer agreement between Moiré results and the small deflection plate theory was obtained in the clamped plate than in the simply supported one.

Square Plates with Cutouts

Simply supported plates with both rectangular and square cutouts and subject to distributed loadings have been studied; the fringe patterns for one of these cutouts are shown in Fig. 19, and the comparisons of Moiré and difference results are given in Fig. 20. These results were calculated using the fringes obtained with q = 1.5" of water. Moment curves and deflection values for other cutouts, obtained both by the difference and the Moiré methods, are given by Raju.[3] In general, the extreme variations between the results obtained by the two methods were about 10 percent. These studies indicated that the effect of a cutout in a simply supported plate extended a distance from the cutout about equal to the dimension of the cutout.

End Supported Rectangular Plates

Two cases of rectangular plates with length equal to twice the width and with concentrated center load are summarized below; in both cases, the side edges were free.

Ends Clamped

The fringes for this case are shown in Fig. 21, and in Fig. 22, the comparison of moments and deflections by the two methods is given. Fig. 2 gives the values of deflections and moments as determined by the difference method, using square grids with spacings of $\lambda = a/8$ and $\lambda = a/12$.

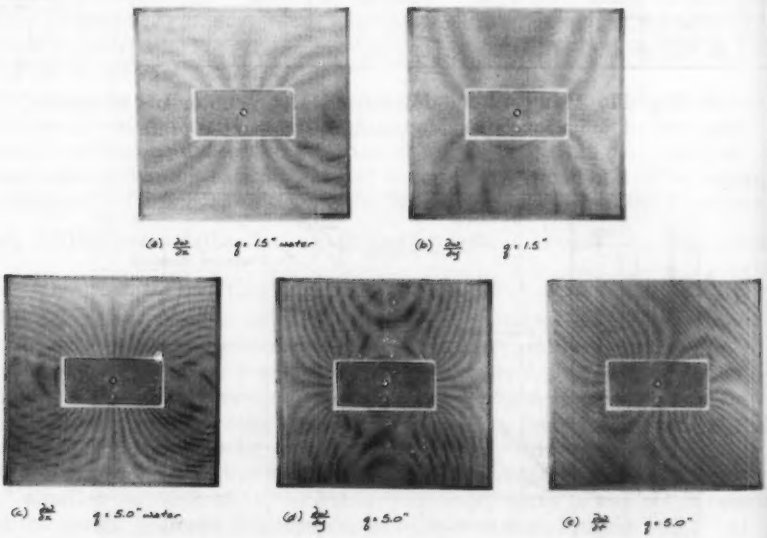
(a) $\frac{\partial^2 w}{\partial x^2}$ q = 1.5" water
(b) $\frac{\partial^2 w}{\partial y^2}$ q = 1.5"
(c) $\frac{\partial^2 w}{\partial x^2}$ q = 5.0" water
(d) $\frac{\partial^2 w}{\partial y^2}$ q = 5.0"
(e) $\frac{\partial^2 w}{\partial x^2}$ q = 5.0"

Fig. 19. Moiré fringes for simply supported plate with uniform load and control cutout.

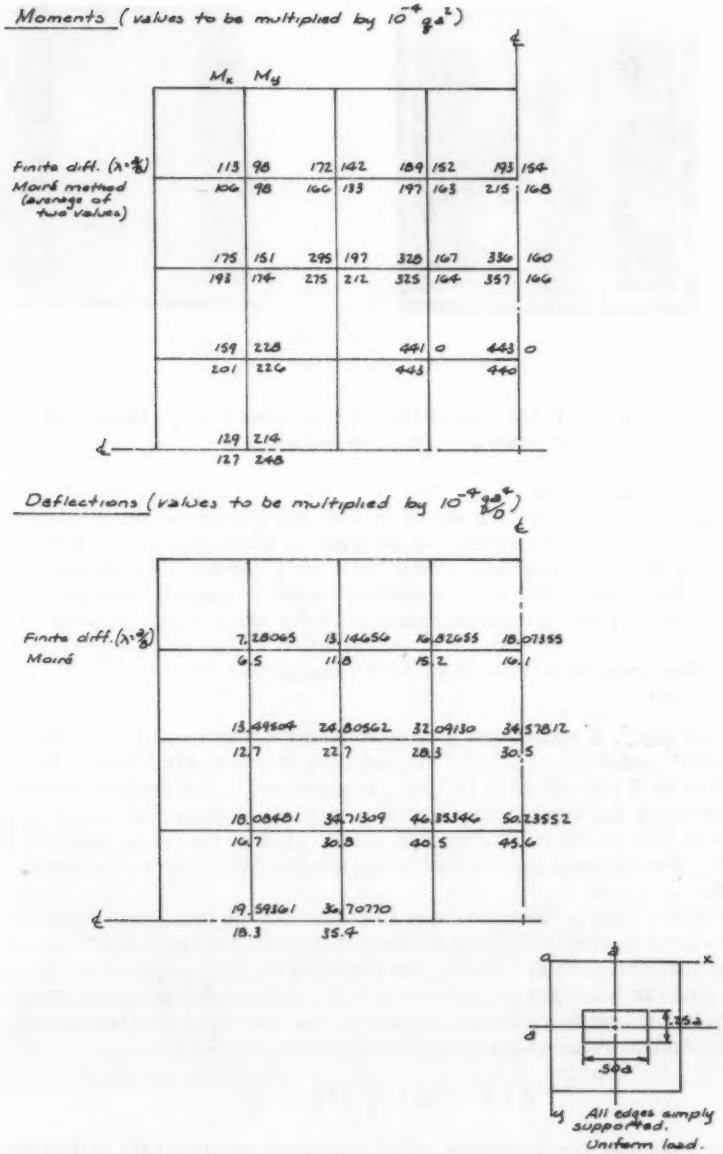

Fig. 20. Moments and deflections for plate with rectangular central cutout.

EM 4

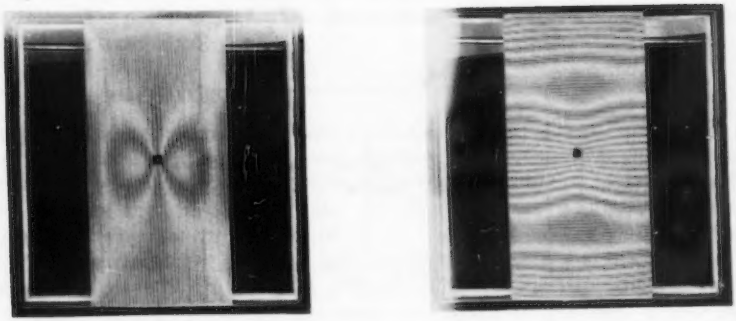

(a) $\frac{\partial w}{\partial x}$ (b) $\frac{\partial w}{\partial y}$

Fig. 21. Fringe patterns for rectangular plate, clamped at the ends and with free edges.

Ends Simply Supported

Fringes for this case are shown in Fig. 24; a comparison of moments and deflections along the centerline of the plate is given in Fig. 25; and, the finite difference moments and deflections for $\lambda = a/8$ and for $\lambda = a/12$ are given in Fig. 26. Note that at the section midway between supports, the deflections at the edge of the plate are greater than the deflections under the load.

Simply Supported Square Steel Plate—Concentrated Center Load

In this study, a square model of stainless steel was used. The thickness was 0.038" and Poisson's ratio and the modulus of elasticity were determined by test to be 0.243 and 29×10^6 psi., respectively. The surface was hand-polished using aluminum oxide powder; that this surface was not of as good quality as that on the plastic models is indicated by the fringe patterns in Fig. 27. The moment and deflection curves for this plate are shown in Fig. 28.

The initial load on the plate was 2 pounds and the final load was 8 pounds, with the incremental deflection between these loads being 0.0398", or slightly greater than the plate thickness. As expected for this large deflection, the actual value is less than calculated by finite differences using the small deflection theory. It was greater, however, than the value calculated using the large deflection relation given by Sturm and Moore,[9,10]

$$w\left[\,87 + 28\left(\frac{w}{t}\right)^2\,\right] = \frac{Pa^2}{D} \qquad (23)$$

For P = 2 pounds, the deflection calculated from equation (23) is 0.0126"; for P = 8 pounds, it is 0.0396"; for the increment of load from 2 to 8 pounds, the deflection is 0.0270", or $0.007743\ Pa^2/D$. Formula (23) is given for a plate with corners held and edges free to rotate. In this test, the corners were not held, so that actual deflections somewhat greater than given by this formula would be expected.

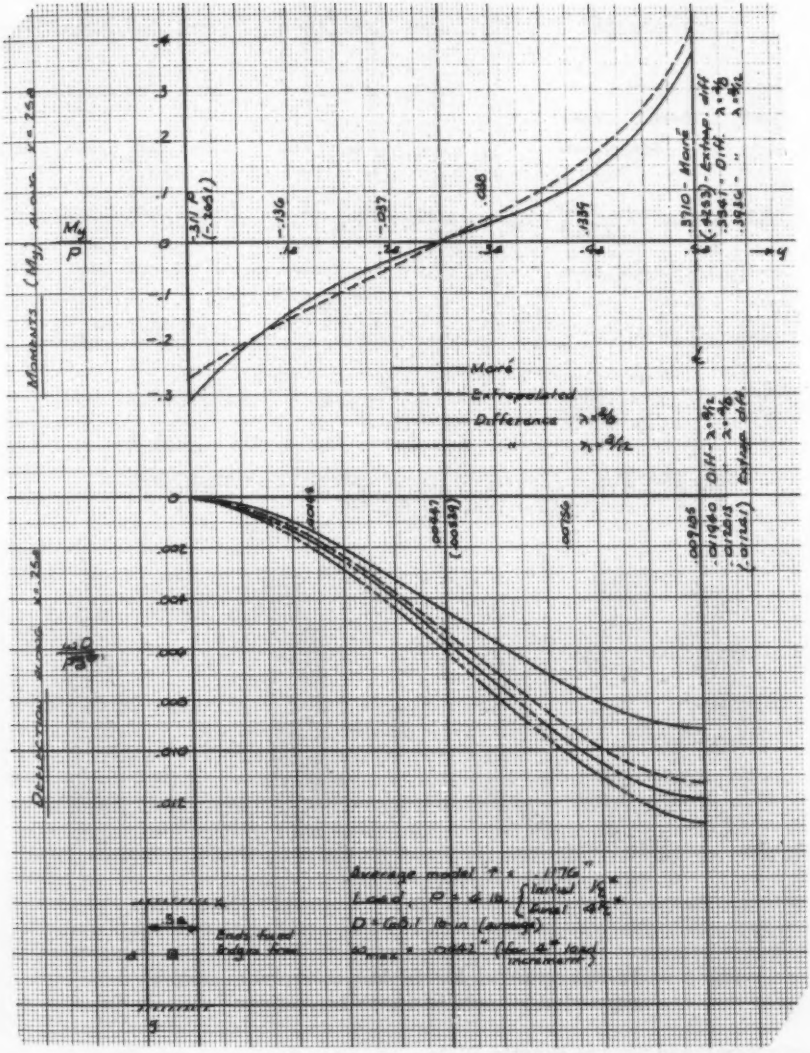

Fig. 22. Moments and deflections along centerline of rectangular plate with ends clamped, edges free, and with concentrated center load.

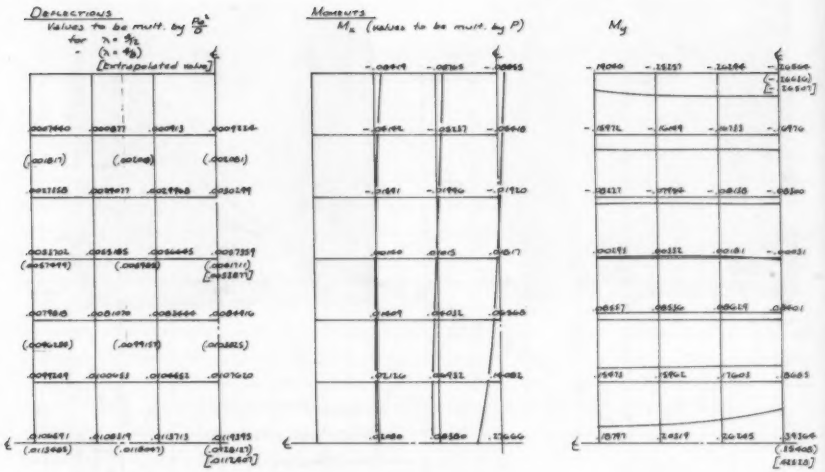

Fig. 23. Finite difference moments and deflections for rectangular plate of Fig. 22.

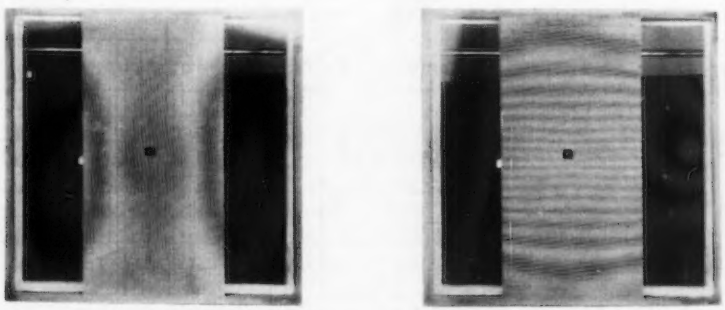

(a) $\frac{\partial \omega}{\partial x}$ (b) $\frac{\partial \omega}{\partial y}$

Fig. 24. Fringe patterns for rectangular plate, simply supported at ends and with free edges.

Simply Supported Square Plastic Plate— Concentrated Center Load

The fringe patterns are shown in Fig. 29, and the moments and deflections along the center line are compared in Fig. 30. The results obtained by the two methods are in close agreement for the deflections, and the center deflections obtained from equation (23) agrees well with the experimental value. The Moire values for moment are about 15 percent lower than the difference values.

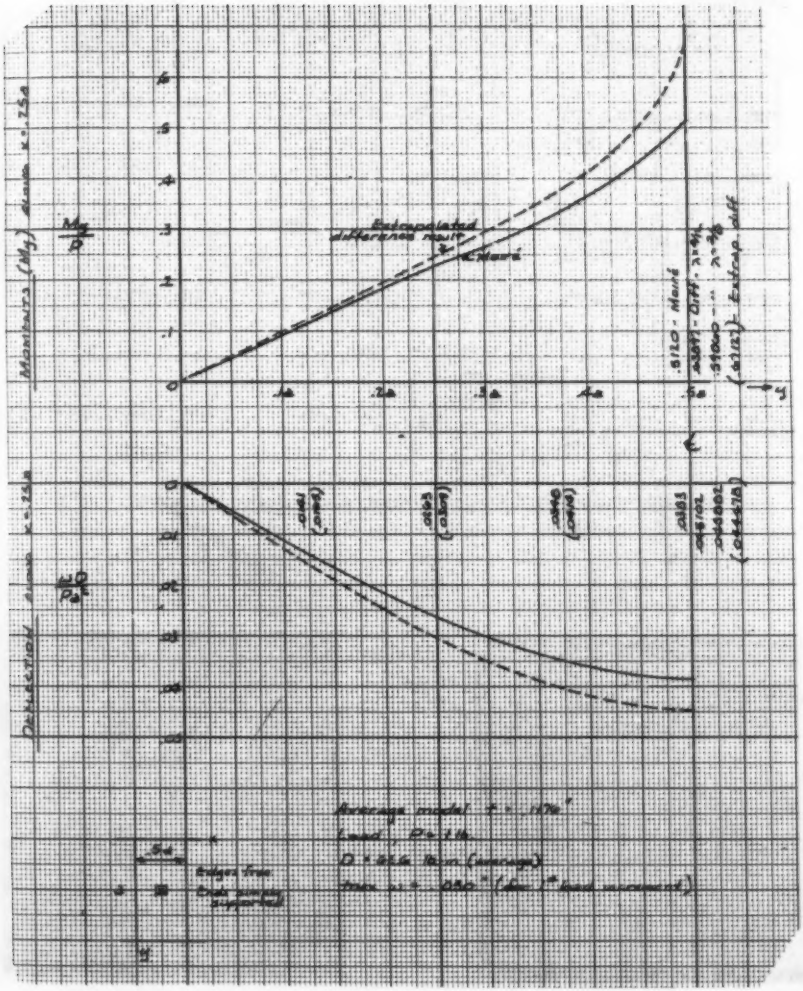

Fig. 25. Moments and deflections along centerline of rectangular plate with ends simply supported, edges free, and with concentrated center load.

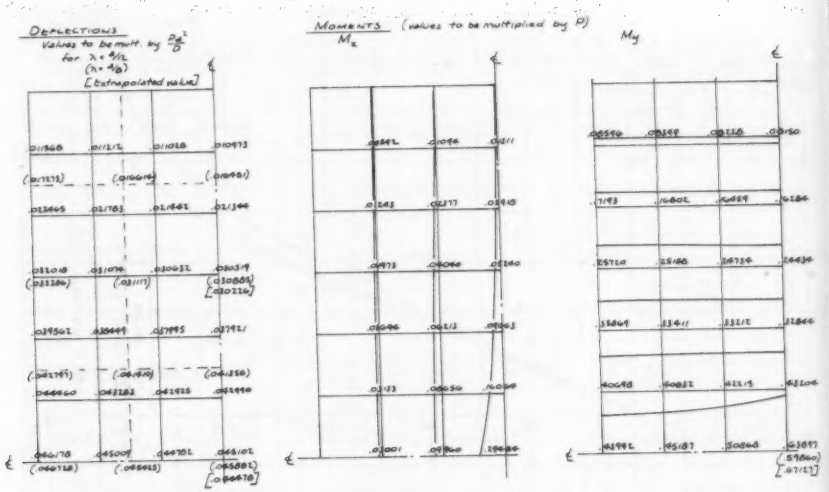

Fig. 26. Finite difference moments and deflections for rectangular plate of Fig. 25.

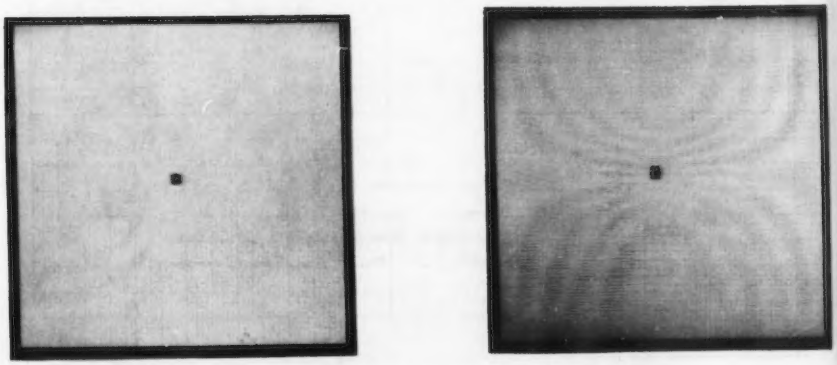

Fig. 27. Fringe patterns for simply supported square steel plate with concentrated center load.

Discussion

In the test procedure followed in these studies, several possible sources of error can be listed. Among these are:

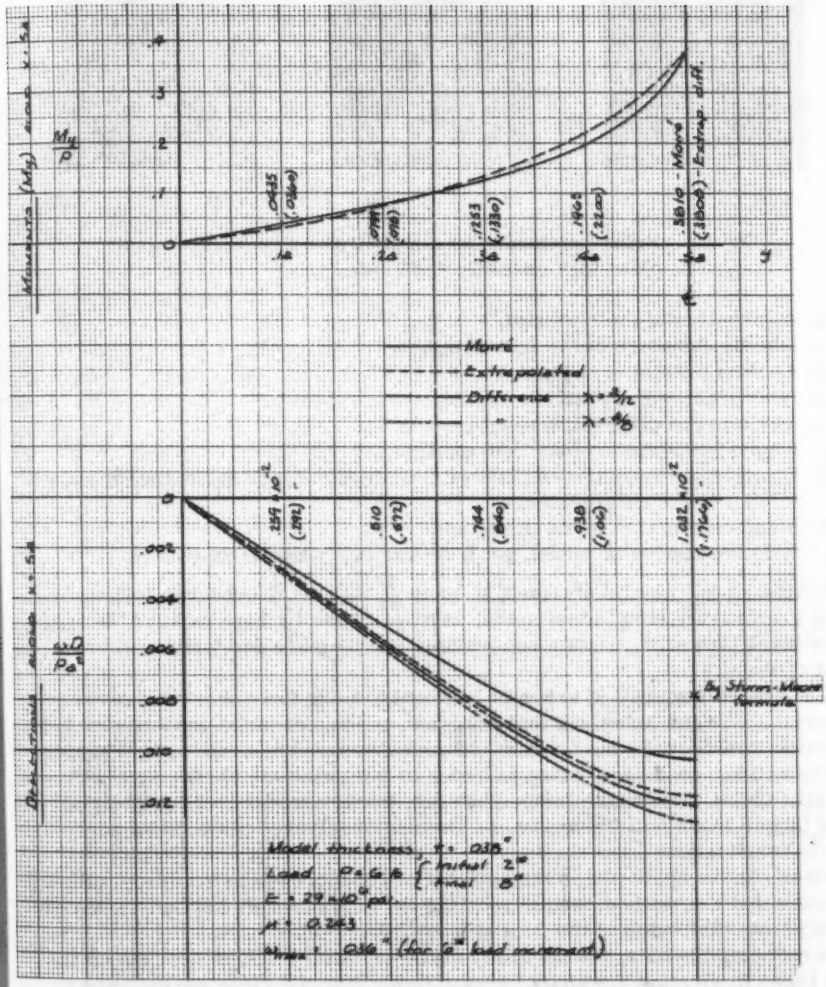

Fig. 28. Moments and deflections for square, simply supported steel plate with concentrated center load.

Fig. 29. Fringe patterns for simply supported square plastic plate with concentrated center load.

a. Calibration of the material,
b. Plastic Behavior of the material,
c. Lack of precision in loads,
d. Inaccuracies in reduction of data,
e. Variation in plate thickness,
f. Support conditions other than assumed,
g. Changes in dimension of photographic film during developing, and distortion in the enlargements,
h. Membrane action in the plate, and
i. Relative motion of model, grid, or camera between exposures.

In view of the results obtained, it appears that the procedures followed, using a relatively simple test setup, have successfully kept most of these at a low level; however, certain suggestions can be made for further improvement of results.

The greatest source of error is believed to be in the calibration of the material. For any extensive test program, the use of metal models should be seriously considered. Such use would probably require a more rigid supporting frame than used here, since in order to minimize membrane stresses and still obtain reasonable fringe patterns, thicker models with correspondingly larger loads will be required. The use of silvered plate glass might also be considered.

Glass photographic plates may offer a slight increase in accuracy, although it seems that the method used in locating the slope fringes kept any error resulting from distortion of the film at a low level.

In reducing the data, the accuracy of the curvature values depends on the care taken in locating the slope fringes, in plotting the slope curves, and in determining the curvatures. It seems possible that two different workers, starting from the same set of slope pictures, might obtain moment results varying by as much as ten percent; the deflection results, however, being obtained by integration, should not vary as widely.

CONCLUSIONS AND FUTURE WORK

The results obtained in this study indicate that useful information can be obtained by the use of Moiré method with the setup described and using plastic

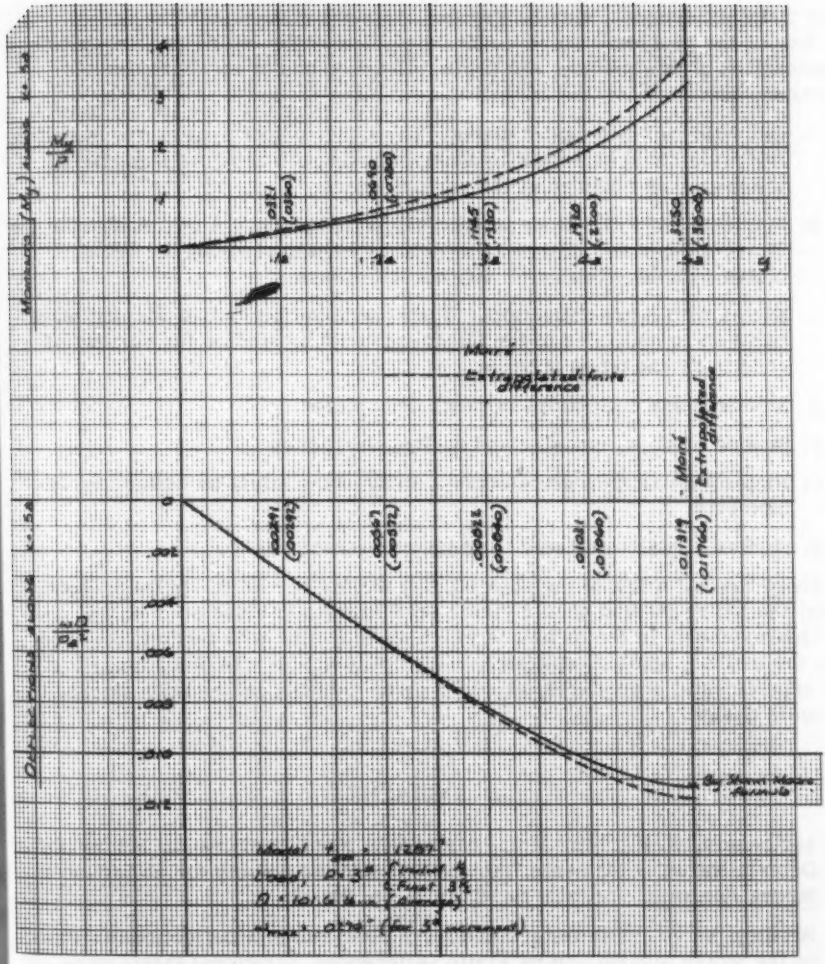

Fig. 30. Moments and deflections for square, simply supported plate with concentrated center load.

models; with the suggested revisions, greater precision should be attainable. The method should be particularly applicable in the study of unusual shaped plates with boundary conditions which are difficult to formulate.

In some cases, however, even though formal mathematical solutions are not possible or practical, numerical approximations, such as those obtained with finite differences, may be quicker and more economical.

Among the problems which might be studied by the Moiré method or by a combination of this method with finite difference and other approximate methods, are:

a. Behavior of viscoelastic plates. The fringe patterns after various time intervals could be sought by superimposing the unloaded negative on the negatives obtained at the various times.

b. Moments and deflections in edge supported plates. A combination of the Moiré method and differences could be used in studying the behavior of plates with edge beams of various stiffnesses.

c. Plates with large deflections. Plates with deflections of varying magnitudes up to multiples of the thickness could be studied for various edge conditions and types of loads.

d. Moments and deflections in continuous plates.

e. Studies of skew, circular and rectangular plates.

f. Plates with reinforced cutouts—a study of the effect on deflections and moments.

g. Studies of plate elements in composite structures.

These are but a few of the possibilities for further work. In its present state, the Moiré method should yield useful results in these studies, and with the improvements in the technique which should come with further and wider use, the method, applied separately and in conjunction with other analytical and experimental procedures, should provide valuable information for application in design.

BIBLIOGRAPHY

1. Ligtenberg, F. K., "The Moiré Method—A New Experimental Method for Determination of Moments," Proceedings of the Society for Experimental Stress Analysis, Vol. XII, No. 2, 1955, pp. 83-98.

2. Bradley, W. A., "The Determination of Moments and Deflections in Plates by the Moiré Method and by Finite Differences," Doctoral thesis submitted to the University of Michigan, 1956.

3. Raju, B. B., "A Study of Simply Supported Square Plates by the Moiré Method and by Finite Differences," Masters thesis submitted to Michigan State University, 1958.

4. Presan Corporation, "Photo Reflective Stress Analysis," a pamphlet prepared by Presan Corp.; Los Angeles 39, California.

5. Salvadori, M. G. and Baron, M. L., Numerical Methods in Engineering, Prentice-Hall, Inc., New York, 1952.

6. Jensen, V. P., Analysis of Skew Slabs, University of Illinois Engineering Experiment Station, Bulletin 332, 1941.

7. Timoshenko, S. P., Theory of Plates and Shells, McGraw-Hill Book Co., New York, 1940.

8. Prescott, J., Applied Elasticity, Dover Publications, New York, 1946.

9. Sturm, R. G. and Moore, R. L., "The Behavior of Rectangular Plates under Concentrated Load," Journal of Applied Mechanics, A.S.M.E., Paper A-75, Vol. 4, No. 2, 1937.

10. Roark, R. J., Formulas for Stress and Strain, McGraw-Hill Book Co., New York, 1943.

Journal of the
ENGINEERING MECHANICS DIVISION
Proceedings of the American Society of Civil Engineers

BEHAVIOR OF STRUCTURES DURING EARTHQUAKES

G. W. Housner,[1] Member ASCE

This paper is one of the group of papers which were the bases for oral presentations at the Joint ASCE-IABSE Meeting, New York, October 1958. The entire group, including those published in CIVIL ENGINEERING, will be reprinted in one volume.

ABSTRACT

The behavior of structures during earthquakes is described by response spectrum curves which show the effect of size and distance of earthquake and period and damping of structure. High elastic stresses are developed during strong ground motion, so the desirability of a type of limit design is indicated.

SYNOPSIS

The behavior of structures during earthquakes is described by so-called response spectrum curves which are, in effect, influence diagrams for the maximum displacements, shears, etc. The spectrum curves show how the response of a structure is affected by the size and distance of the earthquake and by the natural period and damping of the structure. It is found that during strong ground motion ordinary structures will be subjected to larger accelerations than are prescribed by building codes and, therefore, the behavior of the structure depends strongly upon its ability to dissipate vibrational energy when it is overstressed. This indicates the desirability of a type of limit design for structures in seismically active regions.

Note: Discussion open until March 1, 1960. Separate discussions should be submitted for the individual papers in this symposium. To extend the closing date one month, a written request must be filed with the Executive Secretary, ASCE. Paper 2220 is part of the copyrighted Journal of the Engineering Mechanics Division, Proceedings of the American Society of Civil Engineers, Vol. 85, No. EM 4, October, 1959.

1. Prof. of Civ. Engr., California Institute of Technology, Pasadena, Calif.

The damage caused in Mexico City[1] by the earthquake of July, 1957 was a sharp reminder of the importance of aseismic design of structures. The conclusions drawn from observations in Mexico City agreed, in general, with those derived in United States cities after earthquakes and pointed up once again the fact that conservatively designed structures survive with at most minor damage, whereas structures not designed to resist earthquakes may collapse, as a number of them did in Mexico City. Structures unconservatively designed against earthquakes in many instances suffered extensive damage such as shattering of walls, buckling or fracturing of columns, and failing of beams in bending. In some cases large multi-story buildings were so badly damaged that it seemed a miracle that they did not collapse. Although the intensity of ground motion in Mexico City was not high by California standards, it was appreciably more intense than most Mexico City engineers had anticipated. From the point of veiw of what can happen when a city is shaken more severely than the building code anticipates, the Mexico City experience was particularly interesting.

It was already known from United States experience that improper design and construction leads to damage during an earthquake so that this aspect of the Mexico City experience was not particularly informative. However, very interesting building behavior in Mexico City was shown by those buildings that were damaged more or less seriously but did not collapse. At first glance, many of these cases seemed paradoxical. For example, some structures were so badly damaged with failed beams, columns, and walls that from a stress analysis point of view it appeared that hardly any lateral strength remained. Since the duration of ground motion was close to 60 seconds, before the end of the earthquake these structures must have been in an advanced stage of damage but yet they survived.

In other cases a damaged building remained standing even though a standard lateral strength analysis of the building in its damaged state would indicate that its strength was so small that it should have collapsed. On the other hand some relatively sturdy structures having much greater lateral resistance suffered some damage.

It was particularly striking to observe that the old masonry structures in most cases came through with little if any damage, whereas the relatively modern multi-story buildings in many cases suffered severe damage; and this was not because the old buildings were particularly well designed or well constructed. Many of the modern buildings were seriously damaged, whereas some old buildings with low lateral strengths survived with no apparent damage.

It is not possible to account for the foregoing behavior on the basis of the ordinary methods of seismic analysis where the structure is conceived to resist a specified static lateral force. To understand such behavior, it is necessary to examine the performance of structures during earthquakes from the viewpoint of dynamics and to analyze the vibrations induced by the ground motions. If sufficient were known about the physical properties of the structures and about the ground motion during the earthquake, a thorough vibration analysis would, of course, completely explain the observed behavior. Although such detailed information is not available it is possible, by using the results of analyses of past earthquakes to explain the observed behavior.

1. Earthquake Ground Motions. A typical strong ground motion record is shown in Fig. 1. This motion was recorded approximately 30 miles from the center of the fault. Ground motion more intense than this has been recorded during other earthquakes, the most intense being approximately 50% stronger.

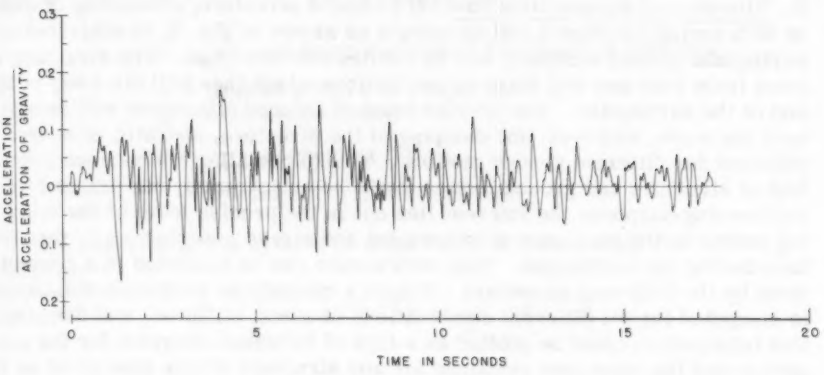

FIG. 1 - ACCELEROGRAM FOR TAFT, CALIFORNIA; EARTHQUAKE OF JULY 21, 1952. COMPONENT S 69 E.

In Fig. 10 is shown the ground motion recorded during this earthquake at a distance of approximately 70 miles from the center of the fault. This illustrates how the intensity of motion diminishes with distance.

Fig. 2 shows the recorded ground motion at a point close to the epicenter of the small earthquake at San Francisco, 22 March 1957. The duration of the motion was very short compared with that of a large earthquake. This motion was recorded on rock whereas the motion shown in Fig. 11 was recorded during the same earthquake on 120 feet of alluvium.

The foregoing ground motions were recorded on U. S. Coast and Geodetic Survey strong-motion accelerometers having a natural frequency of vibration of approximately 18 cycles per second.

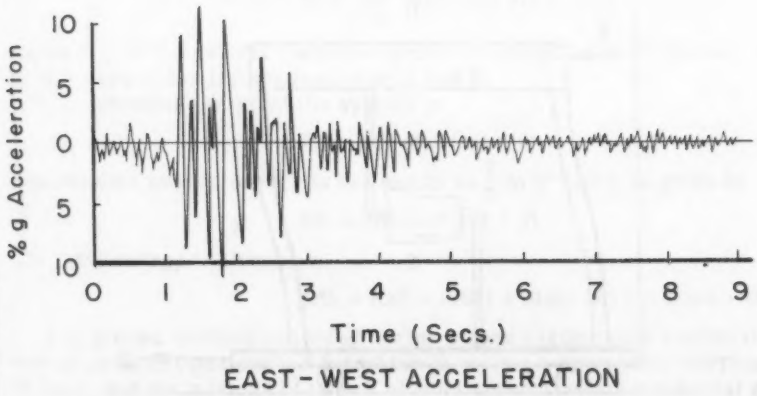

FIG. 2 - GOLDEN GATE PARK ACCELEROGRAM, 22 MARCH 1957

Recorded 7.8 Miles From Center Of Shock

2. Vibration of Simple Structure. If a simple structure, consisting of a mass m with spring constant k and damping c as shown in Fig. 3, is subjected to earthquake ground motion it will be excited into vibration. The structure will start from rest and will build up oscillations which then will die away at the end of the earthquake. The precise form of induced vibrations will depend upon the mass, stiffness, and damping of the structure, and will, of course, be different for different ground motions. To explore all of the various possibilities of structure and ground motion would be an extremely big job; however, for engineering purposes the interest lies not in the precise form of the vibration but rather in the maximum displacement and stress experienced by the structure during the earthquake. This information can be exhibited in a convenient form by the following procedure. If such a quantity as maximum displacement is computed for all different combinations of mass, stiffness, and damping, this information could be plotted as a type of influence-diagram for the ground motion and the maximum response for any structure of this type could be read from the diagram. This has been done as described below.

Newton's equation of motion for the system is

$$m \frac{d^2}{dt^2}(y + z) = -ky - c \frac{dy}{dt}$$

or

$$m\ddot{y} + c\dot{y} + ky = -m\ddot{z} \qquad (1)$$

The relative motion y is thus the same as for a structure resting on an immovable base and subjected to a horizontal force $(-m\ddot{z})$. As is well-known the displacement of the structure is given by

$$y = -\frac{1}{\omega} \int_0^t \ddot{z}(\tau)\, e^{-n(t-\tau)} \sin\omega(t-\tau)\, d\tau \qquad (2)$$

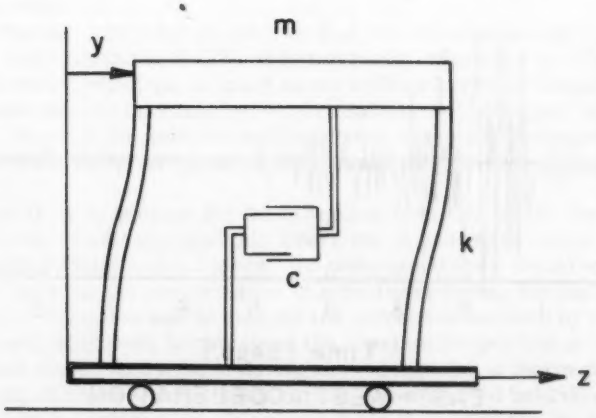

FIG. 3 - ONE DEGREE OF FREEDOM STRUCTURE

where $\omega = \sqrt{p^2 + n^2}$ = circular frequency

$p = \sqrt{\frac{k}{m}}$ = undamped circular frequency of vibration

t = time at which y is evaluated

$\ddot{z}$ = base acceleration

$n = \frac{c}{2m}$ = damping factor

$\frac{n}{p}$ = fraction of critical damping

The behavior of the system is made clear by introducing the following notation

$$\int_0^t \ddot{z}\ e^{-n(t-\tau)} \cos \omega\tau\ d\tau = A$$

$$\int_0^t \ddot{z}\ e^{-n(t-\tau)} \sin \omega\tau\ d\tau = B$$

$$\frac{1}{2}(A^2 + B^2)\left(1 + \frac{n^2}{\omega^2}\right) = E$$

Using trigonometric identities it can be shown that the motion of the system is described by the following equations for relative displacement and velocity, and for absolute acceleration

$$y = -\frac{T_o}{2\pi}\sqrt{2E}\ \sin(\omega t + \alpha) \tag{3}$$

$$\dot{y} = -\sqrt{2E}\ \cos(\omega t + \beta) \tag{4}$$

$$(\ddot{y} + \ddot{z}) = \frac{2\pi}{T_o}\sqrt{2E}\ \sin(\omega t + \gamma) \tag{5}$$

where T_o is the natural undamped period of vibration of the system and α, β, γ are phase factors involving A and B.

The potential energy of the system is

$$PE = mE \sin^2(\omega t + \alpha) \tag{6}$$

The relative kinetic energy is defined to be $\frac{1}{2} m \dot{y}^2$ and it is given by

$$KE = mE \cos^2(\omega t + \beta) \tag{7}$$

The total energy is then

$$(PE + KE) = mE(1 + \sin(\alpha - \beta) \sin(2\omega t - \alpha - \beta) \tag{8}$$

The ground motions recorded during strong earthquakes exhibit the properties of random functions[2, 3] for which E, α, β, γ, are slowly varying functions of time, and the motions of y, $\dot{y}$, $\ddot{y}$ closely approximate a sinusoidal shape. For moderate amounts of damping the factor $(\alpha - \beta)$ may be set equal to zero and the maximum total energy is closely given by

$$m\bar{E} = m\frac{1}{2}(A^2 + B^2)_{max} \tag{9}$$

Where $\overline{E}$ is the maximum total energy per unit mass attained by the structure during the earthquake. The maximum relative displacement, relative velocity, and absolute acceleration attained by the system may be written

$$y_{max} = \frac{T_o}{2\pi}\sqrt{2\overline{E}} = \frac{T_o}{2\pi}\,\dot{y}_{max} = \frac{T_o}{2\pi}\,S_v$$

$$\dot{y}_{max} = \sqrt{2\overline{E}} = S_v \qquad (10)$$

$$(\ddot{y} + \ddot{z})_{max} = \frac{2\pi}{T_o}\,S_v$$

where the notation S_v is used for $\dot{y}$ max. The maximum shear force developed in the structure is

$$F_{max} = ky_{max} = k\frac{T_o}{2\pi}\,S_v = k\sqrt{\frac{m}{k}}\,S_v = \sqrt{km}\;S_v \qquad (11)$$

The maximum inertia force acting on the mass is

$$m(\ddot{y} + \ddot{z})_{max} = m\frac{2\pi}{T_o}\,S_v = m\sqrt{\frac{k}{m}}\,S_v = \sqrt{km}\;S_v$$

which, of course, agrees with equation (11).

The maximum response of the structure is thus characterized by the value of S_v which for moderate damping may be written

$$S_v = \left(\int_o^t \ddot{z}\, e^{-n(t-\tau)} \sin\omega(t-\tau)\, d\tau \right)_{max} \qquad (12)$$

It is found* that the response of an undamped structure builds up roughly proportional to the square root of the duration of the earthquake ground motion, whereas, the response of a damped structure builds up until the energy loss balances the energy input.

A one-mass system that can vibrate in both horizontal directions will respond to both horizontal components of ground motion and the resultant motion is given by the superposition of the two component responses, but the values of S_v will not, in general, occur at the same time for the two components.

3. Complex Structures. A multi-story building will have several modes of vibration and consequently its response to ground motion will be more complicated than is the case for a simple one-mass system. The general nature of the motion can be elucidated by the following considerations. Consider a general elastic structure vibrating in the x-z plane as shown in Fig. 4. Let the structure be linearly elastic and let it be such that its free vibrations can be resolved into normal modes of vibration that are orthogonal. The free vibrations may then be written

$$y = \sum_i C_i\, \phi_i(x) \sin p_i t$$

where

y = displacement at point x
$\phi_i(x)$ = shape of i^{th} mode of vibration
P_i = circular frequency of i-th mode
C_i = amplitude of i-th mode

*This follows from the fact that earthquake ground acceleration is essentially a random function.

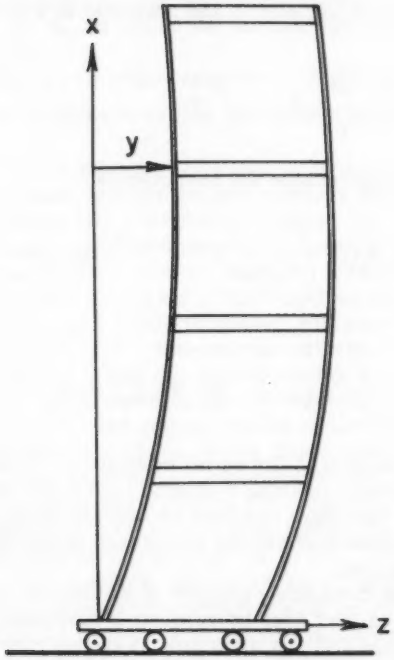

FIG. 4 - MULTI-DEGREE OF FREEDOM STRUCTURE

As in the case of the simple oscillator, the response y to base acceleration $\ddot{z}$ is the same as the response to a lateral force $-m\ddot{z}$ acting on each element of mass m. The effect of $\ddot{z}$ acting for an increment of time dt is to produce an increment of velocity at each point of the structrue.

$$dv = -\ddot{z}\, dt$$

since

$$\dot{y} = \sum_i C_i\, p_i\, \phi_i(x) \cos p_i t$$

at time dt

$$-\ddot{z}\, dt = \sum_i C_i\, p_i\, \phi_i(x)$$

and from the orthogonality of the $\phi_i(x)$

$$C_i = \frac{\int \phi_i\, dm}{p_i \int \phi_i^2\, dm}\,(-\ddot{z}\, dt) = \frac{D_i}{p_i}\,(-\ddot{z}\, dt)$$

where dm indicates that the integrals are to be evaluated over the mass of the structure. The consequent free vibrations are thus given by

$$y = \sum_i \frac{D_i}{p_i}\, \phi_i(x) \sin p_i t\, (-\ddot{z}\, dt)$$

As in the case of the simple oscillator, the response to a continuous $\ddot{z}$ is the summation over t:

$$y = - \sum_i \frac{D_i}{p_i} \phi_i(x) \int_o^t \ddot{z}(\tau) \sin p_i(t - \tau)\, d\tau \qquad (13)$$

If there is damping in the structure the response is

$$y = - \sum_i D_i \phi_i(x) \left\{ \frac{1}{p_i} \int_o^t \ddot{z}\, e^{-n(t-\tau)} \sin p_i(t - \tau)\, d\tau \right\} \qquad (14)$$

or

$$y = - \sum_i D_i \phi_i(x) \left\{ \frac{T_{oi}}{2\pi} \sqrt{2E_i} \sin(p_i t + \alpha_i) \right\}$$

The expression in the brackets is the same as equation (3) which gives the response of a simple structure having a natural undamped period T_{oi}. The response of the complex structure can thus be determined if the mode shapes are known and if the responses of simple structures of the appropriate periods and damping can be computed.

The computation of the complete response of a complex structure is extremely laborious and is best done by computing machines.

By analogy with equation (10) the maximum response may be written

$$y_{max} = \sum_i D_i \left| \phi_i(x) \right| \frac{T_{oi}}{2\pi} S_v \qquad (15)$$

Similar expressions involving S_V can be written for the maximum forces, stresses, shears, bending moments, etc., if in each case the maximum absolute value for each mode is added.(4) The analysis of structures more complicated than the above can also be carried out in a similar fashion and results similar to equations (14) and (15) will be obtained.

From equation (14) it is seen that the true maximum response will, in general, be somewhat less than the right side of equation (15) since each term in equation (14) contains a trigonometric expression which varies between positive and negative values, and in addition the amplitude functions, $\sqrt{2E_i}$, vary with time. Thus, there is only a small probability that all of the terms will reach their peak values and be additive at exactly the same time. Studies made at the California Institute of Technology show that for strong earthquake ground motions, if only two well separated modes of vibration are involved, equation (15) overestimates the true maximum by about 5%-10%. However, if three or four modes are involved and the maximum of each has approximately the same value, equation (15) may significantly overestimate the true maximum value. For such cases it has been proposed(3) to use the geometric mean of the maxima.

4. Earthquake Spectra. As shown by equations (10), (11), (14), (15), the values of S_V will describe the maximum response of a wide class of structures. The S_V is called the velocity spectrum(5, 6) of the ground motion and a plot of it is

in effect an influence diagram for the maximum velocity of a simple structure. S_D, which is equal to $\frac{T}{2\pi} S_V$, is called the displacement spectrum and $S_A = \frac{2\pi}{T} S_V$ is called the acceleration spectrum. A plot of S_V gives a concise picture of the effect of the ground motion and in this sense it characterizes the ground motion.

A plot of S_V for a typical strong earthquake ground motion is shown in Fig. 5. This gives the maximum velocity response over a significant range of periods and for 0%, 10% and 20% of critical damping. The shapes of these curves are typical for ground motion measured moderately close to the epicenter of a large earthquake. In fact, when the normalized spectra for eight components of the four strongest ground motions yet recorded (El Centro 1934, El Centro 1940, Olympia 1949, Tehachapi 1952) are averaged, a quite smooth set of curves is obtained. The average velocity spectrum for strong ground motion shown in Fig. 7 and the corresponding average acceleration spectrum shown in Fig. 8 are based on the average of the four shocks.

The velocity spectrum for the ground motion recorded in Hollywood during the 1952 Tehachapi shock(7) is shown in Fig. 6 and this is very similar to that for the ground motion recorded at Pasadena,(7) both recordings being approximately 70 miles from the center of the fault. It is seen that the shape of this spectrum is different from that of Fig. 5 which is for the same earthquake but at approximately 30 miles from the center. The short period end of the spectrum in Fig. 6 is relatively depressed as compared to Fig. 5 thus indicating that the higher frequency components of the ground motion attenuate with distance more rapidly than the lower frequency components.

For ground motion of relatively small earthquakes, such as the shock at San Francisco, 22 March 1957, recorded quite close to the epicenter the

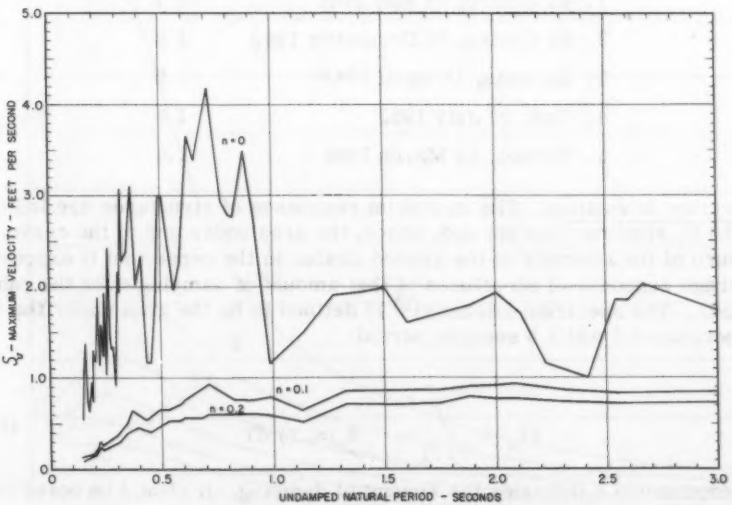

FIG. 5 - VELOCITY SPECTRA FOR TAFT, CALIFORNIA, EARTHQUAKE OF JULY 21, 1952. COMPONENT N 21 E.

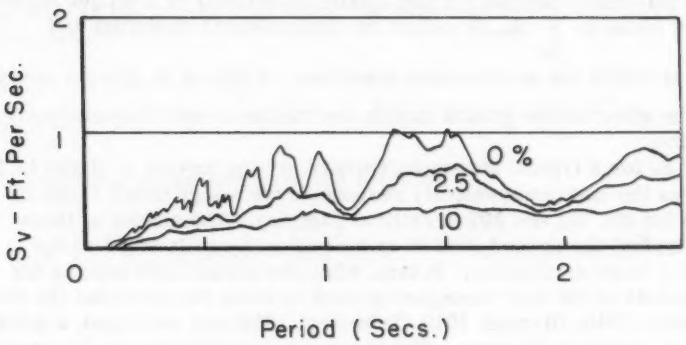

FIG. 6 - E-W VELOCITY SPECTRA, HOLLYWOOD, 21 JULY 1952

velocity spectrum is found[8] to be relatively high in the low period end. Fig. 9 illustrates the differences in shapes of spectra according to whether the shock is large or small and whether the epicenter is near or distant. The curves represent approximately the Taft, 21 July 1952, Hollywood, 21 July 1952, and San Francisco, 22 March 1957 spectra.

The ordinates of Figs. 7 and 8 should be multiplied by the following scale factors to bring them in agreement with the following recorded ground motions:

	Factor
1. El Centro, 18 May 1940	2.7
2. El Centro, 30 December 1940	1.9
3. Olympia, 13 April 1949	1.9
4. Taft, 21 July 1952	1.6
5. Vernon, 10 March 1933	1.5

5. Spectrum Intensities. The maximum responses of structures are indicated by the S_V spectrum curves and, hence, the area under one of the curves is a measure of the intensity of the ground motion in the sense that it expresses the average response of structures of that amount of damping over the range of periods. The spectrum intensity[9] is defined to be the area under the curve between 0.1 and 2.5 seconds period:

$$SI_n = \int_{0.1}^{2.5} S_V(n, T)\, dT \qquad (16)$$

In this expression n indicates the amount of damping. It should be noted that the spectrum intensity is an objective measure of the maximum stresses that would be induced in elastic structures by the ground motion. On the other hand, the comomnly used Modified-Mercalli intensity is a subjective assessment of the degree of damage actually produced by the ground motion.

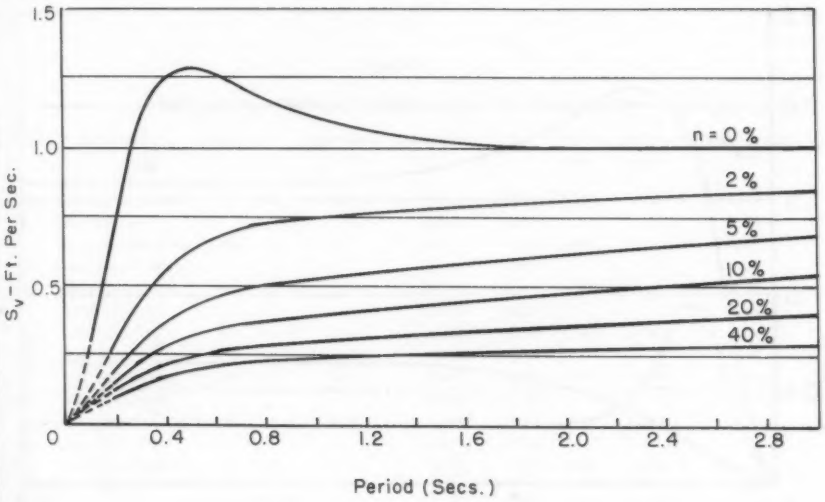

FIG. 7 - AVERAGE VELOCITY SPECTRUM CURVES

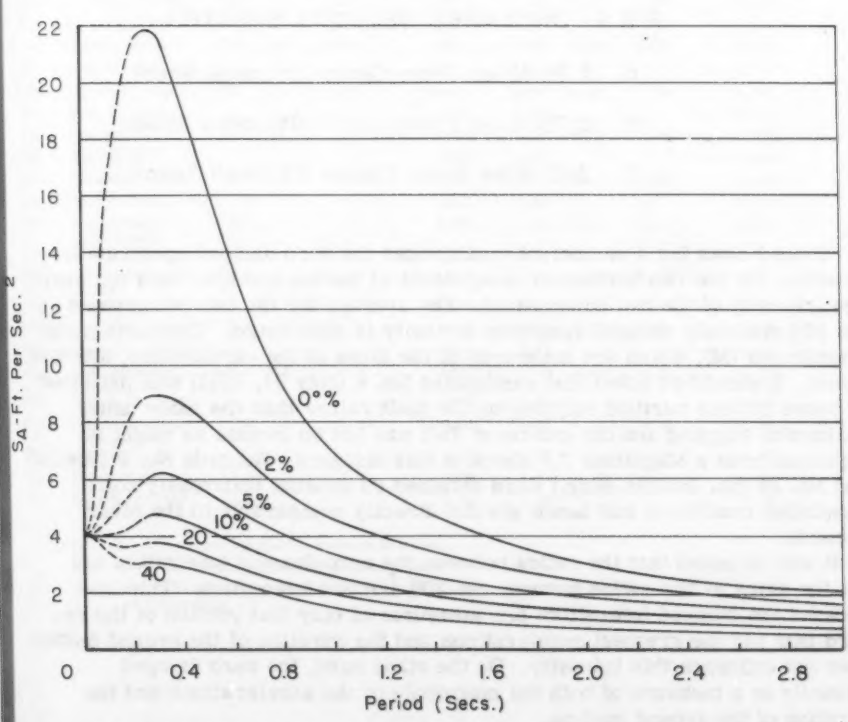

FIG. 8 - AVERAGE ACCELERATION SPECTRUM CURVES

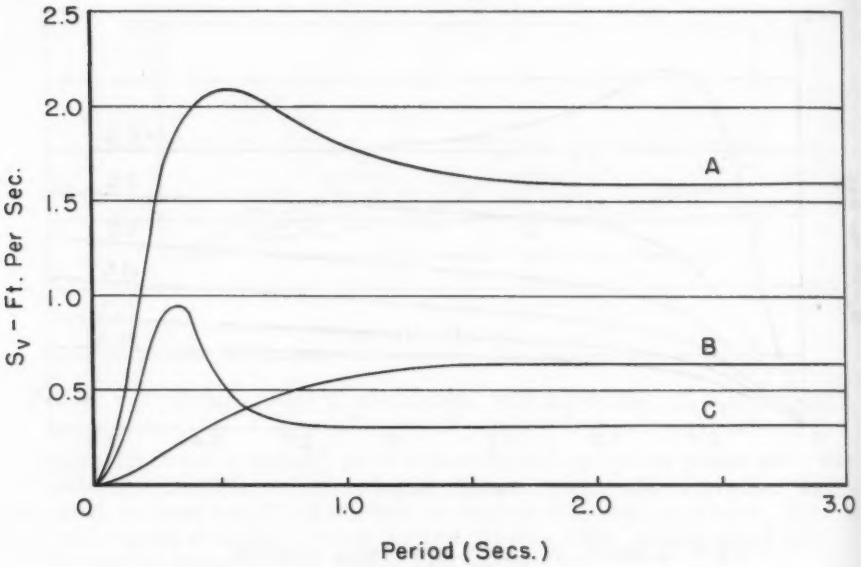

FIG. 9 - UNDAMPED VELOCITY SPECTRA

A. ±25 Miles From Center Of Large Shock

B. ±70 Miles From Center Of Large Shock

C. ±10 Miles From Center Of Small Shock

Table 1 lists for a number of earthquakes the zero damped spectrum intensities for the two horizontal components of motion and also lists the average intensity of the two components. The average for the two components of the 20% critically damped spectrum intensity is also listed. The earthquake Magnitudes (M), which are measures of the sizes of the earthquakes, are also listed. It should be noted that earthquake No. 4 (July 21, 1952) was produced by more or less vertical slipping on the fault rather than the more usual horizontal slipping and the motion at Taft was not so intense as might be expected from a Magnitude 7.7 shock at this distance. Records No. 9 (Seattle) and No. 19 (So. Pacific Bldg.) were obtained on unusual (extremely soft) foundation conditions and hence are not directly comparable to the other records.

It will be noted that the ratios between the zero damped intensities are not the same as the ratios between the 20% damped intensities. This is because the damped intensities are measures of only that portion of the record that had the greatest accelerations and the duration of the ground motion does not influence this intensity. On the other hand, the zero damped intensity is a measure of both the magnitude of the accelerations and the duration of the ground motion.

TABLE 1

SPECTRUM INTENSITIES OF RECORDED GROUND MOTIONS

No.	Location	D	h	Magnitude	Component	SI_o	SI_o Aver.	$SI_{0.2}$ Aver.	Max. Accel. %g
1a	El Centro, Calif.	30	15	6.7	N.S.	8.94	8.35	2.71	0.33
1b	May 18, 1940				E.W.	7.77			0.23
2a	El Centro, Calif.	35	15	6.5	N.S.	5.93	5.88	2.09	0.26
2b	Dec. 30, 1934				E.W.	5.83			0.20
3a	Olympia, Wash.	45	45	7.1	S80W	6.05	5.82	2.21	0.31
3b	April 13, 1949				S10E	5.59			0.18
4a	Taft, Calif.	40	15	7.7	S69E	4.84	4.69	1.91	0.18
4b	July 21, 1952				N21E	4.53			0.17
5a	Vernon, Calif.	28	15	6.3	S82E	4.9	4.62	1.70	0.19
5b	March 10, 1933				N08E	4.35			0.13
6a	Santa Barbara, Cal.	15	19	5.9	S45E	3.43	3.29	1.80	0.24
6b	June 30, 1941				N45W	3.15			0.23
7a	Ferndale, Calif.	50	15	6.4	N45E	3.2	2.99	1.41	0.13
7b	Oct. 3, 1941				S45E	2.78			0.12
8a	L.A. Subway Terminal	33	15	6.25	N51W	3.21	2.94	0.82	0.065
8b	May 10, 1933				N39E	2.67			0.04
9a	Seattle, Wash.	55	45	7.1	N88W	2.81	2.63	1.10	0.075
9b	April 13, 1949				S02W	2.46			0.058
10a	Hollister, Calif.	10	15	5.3	S01W	2.44	2.36	1.27	0.23
10b	March 9, 1949				N89W	2.29			0.11
11a	Helena, Mont.	15	25	6.0	EW	2.49	1.82	1.02	0.16
11b	Oct. 31, 1935				NS	1.16			0.14
12a	Ferndale, Calif.	35	10	5.5	N45E	1.64	1.45	0.64	0.082
12b	Sept. 11, 1938				S45E	1.27			0.16
13a	Vernon, Calif.	17	15	5.3	S82E	1.65	1.32	0.69	0.12
13b	Oct. 2, 1933				N08E	0.99			0.085
14a	Ferndale, Calif.	75	15	6.6	N45E	1.31	1.10	0.40	0.075
14b	Feb. 9, 1941				S45E	0.88			0.04
15a	L.A. Subway Terminal	22	15	5.3	N39E	1.14	0.96	0.45	0.065
15b	Oct. 2, 1933				N51W	0.78			0.060
16a	S.F. Golden Gate Park	7.8	7	5.3	S80E	1.04	0.84	0.49	0.13
16b	March 22, 1957				N10E	0.64			0.095
17a	S.F. State Bldg.	9.8	7	5.3	S9E	1.29	1.12	0.58	0.10
17b	March 22, 1957				S81W	0.95			0.06
18a	S.F. Alexander Bldg.	10.8	7	5.3	N81E	0.50	0.48	0.28	0.05
18b	March 22, 1957				N9W	0.45			0.05
19a	S.F. So. Pacific Bldg.	11.4	7	5.3	N45E	1.32	1.22	0.48	0.05
19b	March 22, 1957				N45W	1.12			0.046
20a	Oakland, Calif.	17.2	7	5.3	N26E	0.46	0.38	0.2	0.05
20b	March 22, 1957				S64E	0.29			0.04

D = Estimated true epicentral distance in miles

h = Estimated depth of center of fault in miles

Magnitude is that reported by Seismological Laboratory of the California Institute of Technology.

6. Measured Building Motions. The foregoing analysis has been checked with measured building motions although only in a few cases has moderately strong ground motion been recorded together with the resulting building vibration. In these cases, the application of the spectrum method to computing the maximum acceleration of the building (equation (15)) has agreed closely with the measured building accelerations.

Fig. 10 shows the recorded aceleration[10] of the roof of a 10-story reinforced concrete building and also shows the earthquake ground motion recorded in the basement.[10] It will be noted that the maximum ground acceleration was 5%g and the maximum recorded roof acceleration was 14%g and came mostly from the first mode of vibration. Fig. 11 shows the recorded acceleration[9] on the 16th floor of a 16-story steel frame office building and also shows the ground motion recorded in the basement. It will be noted that the maximum ground acceleration was 5%g and the maximum recorded 16th floor acceleration was approximately 12%g. For this case, analysis showed that the second and third modes of vibration contributed strongly to the building acceleration. Fig. 12 shows base and building accelerations recorded during an explosive-generated ground shock.[11]

It is seen from the foregoing that appreciable building accelerations are produced by only moderately strong ground motion. In the case of strong ground motion such as the El Centro, 18 May 1940 record accelerations of the order of 30% to 40%g are indicated for buildings like the Hollywood structure. Most buildings could not withstand these accelerations without being overstressed. On the other hand, such structures have survived strong ground motion without collapsing. To understand the reason for this, it is necessary to examine the vibrational energy of structures during earthquakes.

7. Vibrational Energy of Structures. The undamped, multi-degree of freedom structure (Fig. 4) has forced vibrations as given by equation (13) with n = 0. The relative kinetic energy and the potential energy at time t are

$$KE = \int \frac{1}{2} \dot{y}^2 \, dm$$

$$PE = - \int \frac{1}{2} \, y(\ddot{y} + \ddot{z}) \, dm$$

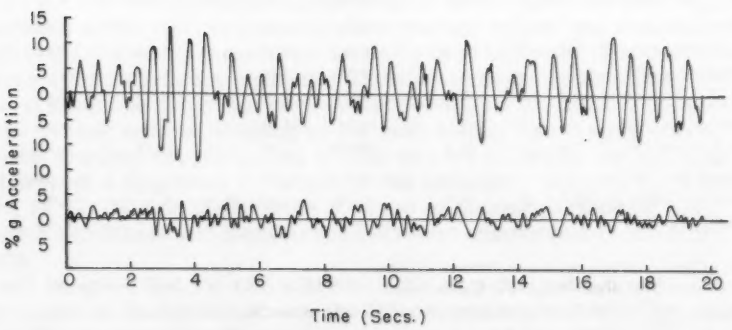

FIG. 10- BASEMENT AND ROOF ACCELERATIONS, HOLLYWOOD STORAGE BUILDING, 21 JULY 1952

Ten-Story Reinforced Concrete Building

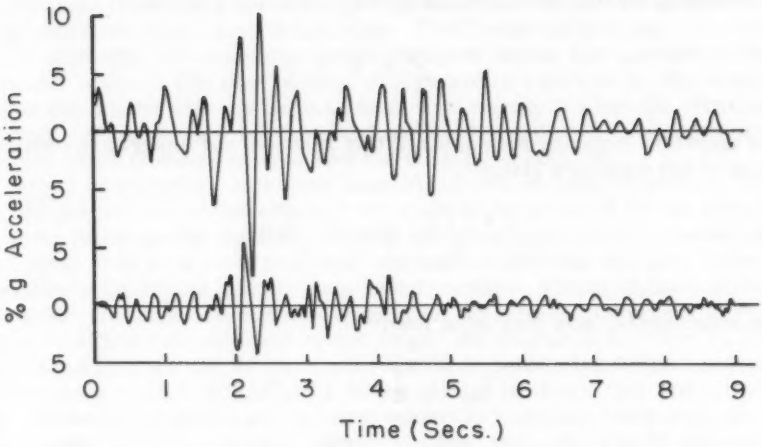

EAST-WEST ACCELERATION

FIG. 11 – BASEMENT AND ROOF ACCELERATIONS, ALEXANDER BUILDING, 22 MARCH 1957

Fifteen Story Steel Frame Structure

The total energy can be expressed by

$$E = KE + PE = \frac{1}{2}\sum_i D_i^2 \int \phi_i^2 \, dm \left\{ \left(\int_o^t \ddot{z} \sin p_i \tau \, d\tau \right)^2 + \left(\int_o^t \ddot{z} \cos p_i \tau \, d\tau \right)^2 \right\}$$

The maximum value of the expression within the brackets is S_{vi}^2, the square of the velocity spectrum value for zero damping. The upper bound for total energy is thus

$$\bar{E} = \frac{1}{2}\sum_i \left(D_i^2 \int \phi_i^2 \, dm \; S_{v_i}^2 \right) \tag{16}$$

The average value over a number of ground motions of the same intensity is

$$\bar{E}_{av} = \frac{1}{2}\sum_i D_i^2 \int \phi_i^2 \, dm \; (S_{v_i}^2)_{av} \tag{17}$$

If the average undamped velocity spectrum were a horizontal line $(S_{vi}^2)_{av}$ would be a constant independent of the period of vibration and the equation could be written

$$\bar{E}_{av} = \frac{1}{2} (S_{v_i}^2)_{av} \sum_i D_i^2 \int \phi_i^2 \, dm \tag{18}$$

It follows from the equations that precede equation (13) that

$$\sum_i D_i \phi_i = 1$$

and therefore squaring both sides of this relation and integrating over the mass of the structure gives

$$\sum_i D_i^2 \int \phi_i^2 \, dm = \int dm = M$$

and equation (18) may thus be written[12]

$$E_{av} = \frac{1}{2} M (S_{v_i}^2)_{av} \qquad (1$$

where M is the total mass of structure.

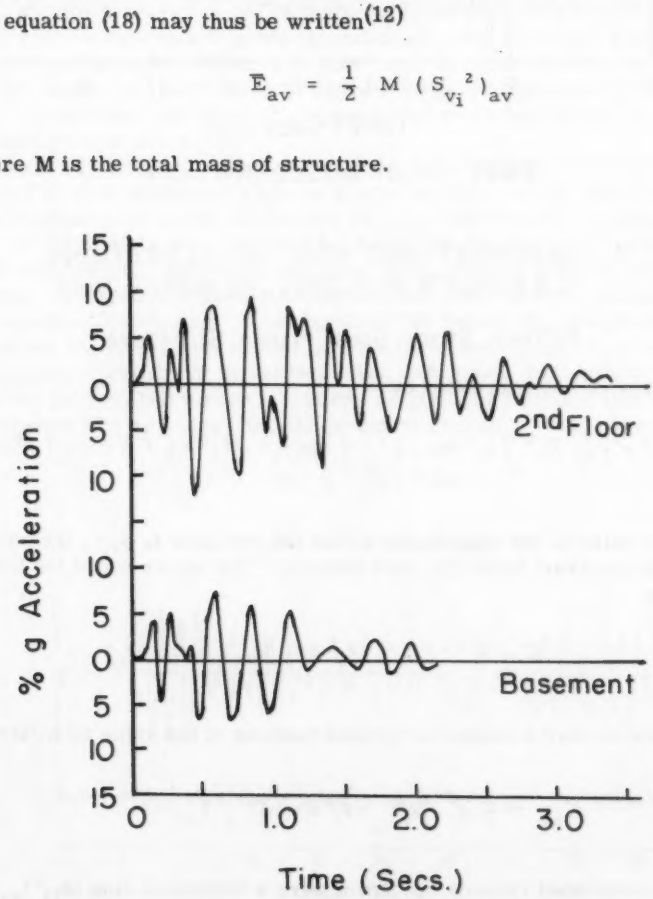

FIG. 12 - BASEMENT AND 2nd FLOOR RECORDS FROM QUARRY BLAST

Although the average zero damped spectrum curve is not a horizontal line, it is seen from Fig. 7 that in the range $T>0.3$ seconds it is not very far from it. Accordingly for structures whose pertinent modes have periods above 0.3 seconds, equation (19) may be used with reasonable accuracy. Equation (19) states that on the average the maximum total energy fed into the structure depends only upon the total mass and on $(S_{v_i}{}^2)_{av}$ and does not depend upon how the mass is distributed or how the framing is laid out.

8. Effect of Damping. It is seen from Fig. 7 that structures with low damping will be subjected to relatively high stresses in the event of strong ground motion. Moderate amounts of damping will give appreciable reduction of stresses. It is also clear that large amounts of damping will give large reductions in the forces and stresses in a structure. Vibration tests show that for small vibrations of ordinary structures the amount of damping is of the order of 10% of critical which is not large. Structures of the types of the Hollywood Storage and the Alexander buildings could experience accelerations of the order of 30 to 40%g during strong ground motion if they had 10% damping. However, if such a structure is subjected to strong vibrations, the consequent cracking, rubbing, plastic yielding, etc., can absorb large amounts of energy and effectively give the structure large damping. Most structures have considerable capacity for energy dissipation when they are overstressed.

An exact analysis[13, 14] of the vibrations of overstressed (non-linear) structures is exceedingly difficult and the results of such analyses are not yet in a form to be used for design. An approximate method, based on equation (19) can be utilized.[15]

Consider a structure starting from rest and excited into vibration by strong ground motion. The vibrations of the structure will continue to increase in amplitude and eventually some part of the structure will be overstressed. If the ground motion is sufficiently strong the amplitude of vibration will continue to increase and overstressing will occur on each swing of the structure. After a time, the intensity of the ground motion will decrease and the structure will quiet down to the point where it is no longer overstressed during the vibrations and following this the vibrations will be gradually damped out by the ordinary damping inherent in the structure. This process can be described by the equation

$$E = D + V \tag{20}$$

where E represents the total energy input into the structure up to the time that the last non-linear overstress occurs; D is the energy dissipated by the structure up to this time: V is the potential energy in the structure at the time that the last energy-absorbing overstress occurs.

If, as in equation (19), it is taken that

$$E = \frac{1}{2} M (S_{v_i}{}^2)_{av}$$

this assumes that the input energy into the overstressed structure is the same as the maximum input energy for an equivalent, elastic, undamped structure. In this case

$$D = \frac{1}{2} M(S_{v_i}{}^2)_{av} - V \tag{21}$$

This equation specifies the amount of energy that must be dissipated if the structure is to remain standing. For ground motion of approximately the intensity of the El Centro 1940 records the equation may be written

$$D = \frac{W}{10} - V \qquad (22)$$

where W = Mg is the weight of the structure. For such ground motion approximately 1/10 of a foot pound of energy must be absorbed for each pound of weight of the structure. In cases where sufficient was known about the properties of the structures and the intensity of the ground motion to make an analysis, equation (22) agrees reasonably well with field observations of damage.(15)

The importance of plastic energy absorption in controlling vibrations is illustrated by the behavior of a steel bar of 1 sq. in. cross-sectional area and 1 in. length. If the elastic limit of the steel is 33,000 psi the strain energy stored at this stress is

$$V = \frac{1}{2} \frac{33,000}{30 \times 10^6} \frac{33,000}{12} = \frac{1}{2} (0.0011) \frac{33,000}{12} = 1.5 \text{ ft lb per cu in.}$$

If the bar is stretched plastically to a strain of 0.02 the energy absorbed plastically is (assuming perfect plasticity)

$$D = 33,000 (0.02 - 0.0011) \frac{1}{12} = 50 \text{ ft lb per cu in.}$$

It is seen from this that a suitably designed structure could be stressed beyond the yield point and could absorb an appreciable amount of energy and still have an adequate factor of safety against collapse. For example,(15) a rod-braced, elevated water tank that would have to be designed for 40%g lateral acceleration to remain elastic during ground motion of the El Centro 1940 intensity could be designed for 12%g and undergo plastic deformation and still have a factor of safety of approximately 2. A plastic design must, of course, be done very carefully to ensure that rupture or brittle fracture does not occur. The total energy absorbed in failing members by oscillatory plastic strain is not as yet well established so that the design should be conservative.

9. Structural Behavior. On the basis of the above analyses, it is possible to explain those apparent anomalies that are frequently observed following a strong earthquake.

a) After almost every strong earthquake it is observed that a few old and apparently very weak buildings survived even though their static lateral strength (as computed on the basis of a %g load on the structural frame) was extremely low. This can be explained as the result of two factors. First, the true ultimate lateral strength of a structure is often much larger than the nominal design lateral strength. Second, such old, loose-jointed structures may absorb large amounts of energy during only moderate vibrations and, as is seen from the spectrum curves, such a structure could survive strong motion without actually being subjected to high stresses.

b) It is not uncommon to observe that the same ground motion that apparently did no damage to an old weak building damaged a relatively strong building. This is readily explainable. Consider a well-designed and constructed building whose lateral strength was so high that it could resist a static lateral load of 25%g without being overstressed. If the design and construction were such that the structure had only small damping during elastic vibrations of such a structure could become worse than the equivalent 25%g load and

some member would than show distress. If a designer were sufficiently clever at incorporating damping in structures he could design a weak structure that would be undamaged and a strong structure that would be damaged by the same ground motion.

c) After the Mexico City earthquake, whose epicenter was 220 miles away, it was observed that in the same district old masonry buildings came through the earthquake on the whole better than modern steel and concrete buildings that had greater lateral strength. This can be explained as resulting from the long distance of the epicenter from the city. As illustrated in Fig. 9, at a long distance from the epicenter the short period end of the spectrum is relatively depressed. The old masonry buildings were mostly low structures with largely multi-story, long-period buildings, so that in effect the old buildings experienced a much weaker ground motion than did the modern buildings. If, in the future, the epicenter of a relatively small earthquake, such as shown in Fig. 2, were to be located close to the city, it could be expected that the low and stiff buildings would suffer more than the tall, flexible structures.

d) After almost every destructive earthquake some buildings are observed to be in such a badly damaged condition that, from the static design point of view, it seems a miracle that they did not collapse. It is often said that if the ground motion had been but a shade more intense many buildings would have collapsed. If the damage to a structure is looked at as a process for absorbing energy, the survival of these structures is not so mysterious. In these cases it is not so much a matter of static lateral strength as it is a question of whether the structure can continue to absorb sppreciable energy during its vibrations. For example, consider a badly damaged building that has cracked a large number of interior partition walls, has extensive cracking in exterior masonry walls, and exhibits many cases of severe overstress in beams and columns. The very fact that the damage is so extensive shows that a large amount of energy has been dissipated and it is likely that further vibrations will continue to dissipate energy. The structure may thus not be in so perilous a condition as would be concluded on the basis of a static lateral force analysis. Opposed to this, consider some one-story concrete-shell structures that collapsed in Mexico City. These were long, narrow concrete roofs, each supported on two concrete columns. With a heavy roof supported on only two columns the inherent damping for small vibrations would be quite small. Furthermore, plastic energy absorption could take place only in overstressing the two columns in bending and this was not very large. Also, if one of the columns lost its strength the entire structure must necessarily collapse. The fact that some of these structures survived the earthquake was really more surprising than the survival of some of the spectacularly damaged structures.

10. Conclusions. The response spectrum curves, which are a type of influence diagram for earthquake loads, describe the important characteristics of strong earthquake ground motions by exhibiting their effects on structures. The spectra also provide a logical measure of the intensity of earthquake ground motion which has engineering sugnificance. By means of the spectrum curves the apparently anomalous behavior of some structures during earthquakes can be explained.

If the point of view is taken that structures should be designed to remain elastic (without damage) when subjected to earthquake ground motion, a satisfactory procedure can be developed using the spectrum curves. It is true that this would be more laborious than the presently used equivalent

static methods but it would not be excessively so. The real difficulty arises from the fact that in this case the structures would have to be designed for lateral loads much larger than are not prescribed by building codes.

It does not seem economically justifiable that in a seismically active region all buildings should be designed to survive the strongest possible ground motion without any damage. It is more reasonable to take the point of view that the design should be such that the structures will survive the more frequent, moderate ground motions without damage but in the more rare event of very strong ground motion, damage would be tolerated so long as it was not a hazard to life and limb. This is the usual point of view of engineers in earthquake areas. It is seen from the material presented in this paper that this point of view is equivalent to requiring two different design analyses for each structure. One would be to ensure that no damage resulted from moderate, elastic vibrations, and the other would be a "limit design" type of analysis to ensure that there was sufficient energy-absorbing capacity to give an adequate factor of safety against collapse in the event of extremely strong ground motion.

For a simple, clean, structure such as a rod-braced elevated water tank, it is not difficult to make a reasonable limit design along the lines set forth in this paper. However, in the case of more complicated structures the problem becomes very difficult, particularly because we do not at present have much precise information about the energy absorbing characteristics of ordinary building materials and structures during vibrations. This is an important problem now facing engineers, and it is being attacked by research projects sponsored by the California State Division of Architecture. One of these projects is a study of how to compute the ultimate lateral strength of structures; another, being of structures; a third, being done at the California Institute of Technology is the development of a large-capacity shaking machine with which it is planned to vibrate some typical structures to the point of serious damage and measure their energy absorbing capacities. These projects are just a beginning, and more research is needed on the general problem.

It is, of course, true that the lateral forces prescribed for design by building codes are based to a certain extent on observed damage behavior of structures during earthquakes and in this sense they do reflect the energy absorbing properties of typical structures. The application of these code requirements to non-typical and unusual structures is not warranted for the energy absorbing capacity of such structures may be quite different from ordinary buildings.

REFERENCES

1. Hiriart, F., R. J. Marsal and E. Rosenblueth, "Los Effectos del Terremoto del 28 de Julio y la Consiguiente Revision de los Criterios para el Diseno Sismico de Estructuras," Revista Ingenieria Universidad Nacional de Mexico, January, 1958.

2. Housner, G. W., "Characteristics of Strong-Motion Earthquakes," Bulletin of Seismological Society of America, Vol. 37, 1947.

3. Goodman, L. E., E. Rosenblueth and N. Newmark, "Aseismic Design of Firmly Founded Structures," Transactions American Society of Civil Engineers, Vol. 117, 1952.

4. Housner, G. W., "Earthquake Resistant Design Based on Dynamic Properties of Earthquakes," Journal of American Concrete Institute, Vol. 28, No. 1, 1956.

5. Housner, G. W., R. R. Martel, J. L. Alford, "Spectrum Analysis of Strong-Motion Earthquakes," Bulletin of Seismological Society of America, Vol. 43, 1953.

6. Hudson, D. E., "Response Spectrum Techniques in Engineering Seismology," Proceedings 1956 World Conference on Earthquake Engineering, Earthquake Engineering Research Institue, 1956.

7. Housner, G. W., "Interaction of Building and Ground During an Earthquake," Bulletin of the Seismological Society of America, Vol. 47, 1957.

8. Hudson, D. E. and G. W. Housner, "Analysis of Strong-Motion Accelerometer Data from the San Francisco Earthquake of March 22, 1957," Bulletin of the Seismological Society of America, Vol. 47, 1957.

9. Housner, G. W., "Spectrum Intensities of Strong Motion Earthquakes," Proceedings of 1952 Symposium on Earthquake and Blast Effects on Structures, Earthquake Engineering Research Institute, 1952.

10. U. S. Coast and Geodetic Survey recording.

11. Hudson, D. E. and G. W. Housner, "Structural Vibrations Produced by Ground Motion," Transactions American Society of Civil Engineers, Vol. 122, 1957.

12. Housner, G. W. and H. Outinan, "The Effects of Torsional Oscillations on Earthquake Stresses," Bulletin of Seismological Society of America, Vol. 48, 1958.

13. Tanabashi, R., "Studies on the Non-Linear Vibrations of Structures Subjected to Destructive Earthquakes," Proceedings 1956 World Conference on Earthquake Engineering, Earthquake Engineering Research Institute, 1956.

14. Berg, G. V., "Analysis of Structural Response to Earthquake Forces," Report IP-291, University of Michigan Engineering College Industry Program, May, 1958.

15. Housner, G. W., "Limit Design of Structures to Resist Earthquakes," Proceedings 1956 World Conference of Earthquake Engineering, Earthquake Engineering Research Institute, 1956.

Journal of the
ENGINEERING MECHANICS DIVISION
Proceedings of the American Society of Civil Engineers

COMMENTARY ON PLASTIC DESIGN IN STEEL: ADDITIONAL DESIGN CONSIDERATIONS - I

Progress Report No. 3 of the Joint WRC-ASCE Committee on Plasticity Related to Design

FOREWORD

This paper is the third in a series of reports on Plastic Design emanating from a Joint Committee of the Welding Research Council and the American Society of Civil Engineers. Reference should be made to Progress Report No. 1 (which appeared in the July EM Journal) for such items as the Foreword, Synopsis, Definitions, and Nomenclature. For information, the complete Table of Contents appears at the beginning of this Progress Report. Articles 6.1 and 6.2 are included in this present paper.

The Joint Committee has approved the publication of this information with the strong recommendation that it be read carefully by all structural engineers.

Note: Discussion open until March 1, 1960. To extend the closing date one month, a written request must be filed with the Executive Secretary, ASCE. Paper 2230 is part of the copyrighted Journal of the Engineering Mechanics Division, Proceedings of the American Society of Civil Engineers, Vol. 85, No. EM 4, October, 1959.

Table of Contents

1. INTRODUCTION
   - 1.1 Structural Design
   - 1.2 Plasticity and Design--Some Advantages and Limitations

2. BASIC PRINCIPLES
   - 2.1 Behavior of Material and Structural Elements
   - 2.2 Plastic Theory

3. ANALYSIS AND DESIGN
   - 3.1 Assumptions
   - 3.2 Statical Method of Analysis
   - 3.3 Mechanism Method of Analysis
   - 3.4 Other Methods

4. GENERAL PROVISIONS
   - 4.1 Introduction
   - 4.2 Types of Construction
   - 4.3 Material
   - 4.4 Structural Ductility
   - 4.5 Yield Stress Level
   - 4.6 Plastic Moment
   - 4.7 Loads
   - 4.8 Load Factors

5. VERIFICATION OF PLASTIC THEORY
   - 5.1 Basic Concepts
   - 5.2 Continuous Beams
   - 5.3 Frames

6. ADDITIONAL DESIGN CONSIDERATIONS
   - 6.1 Shear Force
   - 6.2 Local Buckling
   - 6.3 Lateral Buckling
   - 6.4 Variable Repeated Loading

7. COMPRESSION MEMBERS
   - 7.1 Introduction
   - 7.2 Reduction of the Plastic Moment Due to Axial Thrust
   - 7.3 Moment-Carrying Capacity of Columns
   - 7.4 Rotation Capacity
   - 7.5 The Influence of Lateral-Torsional Buckling
   - 7.6 Frame Stability

8. CONNECTIONS
   - 8.1 Straight Corner Connections
   - 8.2 Haunched Corner Connections
   - 8.3 Tapered Haunched Connections
   - 8.4 Curved Haunched Connections
   - 8.5 Beam-to-Column Connections
   - 8.6 Details with Regard to Welding
   - 8.7 Details with Regard to Bolting

9. DEFLECTIONS
   - 9.1 Introduction
   - 9.2 Deflections in the Elastic Range
   - 9.3 Deflections in the Plastic Range
   - 9.4 Deflection at Ultimate Load
   - 9.5 Step-by-Step Calculations
   - 9.6 Approximate Deflection at Working Load
   - 9.7 Rotation Requirements

CHAPTER 6.
ADDITIONAL DESIGN CONSIDERATIONS

In the application of plastic theory to design, just as in the case of allowable stress design, there are a number of factors the importance of which must be evaluated. Those considered in this chapter include shear force, local buckling of flanges and webs, lateral instability, and repeated loading. The problem of column buckling is treated in chapter 7 (Progress Report No. 5). The background of research is described, including the important assumptions and steps of pertinent theoretical analysis. Experimental correlation is given, and approximations for design use are discussed.

6.1 Shear Force

Statement of the Problem

Simple plastic theory is based on the concept of the attainment of the full plastic moment at certain sections, followed by adequate rotation at this constant moment value as the applied load increases. It must be recognized, however, that the magnitude of the moment at which large inelastic rotations occur is not constant under all circumstances. In calculating the full plastic moment M_p as $\sigma_y Z$, it is assumed that the member is stable and is subjected to pure bending; thus axial thrust and shear force are both ignored.

Since plastic hinges usually occur at positions where shear and axial force are present, it is of importance to be able to predict the changes in the values of the plastic moments due to these causes. In most practical cases the influence of shear force will be very small. In some special cases the combined influence of shear and axial thrust is important.

Previous Research

Horne(6.1) considered the effect of transverse shear force for the case of a beam of rectangular cross section bent about one of its axes of symmetry. An approximate solution was obtained, valid for shear forces less than a certain limit. This solution was also extended to an I-section bent about the axis normal to the web (strong axis).

Leth(6.2) modified this latter solution to determine a lower bound on the value of the full plastic moment in the presence of shear force, valid over the full range of shear forces. He included an upper bound on the full plastic moment when the shear force has its full plastic value. Heyman and Dutton(6.3) proposed a semi-empirical theory which is also valid over the full range of shear forces. Green(6.4) derived an upper bound on the value of the full plastic moment in the presence of shear force for beams of both rectangular and I-section. This upper bound agrees closely with Leth's lower bound for large values of the shear force. Upper bound solutions were also derived independently by Green and by Onat and Shield(6.5) for the case of a beam of rectangular cross section, treated as a problem in plane strain and assuming the material to be plastic-rigid. Drucker(6.6) demonstrated the lack of uniqueness of interaction curves for shear and moment, explored bounds for a beam of rectangular cross section, and proposed an approximate interaction formula

$$\frac{M}{M_p} = 1 - \left(\frac{V}{V_p}\right)^4 \qquad (6.1)$$

where

M = moment

M_p = plastic moment = $\sigma_y \frac{bd^2}{4}$

V = applied shear force

V_p = $\sigma_y \frac{bd}{2}$

Hodge[6.7] derived an expression valid over the full range of shear, in general terms, which is applicable to both rectangular and I-beams. Fujita[6.8] developed a lower bound solution of a cantilever beam with rectangular cross section, assuming the plane stress state and allowing warping at the fixed end. This solution was modified for wide flange sections by Beedle, Thürlimann and Ketter[6.9] including an extreme case of shear failure. The effect of both shear force and axial thrust on the full plastic moment was investigated independently by Horne[6.10] and by Kusuda and Thurlimann[6.11]. The theoretical results obtained in Ref. 6.11 are in fair agreement with experimental observations.

Theoretical Analysis

In most practical situations, WF or I-sections are used. However, the essentials of the problem can be shown by the simple example of a cantilever beam with rectangular cross section of depth d and width b (Fig. 6.1). The following assumptions and limitations are made for the analysis:

1. The problem is analyzed under the assumptions made in ordinary beam theory as a problem of plane stress.
2. Only the elastic portion can carry shearing forces.
3. The Mises - Hencky yield criterion is adopted for the combined stress state.
4. The fixed end is allowed to warp.

As the external loading is increased, yielding will commence at the fixed end of the beam and start to penetrate into the cross section (Fig. 6.1a). External and internal moment and shear at section S-s in Fig. 6.1a are given by

$$M = P(a-x) = M_p - \sigma_y \frac{by^2}{3} \qquad (6.2)$$

$$V = -P = \frac{dM}{dx} \qquad (6.3)$$

where

$$M_p = \sigma_y \frac{bd^2}{4} \text{ (full plastic moment)}$$

In order to determine the shearing stresses τ, the horizontal equilibrium of differential element dx is considered (Fig. 6.1b). A beam element above a horizontal section A-A through the yielded part Fig. 6.1b is in horizontal

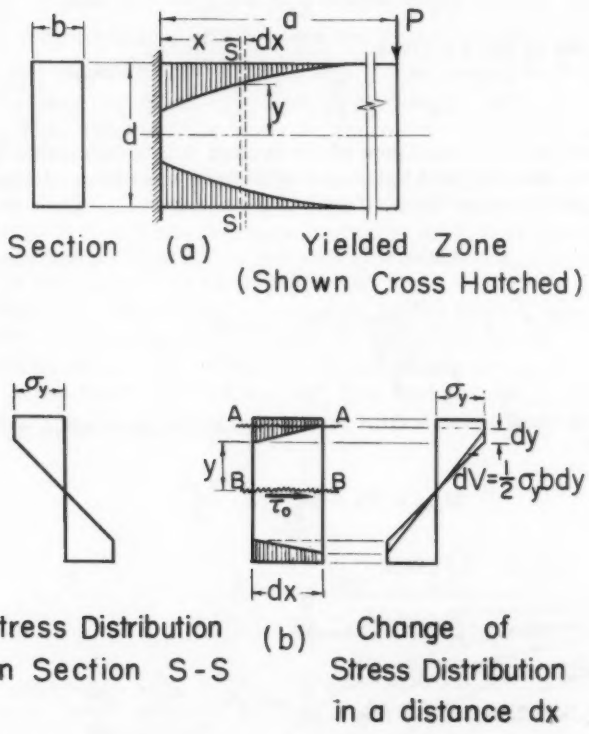

Fig. 6.1. Yielded Zones and Stress Distribution in a Cantilever Beam of Rectangular Cross Section

equilibrium without any shearing stresses τ, since the resultant horizontal forces on both faces are equal. Hence no shearing stresses exist in the plastic zone. The shearing stresses τ_o in the neutral axis along section B-B resist the unbalanced horizontal force,

$$dV = \frac{1}{2}\,\sigma_y\, b\, dy \tag{6.4}$$

Horizontal equilibrium for the element above section B-B (the centerline section) requires

$$\tau_o\, b\, dx = dV = \frac{1}{2}\,\sigma_y\, b\, dy$$

or

$$\tau_o = \left(\frac{\sigma_y}{2}\right)\left(\frac{dy}{dx}\right) \tag{6.5}$$

The rate of change $\frac{dy}{dx}$ is obtained by differentiating Eq. 6.2 with respect to the distance along the beam, x

$$\frac{dM}{dx} = V = -\frac{2}{3}\,\sigma_y\, b\, y\, \frac{dy}{dx} \tag{6.6}$$

which replaced in Eq. 6.5 gives

$$\tau_o = -\frac{3}{4}\,\frac{V}{by} = \frac{3}{4}\,\frac{P}{by} \tag{6.7}$$

It is assumed that the resistance of the section will be exhausted if this shearing stress reaches its yield value at this centerline section. Using the Mises - Hencky yield criterion for yielding under pure shear

$$\tau_{yield} = \frac{\sigma_y}{\sqrt{3}} \tag{6.8}$$

The limiting value for y is given by Eq. 6.7 as

$$y = \frac{3\sqrt{3}}{4}\,\frac{P}{b\,\sigma_y} \tag{6.9}$$

Obviously this condition will first be reached at the fixed end x = 0; therefore from Eq. 6.2

$$M_{ps} = P\,a = M_p - \sigma_y\,\frac{b\,y^2}{3}$$

Replacing y from Eq. 6.9 gives

$$M_{ps} = M_p - \frac{9}{16}\,\frac{P^2}{b\,\sigma_y}$$

$$= M_p - \frac{9}{64}\,P^2\,a^2\,\frac{4}{\sigma_y\, b\, d^2}\,\frac{d^2}{a^2}$$

Since

$$P^2 a^2 = M_{ps}^2$$

and

$$M_p = \sigma_y\,\frac{b\,d^2}{4}$$

then

$$M_{ps} = M_p - \frac{9}{64}\,\frac{M_{ps}^2}{M_p}\,\frac{d^2}{a^2}$$

or

$$\frac{9}{64}\left(\frac{M_{ps}}{M_p}\right)^2\frac{d^2}{a^2} + \frac{M_{ps}}{M_p} - 1 = 0 \tag{6.10}$$

The solution of Eq. 6.10 is given by

$$\frac{M_{ps}}{M_p} = \frac{8}{9}\,\frac{b a^2}{Z}\left(\sqrt{1 + \frac{9}{4}\,\frac{z}{b\,a^2}} - 1\right) \tag{6.11}$$

where $Z = \frac{bd^2}{4}$ = plastic modulus of rectangular cross section. Equation 6.11 gives the desired relationship between the plastic moment M_{ps} as modified by shear and the full plastic moment M_p. It can readily be solved for the parameter a/d (length of cantilever/depth of section) for different values of the ratio M_{ps}/M_p. The result is shown in Fig. 6.2 for the curve marked "rectangle."

The rectangular cross section of Fig. 6.1a can be considered as the web plate of a wide-flange section, and Eq. 6.11 still holds true when the appropriate plastic modulus Z of the wide-flange section is used when yielding due to normal stresses has penetrated into the web of the section and when the web thickness w is used instead of the breadth, b.

Fig. 6.2 shows the comparable reduction of the full plastic moment due to shear force for various ratios of the flange to web areas A_f/A_w. The case $A_f/A_w = 0$ corresponds to a rectangle. The dimensions are given in Fig. 6.3. As indicated on the inset sketch of Fig. 6.2, only that portion of the chart for $\frac{M_{ps}}{M_p} > 0.65$ is shown to the large scale.

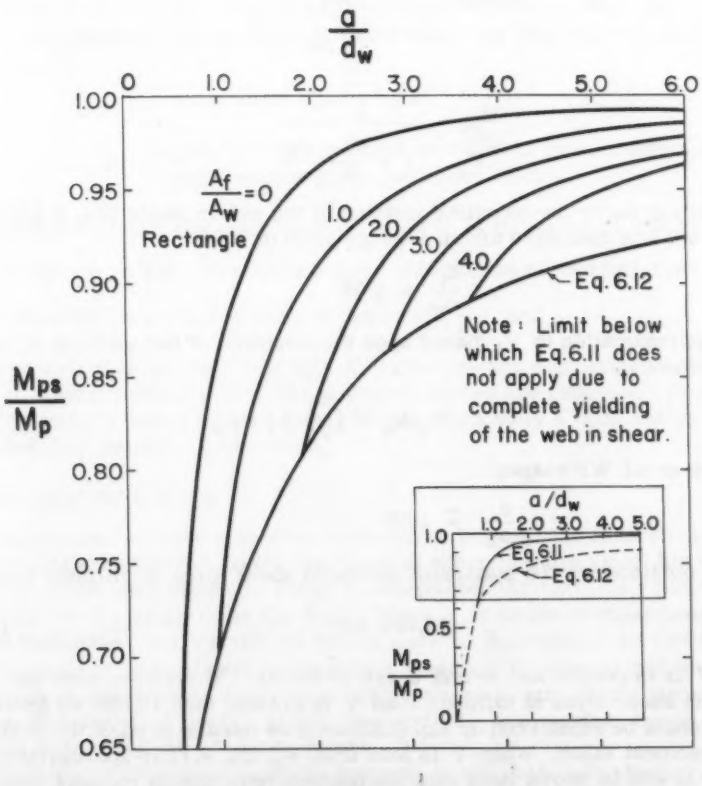

Fig. 6.2. Reduction of Plastic Moment by Shear Force

It is emphasized that this is not a maximum carrying capacity solution, but rather corresponds to "first yield in shear." It would therefore be expected that members tested under this condition would display a greater strength than predicted by the theory.

For cases of high shear to moment values an extreme condition may develop where the entire moment is taken by the flanges and shear produces full yielding of the web as indicated in Fig. 6.3. Then

$$M_{ps} = M_p - \frac{1}{4}\,\sigma_y\, w\, d_w^2 = P\,a$$

$$V_y = \tau_y A_w$$

$$V_y = \frac{\sigma_y}{\sqrt{3}}\; d_w\; w = -P$$

Using these two relations the ratio $\frac{a}{d_w}$ becomes

$$\frac{a}{d_w} = \frac{\sqrt{3}}{4}\;\frac{1}{\frac{M_p}{M_{ps}} - 1}$$

or

$$\frac{M_{ps}}{M_p} = \frac{1}{1 + \frac{\sqrt{3}}{4}\,\frac{dw}{a}} \qquad (6.12)$$

The limiting curve for complete yielding of the web in shear (Eq. 6.12) shown in Fig. 6.2 was computed for an average ratio of

$$\frac{d_f}{d_w} = 1.05$$

An approximation to V_y based upon the condition of full yielding of the web is as follows:

$$V_y = \tau_y A_w = \left(\frac{\sigma_y}{\sqrt{3}}\right)(w\,d_w) \qquad (6.13)$$

Since for usual WF shapes

$$\frac{d}{d_w} \simeq 1.07$$

there is obtained for the maximum allowable shear force at ultimate load,

$$V_y = 18{,}000\ wd \qquad (6.14)$$

where V is in pounds and w and d are in inches. Therefore, when the maximum shear force at ultimate load V is greater than 18,000 wd (pounds), the web could be reinforced or Eq. 6.12 could be used to predict the modified plastic moment value. When V is less than V_y, Eq. 6.11 is appropriate; however it will be shown later that the implied reduction in moment capacity does not actually occur because of strain-hardening.

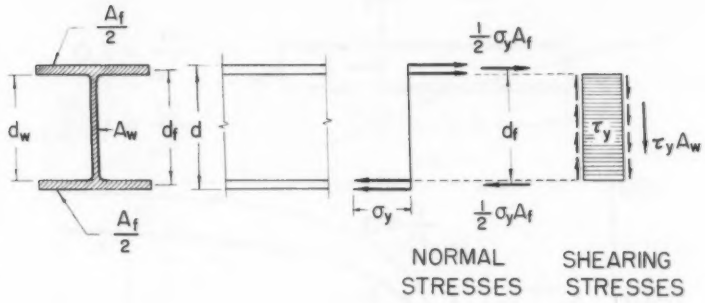

Fig. 6.3. Assumed Stress Distribution in a WF Cross Section Loaded by Shear and Moment

If, in addition to shear, an axial force is also present a similar method of analysis may be applied when both shear and axial force are present. For wide-flange sections with $A_f/A_w = 2.0$ and $d_f/d_w = 1.05$, the problem has been solved in Ref. 6.11. Fig. 6.4 shows the relationship of M_{pm}/M_p to a/d_w for a cantilever beam, the parameter being the magnitude of axial load P. In this fig,

P_y = axial yield load = $\sigma_y A$

M_{pm} = plastic hinge moment modified to include effect of axial compression and shear force

The curve for axial force equal to zero, $\frac{P}{P_y} = 0$, is the same as that given in Fig. 6.2 for $\frac{A_f}{A_w} = 2.0$. The other curves show the combined influence of shear and axial force as functions of the ratios $\frac{a}{d_w}$ and $\frac{P}{P_y}$.

In practice it is unlikely that high shear forces and high axial loads will occur in combination at points where plastic hinges are expected. For such an eventuality, however, Fig. 6.4 may be used to modify a trial design that neglected this unusual combination.

Experimental Correlation

It is not easy to make a precise comparison between the theoretical predictions and experiments, since the effect of shear is quite small for wide-flange sections until the shear force V approaches the extreme value of shear failure V_y as given by Eq. 6.14. When V is in the neighborhood of V_y the load-deflection curves for beams show no appreciable horizontal portion corresponding to plastic hinge action. Instead, it is found that the load-deflection or the moment-rotation curves continue to rise fairly steadily and to such an extent that the full plastic moment M_p is exceeded; hence no sharply defined failure condition exists.

However, the intersection of two tangents to the load-deflection or moment-rotation curves in the elastic and plastic range provides one possible criterion

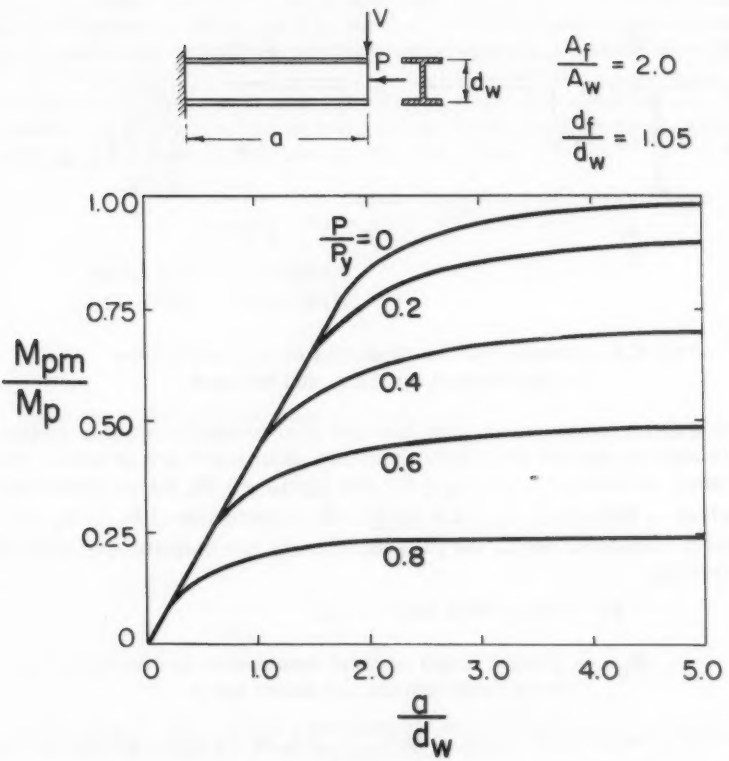

Fig. 6.4. Moment Capacity as Modified by the Combined Action of Shear and Thrust on WF Cross Section

for evaluating experimentally the modified plastic moment of the section due to shear force. Beyond this value of moment the deflection or curvature of the beam increases more rapidly than before.

The determination of M_{ps} is shown in Fig. 6.5; the test data is taken from Ref. 6.17. Predictions from Eqs. 6.11 and 6.14 are also indicated for comparison. The shear force V in this case is greater than 18 ksi, hence Eq. 6.14 would be used.

Fig. 6.6 shows in tabular form a number of tests which indicate the influence of shear on the plastic moment. The structure and loading are shown at the left. Next is indicated the size of member and the ratio $\frac{a}{d}$ where d is the depth of the member and "a" is the ratio $\frac{M}{V}$. For constant shear, "a" is the distance from a plastic hinge to the point of inflection. Thus, the quantity "a" is sometimes referred to as the length of an "equivalent cantilever beam." To the right is a bar graph on which is plotted the maximum moment corresponding to the observed maximum load and observed reduced plastic moment M_{ps} due to shear, the latter being determined as described earlier. The

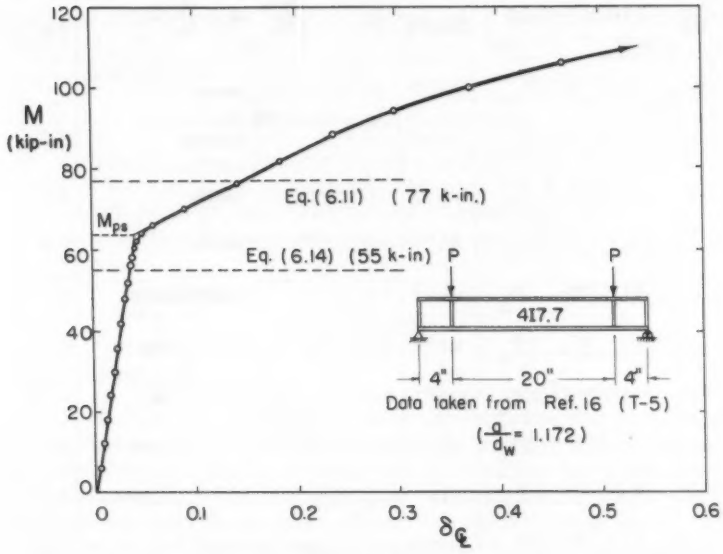

Fig. 6.5. Determination of the Plastic Moment as Modified by Shear, M_{ps}, Using Tangent Intersection Method

theoretical limit according to Eq. 6.11 or Eq. 6.12, (depending on which case is the controlling one) is shown by the dotted line. In the range where the shear force V is high and greater than 18,000 wd (pounds), Eq. 6.12 is used to compute the limit predicted by the theory. This figure shows that the actual strength of the structure usually exceeds the full plastic moment M_p if the shear force V is less than 18,000 wd (the value which assumes full web yielding, V_y). The exception is Beam No. 13 which was only deficient 4%. The influence of shear force may thus be neglected when this condition exists. Even when the shear force is greater than 18,000 wd, the test results show a moment strength greater than predicted by Eq. 6.12. It is evident, however, that the latter is a reasonable limit.

While it might appear from these results that a more than ample load factor exists with regard to shear force when $V \leq 18{,}000$ wd, this fact cannot be utilized because of practical limitations. A beam with pure moment, for example, usually buckles when strain-hardening commences, and therefore cannot be counted upon to support a moment greater than M_p.

The test results on the effect of both shear and axial forces(6.10) show a tendency similar to that of the bar graph in Fig. 6.6. The observed values of M_{pm}/M_p are in good agreement with the theoretical predictions in Fig. 6.4.

Design Approximation

The effect of shear on the full plastic moment will usually be negligible for frames. High shear and moment occur in very localized zones so that strain-hardening will set in quickly and, in most cases, permit the moment to reach

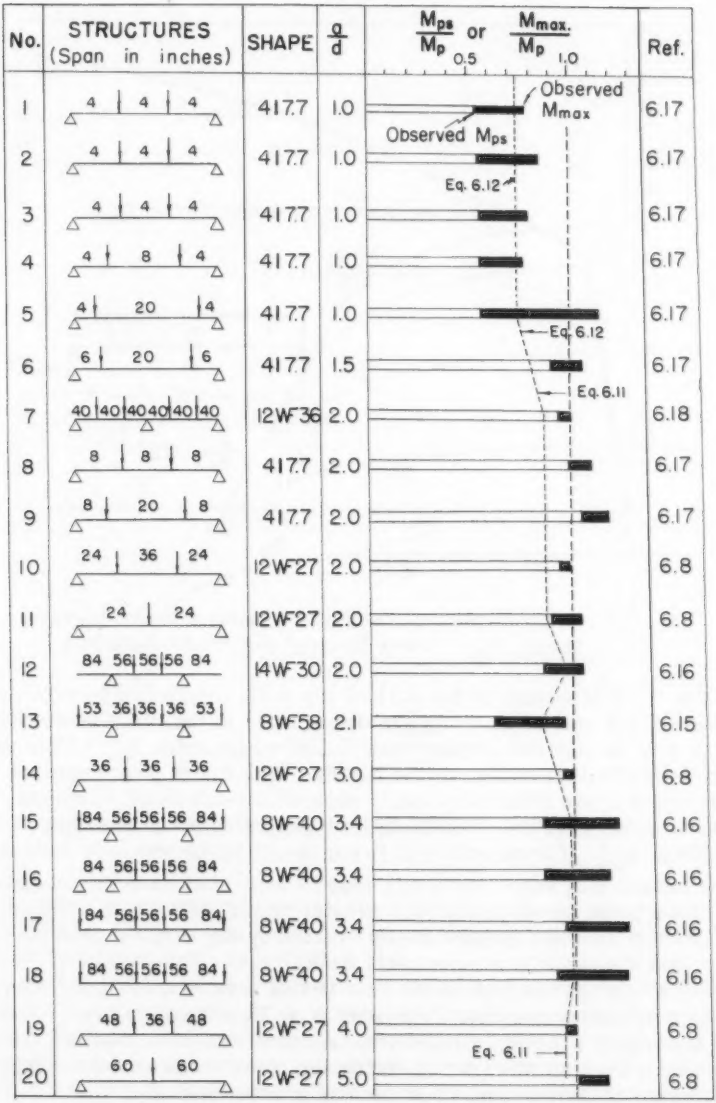

Fig. 6.6. Summary of Test Results for Beams Under Combined Action of Shear and Moment

the full plastic value. Therefore no reduction in the plastic moment M_p is required for the effect of shear if at ultimate load V is less than 18,000 wd pounds (Eq. 6.14).

> Combined Moment and Shear Force
>
> The design is satisfactory as regards shear force V if its magnitude at ultimate load does not exceed 18,000 wd (V in pounds and w and d in inches). No modification of the plastic moment is required.

Local Buckling

Statement of the Problem

Rolled structural steel WF shapes are so proportioned that premature local buckling will not occur for members proportioned in accordance with allowable stress specifications. Plastic design requires that a member have capacity to sustain sufficiently large plastic hinge rotations so that such hinges may form at certain sections without the occurrence of inelastic instability and consequent loss of moment capacity. Hence plastic design may impose more severe conditions on the local buckling behavior of the plate elements of structural members. Local failure, both of the flange and the web can be treated separately as plate buckling problems making use of proper boundary conditions and restraints provided from the adjacent plate.

Previous Research

The problem of elastic and inelastic buckling below the yield stress is discussed by Bleich.[6.19] Bijlaard[6.20] was the first to apply the deformation theory (finite stress-strain relations) to the plastic plate buckling problem. The theory was further developed by Ilyushin[6.21] and modified by Stowell.[6.22] Winter[6.23] called attention to the problem of local flange buckling, discussing possible limitations in width-thickness ratios. The flow theory (incremental stress-strain relations) was applied by Handelman and Prager[6.24] to perfectly flat plates. The latter theory does not compare well with experimental results. Onat and Drucker[6.25] suggested that the deviations between theory and experimental results were due to the initial imperfections of the plate. Bleich[6.19] has proposed an approximate method for the analysis of inelastic local buckling and has considered various structural shapes.

Maaijer and Thürlimann[6.27] have presented the results of further study of the stability of plates compressed beyond the yield point and even into the strain-hardening range. Theoretical results verified by experimental data were also presented in this reference.

Theoretical Analysis

The theoretical analysis of Ref. 6.27 is based on the following assumptions:

1. The material follows an idealized stress-strain diagram (Fig. 6.7)*
2. Yielding occurs discontinuously in slip bands such that the material is either elastic or strain hardened.
3. The material in the elastic range is homogeneous and isotropic, while in the strain-hardening range it is homogeneous and orthotropic.
4. A linear strain variation is assumed as shown in Fig. 6.8.
5. Yielding of a compressed element starts either from both ends simultaneously or from the middle section of the element.
6. An incremental stress-strain relationship is used. However consideration is given to initial imperfections of the plate by introducing effective moduli for the strain-hardening range.
7. Interaction between plate elements is taken into account by a coefficient of restraint.

Assuming that buckling occurs without strain reversal, the equilibrium condition for a differential plate element of orthotropic material yields**

$$D_x \frac{\partial^4 w}{\partial x^4} + 2H \frac{\partial^4 w}{\partial x^2 \partial y^2} + D_y \frac{\partial^4 w}{\partial y^4} = -\frac{t\sigma_x}{I} \frac{\partial^2 w}{\partial x^2} \qquad (6.15)$$

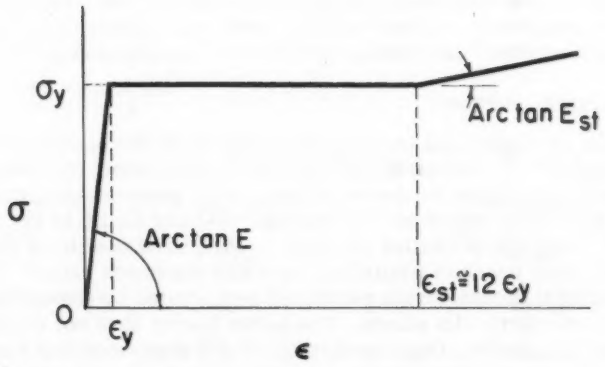

Fig. 6.7. Typical Idealized Stress-Strain Diagram for A7-Type Structural Steel

*In order to derive a rational plate buckling equation for the inelastic range between the proportional limit and the point of strain-hardening, residual stresses must be considered. However, no general solution to the problem has been developed to date. Therefore an empirical transition curve has been proposed in Ref. 6.27.

**The reader is referred to Chapter 3, of "Mathematical Theory of Elasticity" by I. S. Sokolnikoff for discussion of orthotropic material.

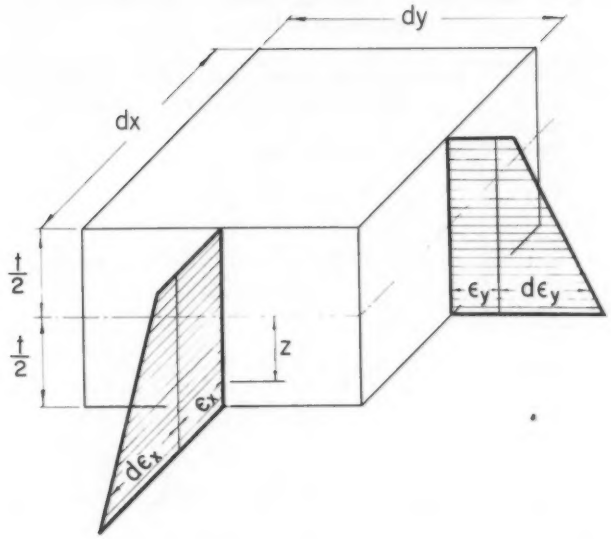

Fig. 6.8. Assumed Linear Strain Distribution (No Strain Reversal Occurs)

where

$$D_x = \frac{E_x}{1 - V_x \gamma_y}$$

$$D_y = \frac{E_y}{1 - V_x \gamma_y}$$

$$D_{xy} = \frac{V_y E_x}{1 - V_x \gamma_y}$$

$$D_{yx} = \frac{V_x E_y}{1 - V_x V_y}$$

$$2H = D_{xy} + D_{yx} + 4G_t$$

G_t = tangent modulus in shear

The reader is referred to Table 6.1 and Figs. 6.9 and 6.10 for solutions of various limiting cases of Eq. 6.15. References 6.26 and 6.27 may be consulted for detailed derivations.

The effective plate moduli D_x, D_y, and D_{xy} and G_t were evaluated in Ref. 6.26 for A7-type steel. Their values are as follows:

D_x = 3,000 ksi

Table 6.1. Summary of Limiting Cases of the Solution of Equation 6.15

PLATE	BOUNDARY CONDITIONS	EXPRESSIONS FOR CRITICAL STRESSES AND FOR EFFECTIVE LENGTH
Flange Plate (Fig. 6.9)	$x = 0$ Simply Supported $x = \ell$ Simply Supported $y = 0$ Free $y = b_o$ Free	$\sigma_{cr} = \left(\frac{t}{b_o}\right)^2 \left[\frac{\pi^2}{12} D_x \left(\frac{b_o}{\ell}\right)^2 + G_t\right]$ for long plate $\sigma_{cr} = \left(\frac{t}{b_o}\right)^2 G_t$
	$x = 0$ Simply Supported $x = \ell$ Simply Supported $y = 0$ Fixed $y = b$ Free	$\sigma_{cr} = \left(\frac{t}{b_o}\right)^2 \left[0.769\sqrt{D_x D_y} - 0.270\,(D_{xy} + D_{yx}) + 1.712\,G_t\right]$ $\frac{t}{d_f} = 1.46\sqrt[4]{\frac{D_x}{D_y}}$
Web Plate (Fig. 6.10)	$x = 0$ Simply Supported $x = \ell$ Simply Supported $y = \frac{d_f}{2}$ Simply Supported $y = \frac{d_f}{2}$ Simply Supported	$\sigma_{cr} = \frac{\pi^2}{12}\left(\frac{w}{d_f}\right)^2 \left[2\sqrt{D_x D_y} + D_{xy} + D_{yx} + G_t\right]$ $\frac{t}{d_f} = 0.66\sqrt[4]{\frac{D_x}{D_y}}$
	$x = 0$ Simply Supported $x = \ell$ Simply Supported $y = \frac{d_f}{2}$ Fixed $y = \frac{d_f}{2}$ Fixed	$\sigma_{cr} = \left(\frac{\pi^2}{12}\right)\left(\frac{w}{d_f}\right)^2 \left[4.554\sqrt{D_x D_y} + 1.237\,(D_{xy} + D_{yx}) + 4.943\,G_t\right]$ $\frac{t}{d_f} = 0.66\sqrt[4]{\frac{D_x}{D_y}}$

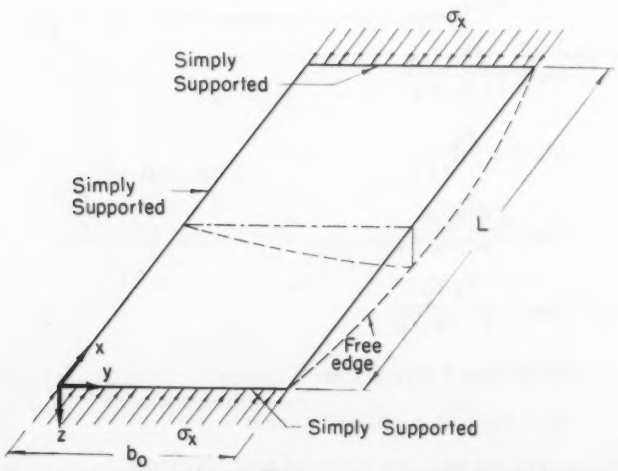

Fig. 6.9. Plate with One Edge Free Simulating One Half of the Flange Element of a WF shape

$D_y = 32{,}800$ ksi

$D_{xy} = V_y D_x = V_x D_y = 8{,}100$ ksi

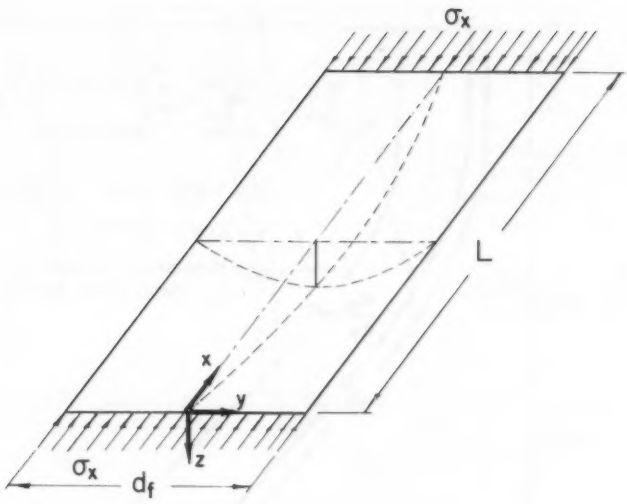

Fig. 6.10. Plate with All Edges Simply Supported Simulating the Web Plate of a WF Shape

G_t = 2,400 ksi

It should be kept in mind that the foregoing expressions and moduli are applicable only for A7-type steel plates stressed to the onset of strain-hardening.

The problem of an axially loaded plate subjected also to bending in the plane of the plate is of practical importance. The web of a WF beam subjected to both axial load and bending moment presents such a case. This problem has been studied in Ref. 6.27 and a diagram is presented for the allowable $\frac{d_f}{w}$ - ratio of the web of a WF section. As shown in Fig. 6.11, the curves are plotted for different ratios of maximum strain to yield strain, $\frac{\epsilon_m}{\epsilon_y}$. As the maximum strain of the compression flange increases, the critical d_f/w - ratio decreases. The critical value of the axial force P also decreases as the ratio of the depth to the thickness of the web increases.

Experimental Correlation

Tests were carried out to check the theory for local buckling of WF shapes. It was found that the theoretical curves gave a good description of the actual behavior of flanges and webs. Fig. 6.12 gives the experimental correlation with theory for the buckling of flange plates. Fig. 6.13 gives the same comparison for the buckling of web plates. The specimens tested in this program[6.27] included 8WF24, 8WF35, 10WF21, 10WF33, 10WF39 and 12WF50 shapes.

Few experimental data are available to compare with the theory in the case of bending with axial force (Fig. 6.11). Partial correlation may be found by examining the results of some corner connection tests,[6.28] if one accepts

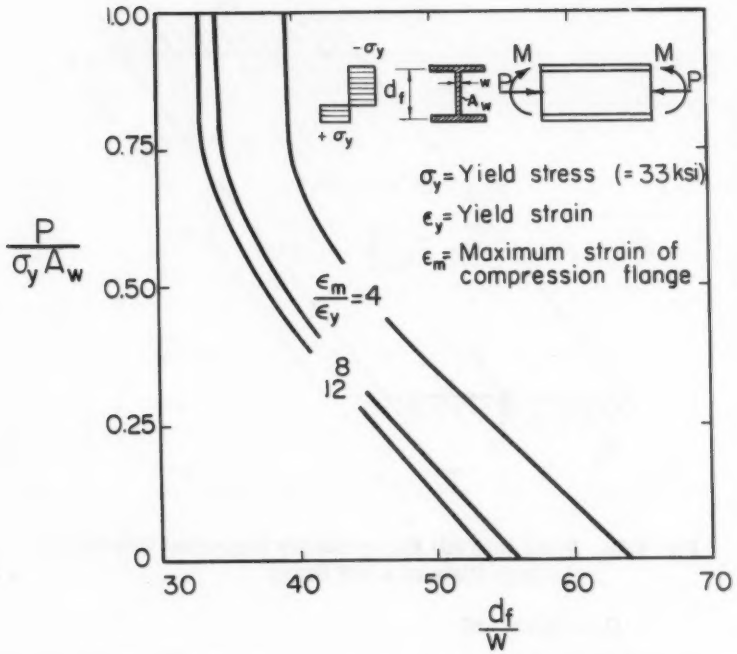

Fig. 6.11. Allowable d_f/w-Ratio of Web of Fully Plastified WF Sections for $\sigma_y = 33$ ksi

the fact that the conditions of these tests were somewhat different from those upon which the theory is based. This comparison is shown in non-dimensionalized form in Fig. 6.14 where the rotation of a selected length of member is plotted vs. the $\frac{d_f}{w}$ - ratio for $\frac{P}{P_y} = 0.10$. The curve is obtained by taking cross-curves of Fig. 6.11. Test results do not check the predictions precisely, but they do indicate a large rotation capacity. The 14WF30 shape rotated an amount less than predicted; on the other hand, the 30WF108 with greater $\frac{d_f}{w}$ - ratio and a somewhat higher axial load ratio rotated much more than the required amount.

Design Approximations

For flange elements Fig. 6.12 shows that if $b/t < 17$, then a section under uniform compression can be strained to the point of strain-hardening before local buckling influences its carrying capacity.

Fig. 6.13 shows that the web of a shape under uniform compression would be limited to $\frac{d_f}{w} < 33$ in order to reach the onset of strain-hardening. However, no such strain is needed in a plastically designed structure and it would be adequate to require only that the strain be able to reach the yield value.

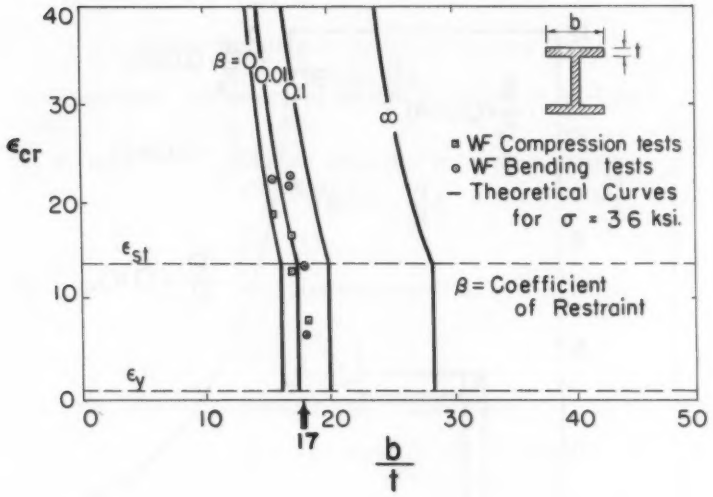

Fig. 6.12. Results of Tests on WF shapes Showing Correlation with Predicted Strain at Buckling of Flanges

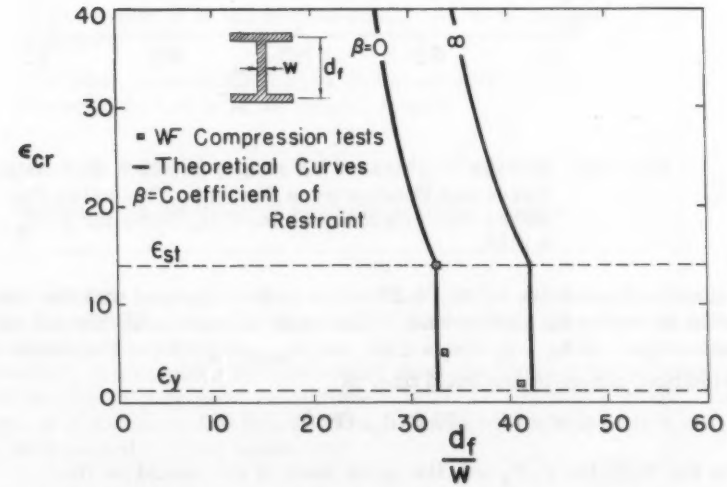

Fig. 6.13. Results of Tests on WF Shapes Showing Strain at Which Web Buckling Occurred

Thus on the basis of Fig. 6.13 the limiting value would be $d_f/w = 41$. Using $d/d_f = 1.05$, the ratio of d/w may go as high as 43 under uniform compression.

For combined bending and compression a design approximation may be developed that is based on the results given in Fig. 6.11. This approximation

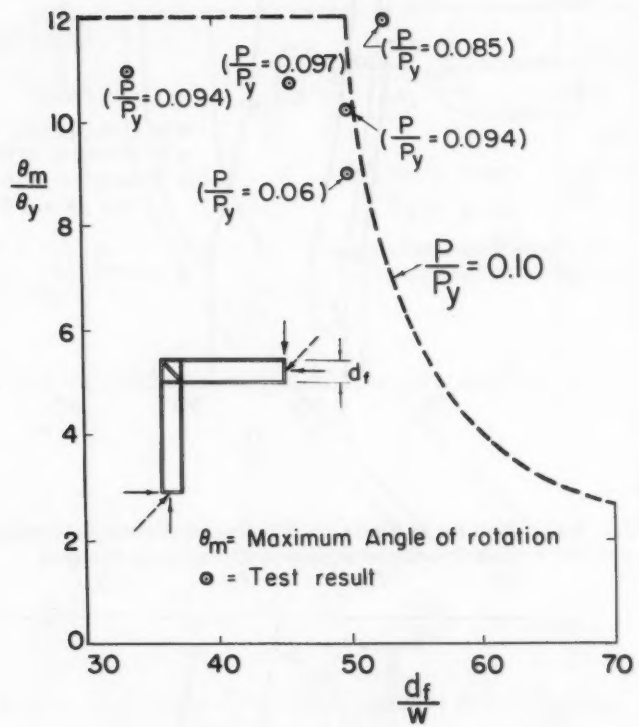

Fig. 6.14. Results of Tests on WF shapes in which Both Axial Force and Bending were Present. The dotted line shows the predicted web buckling curve for $P/P_y = 0.10$.

is shown as a solid line in Fig. 6.15 and is to be compared with the theoretical solution shown by the dashed line. This latter solution assumes the following relationships: $A/A_w = 2$, $d/d_f = 1.05$, and $\epsilon_{max}/\epsilon_y = 4.0$. The design approximation, shown by the solid line, is

$$d/w = 70 - 100\ P/P_y,\ (P/P_y \leq 0.27) \qquad (6.16)$$

From Eq. 6.16, for $P/P_y = 0$, the upper limit of d/w would be 70.

In summary, for use in plastic design involving shapes of ASTM A7-type steel ($\sigma_y = 33$ ksi), the following values are suggested to assure that premature local buckling will not occur:

Local Buckling of Structural Shapes

For I-sections, WF beams of Welded H-Shapes of A7-type steel

(1) Flanges — Compression due to bending, and/or axial force

$$\frac{b}{t} \leq 17$$

(2) Web — Uniform compression

$$\frac{d}{w} \leq 43$$

(3) Web — Bending and compression

$$\frac{d}{w} = 70 - 100\frac{P}{P_y} \quad \left(\frac{P}{P_y} \leq 0.27\right)$$

$$\frac{d}{w} = 43$$

where b and t are the width and thickness of the flange respectively, d is the section depth, and w is the web thickness.

For other outstanding flanges and plate stiffeners intended to be stable in the plastic region.

(4) $$\frac{b'}{t} = 8.5$$

where b' is the width of outstanding plate element.

For rolled shapes, a small upward variation of the b/t ratio to include, for example, the 14WF30 (b/t = 17.58) would be reasonable. This section performed adequately under test.

In practice, if a selected section cannot meet the above requirements, a different section may be used for stiffeners could be added to prevent local buckling. It is fortunate that nearly all rolled I and WF shapes are satisfactory with regard to local instability.

ACKNOWLEDGMENT

The Joint Committee acknowledges the work of a research group at Fritz Engineering Laboratory, Department of Civil Engineering, Lehigh University. This group has been engaged through the Institute of Research in an investigation entitled "Welded Continuous Frames and Their Components." The results of that investigation were the basis of preliminary reports which were later revised and supplemented by the Joint WRC-ASCE Committee. The staff members at Fritz Laboratory included L. S. Beedle, G. C. Driscoll, Jr.,

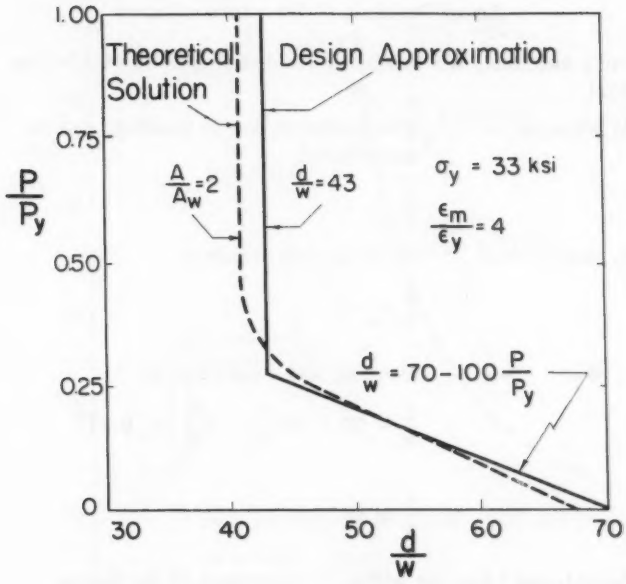

Fig. 6.15. Limiting Slenderness Ratios for the Web Plate of WF Shapes under Combined Bending and Axial Compression.

T. V. Galambos, R. L. Ketter, T. Kusuda, G. C. Lee, T. Lee, L. W. Lu, A. Ostapenko and B. Thürlimann. Wm. J. Eney is Director of Fritz Laboratory and Head of the Civil Engineering Department.

The organizations that supported the research projects out of which the preliminary reports were prepared were the following: American Institute of Steel Construction, American Iron and Steel Institute, Column Research Council, the Department of the Navy (Office of Naval Research, Bureau of Ships, Bureau of Yards and Docks) and the Welding Research Council.

Respectfully submitted,

A. Amirikian
Lynn S. Beedle
J. M. Crowley
F. H. Dill
Samuel Epstein
LaMotte Grover
William H. Jameson
Bruce G. Johnston
Jonathan Jones
R. L. Ketter
Carl Kreidler
H. W. Lawson
Frank Baron
John M. Biggs
Daniel C. Drucker
John D. Griffiths
William J. Hall
T. R. Higgins
Harry N. Hill
Eivind Hognestad
Robert L. Janes
Bruce G. Johnston
William H. Hunse, Jr.
Egor P. Popov

Nathan M. Newmark
R. M. Stuchell
John Vasta

T. R. Higgins, Chairman

Lehigh Project Subcommittee
Structural Steel Committee
Welding Research Council

John B. Scalzi
Paul S. Symonds
Bruno Thurlimann
George Winter
Douglas T. Wright
Lynn S. Beedle, Chairman

Committee on Plasticity Related to Design
Engineering Mechanics Division
American Society of Civil Engineers

ADDITIONAL NOMENCLATURE

(See Progress Report No. 1 for basic nomenclature)

b = width of stiffener

$D_x = \dfrac{E_x}{1 - V_x V_y}$

$D_y = \dfrac{E_y}{1 - V_x V_y}$

$D_{xy} = V_y D_x$

$D_{yx} = V_x D_y$

E_x = tangent modulus in x-direction

E_y = tangent modulus in y-direction

G_t = tangent modulus in shear

M_{pm} = plastic hinge moment modified to include effect of axial compression and shear force

M = bending moment along a beam about strong axis

M_x = bending moment per unit width of plate in x-direction

M_y = bending moment per unit width of plate in y-direction

P = axial load

P_y = yield load

w = deflection of the plate
= web thickness

y_o = distance between neutral axis and compression flange

β = coefficient of restraint

γ = shearing strain

ϵ_m = Maximum strain of compression flange

ϵ_x = strain in x-direction

ϵ_y = strain in y-direction

V = Poisson's ratio

V_x = coefficient of dilatation for stress increment in x-direction

V_y = coefficient of dilatation for stress increment in y-direction

σ_{cr} = critical stress

ψ = edge moment per unit length to produce unit rotation of edge

REFERENCES

Art. 6.1

6.1. Horne, M. R.
THE PLASTIC THEORY OF BENDING OF MILD STEEL BEAMS WITH PARTICULAR REFERENCE TO THE EFFECT OF SHEAR FORCES, Proc. Royal Society, A, (207) p. 216 (1951).

6.2. Leth, F. A.
THE EFFECT OF SHEAR STRESSES ON THE CARRYING CAPACITY OF I-BEAMS, Technical Report 107, Brown University (1954).

6.3. Heyman, J., Dutton, V. L.
PLASTIC DESIGN OF PLATE GIRDERS WITH UNSTIFFENED WEBS, Welding and Metal Fabrication, Vol. 22, p. 265 (1954).

6.4. Green, A. P.
A THEORY OF THE PLASTIC YIELDING DUE TO BENDING OF CANTILEVERS AND FIXED-ENDED BEAMS, Journal of Mechanics and Physics of Solids, 3 (1) p. 143 (1954).

6.5. Onat, E. T., Shield, R. T.
THE INFLUENCE OF SHEARING FORCES ON THE PLASTIC BENDING OF THE WIDE BEAMS, Proceedings of the 2nd U.S. National Congress of Applied Mechanics, Ann Arbor, Michigan pp. 535-537 (1954).

6.6. Drucker, D. C.
THE EFFECT OF SHEAR ON THE PLASTIC MOMENT OF BEAMS, Journal of Applied Mechanics, A.S.M.E. 23 (4) pp 509-514 (December 1954).

6.7. Hodge, P. G. Jr.
INTERACTION CURVES FOR SHEAR AND BENDING OF PLASTIC BEAMS, Journal of Applied Mechanics, A.S.M.E. 24 (3)-pp. 453-456 (September 1957).

6.8. Fujita, Y.
INFLUENCE OF SHEAR ON THE FULL PLASTIC MOMENT OF BEAMS, Fritz Lab Report, Lehigh University, (1955).

6.9. Beedle, L. S., Thürlimann, B., Ketter, P. L.
PLASTIC DESIGN IN STRUCTURAL STEEL, (Lecture Notes) Lehigh University and AISC, (New York) (September 1955).

6.10. Horne, M. R.
THE FULL PLASTIC MOMENTS OF SECTIONS SUBJECTED TO SHEAR FORCE AND AXIAL LOAD, British Welding Journal, (April 1958).

6.11. Kusuda, T., Thurlimann, B.
STRENGTH OF WIDE-FLANGE BEAMS UNDER COMBINED INFLUENCE OF MOMENT, SHEAR AND AXIAL FORCE, Fritz Lab Report 248.1, Lehigh University (1958).

6.12. Baker, J. F., Roderick, J. W.
FURTHER TESTS ON BEAMS AND PORTALS, Transactions, Institute of Welding Vol. 3, p. 83 (1940).

6.13. Hendry, A. W.
THE STRESS DISTRIBUTION IN A SIMPLY SUPPORTED BEAM OF I-SECTION CARRYING A CENTRAL CONCENTRATED LOAD, Proceedings, Society for Experimental Stress Analysis, Vol. 7, p. 91 (1949).

6.14. Longbottom, E., Heyman J.
TESTS ON FULL-SIZE AND ON MODEL PLATE GIRDERS, Structures Paper No. 49, Institute of Civil Engineers, (1956).

6.15. Hall, W. J., NewMark, N. M.
SHEAR DEFLECTION OF WIDE-FLANGE STEEL BEAMS IN THE PLASTIC RANGE, Transactions, ASCE, 122 (2878) p. 666 (1957).

6.16. Yang, C. H.
THE PLASTIC BEHAVIOR OF CONTINUOUS BEAMS, Ph.D. Dissertation, Lehigh University, (1951).

6.17. Yang, C. H., Beedle, L. S.
BEHAVIOR OF I AND WF BEAMS IN SHEAR, Fritz Lab Report 205B.21, Lehigh University, (1951).

6.18. Driscoll, G. C., Beedle, L. S.
THE PLASTIC BEHAVIOR OF STRUCTURAL MEMBERS AND FRAMES, Welding Journal 36 (6) p. 275-s (June 1957).

Art. 6.2

6.19. Bleich, F.
BUCKLING STRENGTH OF METAL STRUCTURES, Chapter 9, McGraw-Hill Book Co., New York (1952).

6.20. Bijlaard, P. P.
SOME CONTRIBUTIONS TO THE THEORY OF ELASTIC AND PLASTIC STABILITY, Publication, International Association for Bridge and Structural Engineering Vol. VIII (1947).

6.21. Ilyushin, A. A.
STABILITY OF PLATES AND SHELLS BEYOND THE PROPORTIONAL LIMIT, NACA TM - 1116 (1947).

6.22. Stowell, E. Z.
A UNIFIED THEORY OF PLASTIC BUCKLING OF COLUMNS AND PLATES, NACA Report 898 (1958).

6.23. Winter, G.
FLANGE BUCKLING, A LIMITATION OF PLASTIC DESIGN, Final Report, International Association for Bridge and Structural Engineering, p. 139 (1952).

6.24. Handelman, D. C., Prager, W.
PLASTIC BUCKLING OF A RECTANGULAR PLATE UNDER EDGE THRUST, NACA TN-1530 (1948).

6.25. Onat, E. T., Drucker, D. C.
INELASTIC INSTABILITY AND INCREMENTAL THEORIES OF PLASTICITY, Journal of the Aeronautical Science 20, (3) (March 1953).

6.26. Haaijer, G.
PLATE BUCKLING IN THE STRAIN-HARDENING RANGE, ASCE Journal 83 (EM-2) p. 1212 (April 1957).

6.27. Haaijer, G., Thürlimann, B.
ON INELASTIC BUCKLING IN STEEL, ASCE Journal 84 (EM-2) p. 1581 (April 1958).

6.28. Fisher, J. W., Driscoll, G. C., Schutz F. W.
BEHAVIOR OF WELDED CORNER CONNECTIONS, Welding Journal 37 (5) p. 216-s (May 1958).

Journal of the
ENGINEERING MECHANICS DIVISION
Proceedings of the American Society of Civil Engineers

COMMENTARY ON PLASTIC DESIGN IN STEEL: ADDITIONAL DESIGN CONSIDERATIONS - II

Progress Report No. 4 of the Joint WRC-ASCE Committee on Plasticity Related to Design

FOREWORD

This paper is the fourth in a series of reports on Plastic Design emanating from a Joint Committee of the Welding Research Council and the American Society of Civil Engineers. Reference should be made to Progress Report No. 1 (which appeared on the July EM Journal) for such items as the Foreword, Synopsis, Definitions, and Nomenclature. For information the complete Table of Contents appears at the beginning of Progress Report No. 3 immediately proceeding this paper. Articles 6.3 and 6.4 are included herein.

The Joint Committee has approved the publication of this information with the strong recommendation that it be read carefully by all structural engineers.

Note: Discussion open until March 1, 1960. Separate discussions should be submitted for the individual papers in this symposium. To extend the closing date one month, a written request must be filed with the Executive Secretary, ASCE. Paper 2231 is part of the copyrighted Journal of the Engineering Mechanics Division, Proceedings of the American Society of Civil Engineers, Vol. 85, No. EM 4, October, 1959.

6.3. Lateral Buckling

Statement of the Problem

In order to realize the necessary inelastic rotations at plastic hinge locations the members must have sufficient lateral support so that lateral-torsional buckling will not reduce the resisting moment at these sections. When a member buckles laterally it undergoes lateral bending and twisting. Elastic regions of the beam resist this buckling through lateral bending stiffness I_y and torsional resistance. The latter consists of two parts:*

a) Resistance associated with St. Venant's torsion

b) Resistance associated with warping torsion (or cross bending)

A member with an adequate combination of these properties will have effective resistance to lateral-torsional buckling.(6.29)

The types of lateral support available in actual structures vary greatly. For most structures, however, the points of applied loading also constitute points of lateral support.

Previous Research

Although many studies on the lateral-torsional buckling of elastic members have been carried out since Timoshenko (1906, 1913), Wagner (1936), Kappus (1938) and Goodier (1941), there are few solutions available in the inelastic range. Bleich(6.19) suggests that this inelastic effect can be allowed for by determining the most critically stressed section and using a tangent modulus reduction factor ($\tau = E_t/E = G_t/G$) in the elastic solutions. This approach forms a simple and expedient means of approximating the inelastic effects. It is generally held that this practice is conservative. However, recent investigations made by Campus and Massonnet(6.32) indicated that in some cases it may be on the unsafe side. Clark and Hill(6.33) refer to these and other approximations in connection with application to design. In Ref. 6.34 it is shown that test results for laterally unsupported wide-flange shapes agree very well with the concept that the ratio between the elastic critical buckling stress and the actual critical buckling stress is the same in the inelastic range for beams and columns.

Neal(6.35) studied this problem by considering, in detail, the effect of yielding (idealized stress-strain curve) on the lateral flexural rigidity and initial torsional rigidity of a rectangular cross section. His solution corresponds to the reduced modulus solution of an axially loaded column. Wittrick(6.36) pointed this out and deduced an equivalent formula on the basis of a tangent modulus load, assuming no unloading of the cross section.

Horne(6.37) extended these results for pure bending to the case of I-beams. His conclusions, however, were modified by other practical considerations. Eventually, from this work, limiting critical lengths of I-beams were presented as a basis for design by Baker, Horne, and Heyman.(6.38) The fundamental concept behind this work is a tacit reliance on the post-buckling strength of a member to provide the necessary moment resistance over a large range of its deformation.

*See, for example, Ref. 6.29 for a discussion of St. Venant's torsion and warping torsion.

The solution of the various cases on a systematic basis was obtained by White.(6.31) He also presented a design procedure for determining the spacing of lateral supports such that the members would not buckle laterally before the required plastic hinges had formed. Although a simplifying approximation has been made for practical use, the method still presents three main difficulties:

1) Under conditions of loading where the moment diagram has a small gradient, the procedure gives results which are too conservative when compared with test results.

2) The method of design is an iterative procedure because of the restraining influence of adjacent segments on the segment being braced.

3) One of the necessary parameters is the amount of plastic hinge rotation required to obtain a complete re-distribution of moments corresponding to the ultimate load. Unless an assumption is made of a single given amount of rotation, this would have to be computed analytically and would therefore complicate the design procedure.

Theoretical Analysis

Assuming as in the solution to local instability problems that the process of yielding of structural steel is non-homogeneous,(6.30) the actual material will be in either the elastic or the strain-hardened state. Since the material in each of these regions behaves in a linear homogeneous manner characterized by its appropriate moduli, it is reasonable to assume that the problem can be reduced, in a somewhat simplified manner, to the consideration of a member with an abrupt change in stiffness.(6.27) In the case of a completely strain-hardened member the resistance to buckling depends almost entirely on warping torsion instead of on a combination of St. Venant's torsion and lateral bending strength as in the fully elastic case. For a member with partial strain-hardening, the effects of St. Venant's torsion, moment gradient and end restraint are then considered as modifications of the basic solution.

The basic assumptions for the theoretical analysis(6.31) are as follows:

1) The material in a member deformed beyond the elastic limit either is at a strain less than the yield strain or has reached the strain-hardening range.

2) The distribution of the elastic and strain-hardening zones depends on the magnitude and location of the over-all inelastic deformation. Strain-hardening is assumed to start at the end of the member at the point of maximum moment and to spread from that point.

3) It is assumed that the member is initially straight and that no lateral or torsional deflection takes place before buckling. This approach leads mathematically to an eigenvalue problem. The lowest point of bifurcation of equilibrium is obtained by considering no strain reversal. At this point of buckling, therefore, the linear incremental stress-strain relations can be used, the two different zones being characterized by the incremental elastic and strain-hardening moduli, respectively.*

*Another possible solution would be to analyze for the ultimate strength of the member; this latter solution, however, has not been obtained up to the present.

4) A solution can be obtained by solving the normal linear differential equation for both regions and matching the boundary conditions between them.

5) The cross section is restricted to an open, doubly-symmetrical, thin-walled shape.

6) The cross section is idealized so that the whole section will be considered as either elastic or strain-hardened under flexure. The condition of having a non-homogeneous material over the cross section is difficult to handle analytically, since then the differential equations of equilibrium would have variable coefficients. As shown in Ref. 6.31 this assumption of an idealized cross section gives conservative results.

When the loading is restricted to the case of loading in one principal plane at the boundary only, with zero axial force and zero applied forces along the beam, the basic equations can be re-written in the following form:

$$EC_w \frac{d^4\beta}{dz^4} - GK \frac{d^2\beta}{dz^2} + M_\xi \frac{d^2u}{dz^2} = 0$$

$$EI_x \frac{d^4v}{dz^4} = 0 \qquad (6.17)$$

$$M_\xi \frac{d^2\beta}{dz^2} + 2\frac{dM_\xi}{dz} \frac{d\beta}{dz} + EI_y \frac{d^4u}{dz^4} = 0$$

where

EC_w = warping rigidity

GK = St. Venant's torsional rigidity

EI_x = bending rigidity of the beam about strong axis

EI_y = bending rigidity of the beam about weak axis

β = angle of twist about shear center

u = displacement of shear center in weak direction

v = displacement of shear center in strong direction

z = axis along the beam, $0 \leq z \leq L$

M_ξ = applied bending moment along the beam about the strong axis

L = length of beam

The problem solved in Ref. 6.31 was a single-span beam with load applied in the maximum principal plane of bending. Both simply supported and fixed-end conditions were considered. The simple supports, however, were assumed to be able to resist twisting. Part of the beam was considered elastic and part strain-hardened as shown in Fig. 6.16. For the strain-hardened portion (length αL) in the above equations were modified by introducing the strain-hardening moduli in lieu of the elastic values. The continuity conditions were introduced at the juncture of the elastic and strain-hardened portions. The effect of moment gradient is shown in Fig. 6.17 and the effect of

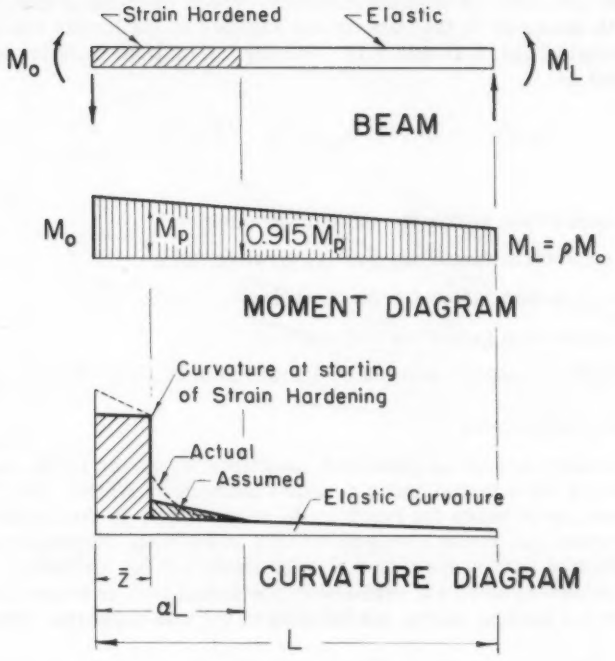

Fig. 6.16. Moment-Curvature Diagram for a Partially Yielded Beam Under Moment Gradient

St. Venant's torsion is shown in Fig. 6.18. The differential equations mentioned above were solved by a numerical procedure based on finite differences, using the appropriate boundary conditions. The computations for determining the eigenvalue for various conditions of restraint, loading, and extent of strain-hardening were carried out on a digital computer.

Four series of results were obtained as follows:

1) Member simply supported at each end
2) Member fixed at each end
3) Member fixed at end z = 0, simple at end z = L
4) Member simply supported at end z = 0, fixed at end z = L

The basic critical buckling length for simply supported beams under uniform moment is determined from the expression $A = L_{cr}\sqrt{\frac{Z}{h\ I_y}}$, where A, the eigenvalue, equals 11.28 and Z is the plastic modulus of the cross section. For a WF beam it has been shown that $\sqrt{h\ I_y/Z} = 1.60\ r_y$, therefore $L_{cr}/r_y = 18$. This length is then corrected for the effects of moment gradient and extent of yielding over the unbraced length of the member. Correction factors are also determined for the St. Venant's torsional resistance of the

member and the effect of moment gradient. These correction factors can be expressed in terms of ρ, the ratio of the smaller to the larger end moments. See for example Figs. 6.17 and 6.18. Finally the critical buckling length can be expressed as

$$L_{cr}/r_y = 18 \quad \nu_\rho \ \nu_\alpha \ \nu_s \ \nu_\gamma \ \sqrt{M_p/M_o} \tag{6.18}$$

where

ν_ρ = correction factor for moment gradient

ν_α = correction factor for partial yielding (αL)

ν_s = correction factor for St. Venant's torsion

ν_γ = correction factor for end fixity

M_p/M_o = ratio of plastic moment to actual moment at $z = 0$

Experimental Correlation

Two specimens providing fixed-end conditions by boxing in the end sections of the members were tested under constant moment by White. The "fixed-end" condition was one in which the beam could rotate freely in the loading plane (strong direction) but rotation was prevented in the weak direction and twisting was prevented with respect to the longitudinal axis of the beam. These conditions, however, were not realized in the actual test as evidenced by movement of the loading points and twisting of the end supports. Therefore,

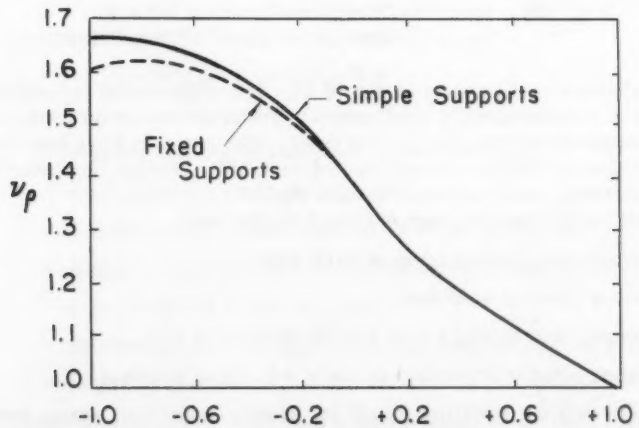

Fig. 6.17. Effect of Moment Gradient as Compared to Uniform Moment for Lateral-Torsional Buckling for Beams Simply Supported or Fixed-Ended (Warping Torsion Only)

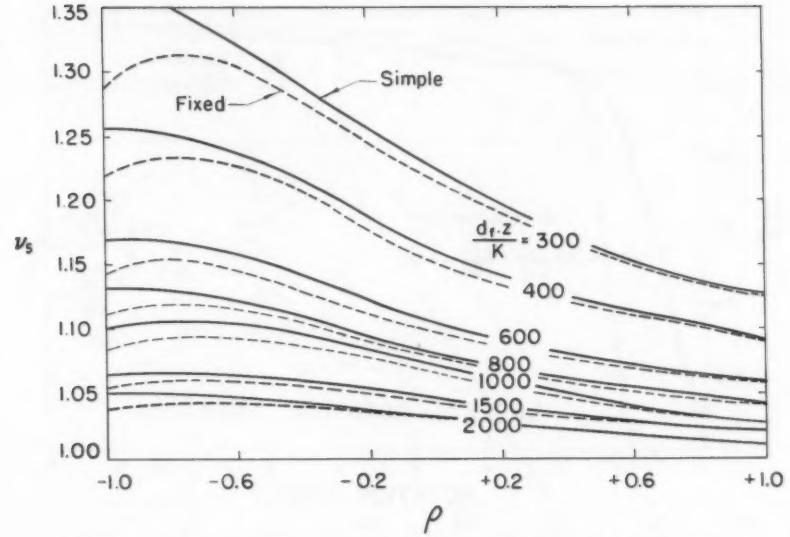

Fig. 6.18. Effect of Saint Venant's Torsion ($d_f Z/K$) on the Critical Buckling Length for Beams Simply Supported or Fixed-Ended

the values of ν_α obtained from the test results were considerably lower than values predicted by the theoretical analysis for the fixed-end beam.

Further tests were conducted by R. Sarubbi[6.39] in order to find the effect of moment ratio ρ on the critical buckling length of the simply supported beam. Four specimens were tested with moment ratios of 0.40, 0.71, 0.90 and 0.98 respectively. Fig. 6.19 shows a typical curve of moment vs. lateral rotation for $\rho = 0.71$, together with the relation of the moment and rotation about the strong axis. The plastic moment M_p is computed using the average value of static yield level σ_{ys} for the flanges and the value of the plastic modulus derived on the basis of measured dimensions. The non-dimensional inelastic angle change $H/L\phi_p$ is computed from this curve for three cases: the point of buckling, the point of maximum load, and the last recorded load. The ratio $H/L\phi_p$ is used to express rotation in which H is the total inelastic angle change between the two load points, L is the distance between the points of lateral supports, and $\phi_p = M_p/EI$ is the elastic part of the curvature at the plastic moment. The observed values of $H/L\phi_p$ are shown on Fig. 6.20 at the corresponding moment ratios and slenderness ratios, L/r_y, of the sections tested. These tests indicate that the theoretical considerations give conservative results.

Design Approximation

The critical buckling length L_{cr}/r_y is given by

$$L_{cr}/r_y = 18\ \nu_\rho\ \nu_\alpha\ \nu_s\ \nu_\gamma \sqrt{\frac{M_p}{M_o}} \qquad (6.18)$$

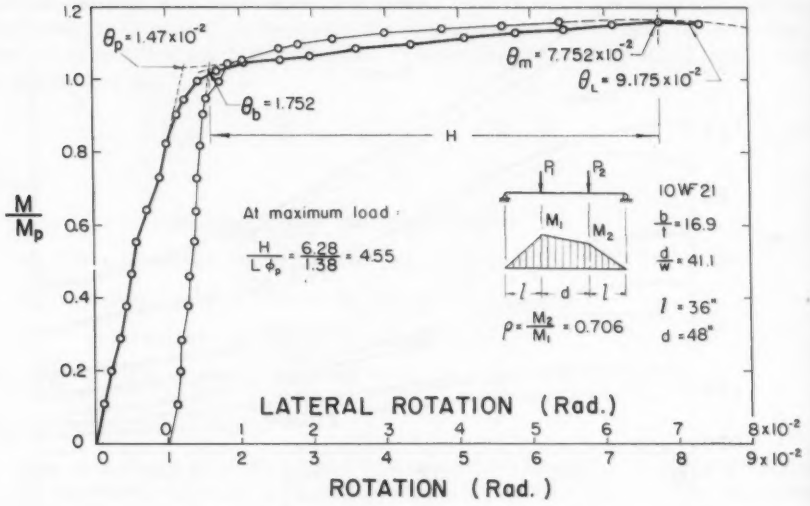

Fig. 6.19. Moment Vs. Rotation Curves of a Lateral Buckling Test Under Moment Gradient

as mentioned above and these correction factors can be obtained by a trial and error procedure using tables and figures given in Ref. 6.31. For instance, the correction factor ν_α for the effect of partial strain-hardening of the member depends upon the moment ratio ρ and the yielded length α L. The value of α depends also on the moment ratio ρ and the angle of rotation of the beam at hinge points. It may be too tedious to compute the critical length between two adjoining points using many figures and tables. Therefore, the following approximations are made for each correction factor.

1) $\nu_\rho = 1.34 - 0.34\,\rho$
2) ν_α is assumed to be related to α only
3) α is obtained from the moment ratio ρ and angle of rotation $H/L\phi_p$
4) Then ν_α can be expressed in terms of ρ with a parameter of rotation angle. A reasonable value of $H/L\phi_p = 3$ is chosen on the basis of practical considerations.
5) $\nu_s = 1.08 - 0.04\,\rho$

This expression corresponds to a ratio $\frac{d_f Z}{K} \simeq 800$ and is based on the following values for WF beams:

$$\sqrt{\frac{hI_y}{Z}} \Big/ r_y \simeq 1.60, \quad \frac{A_f}{A_w} \simeq 2.0, \quad \frac{d_f}{d_w} \simeq 1.05$$

where A_f is flange area, A_w is web area, d_f is flange distance and d_w is web depth.

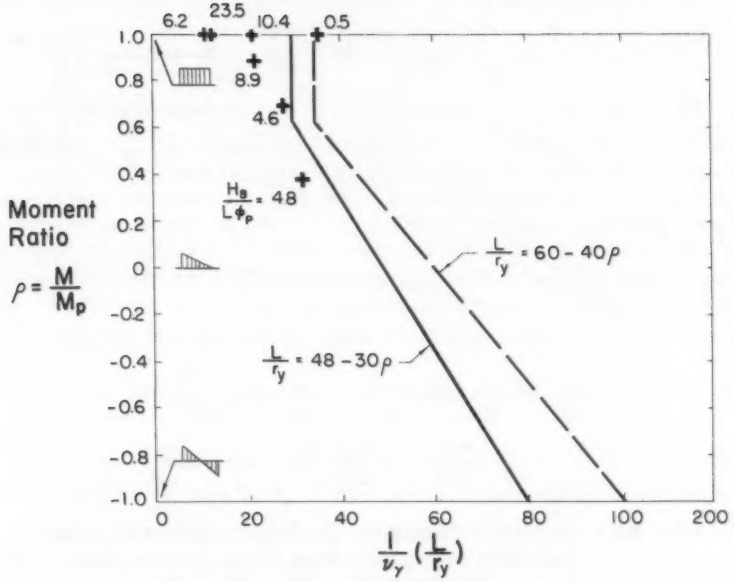

Fig. 6.20. Critical Slenderness Ratio as a Function of the Moment Ratio for Lateral Buckling of Beams

6) $\sqrt{M_p/M_o} \cong 1.0$

From these approximations the correction factors (except that due to end restraint) are simplified, and the final relationship between the critical length and moment ratio can be expressed as a straight line,

$$L_{cr}/r_y = 48 - 30\rho \qquad (6.19)$$

L_{cr}/r_y need not be less than 30, since the theory is known to be overly conservative when $\rho > 0.6$.

7) The correction factor ν_γ for end restraint depends upon the stiffness of the adjacent segments as shown in Fig. 6.21 where k_ℓ is the larger stiffness and k_s the smaller stiffness of adjacent segments respectively.(6.39) The stiffness factor k under thrust is approximately given by

$$k = \frac{3EI}{L}\left[1 - \left(\frac{L}{L_{cr}}\right)^2\right] \qquad (6.20)$$

where L is the actual length of the adjacent segment and L_{cr} is given by Eq. 6.19 for the adjacent segment if it is plastic-elastic or, if the adjacent segment remains elastic then L_{cr} is given by

$$\frac{L_{cr}}{r_y} = \frac{134}{\sqrt{\rho_{BC}}} + 60\,(1 - \rho_{AB}) - 1100\,(\rho_{BC} - 0.9) \qquad (6.21)$$

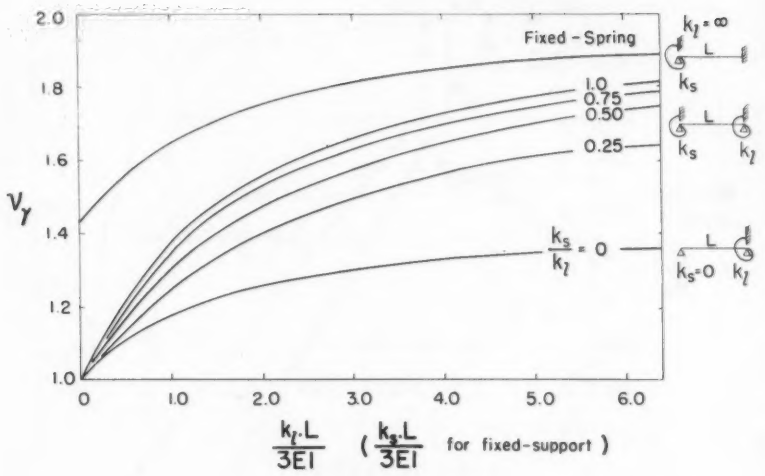

Fig. 6.21. Restraint Factor for Continuous Beams Showing Influence of Adjacent Span on the Critical Span

where ρ_{AB} = moment ratio in the adjacent segment

ρ_{BC} = moment ratio in the segment being investigated

The last term gives the reduction of L/r_y due to plastic deformation for $\rho_{BC} > 0.9$, and if $\rho_{BC} < 0.9$ then the last term vanishes.

A value for ν_γ is obtained by entering Fig. 6.21 with k_s/k_ℓ and $k_\ell L/3EI$, where L is the actual length of the segment being investigated.

Design Approximation for Equal EI/L

For a continuous beam with constant EI and equal unbraced segment lengths, the ratio

$$\frac{k_s}{k_\ell} = \frac{1 - (\frac{L_s}{L_{scr}})^2}{1 - (\frac{L}{L_{\ell cr}})^2} \leq 1.0 \qquad (6.22)$$

and the value

$$\frac{k_\ell L}{3EI} = 1 - (\frac{L}{L_{\ell cr}})^2 \leq 1.0 \qquad (6.23)$$

Then ν_γ is found from Fig. 6.21 as before.

Since the value of $k_\ell L/3EI$ is less than 1.0, as can be shown with the aid of Fig. 6.21, the variation of ν_γ vs $\frac{k_s}{k_\ell}$ for $0 < \frac{k_s L}{3EI} < 1.0$ is nearly a

straight-line function and is approximated[6.39] by the expression

$$\nu_\gamma = 1.0 + 0.2 \frac{k_\ell L}{3EI} (0.9 + k_s/k_\ell) \qquad (6.24)$$

Simplified Design Procedure

Recognizing that the effect of end restraint, extent of yielding, St. Venant's torsion, moment gradient, required hinge rotation, and axial force are interrelated and that the exact value of one of these parameters cannot be determined without knowledge of the others, a practical design approach would be to assign a representative value to the restraint factor ν_γ in lieu of the consideration of the separate effects. From Fig. 6.21 it may be seen that an average value of ν_γ is 1.25 for the continuous beam with constant EI and equal unbraced segment lengths. An equation developed on this basis is as follows:

$$L_{cr} = (60 - 40 \frac{M}{M_p}) r_y, \text{ but not less than } 35\ r_y \qquad (6.25)$$

This equation is shown in Fig. 6.20 as a dashed line. When $M/M_p = 1.0$, $\nu_\gamma = 1.17$. When $\frac{M}{M_p} = -1.0$, $\nu_\gamma = 1.28$. Such a variation is reasonable because the correction factor ν_ρ for the moment ratio M/M_p increases with that ratio.

Thus, an approximate value has been established for the effect of all of the correction factors required by the theoretical analysis. In the event the designer would like to use unbraced lengths greater than those indicated by this expression he may use the method based on the theoretical analysis by taking into account each parameter individually and performing the necessary iteration if he feels the slightly increased allowable unbraced length which might result would be justified by the additional design time involved.

Lateral Bracing

The spacing of bracing in the region of plastic hinges where rotation would be required may be determined from the following simplified formula

$$\left.\begin{aligned} \frac{L}{r_y} &\leq 60 - 40 \frac{M}{M_p} \quad \text{for} \quad \frac{M}{M_p} < 0.625 \\ \frac{L}{r_y} &\leq 35 \quad \text{for} \quad \frac{M}{M_p} > 0.625 \end{aligned}\right\} \qquad (6.25)$$

where L = distance between bracing points

r_y = radius of gyration in the weak direction

$\frac{M}{M_p}$ = end moment ratio

To obtain somewhat greater unbraced lengths, the procedures outlined above can be used.

The spacing of bracing in the non-yielded portions of the structure may be determined by methods used in allowable stress design.

Illustrative Examples

The design procedure is essentially a trial and error method if the unbraced length is determined by the consideration of lateral-torsional buckling only. However, in practical design the unbraced length may be fixed by other structural considerations and then must be examined for lateral-torsional buckling. The general procedure for investigating a given unbraced length is:

1) From the moment diagram find moment ratios for this segment and its adjacent unbraced segments.
2) Find L_{cr}/r_y for each segment from Eq. 6.19 or Eq. 6.21.
3) Compute stiffnesses of the adjacent segments from Eq. 6.20.
4) Compute the ratio k_s/k_ℓ and the value $k_\ell L/3EI$.
5) Find ν_γ from Fig. 6.21.
6) The actual length of the segment being investigated should be less than $\nu_\gamma L_{cr}$.

Since the spacing of purlins and girts is usually uniform, the particular unbraced length that must be investigated in a design will be the one with the largest moment ratio at a hinge point where rotation would be required. Ordinarily this means that the bracing spacing would be checked in the region of formation of the first plastic hinge.* Or course, if all segments meet the requirement that would be stipulated for a first plastic hinge location, then no further consideration of hinge sequence would be needed.

Example I: Continuous Beam as shown in Fig. 6.22.

The example will first be worked without any regard to sequence of hinge formation. The problem will then be solved again on the basis that the first hinge forms at the ends.

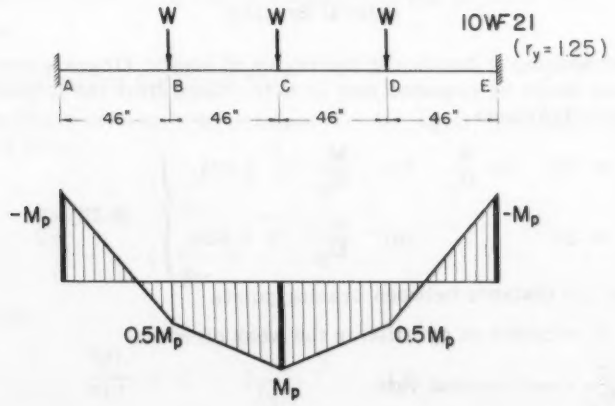

Fig. 6.22. Illustrative Example I of Lateral Bracing

*Sequence of hinge formation is discussed in Chapter 9.

1) Considering only the effect of moment ratio, the critical span is either BC or CD. The moment ratios are $\rho_{AB} = \rho_{DE} = -0.5$, $\rho_{BC} = \rho_{CD} = 0.5$

2) All spans are in the plastic-elastic state, therefore the critical length of each span considered as a simple beam, $\nu_\gamma = 1.0$, is given by Eq. 6.19 as

$$\frac{L_{ABcr}}{r_y} = \frac{L_{DEcr}}{r_y} = 63, \text{ then } L_{ABcr} = L_{DEcr} = 78.75''$$

$$\frac{L_{BCcr}}{r_y} = \frac{L_{CDcr}}{r_y} = 33, \text{ then } L_{BCcr} = L_{CDcr} = 41.25''$$

3) Since the beam is symmetrical about point C, then $k_{CD} = 0$, which means that there is no restraint on span BC due to span CD. From Eq. 6.21,

$$k_{AB} = \frac{3EI}{L_{AB}} \left[1 - \left(\frac{L_{AB}}{L_{ABcr}} \right)^2 \right] = \frac{3EI}{L_{AB}} \left[1 - \left(\frac{46}{78.75} \right)^2 \right]$$

$$= \frac{3EI}{L_{AB}} \; 0.66, \; k_{CD} = 0$$

4) $\dfrac{k_s}{k\ell} = \dfrac{k_{CD}}{k_{AB}} = 0$

$$\frac{k_{AB}L}{3EI} = \frac{k_{AB}L_{BC}}{3EI} = 0.66$$

5) From Fig. 6.21, $\nu_\gamma = 1.13$

6) $L_{BCcr} = 1.13 \times 41.25'' = 46.6'' > 46''$ (OK)

Approaching the problem with the added information that the first hinges form at ends A and E, the critical span is AB (and DE, by symmetry). Then

$$k_{CD} = \frac{3EI}{L_{CD}} \left[1 - \left(\frac{L_{CD}}{(L_{CD})_{cr}} \right)^2 \right] = \frac{3EI}{L_{CD}} \left[1 - \left(\frac{46}{42.5} \right)^2 \right]$$

Since the resulting value is negative, $k_{CD} = 0$. For the special case of a fixed-end (Fig. 6.21) $\nu_\gamma = 1.43$. Then

$$(L_{AB})_{cr} = 1.43 \times 78.75'' = 112.5'' > 46'' \text{ (OK)}$$

Thus, the chosen length is satisfactory. In fact, this was evident in step 2 where it was found that $(L_{AB})_{cr} = 78.75''$ with $\nu_\gamma = 1.0$.

If the approximation of Eq. 6.25 had been used,

$$L_{cr} = \left[60 - 40 \, (-0.50) \right] 1.25 = 100'' \text{ (OK)}$$

Example II: (Fig. 6.23) corner of rectangular frame

The critical segment is BC.

1) Moment ratios:

ρ_{AB} = -0.05 (elastic-plastic)

ρ_{BC} = +0.75 (plastic-elastic)

ρ_{CD} = +0.67 (elastic)

2) $\frac{(L_{AB})_{cr}}{r_y}$ = 48-30 (-0.05) = 49.5, $(L_{AB})_{cr}$ = 75.6"

$\frac{(L_{BC})_{cr}}{r_y}$ = 30 for $\rho > 0.6$, $(L_{BC})_{cr}$ = 46"

$\frac{(L_{CD})_{cr}}{r_y} = \frac{134}{\sqrt{0.75}} + 60\,(1 - 0.67) = 175$, L_{CD} = 266"

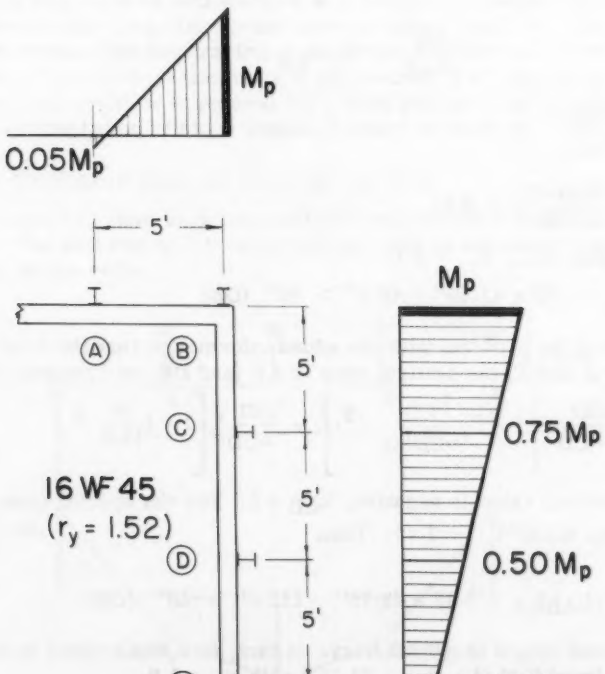

Fig. 6.23. Illustrative Example II of Lateral Bracing

3) $k_{AB} = \frac{3EI}{L_{AB}} \quad 1 - (\frac{60}{75})^2 \quad = \frac{3EI}{L} \times 0.36 = k_s$

$k_{CD} = \frac{3EI}{L_{CD}} \quad 1 - (\frac{60}{266})^2 \quad = \frac{3EI}{L} \times 0.95 = k_\ell$

4) $\frac{k_s}{k_\ell} = 0.38$

5) Using Eq. 6.24,

$$\nu_\gamma = 1.0 + 0.2\,(0.95)\,(0.9 + 0.38) = 1.25$$

6) $(L_{BC})_{cr} = (1.25)\ (46) = 58'' < 60''$ (call OK)

Note: By Eq. 6.25, $\frac{(L_{BC})_{cr}}{r_y} = 35$,

$$(L_{BC})_{cr} = (35)\ \ (1.53) = 53.2''$$

6.4. Variable Repeated Loading

Statement of the Problem

In the previous discussions it has been assumed that the structures under consideration were subjected to all of the applied loads acting simultaneously. It has been further assumed that the applied loads increase in their magnitude until the limit load is reached. During this process none of the applied loads are permitted to change their directions and the ratio of load magnitudes to each other remains fixed. Such loading is termed proportional loading.

In practice the separate loads on a structure may not satisfy the condition of proportionality. Instead, the separate loads may change in magnitude independently from each other. These non-proportional loads are called "variable repeated loads" in the literature. Although these loads act generally in a random manner, it is convenient to assume a cyclic pattern in discussing the problem.

Two modes of failure that may result from repeated loading are considered in the following:

a) Fatigue and Alternating Plasticity

Fatigue is failure of the material by fracture as a result of repeated loading on the structure. In particular, failure will occur at a relatively low number of cycles when the repeated loading is such that yielding of the material occurs alternately in tension and compression at a given cross section. This phenomenon is known as "alternating plasticity." During each cycle of load application plastic flow will take place and eventually will lead to fracture.

Fatigue within the nominally elastic range is of little concern in usual building frames.

b) Deflection Stability

This type of failure is characterized by an increase in deflection during each cycle of loading, the increments of deflection being in the same direction. This mode of failure is termed "incremental collapse." The problem is to determine the limits on the loads for which these increments cease after a few cycles of load application and the deflection "stabilizes." When a structure reaches this state of stabilized deflection it is said to have "shaken down" and the corresponding set of loads is referred to as the "stabilizing load" or the "shakedown load." The structure henceforth responds to the load in a purely elastic manner.

Previous Investigations

Gruning(6.40) was the first to recognize that under variable repeated loading a structure may fail due to a lack of deflection stability. Further extensive studies in this field were made by Bleich(6.41), Melan(6.42) and Horne.(6.43) In recent years, analyses and experiments were also made by many other investigators including Symonds(6.44,6.45) Neal,(6.46,6.47,6.48) Hodge,(6.49) Massonnet,(6.50) Gozum and Haaijer.(6.51) Most recently McCarthy and Popov(6.52) have carried out a series of experimental investigations of portal frames. Neal and Symonds(6.45) have recently published the test results of a number of rectangular model frames.

Theoretical Analysis

a) Alternating Plasticity

A condition of alternating plasticity is illustrated by the example of a cantilever beam with a concentrated load acting at the free end. (Fig. 6.24). The load P is assumed at first as being applied in a downward direction and the resulting moment-curvature relationship at the built-in section is shown from (o) to (a) in Fig. 6.24. If, instead, the load were applied in the opposite direction, the corresponding M-ϕ curve would be that shown in Fig. 6.24 from (o) to (c). If at point (a) the load P is gradually released and finally applied in the opposite direction, the M-ϕ relationship is linear for a range of moment designated as ΔM_y. The magnitude of ΔM_y is less than or at most equal to $2M_y$, the precise value being a function of the residual stress and the Bauschinger effect. At point (b), yielding starts in the opposite direction. Finally a point (d) corresponding to $-P_{max.}$ is reached. To complete the cycle, as loads are released and then reversed, the resulting behavior would be as shown by the dashed line d-e-f-a.

Failure due to alternating plasticity will not occur when ranges of moment values exist for which a section behaves elastically regardless of its previous loading history. As a first approximation the Bauschinger effect may be ignored and this range of moment (ΔM_y in Fig. 6.24) may be taken as

$$\Delta M_y = 2\ M_y = 2\ M_p/f \qquad (6.26)$$

The necessary condition for eliminating the possibility of alternating plasticity is:

$$(M_i)_{max.} - (M_i)_{min.} \leq \Delta M_y = 2\ M_p/f \qquad (6.27)$$

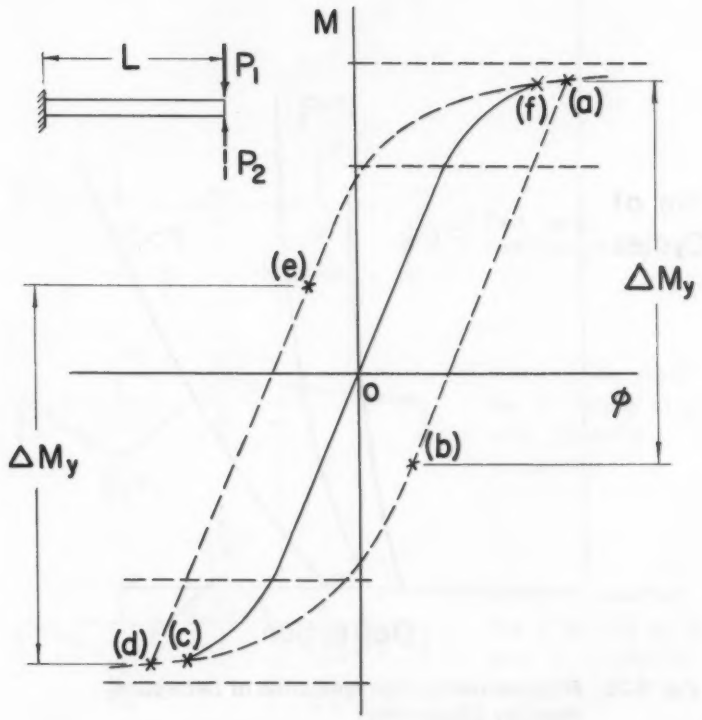

Fig. 6.24. Moment-Curvature Relationship at the Built-in End of a Cantilever Beam Under Alternating Plasticity

where M_i denotes the elastic moment values at any section "i" being investigated. Procedures for calculating the limit for alternating plasticity in the case of indeterminate structures may be found in Ref. 6.53.

d) Deflection Stability

As noted earlier, under repeated application of a certain sequence of loads an increment of plastic deformation in the same sense may occur during each cycle. The maximum load for which these increments cease after a few cycles is called the stabilizing (or shakedown) load. In Fig. 6.25 is plotted diagrammatically the number of loading cycles versus the deflection under the load at the end of each cycle. When P is equal to or less than a certain critical value P_S, a set of residual moments will be set up in the structure after a few cycles during which the deflection approaches a limit value. All further repetitions of load are carried elastically. If P is greater than P_S, the deflection does not stabilize but continues to grow for each cycle of load application. A description of this phenomenon may be found in the several references that pertain to this article.

EM 4

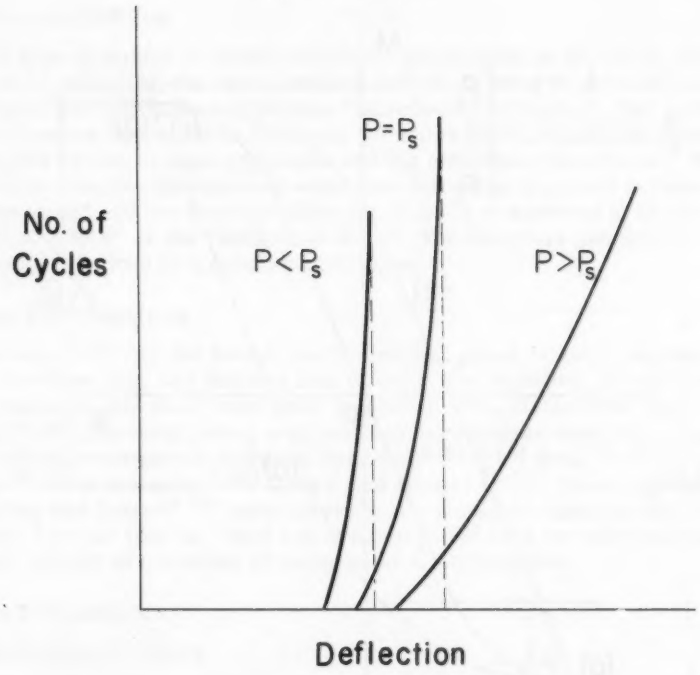

Fig. 6.25. Diagrammatic Representation of Deflection Stability (Shakedown)

It is possible to determine mathematically the maximum load P_s for which the deflection of the structure will finally stabilize. The condition to be fulfilled is that at points of maximum moment the absolute value of the sum of the residual moment M_r and the elastic moment M produced by the loads does not exceed the full plastic moment value M_p. In general terms:

$$\left| (M_i)_r + (M_i)_{max.} \right| = M_p \qquad (6.28)$$

Equation 6.28 may be applied to the problem shown in Fig. 6.26a, a continuous beam of two equal spans, the supports of which can take upwards and downwards reactions. Suppose the load P is first applied at B. An elastic analysis would produce the moment diagram shown in Fig. 6.26b with $M_B = 13/64$ PL. As a second phase of the loading, two equal loads applied at B and D would give the elastic moment diagram shown in Fig. 6.26c. Due to any inelastic deformation that may occur under load, the only possible shape of the residual moment diagram is that shown in Fig. 6.26d.

Applying Eq. 6.28, and defining the residual moment diagram positive as shown in Fig. 6.26d, the conditions to be satisfied are as follows:

At section B: $$\left| 13/64\ (PL) + (M_r)_B \right| = M_p \qquad (6.29)$$

At section C: $$\left| -12/64\ (PL) + (M_r)_C \right| = M_p \qquad (6.30)$$

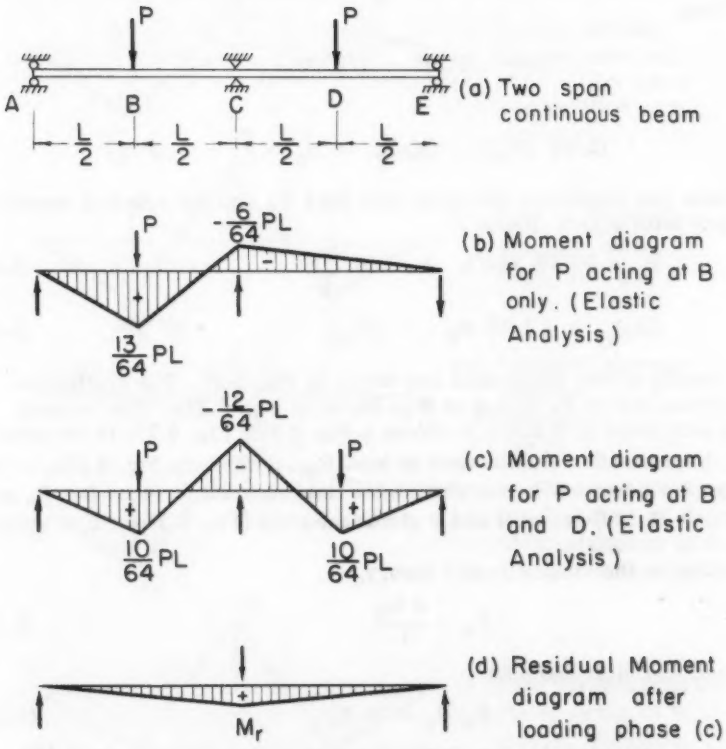

Fig. 6.26. Two-Span Continuous Beam Under Variable Repeated Loading (Deflection Stability)

However, the residual moments can have only a linear variation across the span with the maximum value at C (Fig. 6.26d) so that

$$(M_r)_B = 1/2\ (M_r)_C \tag{6.31}$$

Expressions for the stabilizing load P_s are obtained from Eqs. 6.29, 6.30 and 6.31. Thus,

$$13/64\ \ (P_s)L + 1/2\ (M_r)_C = M_p$$

and

$$12/64\ \ (P_s)L - (M_r)_C = M_p$$

From these two conditions the stabilizing load P_s and the residual moment $(M_r)_C$ are determined. Hence

$$P_s = 96/19\ M_p/L = 5.06\ \frac{M_p}{L} \tag{6.32}$$

$$(M_r)_C = -\ 1/19\ M_p \tag{6.33}$$

The results of this calculation are shown in Fig. 6.27. The elastic moment diagram due to P_s acting at B is shown in Fig. 6.27a. The moment diagram with loads at B and D is shown in Fig. 6.27b. Fig. 6.27c is the residual moment diagram after stabilization at load P_s. Combining Fig. 6.27c, in turn, with Figs. 6.27a and 6.27b, one obtains the final moment diagram for P_s acting at B only (6.27d) and at B and D simultaneously (Fig. 6.27e). It is evident that Eq. 6.28 is satisfied.

According to the simple plastic theory,

$$P_u = \frac{6\ M_p}{L} \tag{6.34}$$

Thus, from Eqs. 6.32 and 6.34

$$P_s/P_u = 84.4\% \tag{6.35}$$

Equation 6.35 indicates that the stabilizing load is theoretically about 16% lower than the ultimate load P_u in this example.

As a check on alternating plasticity, the following condition must be satisfied

$$(M_i)_{max.} - (M_i)_{min.} \leq 2\ \frac{M_p}{f} = 2\ M_y$$

In the previous example at section B

$$(M_B)_{max.} = 13/64\ \ (96/19\ M_p) = 39/38\ M_p$$

$$(M_B)_{min.} = -3/64\ \ (96/19\ M_p) = -9/38\ M_p$$

$$(M_B)_{max.} = (M_B)_{min.} = 48/38\ M_p < 2\ M_y$$

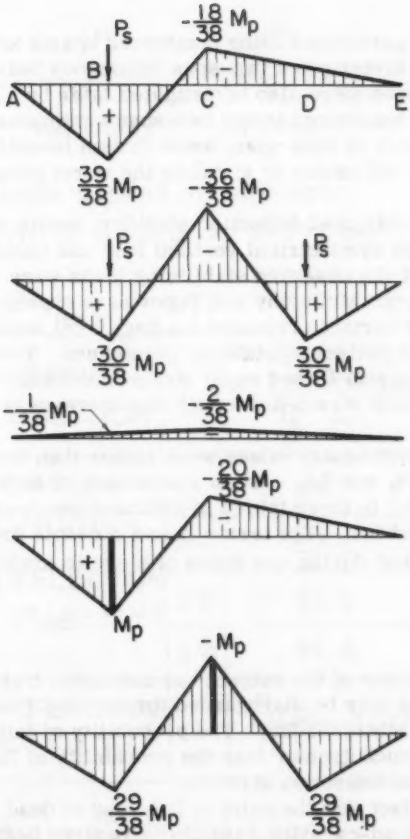

(a) Elastic Moment diagram with load at B. (for use in combination with sketch (c))

(b) Elastic Moment diagram with loads at B and D.

(c) Residual Moment diagram after stabilization at loads P_s

(d) Final Moment diagram for P_s acting at B only. (Residual + Elastic moment)

(e) Final Moment diagram for P_s acting at B and D. (Residual + Elastic moment)

Fig. 6.27. Two-Span Continuous Beam of Fig. 6.26 Under Stabilizing Load P_s

Actually, the increase in deflection for a load $P < P_S$ will cease as strain-hardening sets in. A discussion of the effect of strain-hardening can be found either in Ref. 7.48 or Ref. 6.51.

Experimental Correlation

Experimental studies have been performed using continuous beams and rectangular frames. Kloppel[6.54] investigated two-span continuous beams with simple supports. Such structures were also investigated later by Massonnet[6.50] and Gozum.[6.51] Massonnet tested two-span continuous beams with loads applied at the center of each span, while Gozum investigated the same structure with loads off center to simulate the worst possible condition.

Neal and Symonds[6.45] have investigated deflection stability, testing small scale rectangular portal frames with symmetrical vertical load and horizontal load. Test results indicated that the observed stabilizing loads were about 10% higher than those given by theory. McCarthy and Popov have experimented on a series of frames under variable repeated loading,[6.52] investigating both alternating plasticity and deflection stability phenomena. Test results show that the theoretical analysis (based on no strain-hardening) gives conservative predictions and that strain-hardening may increase the stabilizing load.[6.48, 6.51]

All results indicated that the experimental values were higher than those given by theory. Tables 6.2, 6.3, 6.4, and 6.5, contain a summary of each of the previous important observations. In these tables is indicated the loading sequences used in a given cyclic load test. The terms α and β denote the proportion of a particular load applied during one phase of a cyclic loading sequence.

Relationship to Design

Practically every recent investigator of the subject has concluded that the problem of variable repeated loading may be disregarded for building frames designed for the usual conditions of static loading. The probability of failure by a single overload appears to be much greater than the probability of failure by alternating plasticity or by loss of deflection stability.

Of particular significance is the fact that the ratio of live load to dead load must be very large before the load-carrying capacity is reduced because of load repetitions. In nearly all of the tests described in Section 4, extreme examples were chosen in which all of the load was considered to be live load. It is unusual to find such extreme load variations in building structures. The live load is seldom more than two-thirds of the total load and usually it is of the order of one-third of the total.

It must be remembered that the safety factor F does not provide for possible overloads alone. It also accounts for such additional factors as variation in material properties, dimensions, workmanship, fabrication, methods of analysis, etc. Therefore, variation in live load alone could not properly be assumed to account for the full value of the factor of safety.

Neal[6.48] has emphasized the fact that failure due to increase of deflection is a gradual process so that ample warning of danger is available. This implies that a lower load factor is acceptable for P_S than that provided for P_u.

Table 6.2. Test Results of Deflection Stability of Two-Span Continuous Beams[6.50]

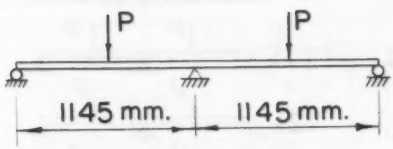

Loads applied at mid-span
(P.N. 12 Bent about strong axis)

Loading Sequence

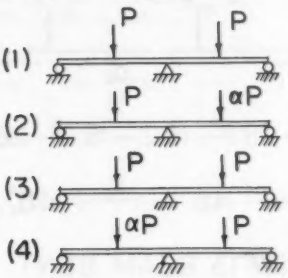

LOADING CONDITION	α	THEORETICAL RELATIONSHIP $\frac{P_s}{P_u}$ (%)	OBSERVED RELATIONSHIP	$\frac{P_s\,(obs.)}{P_s\,(theo.)}$
CYCLIC LOADING (DEFLECTION STABILITY)	0	84.2	85.7	102
	1/4	87.6	86.7	99
	1/2	91.5	96.2	105
	3/4	91.6	95.6	100
PROPORTIONAL LOADING	1	$\frac{P_{max.}}{P_u} = 100$	$\frac{P_{max.}}{P_u} = 105$	

P_s = Stabilizing Load
P_u = Theoretical failure load by simple plastic theory
P_{max} = Observed plastic failure load

Finally, the results of the most recent tests using rolled shapes have shown that the observed stabilizing load was always greater than the theoretically predicted value. Since the theoretical values of P_s are seldom more than 20% below P_u, the practicality of this problem loses much of its significance. Although account could be taken of variable repeated loading by using a higher load factor, such a procedure is neither reasonable nor necessary for ordinary building frames.

Table 6.3. Test Results of Deflection Stability of Two-Span Continuous Beams(6.51)

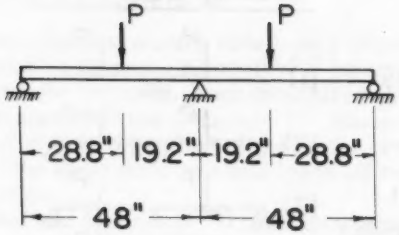

4WF13 BEAM BENT ABOUT THE WEAK AXIS

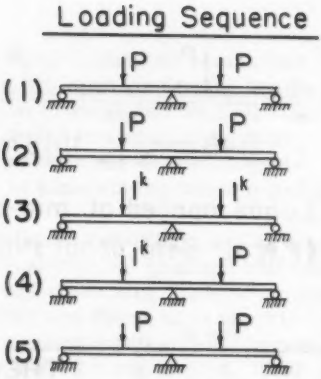

LOADING CONDITION		P (Theo.) (kips)	P (Obs.) (kips)	P (Obs.) / P (Theo.) (%)
PROPORTIONAL LOADING	TWO LOADS	P_u = 16.81	P_{max} = 17.08	101.6
	SINGLE LOAD	P_u = 16.81	P_{max} = 17.68	105.2
CYCLIC LOADING (DEFLECTION STABILITY)		P_s = 13.72	P_s = 14.8	$\frac{P_s}{P_u}$ = 88

Variable Repeated Loading

Deflection stability need not be investigated in the design of statically-loaded building frames.

Table 6.4. Test Results of Rigid Frames Under Variable Repeated Loading(6.52)

LOADING CONDITION	STRUCTURES	P_s or P_0 (theo.) kips	P_s or P_0 (obser) kips	P(obs.)/P(theo.) (%)	P_u (theo.) kips	$\frac{P_s}{P_u}$ or $\frac{P_0}{P_u}$ (%)
ALTERNATING PLASTICITY	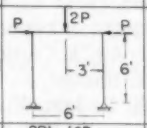	5.68	6.00	106	5.76	104.0
DEFLECTION STABILITY	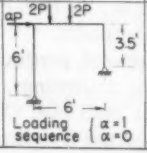	5.81	6.80	117	7.76	87.7

Table 6.5. Test Results of Rigid Frames Under Variable Repeated Loading(6.45)

LOADING CONDITION	STRUCTURES*	P_u (Theo) lbs.	P_s (Obs.) lbs.	P(obs.)/P(theo) (%)	P(obs)/P_u(theo) (%)
Proportional Loading	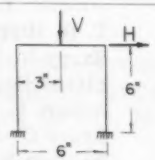 (2 Tests)	92.5	101	109.2	109.2
		92.4	101	109.2	109.2
Cyclic Loading	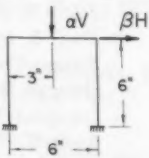 (3 Tests)	87.9	93.5	106.5	101.0
		87.2	95.5	109.5	103.0
	Loading sequence { α=1 β=1; α=0 β=0; α=0 β=1; α=0 β=0 }	88.9	93.0	104.8	101.5
	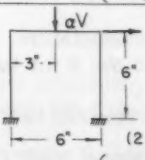 (2 Tests)	78.0	89.5	114.8	96.8
	Loading sequence { α=1 β=1; α=0 β=0; α=-1 β=1; α=0 β=0 }	79.3	90.5	114.1	97.9

*All members were 1/4"sq. sections

ACKNOWLEDGMENT

The Joint Committee acknowledges the work of a research group at Fritz Engineering Laboratory, Department of Civil Engineering, Lehigh University. This group has been engaged through the Institute of Research in an investigation entitled "Welded Continuous Frames and Their Components." The results of that investigation were the basis of preliminary reports which were later revised and supplemented by the Joint WRC-ASCE Committee. The staff members at Fritz Laboratory included L. S. Beedle, G. C. Driscoll, Jr., T. V. Galambos, R. L. Ketter, T. Kusuda, G. C. Lee, T. Lee, L. W. Lu, A. Ostapenko and B. Thurlimann. Wm. J. Eney is Director of Fritz Laboratory and Head of the Civil Engineering Department.

The organizations that supported the research projects out of which the preliminary reports were prepared were the following: American Institute of Steel Construction, American Iron and Steel Institute, Column Research Council, The Department of the Navy (Office of Naval Research, Bureau of Ships, Bureau of Yards and Docks) and the Welding Research Council.

Respectfully submitted,

A. Amirikian	Frank Baron
Lynn S. Beedle	John M. Biggs
J. M. Crowley	Daniel C. Drucker
F. H. Dill	John D. Griffiths
Samuel Epstein	William J. Hall
LaMotte Grover	T. R. Higgins
William H. Jameson	Harry N. Hill
Bruce G. Johnston	Eivind Hognestad
Jonathan Jones	Robert L. Janes
R. L. Ketter	Bruce G. Johnston
Carl Kreidler	William H. Munse, Jr.
H. W. Lawson	Egor P. Popov
Nathan M. Newmark	John B. Scalzi
R. M. Stuchell	Paul S. Symonds
John Vasta	Bruno Thurlimann
	George Winter
	Douglas T. Wright
T. R. Higgins, Chairman	Lynn S. Beedle, Chairman
Lehigh Project Subcommittee	Committee on Plasticity Related to Design
Structural Steel Committee	Engineering Mechanics Division
Welding Research Council	American Society of Civil Engineers

Additional Nomenclature
(See Progress Reports No. 1 and No. 3 for basic nomenclature)

H = Total inelastic angle change between two load points

L = Distance between points of lateral support or length of a critical segment

M_i = Elastic moment at section "i"

M_L = Bending moment about strong axis at z=L

M_o = Bending moment about strong axis at z=0

M_r = Residual moment

ΔM_y = Range of moment in which M-ϕ curve is linear

P_a = Maximum load for alternating plasticity

α = Proportion of a given length in strain-hardened state

β = Angle of twist about shear center

θ = Inelastic angle change between points of lateral support

ν_s = Correction factor for St. Venant's torsion

ν_α = Correction factor for extent of yielding

ν_γ = Correction factor for end fixity

ν_ρ = Correction factor for moment gradient

$\mathcal{J}$ = Ratio of end moments for a segment = M_L/M_o

REFERENCES

Art. 6.3

6.29. Timoshenko, S.
THEORY OF BENDING, TORSION AND BUCKLING OF THIN-WALLED MEMBERS OF OPEN CROSS SECTION, Journal, Franklin Institute, Vol. 239, pp. 201, 249, 343 (1945).

6.30. Nadai, A.
THEORY OF FLOW AND FRACTURE OF SOLIDS, McGraw-Hill Book Company, New York (1950).

6.31. White, M. W.
THE LATERAL-TORSIONAL BUCKLING OF YIELDED STRUCTURAL STEEL MEMBERS, Ph. D. Dissertation, Lehigh University, (1956).

6.32. Campus, F.; Massonnet, C.
RECHERCHES SUR LE FLAMBEMENT DE COLONNES EN ACIER A 37, A PROFIL EN DOUBLE TE, SOLLICITEES OBLIQUEMENT, I.R.S.I.A. Comptes Rendus de Recherches, No. 17, (April 1956).

6.33. Clark, J. W.; Hill, H. N.
LATERAL BUCKLING OF BEAMS AND GIRDERS, ASCE Publication Forthcoming.

6.34. CRC
GUIDE TO DESIGN CRITERIA FOR METAL COMPRESSION MEMBERS, Column Research Council (to be published).

6.35. Neal, B. G.
THE LATERAL INSTABILITY OF YIELDED MILD STEEL BEAMS OF RECTANGULAR CROSS SECTION, Philosophical Transactions of the Royal Society of London, 242 (846) (January 1950).

6.36. Wittrick, W. H.
LATERAL INSTABILITY OF RECTANGULAR BEAMS OF STRAIN-HARDENING MATERIAL UNDER UNIFORM BENDING, Journal of the Aeronautical Science 19 (12) 835 (December 1952).

6.37. Horne, M. R.
CRITICAL LOADING CONDITIONS IN ENGINEERING STRUCTURES, Ph.D. Thesis, Cambridge University, (1950).

6.38. Baker, J. F.; Horne, M. R.; Heyman, J.
THE STEEL SKELETON, VOL. 2, PLASTIC BEHAVIOR AND DESIGN, Cambridge University Press, (1956).

6.39. Kusuda, T.; Sarubbi, R. G.; Thurlimann, B.
LATERAL BRACING OF BEAMS IN PLASTICALLY DESIGNED STEEL STRUCTURES, Fritz Lab Report 205E.11, Lehigh University, (1958).

Art. 6.4

6.40. Gruning, M.
DIE TRAGFAHIGKEIT STATISCH UNBESTIMMTER TRAGWERKE AUS STAHL BEI BELIEBIG HAUFIG WIEDERHOLTER BELASTUNG, Julius Springer, Berlin, (1926).

6.41. Bleich, H.
UBER DIE BEMESSUNG STATISCH UNBESTIMMTER STAHLTRAGWERKE UNTER BERUCKSICHTIGUNG DES ELASTISCH - PLASTISCHEN VERHALTENS DES BAUSTOFFES, Bauingenieur 13, p. 261 (1932).

6.42. Melan, E.
THEORIE STATISCH UNBESTIMMTER SYSTEME AUS IDEAL PLASTISCHEN BAUSTOFF, Sitzber, Akad. Wiss, Wien. 145 (IIa) p. 195 (1936).

6.43. Horne, M. R.
THE EFFECT OF VARIABLE REPEATED LOADS IN BUILDING STRUCTURES DESIGNED BY THE PLASTIC THEORY, Proceedings of the IABSE, 14, p. 53 (1954).

6.44. Symonds, P. S.
THE BASIC THEOREMS IN THE PLASTIC THEORY OF STRUCTURES, Journ. Aero. Science, 17 (18) (1950).

6.45. Neal, B. G.; Symonds, P. S.
CYCLIC LOADING OF PORTAL FRAMES, THEORY AND TESTS, Proceedings of the IABSE, 18, p. 171 (1958).

6.46. Neal, B. G.; Symonds, P. S.
A METHOD FOR CALCULATING THE FAILURE LOAD FOR A FRAMED STRUCTURE SUBJECTED TO FLUCTUATING LOADS, Journ. Inst. Civil Engineers, 35, p. 186, (1950).

6.47. Neal, B. G.
THE BEHAVIOR OF FRAMED STRUCTURES UNDER REPEATED LOADING, Quarterly Journ. of Mechanics and Applied Math., 4, p. 78 (1951).

6.48. Neal, B. G.
PLASTIC COLLAPSE AND SHAKEDOWN THEOREMS FOR STRUCTURES OF STRAIN-HARDENING MATERIAL, Journ. Aero. Science, 17, p. 297 (1950).

6.49. Hodge, P. G.
SHAKEDOWN OF ELASTIC-PLASTIC STRUCTURES, Residual Stresses in Metals and Metal Construction, (Ed. W. R. Osgood), Reinhold, New York, (1954).

6.50. Massonnet, C.
ESSAIS D'ADAPTATION ET DE STABILIZATION PLASTIQUES SUR DES POURTRELLES LAMINEES, Proceedings of the IABSE, 13, p. 239 (1953).

6.51. Gosum, A. T.; Haaijer, G.
DEFLECTION STABILITY OF CONTINUOUS BEAMS, Fritz Laboratory Report No. 205G.1 Lehigh University, (1955).

6.52. Popov, E. P.; McCarthy, R. E.
DEFLECTION STABILITY OF RIGID FRAMES UNDER REPEATED LOADS, presented at the ASCE Los Angeles Convention, (March, 1959).

6.53. Neal, B. G.
THE PLASTIC METHODS OF STRUCTURAL ANALYSIS, John Wiley and Sons, New York, (1956).

6.54. Kloppel, K.
BEITRAG ZUR FRAGE DER AUSNUTZBARKEIT DER PLASTICITAT DER DAUERBEANSPRUCHTEN DURCHLAUFTRAGERN, Final Report, 2nd Congress IABSE, 77 (1939).

Journal of the
ENGINEERING MECHANICS DIVISION
Proceedings of the American Society of Civil Engineers

CONTENTS

DISCUSSION

Page

On Inelastic Buckling in Steel, by G. Haaijer and B. Thurlimann. (Proc. Paper 1581, April, 1958. Prior Discussion: 2008. Discussion closed.)
by G. Haaijer and B. Thurlimann (closure) 189

Dynamic Elasto-Plastic Response of Rigid Frames, by Frank L. DiMaggio. (Proc. Paper 1693, July, 1958. Prior Discussion: 1917. (Discussion closed.)
by Frank L. Dimaggio (closure and errata) 191

The Elastic Stability of Thin Spherical Shells, by Gideon P. R. Von Willich. (Proc. Paper 1897, January, 1959. Prior Discussion: 2008. Discussion closed.)
by Gideon P. R. Von Willich (closure) 195

Columns Under Combined Bending and Thrust, by Galambos and Ketter. (Proc. Paper 1990, April, 1959. Prior Discussion: none. (Discussion open until September 1, 1959.)
by George Winter 197

Note: Paper 2234 is part of the copyrighted Journal of the Engineering Mechanics Division, Proceedings of the American Society of Civil Engineers, Vol. 85, EM 4, October, 1959.

ON INELASTIC BUCKLING IN STEEL[a]

Closure by G. Haaijer and B. Thürlimann

G. HAAIJER[1] AND B. THÜRLIMANN,[2] M. ASCE.—Professor Bijlaard is correct in pointing out that the authors' formula (13) does not reduce to the elastic buckling stress when the elastic moduli are substituted. Formula (13) was derived for the strain-hardening range of mild steel as shown in the thesis on which the authors' reference 3 was based. In the strain-hardening range Professor Bijlaard's formula gives slightly larger values for the critical stress than formula (13). Because of the small value of the tangent modulus, however, the differences in critical strain values would be considerable.

Furthermore, Professor Bijlaard's discussion corrects the statement made by the authors that his theory is of the deformation type. Although his theory as it is used today in aircraft design is a deformation theory, his complete theory as published in 1938 includes both deformation and incremental theory.

Professor Bijlaard has been able to reduce all subsequent contributions to inelastic plate buckling such as the papers by Ilyushin, Stowell, Handelman-Prager, and the one by the authors he discussed to his original theory.

Concerning the case of the authors' paper it may be well to quote Professor Bijlaard's own statement presented at the Annual Meeting of the Column Research Council, May 1957 (Ref. (a), p. 55):

> "The writer's theory (Prof. Bijlaard's theory) of plastic buckling of plates is in excellent agreement with test results with aluminum plates (references 12-15). It is also in good agreement with tests on structural steel for small plastic deformations as occur below the yield stress. However, in the horizontal part of the stress strain diagram at the yield stress where the material flows in layers and thus behaves discontinuously, in contrast with the continuous behavior assumed in the theory, it obviously does not apply* and is too conservative, as was pointed out for columns in reference 16(b). This was taken into account by using the requirements $b/t < 8.5$ and 34 from reference 8(c) for hinged flanges and plates where large strains at the yield stress are necessary."

This statement obviously implies that Prof. Bijlaard himself did not feel that his theory could be extended to the case treated by the authors prior to the publication of their paper.

Instead of starting from a general theory of plasticity the authors determined expressions for the plate buckling stresses based on orthotropic behavior of the material. Agreement should exist between these expressions and others

a. Proc. Paper 1581, April, 1958, by G. Haaijer and B. Thürlimann.
1. Research Engr., Appl. Research Lab., U. S. Steel Corp., Monroeville, Pa.
2. Research Associate Prof., Fritz Lab., Lehigh Univ., Bethlehem, Pa.
* Underlined by the authors.

based on plastic reduction factors that imply proper orthotropic behavior. The advantage of giving general expressions for the buckling strength of orthotropic plates was to clearly indicate the influence of the various stiffness factors that are involved. This approach enabled the authors to show the source of diffenences in the buckling stresses predicted by various theories (see authors' Table I).

The authors sincerely appreciate Professor Bijlaard's careful review and discussion of their paper.

REFERENCES

Ref. (a) P. P. Bijlaard, "Buckling of Columns, with Special Attention to Eccentricity, Plasticity and Local Buckling," Proceedings of the Seventh Technical Session, Column Research Council, (May 1958).

Ref. (b) P. P. Bijlaard, "Exact Computation for the Buckling of the Webs of Truss Members Used in Bridge Building," De Ingenieur in Ned. Indie, No. 2, pp. 1.17-1.23, (1939).

Ref. (c) L. S. Beedle, B. Thürlimann, and R. L. Ketter, "Plastic Design in Structural Steel," Lecture Notes, Lehigh University, Summer Course, (September 1955).

DYNAMIC ELASTO-PLASTIC RESPONSE OF RIGID FRAMES[a]

Closure and Errata by Frank L. DiMaggio

FRANK L. DIMAGGIO,[1] M. ASCE.—The author wishes to thank Miss Mathews for her pertinent comments. It is true that in general the location of the plastic hinges is not known a priori. The method presented is valid regardless of where the first hinge forms, but the specific results presented in the paper obtain only for the case when it forms at the knee. It certainly would be advantageous to consider the effect of the axial forces on the yield criterion in some cases, but the method presented is not amenable to this extension.

For those cases where many elasto-plastic stages occur, the author agrees that the recent method proposed by H. H. Bleich is far superior. Miss Mathews states that the author's procedure is applicable when the load duration is short compared with the period of the first elasto-plastic mode. Since the elasto-plastic response is governed primarily by the rigid body mode when such a mode exists, and since this mode has an infinite period, it would be more correct to say that the load duration should be short compared to the time corresponding to the end of the (first) elasto-plastic stage.

Errata

p. 5 - In eq. (10) change p_i^u to P_i^u

p. 6 - Insert equation number for eq. (33)

p. 14 - In eq. (73) $\alpha_i = 1/\lambda_i^2$

In eq. (74) change ω_i in denominator to ω_i^2

p. 16 - In eq. (87) change sin a in first term to sinh a and interchange expressions (sin a $\neq$ D_i sinh a) in third and fourth lines.

In eq. (89) $\gamma_i = 1/\lambda_i$

In eq. (91) change $\frac{1}{3}$ te to $\frac{1}{12}$ te

This is not a typographical error, but a mistake in the original work. It makes all numerical results in the elasto-plastic stage incorrect.

p. 18 - In first paragraph under title First Elastic Stage change t_e to t_o

p. 21 - Delete Tables 7 and 8. They are incorrect due to error in eq. (91).

p. 22 - In Fig. 7, deflections after first elastic stage are incorrect due to

---

a. Proc. Paper 1693, July, 1958, by Frank L. DiMaggio.

1. Assistant Prof. of Civ. Engr., Columbus University, New York, N. Y.

error in eq. (91). If correct equation is used, a maximum deflection of 665 inches is predicted at the end of 2.75 seconds—a completely academic result. A straight rigid-plastic calculation gives results essentially identical with this "exact" analysis. This should be expected because the load F_0 = 345600 lbs. is 10.8 times the static collapse load.

p. 23 - In Fig. 8 τ_0 is incorrect (see errata re. p. 22)

p. 24 - On the half page starting with "If eqs. (90)" and ending with "at the top of the column," the numerical results quoted and referred to are incorrect (see errata re. p. 22)

Under "Response to Load with F_0 = 57600," Figs. 10 and 12 are incorrect due to error in eq. (91). Corrected graphs constitute Figs. 1 and 2 of this errata. The rigid body mode of course still contributes almost all of the response in the plastic stage. Note that in this case, where the load F_0 is only 1.8 times the static collapse load, a rigid plastic analysis gives results which are too low. This will always be true in problems of this type because in a rigid plastic analysis, the coordinate P_0 has no initial velocity. In Fig. 11 change τ_0 = .283 to τ_0 = .385.

p. 25 - Fig. 9 is incorrect (see errata for p. 22 above).

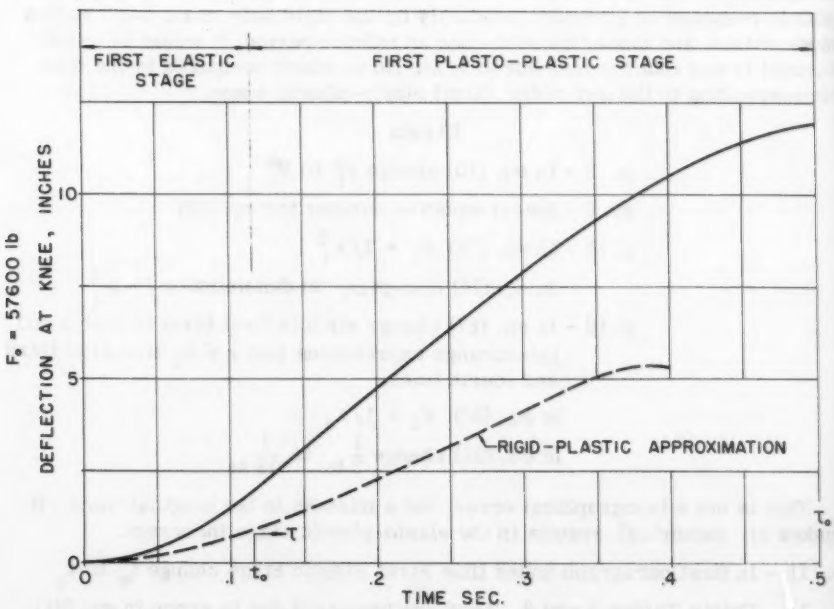

FIG. 1

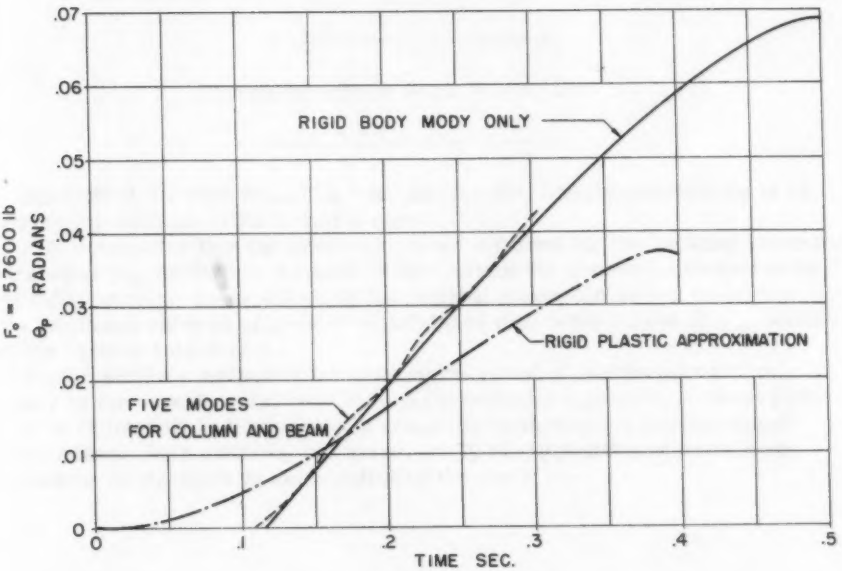
.07
.06
.05
.04
.03
.02
.01
0
0
.1
.2
.3
.4
.5
TIME SEC.
F_o = 57600 lb
θ_p RADIANS
RIGID BODY MODY ONLY
RIGID PLASTIC APPROXIMATION
FIVE MODES
FOR COLUMN AND BEAM

FIG.2

THE ELASTIC STABILITY OF THIN SPHERICAL SHELLS[a]

Closure by Gideon P. R. Von Willich

GIDEON P. R. VON WILLICH,[1] M. ASCE.—Mr. Chen's contribution is an interesting addition to the writer's paper.

It is noteworthy that the minimum values obtained for the buckling pressure parameter p_{cr} by the two methods of minimizing the potential expression do not differ widely. As explained in the original paper, the writer feels that this minimum value is of greater significance than other values of p_{cr} obtained for various values of λ.

As the writer's method of minimizing the potential yields values of p_{cr} closer to the experimental results than the orthodox approach, it would probably be of interest to investigate in detail the mathematical implication of this method. Both methods, of course, imply the imposition of certain restrictions on the mode of deformation of the shell.

a. Proc. Paper 1897, January, 1959, by G. P. R. von Willich.

1. Senior Lecturer, Dept. of Civ. Engr., Univ. of Pretoria, South Africa.

COLUMNS UNDER COMBINED BENDING AND THRUST[a]

Discussion by George Winter

GEORGE WINTER,[1] F. ASCE.—The authors have rendered a significant service by using Newmark's well known numerical method for obtaining information on the carrying capacity of steel beam-columns for some special cases, and by comparing their analytical results with experimental information.

The first of the various test series with which comparison is made is the one carried out at Cornell University by the writer and two of his colleagues. This information has long since been published and, therefore, reference should be made not to a preliminary, mimeographed report (ref. 9) but to the published version, as follows:

Mason, R. E., Fisher, G. P., and Winter, George: Eccentrically Loaded, Hinged Steel Columns. Proc. ASCE (J. Engr. Mech. Div.) EM 4, Paper 1792, October 1958, with discussion in Paper 2099, July 1959.

It worth noting that in the latter paper comparison is made of the test results with the so-called "C.R.C. interaction equation," the authors' Eq. 9. Agreement is about as close as with the authors' proposed formula, Eq. 5, as represented on their Fig. 12. As noted in the quoted paper, the general interaction formula Eq. 9 has been found in satisfactory agreement with tests on a great variety of cases not covered by the authors' analysis. Consequently, while only "semi-rational," Eq. 9 has a wide range of validity, having been checked by various investigators against tests on both aluminum and steel members, in major and minor axis bending, without and with torsional deformation, and for a variety of ratios of end moments.

Objection is sometimes raised to the presumed "complexity" of the interaction formula of Eq. 9 for practical design use. In discussing Eq. 9 the authors have shown that the form of this equation is the same as that of their proposed Eq. 5. Since the American Institute for Steel Construction has seen fit to incorporate Eq. 5 in their Rules for Plastic Design and Fabrication, the complexity of Eq. 5 and, therefore, of Eq. 9 (if suitably transformed) is apparantly not excessive for practical design purposes.

Naturally, the writer is pleased that the relation which the authors have found to hold for concentric columns, Eq. 11, is in substantial agreement with that given in another, earlier paper of which the writer was a co-author (Ref. 17).

It is gratifying to note that as a consequence of sustained research effort in a considerable variety of places during the last ten years, as reflected in the authors' and the writer's papers and, even more so, in their extensive

---

a. Proc. Paper 1990, April, 1959, by Theodore V. Galambos and Robert L. Ketter.

1. Prof. & Head, Dept. of Structural Engr., Cornell University, Ithaca, N. Y.

bibliographies, the elusive problem of the real strength of eccentrically loaded columns is at last being brought under control. The authors should be congratulated on having furnished a valuable building block in this edifice.